Developing retinal cell therapy: cones and cone-like cells in transplantation and development

Paul Vincent Waldron

Institute of Ophthalmology

University College London

2017

A thesis submitted for the degree of Doctor of Philosophy

[RRDNEUS4YR01]

I, Paul Vincent Waldron, confirm that the work presented in this thesis is my own. Where information has been derived from other sources, I confirm that this has been indicated in the thesis.

Abstract

Retinal cell replacement therapy aims to restore vision in retinal degenerative diseases by replacing dead photoreceptors. Injecting GFP+ rod photoreceptor precursors into the subretinal space of recipient mice leads to GFP+ cells being seen in the recipient retina. In models of retinal degeneration, replacement of proteins lacking in the recipient, as well as functional improvement, has been seen. This thesis aimed to extend this work to use cone photoreceptors, which are more important for human vision.

The Chrnb4.eGFP model was selected as a source of cones, as well as the $Nrl^{-/-}$ and $Nr2e3^{rd7/rd7}$ models which generate an increased number of cone-like cells. Cells were injected into the subretinal space of several different mouse recipients, and a number of retinal degenerative models representing a range of cone to rod ratios and functionalities.

GFP+ photoreceptors, including unambiguous morphology and immunohistochemical markers were seen in recipient retinas after transplantation into all tested recipient types. The highest numbers occurred in Nrl-deficient and Prph2 mutant mice. The majority of GFP+ cells resembled rod photoreceptors in morphology, and did not express cone-specific markers, except in Nrl-deficient recipients. Evidence from these and other experiments showed that these results were most likely due not to cell integration but instead to the transfer of material including GFP from injected cells to existing recipient photoreceptors.

To investigate functional outcomes of transplantation, electroretinography and multi-electrode array (MEA) techniques were used. MEA data showed no clear improvement in light response in treated retinas.

Time-lapse imaging of explanted early postnatal retinal tissue using multi-photon microscopy was used to investigate the migratory behaviour of developing cone photoreceptor precursors around the ages of transplantation. This revealed a cyclical pattern of migration similar to interkinetic nuclear migration, with slow basal and rapid apical movements. Pharmacological intervention implicated the dynein/kinesin motor proteins in the apical movement seen.

Acknowledgements

I would like to thank the many people who have been of great help throughout my PhD. Above all, I would like to thank my supervisors, Rachael Pearson and Robin Ali, for their support and direction. In the group, Dom Aghaizu has been hugely helpful with the migration aspects of my project, and Anna Graca has also been a frequent aid in particular with her additions to the OLM investigations. I would also like to thank Sander Smith, Claire Hippert and Su Jayakody for their guidance.

At the Rockefeller Institute, Chris Thrasivoulou, Daniel Ciantar and Tim Robson assisted with the time-lapse imaging equipment while elsewhere Ayad Eddaoudi and Rob Sampson ran FACS machines for me more times than I can remember. At the Institute of Child Health, my thanks go to Jane Sowden and Fabiana Di Marco for their contributions to the transplantation data.

For technical support, assistance with animals, sectioning and PCR I would like to thank Yanai Duran, Sam Blackford, Laura Abelleira-Hervas and Joana Ribeiro. Kate Oversby-Powell and Matteo Rizzi helped me develop and run the MEA experiments, and Martha Robinson was invaluable for her programming expertise.

Finally, huge thanks go to those in the lab and outside who have provided much needed companionship and emotional support over the years, in particular Mark Basche, the other members of my group on the Wellcome Trust PhD course, and most of all my partner Marketa, for her patience and for being a constant reminder of the outside world.

Table of Contents

List of Figures and Tables

** Denotes copyright licence from another publication. Details are specified on Figure legends.*

CHAPTER 1 .....

CHAPTER 2 .....

CHAPTER 3 .....

CHAPTER 4 .....

CHAPTER 5 .....

CHAPTER 6 .....

CHAPTER 7 .....

APPENDIX A .....

APPENDIX B

CD-ROM FILES

Abbreviations

Abbreviation	Meaning
(e)GFP	(enhanced) Green Fluorescent Protein
AMD	Age-related Macular Degeneration
Arr3	Arrestin 3
cba	Chicken beta-actin
Chrnb4	Nicotinic acetylcholine receptor subunit b4
CMV	Cytomegalovirus
Cnga3	Cyclic nucleotide gated channel alpha 3
CNS	Central nervous system
Cpfl	Cone photoreceptor function loss (mutation)
Crx	Cone-rod homeobox
E(15.5)	Embryonic/post-conception day (15.5)
ECM	Extracellular matrix
FACS	Fluorescence-activated cell sorting
FITC	Fluorescein isothiocyanate
Fgfr4	Fibroblast growth factor receptor 4
GCL	Ganglion cell layer
GFP	Green Fluorescent Protein
Gnat	Guanine nucleotide-binding-protein (transducin)
INM	Interkinetic nuclear migration
INL	Inner nuclear layer
IPL	Inner plexiform layer
Nr2e3	Nuclear receptor subfamily 2 group E member 3 (transcription factor)

MEA	Multi-electrode Array
Nrl	Neural retinal leucine zipper (transcription factor)
OLM	Outer limiting membrane
ONL	Outer nuclear layer
OPL	Outer plexiform layer
OPN1LW	Human long-wave opsin (red and green pigment)
Opn1mw *or* M-opsin	Medium-wave cone opsin
Opn1sw *or* S-opsin	Short-wave cone opsin
P(1)	Postnatal day (one)
Pde6c	Phosphodiesterase 6c
PNA	Peanut agglutinin (cone photoreceptor marker)
Prph2	Peripherin 2
rd1	Retinal degeneration 1 (Pde6b mutant)
rd2 (rds)	Retinal degeneration 2 (Prph2 mutant)
rd7	Retinal degeneration 7 (Nr2e3 mutant)
rd8	Retinal degeneration 8 (Crb1 mutant)
RGC	Retinal ganglion cell (incl. layer)
Rho	Rhodopsin
RPC	Retinal progenitor cell
RPE	Retinal pigmented epithelium
Rxrγ	Retinoid X receptor gamma
WT	Wild-type

Chapter 1 – Introduction

1.1 The eye

The eye is a highly specialised organ with the function of transmitting information about light images of the world to the brain, in order to provide visual perception of the environment and direct physical responses to external stimuli. The gross anatomy of the eye can be seen in cross section in Figure 1.1A.

Light enters via the cornea and is focussed by refraction in the transparent cornea and lens through the vitreous humour in the centre of the eye onto the neural tissue of the retina at the back, forming the image. Here the light sensitive photoreceptor cells change their response based on their illumination and transmit a signal to the retinal ganglion cells (RGCs) via the second order neurons, the bipolar cells. The optic nerve, made of the axons of RGCs, conveys the visual signal through the optic tract to synapses in the lateral geniculate nucleus in the thalamus of the brain and from there to the visual cortex, where information processing is continued. Some axons project instead to the superior colliculus in the midbrain, which is involved in controlling saccadic movements and generating a retinotopic visual map of the environment.

The retina is supported by the vascular underlying tissue of the choroid, which maintains blood flow through the eye, and supplies oxygen and nutrients to the retina. The external surface of the eye is made of the cornea and sclera, the latter being a tough tissue that maintains the shape of the eye against intraocular pressure.

A

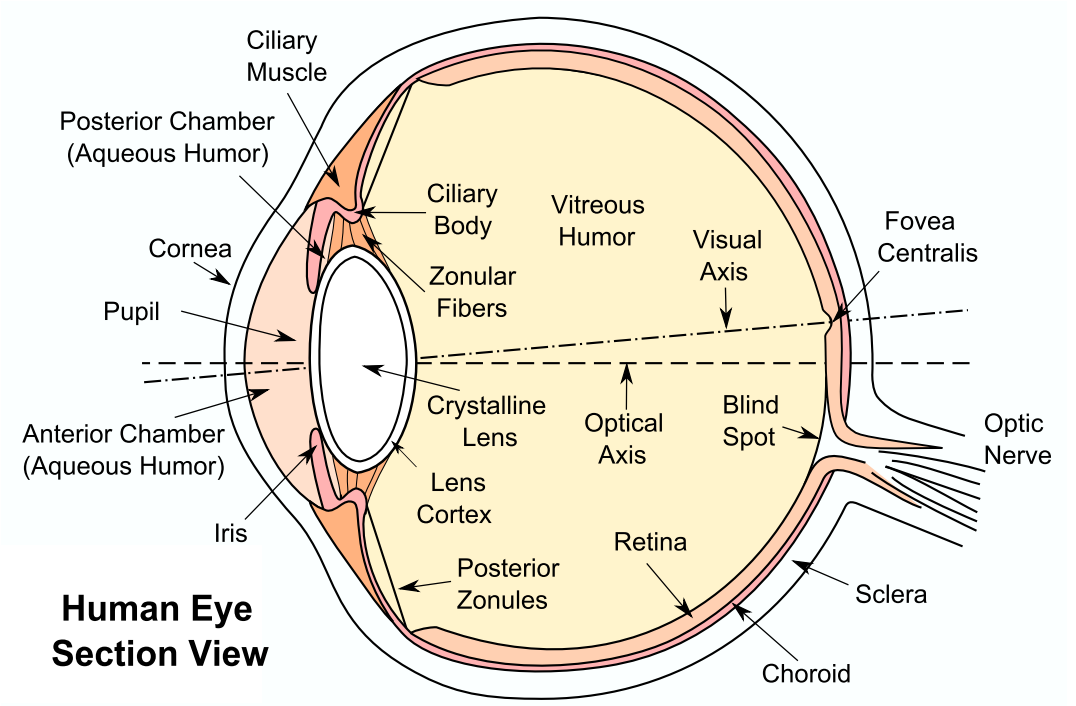
Ciliary Muscle
Posterior Chamber (Aqueous Humor)
Ciliary Body
Vitreous Humor
Visual Axis
Fovea Centralis
Cornea
Zonular Fibers
Pupil
Crystalline Lens
Optical Axis
Blind Spot
Optic Nerve
Anterior Chamber (Aqueous Humor)
Lens Cortex
Iris
Retina
Posterior Zonules
Sclera
Choroid
Human Eye Section View

B

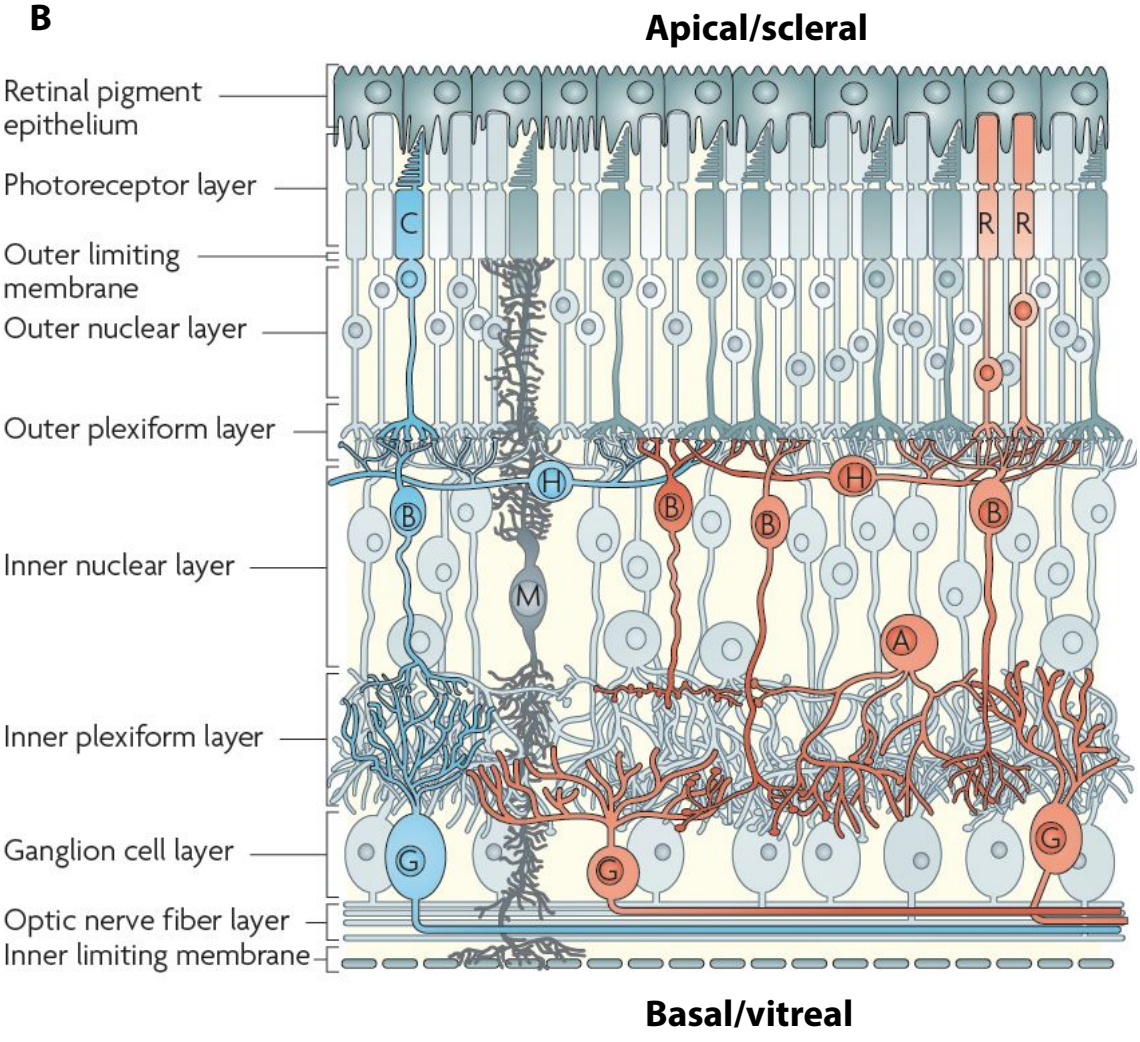
Apical/scleral
Retinal pigment epithelium
Photoreceptor layer
Outer limiting membrane
Outer nuclear layer
Outer plexiform layer
Inner nuclear layer
Inner plexiform layer
Ganglion cell layer
Optic nerve fiber layer
Inner limiting membrane
C
R
R
H
H
B
B
B
B
M
A
G
G
G
Basal/vitreal

Figure 1.1 The anatomy of the eye, and the cells and structure of the neural retina.

A A diagram of the human eye showing the major tissue layers and structural features. Public domain image reproduced from https://commons.wikimedia.org.

B The retina, showing the layers of this laminar tissue and the major cell types:

C - Cone photoreceptors
R - Rod photoreceptors
H - Horizontal cells
B - Bipolar cells
M - Müller glia cells
A - Amacrine cells
G - Retinal Ganglion Cells

The axis of the retina is shown, with the photoreceptors and RPE located most apically and closest to the sclera, and the RGCs located basally, nearest the vitreous humour. Photoreceptors have cell bodies in the outer nuclear layer, while those of bipolar, horizontal, amacrine and Müller glia cells make up the inner nuclear layer.

The outer segments of both photoreceptor types are surrounded by the retinal pigmented epithelial cells which regenerate chromophores and phagocytose spent photoreceptor discs. Signals from photoreceptors are passed to bipolar cells at synapses in the outer plexiform layer and then to the retinal ganglion cells. Typical pathways for cones (blue) and rods (orange) are shown. Note the increased convergence of signals from multiple photoreceptors in the rod cells, compared to the cones. Axons of the RGCs transmit visual information by action potentials via the optic nerve to the brain.

The Müller glia span the whole depth of the neural retina, are involved in chromophore regeneration and response to injury, and also form the inner and outer limiting membranes, the latter through adherens junctions with each other and with photoreceptor cells. Reprinted by permission from Macmillan Publishers Ltd: *Nature Reviews Neuroscience* (Swaroop et al, 2010), copyright 2010.

The sphincter muscle of the iris controls the size of the pupil, the aperture at the anterior of the eye through which light enters. The pupil alters its size depending on ambient light levels, in a reflexive mechanism controlled by a minority of intrinsically light sensitive RGCs.

1.1.2 The retina

The retina contains the light sensitive cells of the eye – the photoreceptors - and the neural tissue responsible for initial processing of the visual signal and its transmission to the brain. It displays a laminar structure characteristic of the central nervous system; this structure, together with the cells that comprise it, can be found in Figure 1.1B. This structure is ordered with the light sensitive photoreceptors at the back of the eye, such that light must pass through the cell bodies of the rest of the cells in order to reach the photosensitive photoreceptor layer. The orientation of the retina is referred to, variously, as an apico-basal, or scleral/vitreal axis, as shown.

1.1.2.1 Retinal neurons

The photoreceptors are the primary light-sensitive cells and have nuclei located in the outer nuclear layer (ONL). The two major classes of photoreceptors are the rod cells, mediating vision at low (scotopic) light levels, and cones, which respond at higher (photopic) light levels and allow for colour vision. They hyperpolarise in response to the absorption of light by photopigment in their outer segments, and have synapses located in the outer plexiform layer (OPL). These cells are described in more detail below (section 1.2).

Bipolar cells have nuclei residing in the inner nuclear layer (INL) and relay signals from the photoreceptors to the RGCs. Each bipolar cell will make primary

connections with either rod or cone cells, with multiple types of cone bipolar cell (at least nine identified to date) existing, but only one type of rod bipolar in the mammalian retina (Ghosh et al. 2004). In response to a light signal from the associated photoreceptor, an ON bipolar cell becomes excited (depolarised) and an OFF bipolar cell becomes inhibited by hyperpolarisation, due to differences in the reception of the photoreceptor signal. These divisions in cell type are a result of the expression of different glutamate receptors at the synapse with photoreceptor cells (Wässle et al., 2009).

Horizontal and amacrine cells are both located in the INL and are involved in the neural processing of the visual signal at the earliest stages. Horizontal cells are GABAergic inhibitory neurons that make synapses in the OPL with both photoreceptors and bipolar cells and regulate a negative feedback mechanism. Similarly, amacrine cells are generally inhibitory interneurons (GABA- or glycinergic) that make connections in the IPL with RGCs and bipolar cell terminals.

The cell bodies of RGCs are present in their own layer, the GCL, the most basal of the retina. They receive input from bipolar and amacrine cells in the IPL. The axons of the RGCs project to the brain through the optic nerve. As the RGCs are located vitreal to the photoreceptors, the axons must pass through the retinal tissue to leave the eye, which occurs at the optic disc, or optic nerve head. This break in the retinal tissue causes the blind spot, a gap in the visual field.

Multiple types of RGC exist differing in their response to illumination and in the amount of the visual field they cover. The two major types are midget cells, with small dendritic trees, which sample from few input cells and thus have a small receptive field. Parasol cells have larger receptive fields, sampling inputs from large numbers of bipolar cells with their wide dendritic trees.

1.1.2.2 Other retinal cells and features

The Müller glia are the primary glial cell type in the retina. These cells span the depth of the retina and are involved in maintaining a healthy retinal environment: recycling glutamate for synaptic transmission and providing metabolic support to the other retinal cells. These cells are also involved in the response to retinal damage, undergoing a process of gliosis (see section 1.5.1.2). It has also been shown that Müller glia act as optical fibres, guiding photons through the retinal tissue to the photoreceptor layers (Franze et al., 2007).

The outer limiting membrane (OLM) is formed of adherens junctions between the Müller glia end feet and the inner segments of the photoreceptors, at the apical edge of the ONL. The OLM forms a barrier between the cell layers of the neural retina and the subretinal space containing the photoreceptor segments. It acts to prevent the diffusion of components involved in the phototransduction cascade (the mechanism by which photoreceptors respond to light), and to maintain the physical structure of the retinal tissue. The other end feet of the Müller glia form the inner limiting membrane (ILM), together with astrocytes, beyond the GCL at the vitreal surface of the retina.

The cells of the RPE, located beyond the outer segments of the photoreceptors, are pigmented to absorb the light not captured by the photoreceptors, improving image resolution by the avoidance of backscatter. These cells extend processes which surround the outer segments of the photoreceptor cells, and act to provide trophic support and the light-sensitive molecules needed for photosensitivity to these cells, and transport metabolic waste to the underlying choroid.

1.2 Rods and cones

1.2.1 Photoreceptor structure

The structure of rod and cone cells is specialised to enable their function as photosensitive neurons. A diagram of this structure can be found in Figure 1.2. The outer segment, a heavily modified cilium, is the location of the photosensitive molecules of the photoreceptors. Both types of photoreceptor contain discs, made from infoldings of the plasma membrane. In cones, the discs are continuous with the plasma membrane. However, in rods these are not continuous with the outer cell membrane but are each whole structures within the cell. The photosensitive visual pigment (rhodopsin or cone opsin), as a transmembrane protein, is held within these discs. The function of these proteins is explained below (section 1.2.2). The inner segment contains most of the cytoplasm of a photoreceptor, along with mitochondria, which produce the ATP necessary for the function of the cell and is much larger in cone cells than in the rods. The majority of protein production, including the generation of visual pigment also occurs in this part of the cell.

Photoreceptor nuclei are located in the ONL. Notably, in mammalian retina, cone photoreceptor nuclei are located apically, at the edge of the ONL closest to the OLM, while rod nuclei make up the rest of the ONL, and are found throughout its depth. The appearance of the nuclei in rods and cones differs, with rods possessing a smaller nucleus with a single large central point of condensed heterochromatin (Solovei et al., 2009). In contrast, cone nuclei are larger and show multiple smaller points of condensed heterochromatin. Cone photoreceptors, with their nuclei and segments, are arranged in a regular pattern across the mouse retina known as the cone mosaic (Fei, 2003; Ogden, 1975; Reese et al., 1995).

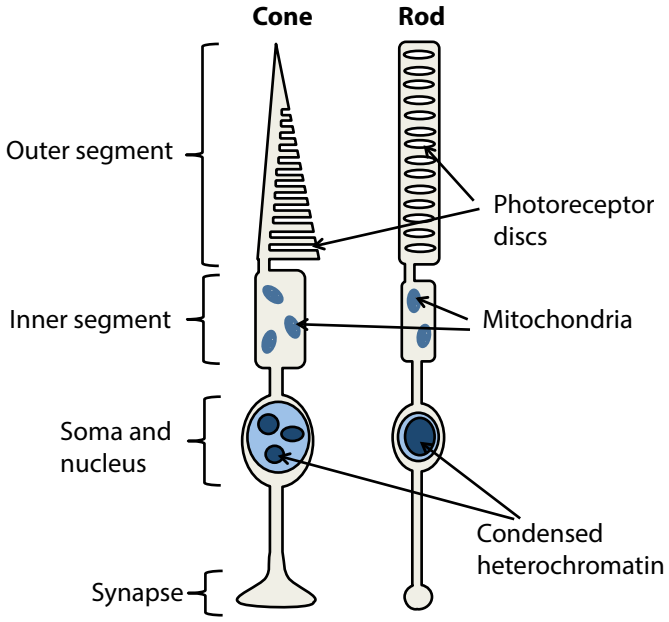

Figure 1.2 Mammalian photoreceptor structure. The major features of these cells are shown, including inner and outer segments, the nucleus and synapses.

The synapses of rods and cones are found in the OPL. Photoreceptors do not fire action potentials, and as such their glutamate release is controlled by the membrane potential changes caused by the activity of photopigment in the outer segments (see below). Rod synaptic terminals are generally found basal to those of cones and are referred to as spherules. A rod will make a single connection to a rod bipolar cell, which will itself receive input from several rods. This summation of the response of several rods is one factor in how rods mediate scotopic vision.

Cone synapses are called pedicles, and have a larger triangular shape. These terminals contain multiple ribbon synapses, which are specialised for rapid glutamate release and are made with one or more cone bipolar cells, with a single cone pedicle able to make up to 500 contacts in primate retina (Wässle et al., 2009; see also Wässle, 2004).

1.2.2 The phototransduction cascade

The phototransduction cascade is the process by which a light stimulus is converted into a change in neurotransmitter release by a photoreceptor (see Ebrey & Koutalos 2001). The chromophore 11-cis-retinal is the light sensitive component of this system. Derived from Vitamin A, this molecule is bound to the opsin class of molecules in the photoreceptor. Opsins are transmembrane proteins which are part of the G protein-coupled receptor family (GPCR). They are found in all photoreceptors, and are located on the photoreceptor discs in the outer segments of these cells.

On absorbing a photon, 11-cis-retinal undergoes photoisomerisation to all-trans-retinal, causing a conformational change in the opsin to which it is bound. This leads to the dissociation of the retinal molecule from its opsin, and the commencement of

the GPCR activity of the opsin. The resulting signalling cascade which subsequently occurs is somewhat unusual compared to the GPCR pathway found in other neurons, and will be discussed below.

In darkness, the cyclic nucleotide cGMP is produced by guanylyl cyclase proteins and binds to cyclic nucleotide gated channels, keeping them in the open state. This allows an inward current, meaning that the cell is depolarised, and so releases glutamate at its synapse, through Ca^{2+} mediated neurotransmitter release. The activated opsin protein binds the heterotrimeric G-protein transducin, and causes the disassociation of the α-subunit by replacing the bound GDP for GTP. The remaining βγ-subunit is thereby freed; this can be prolonged by the action of phosducin, which associates with transducin and prevents the hydrolysis of the GTP activator.

Activated βγ-transducin stimulates the activity of cGMP-phosphodiesterase. The phosphodiesterase protein hydrolyses cGMP to produce GMP, which no longer binds to the ion channels, which thus close, preventing the inward current. This causes the cell to hyperpolarise, and so reduces the amount of neurotransmitter released at the synapse with the cell's associated bipolar cell or cells. Light stimulation therefore reduces the release of glutamate at the synaptic terminal of photoreceptors, and this reduction alters the activity of the connected bipolar and horizontal cells.

In the recovery phase following light stimulation, these processes are reversed. The opsin molecules are phosphorylated by the action of rhodopsin kinase, and 'capped' to further prevent its action by the arrestin protein. The phosphorylation activity can be further regulated through the activity of the recoverin protein. The retinal molecule, now in its all-trans conformation, must be regenerated into 11-cis retinal.

First, it is converted to all-trans retinol by retinal dehydrogenase in the photoreceptor. The molecule is transported to the RPE cells, where it is converted into all-trans-retinyl ester, and then to 11-cis retinol by the action of retinyl-ester isomerase. Finally, it is converted to 11-cis retinal by retinol dehydrogenase and transported back into the photoreceptor cells. In cone cells, an alternative pathway exists, which utilises the Müller glia cells. These cells absorb 11-cis retinol leaving the photoreceptors, and convert it to 11-cis retinol through the action of all-trans-retinol isomerase before releasing it to the cones, which use a cone specific dehydrogenase enzyme to produce 11-cis retinal (Arshavsky, 2002). It is hypothesised that this system is one way in which cone cells are able to maintain function at high light levels, as it provides a source of retinal independent of the RPE and unavailable to the rod cells.

The differences in response to light between rod and cone photoreceptors are, in part, a product of the cellular machinery that carries out this response. While very similar in nature, the majority of the proteins involved in mediating the response are distinct between rod and cone photoreceptors. Most importantly, the opsin protein that houses the 11-cis-retinal molecule is different between rods and cones, and between the different cone subtypes. This determines the wavelength at which the retinal molecule will absorb light, and so changes the spectral sensitivity of the photoreceptor. In mice, two cone opsins are produced, with different peak sensitivities. Short-wave opsin (S-opsin) is most sensitive to ultraviolet light (360nm) and medium wave-opsin (M-opsin) to green light (508 nm). This difference in sensitivity is how cone responses encode colour perception. The majority of mouse cones coexpress both opsins, but in variable ratios, such that a cone can be said to have a primary opsin type. A gradient of expression is evident across the mouse retina, such that cone cells in the inferior/ventral retina primarily express S-opsin, while cones in the superior/dorsal retina predominantly express M-opsin (Applebury

et al., 2000; Ng et al., 2001; Roberts et al., 2005). These observations are matched by the analysis of single-cell recordings from different cone cells (Nikonov et al., 2006), which also show that the absolute sensitivity of both classes of cones are very similar, and that both types are more tolerant to bleaching of their photopigment than are rods – part of the reason for the ability of these photoreceptors to function at high light intensities.

As well as the opsins, cone photoreceptors have distinct varieties of the phosphodiesterase protein (Pde6c), transducin protein (Gnat2), and cGMP gated channels (Cnga3) all involved in the signalling cascade, as well as the recovery protein arrestin (Arr3), with this not being a comprehensive list.

1.2.3 Role in vision

As already stated, rods and cones differ in their response to light, in a number of ways. Rods are sensitive to much lower light levels than cones, but rapidly saturate at higher light intensities. The colour vision resulting from cones is a function of their different visual pigments, with the three opsin types in humans giving trichromatic vision (Bowmaker and Dartnall, 1980), and the two in other mammals such as mice giving dichromatic vision. Rods, with the single rhodopsin pigment, do not encode colour information.

The connections made with other retinal neurons are also relevant to the contribution to vision. Many midget RGCs are connected to single midget bipolar cells, which themselves receive input from only one cone, thus giving a single-cell resolution of the light information reaching the retina. In contrast, rod responses are more usually subject to summation from multiple rods to single bipolar cells, increasing light sensitivity at the expense of detail.

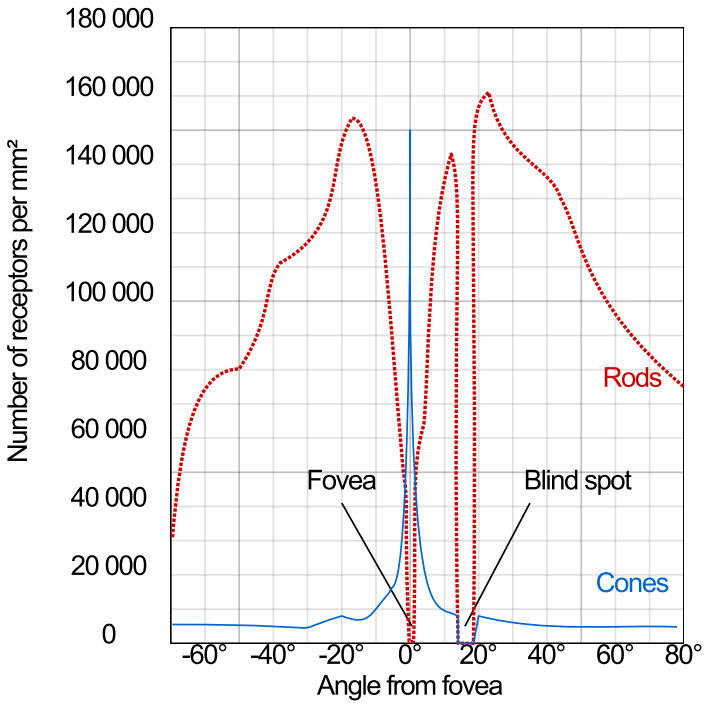

Figure 1.3 Photoreceptor distribution in the human retina. Cones (blue) are outnumbered by rods in all areas of the retina except in the fovea, which has no rods and dense cones. Both photoreceptor types are absent in the 'blind spot' at the optic nerve head. This image by Cmglee via Wikimedia Commons, and based on Foundations of Vision by Brian A Wandell. Reproduced under the GNU Free Documentation License.

While cones are far less common than rods in most mammals, making 3% of mouse photoreceptors (Jeon et al., 1998) and approximately 5% in humans (approximately 5 million cones to 92 million rods) (Curcio et al., 1990), in humans, at least, their contribution to vision is highly significant. Rods are approximately evenly distributed in the mouse retina, but, as shown in Figure 1.3, the distribution of rods and cones across the human retina differs in different areas. In the central fovea, rods are absent and the concentration of cones much increased. In addition, the cell bodies and processes of the retina are laterally displaced away from the light path in order to decrease the impedance of cytoplasm on the incoming light. In this way, central vision in humans is highly detailed and colour sensitive, and is therefore necessary for many aspects of useful vision.

1.3 Retinal development

As described below, previous studies have shown that the developmental stage of transplanted photoreceptors is of critical importance in their capacity for use in cell therapy. It is therefore necessary to provide an overview of the major stages in retinal development, with particular focus on the generation and specification of rod and cone photoreceptors.

The neural retinal tissue is part of the central nervous system (CNS) and is accordingly derived from the dorsal neurectoderm. Other parts of the eye derive from separate germ layers, with the cornea and sclera produced by the mesoderm, and the lens a product of the surface ectoderm. The neural plate, the basis for the nervous system, forms from the ectoderm and the neural tube develops from a fold made in this structure. The optic vesicles develop at the dorsal end of the animal from outpockets of the neural tube, with the optic stalk connecting them to the rest of the tube, and eventually linking the eye and the brain as the optic nerve. Figure

1.4A shows the development of the eye from these optic vesicles. The optic cup is formed from invagination of the surface ectoderm together with the underlying neuroepithelium of the neural tube. The lens is formed and surrounded by two layers of the neuroepithelium, with the outer layer becoming the RPE monolayer and the inner layer beginning to divide repeatedly in order to become the neural retina.

During the proliferative stage, multipotent retinal progenitor cells (RPCs) divide in the neuroblastic layer, initially in symmetric divisions. During this process they undergo a migratory process where they divide only at the ventricular zone, on the apical edge of the developing tissue, but are found displaced from this area during the other phases of the cell cycle, a process called interkinetic nuclear migration (see section 1.6.1). The RPCs thus increase in number as they divide but after a peak at P0 (Alexiades and Cepko, 1996) decline steeply in number as fewer continue to divide and instead begin to undergo asymmetric division, with some daughter cells beginning to differentiate into postmitotic retinal cells. In this way, the seven main classes of retinal cell are produced in an overlapping temporal sequence which is conserved across vertebrate species (Cepko et al., 1996). RGCs are produced first, then cones, horizontal cells and amacrine cells are produced at approximately the same age. A second wave of cell genesis generates rods, bipolar and Müller glial cells. Figure 1.4B shows the order of the production of the retinal cells. The activity of Notch is required for maintaining progenitors in the cycling proliferative state, preventing them from leaving the cell cycle. Inhibition of Notch leads to cells leaving the cycle early, and a consequent over-production of cone cells at early developmental stages, and rod cells at later ages (Wall et al., 2009; Yaron et al., 2006).

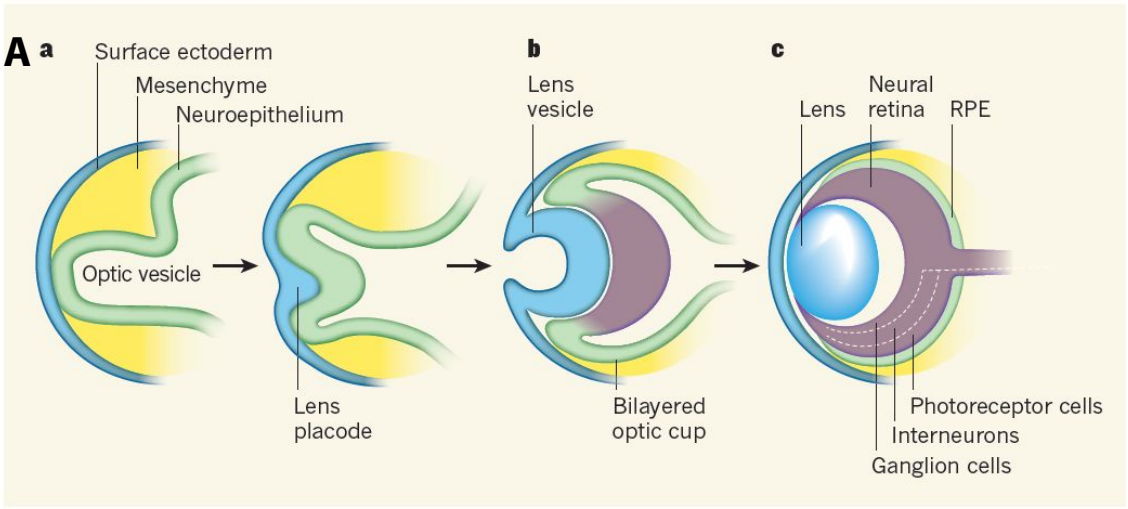
A
a
Surface ectoderm
Mesenchyme
Neuroepithelium
Optic vesicle
Lens placode
b
Lens vesicle
Bilayered optic cup
c
Lens
Neural retina
RPE
Photoreceptor cells
Interneurons
Ganglion cells

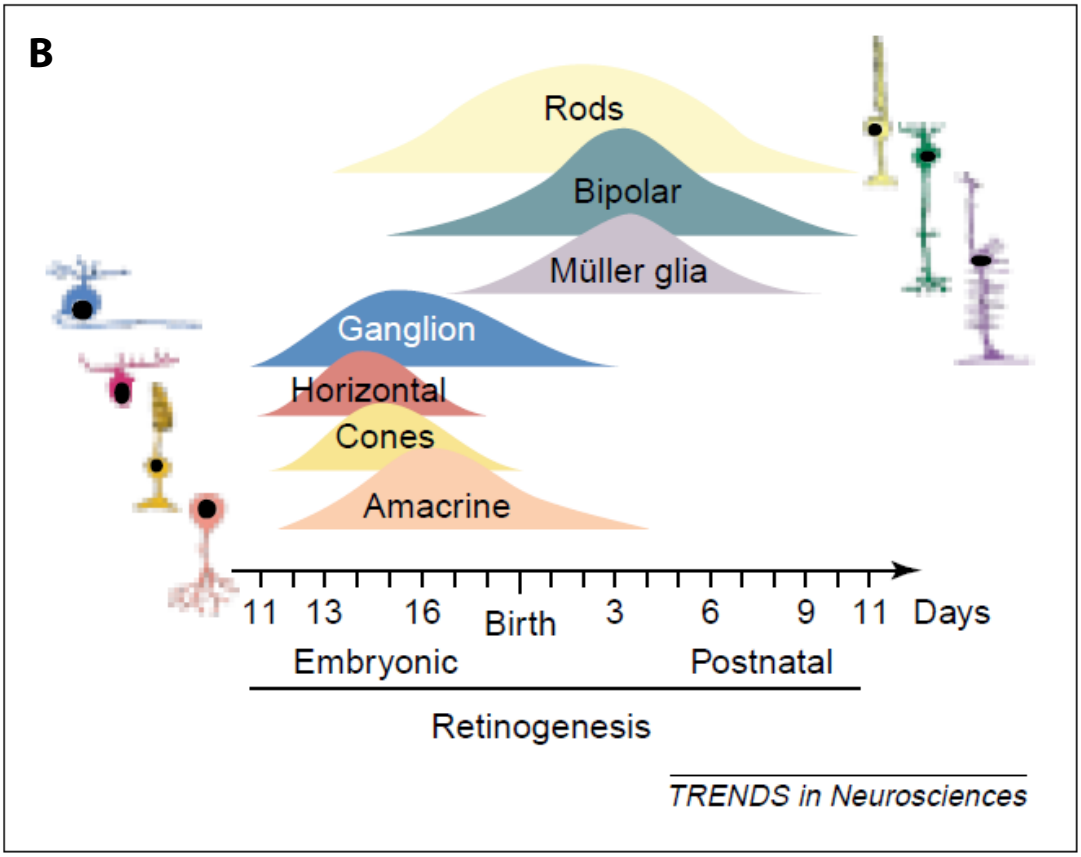
B
Rods
Bipolar
Müller glia
Ganglion
Horizontal
Cones
Amacrine
11 13 16 Birth 3 6 9 11 Days
Embryonic
Postnatal
Retinogenesis
TRENDS in Neurosciences

Figure 1.4 Eye formation and retinal neurogenesis.

A The formation of the eye. The surface ectoderm and underlying neuroepithelium invaginate and form the optic cup, with the outer and inner neuroepithelium forming the RPE and neural retina, respectively. Reprinted by permission from Macmillan Publishers Ltd: *Nature* (Ali & Sowden, 2011), copyright 2011.

B The generation of the 7 neural retinal cell types from differentiating daughter cells of RPCs occurs in overlapping sequence as shown, in the mouse eye. Groups do not show relative quantity of cells produced between cell types, but only within cell type. This image reprinted by permission from Elsevier: *Trends in Neuroscience* (Marquardt & Gruss, 2002), copyright 2002, itself adapted from Young, 1985, reprinted with permission from Wiley: *The Anatomical Record*, copyright 2005.

Due to the overlapping order in which these cells are produced, in order to construct the ordered layers of the retina, the newly post-mitotic cells must move to their final position through the developing retinal tissue. I will discuss this stage of migration in the retina and other parts of the CNS in section 1.6.2.

1.3.1 Photoreceptor development

Rods and cones are produced by mitosis at different but overlapping ages in the mouse retina, as shown in Figures 1.4B and 1.5A. Photoreceptors undergo process growth, synaptogenesis and a period of postmitotic migration (see section 1.6.3) in the late embryonic and early postnatal period, with the onset of a functional retina occurring after the elaboration of outer segments beginning at P10. The onset of functional proteins such as opsins occurs at various times depending on the cell subtype, with S-opsin and Rhodopsin expression preceding that of M-opsin, in the mouse. In humans, sight is more developed at birth, with terminal photoreceptor mitosis and opsin expression beginning around foetal week 9, and continuing until birth (see Swaroop, Kim, & Forrest, 2010).

Evidence that rod photoreceptors are generated in two distinct phases was found in rat retinas (Morrow et al., 1998). This study found that rod precursors born after E19 had a shorter time lag between terminal mitosis and the expression of rhodopsin than did those generated before E19, with the effect that rhodopsin expression was approximately synchronous between all rods, despite the wide range in the date of terminal mitosis.

1.3.1.1 Fate specification

The activity of a series of transcription factors is necessary for the correct development of both rod and cone photoreceptors. Combinations of these factors,

expressed in sequence, are necessary for the production of specific subtypes of photoreceptors, as summarised in Figure 1.5B (Swaroop et al., 2010).

The transcription factors associated with all photoreceptor cells in mammalian retina are Crx, Rorβ, and Otx2. Otx2, a homeobox protein, is the first to be expressed, being produced during and after terminal mitosis, and also produced in postnatal bipolar cells. Ablation of Otx2 in RPCs leads to a decrease in the production of both bipolar cells and photoreceptors (Koike et al., 2007). Rorβ, a retinoid orphan nuclear receptor, (Schaeren-Wiemers et al., 1997) is expressed in the brain and pineal gland in addition to the retina. When knocked out in mice, an absence of Rorβ causes a loss of rod cells and an overproduction of cones, although these cells are functionless, lacking outer segments (Jia et al., 2009).

Crx, another homeobox gene, is expressed in all photoreceptors and is necessary for the transcription for a number of photoreceptor genes, including the opsins (Chen et al., 1997). Crx mutations are associated with a number of retinal diseases including retinitis pigmentosa and Leber's congenital Amaurosis (see below) in humans. In mice, a lack of Crx leads to photoreceptors failing to produce outer segments and a lack of rod or cone function (Furukawa et al., 1999, 1997).

Determination of the specific photoreceptor type – rod or cone – is a result of the activity of two transcription factors found in rods: Nrl and Nr2e3. Nrl is a Maf-family transcription factor, which interacts with Crx and regulates rod gene expression (Mears et al., 2001; Oh et al., 2008). In the absence of Nrl, rod photoreceptors are not produced and the ONL is instead composed of cells that resemble S-opsin containing cones (Brooks et al., 2011; Roger et al., 2012; Yoshida et al., 2004). These cells are similar in most morphological, molecular and electrophysiological

A

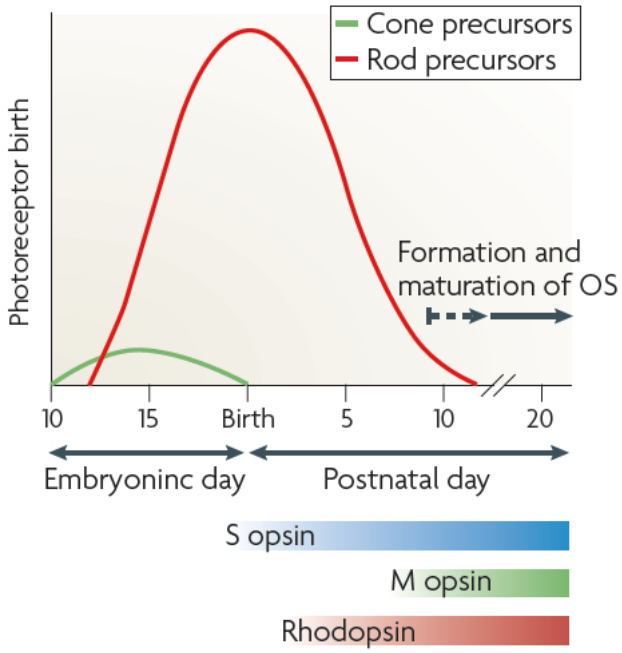
Cone precursors
Rod precursors
Photoreceptor birth
Formation and maturation of OS
10
15
Birth
5
10
20
Embryoninc day
Postnatal day
S opsin
M opsin
Rhodopsin

B

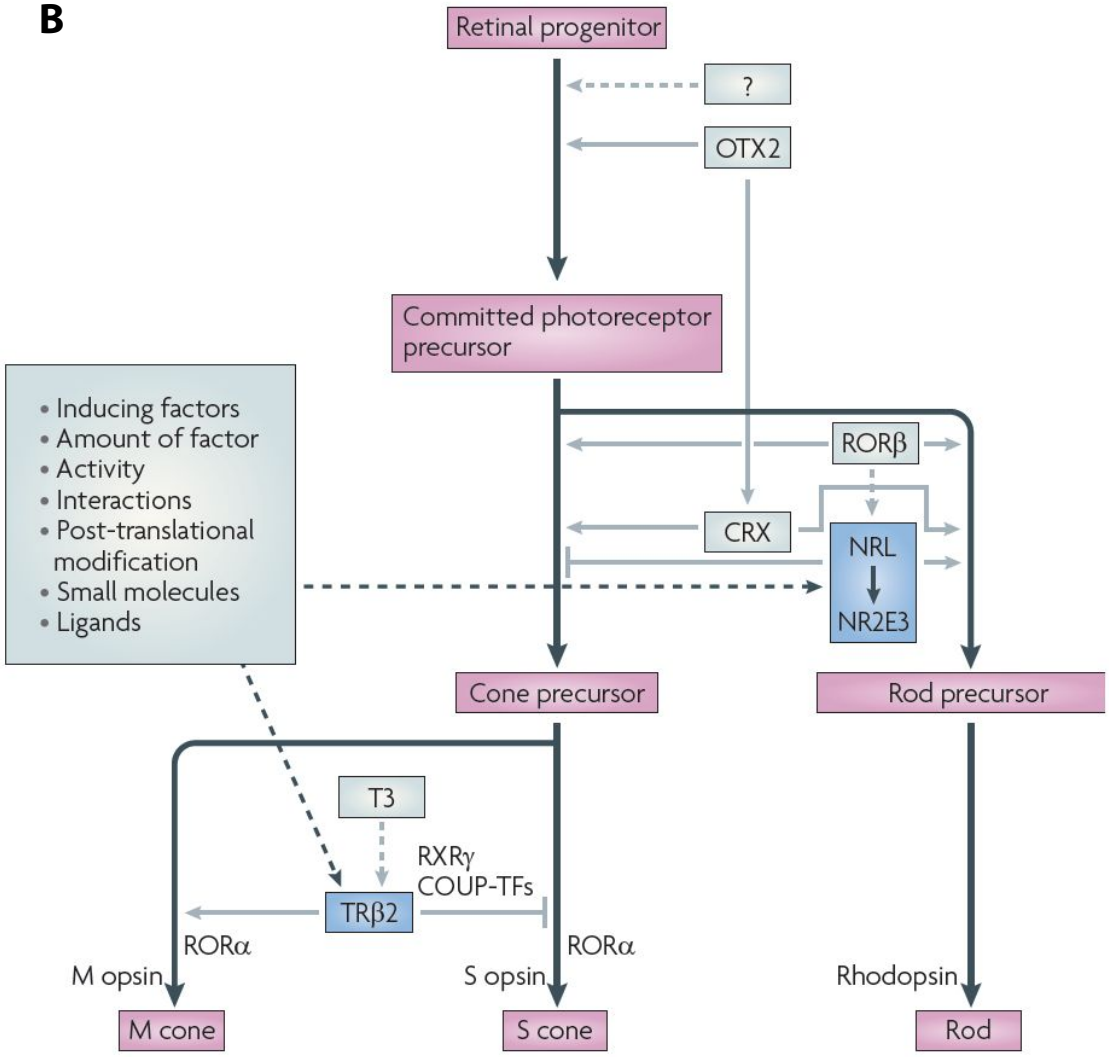
Retinal progenitor
?
OTX2
Committed photoreceptor precursor
• Inducing factors
• Amount of factor
• Activity
• Interactions
• Post-translational modification
• Small molecules
• Ligands
RORβ
CRX
NRL
NR2E3
Cone precursor
Rod precursor
T3
RXRγ
COUP-TFs
TRβ2
RORα
RORα
M opsin
S opsin
Rhodopsin
M cone
S cone
Rod

Figure 1.5 Photoreceptor genesis and fate determination in the mouse.
A The age at which photoreceptors become postmitotic. Cone genesis begins and ends before birth, with the peak of rod genesis occurring around birth. The cone ratio is therefore higher at early developmental stages.
B Fate specification of classes of photoreceptor cells. Otx2, Rorβ and Crx are necessary for the general specification of photoreceptor fate. Nrl, along with its target Nr2e3, suppress cone identity and promote differentiation into rod precursor cells. In the absence of these factors, photoreceptors become S-opsin expressing cones, with Rxrγ expression evident in cone precursors. Thrβ2 is involved in the specification of M-opsin expression, and is instrumental in the generation of the dorsal-ventral axis of cone types.

---

features to normal cones, with a consequent removal of rod-mediated vision in these mice (Daniele et al., 2005). Conversely, the introduction of Nrl expression into developing cone cells has been shown to convert them to a rod fate in *Xenopus* (McIlvain and Knox, 2007) and mouse (Oh et al., 2007), where it has also been shown to rescue the excess cone production in Rorβ$^{-/-}$ cells (Jia et al., 2009).

Nr2e3, an orphan nuclear receptor, is a target of Nrl, also interacting with Crx, and has been shown to suppress the expression of cone-specific genes (Chen, 2005; Cheng et al., 2006, 2004; Haider et al., 2006; Peng et al., 2005). In the rd7 mutant mouse, Nr2e3 is functionless, with a phenotype similar to that of the Nrl deficient mouse: supernumerary S-opsin expressing cones are produced, especially in the ventral/inferior retina, and while not all photoreceptors become cones, the remaining photoreceptors are hybrids, expressing all rod but also some cone-specific genes (Corbo and Cepko, 2005; Haider et al., 2006, 2001). The excess cones produced are derived from early-born photoreceptor precursors (Cheng et al., 2011). Similarly, in humans, enhanced S-cone syndrome is caused by an Nr2e3 mutation, causing an increase in S-opsin mediated vision and a reduction in Rhodopsin and L/M-opsin related vision (Haider et al., 2000; Milam and Rose, 2002).

Both the Nrl and Nr2e3 mutant mice display defects in the structure of the retina, with rosettes forming and some loss of photoreceptors over time (Haider et al., 2001; Roger et al., 2012; Stuck et al., 2012). The formation of the rosettes is hypothesised to arise due to defects seen in the integrity of the OLM, or by the disruption to the tissue involved with the production of supernumerary cones.

As evidenced by defects in Nrl and Nr2e3 function, the S-opsin expressing cone can be thought of as a ‘default’ outcome for Crx-specified photoreceptor precursors. The specification of other cone subtypes is a function of Thyroid Hormone receptor β2 (Thrβ2), which controls the patterning of the gradient of M-opsin and S-opsin expression in cones (Liu et al., 2008; Ng et al., 2009). In mice without Thrβ2, M-cones are lost and S-opsin cones produced instead (Ng et al., 2001).

1.4 Retinal degenerative diseases

Retinal degenerative diseases involve the death of the cells of the retina, and progressive loss of function as a result of their removal. Commonly, the cells that die are the photoreceptor cells, and vision loss occurs as their photosensitive input is removed. Degeneration can be caused by a number of factors, including environmental, aging, and genetic components, as well as occurring as a result of other conditions, such as diabetes. Inherited retinopathies affect approximately 1 in every 2000 individuals worldwide. I will discuss two of the most common types of retinal disease that culminate in photoreceptor loss.

1.4.1 Retinitis pigmentosa

Retinitis pigmentosa refers to a group of hereditary retinal degenerative diseases that involve photoreceptor degeneration and loss of peripheral vision (Hartong et al., 2006). Retinitis pigmentosa is the most common form of inherited retinal degeneration, affecting about 1 in 4000 people worldwide.

Most examples of retinitis pigmentosa manifest as problems with adaptation to low light levels, a loss of night vision and peripheral vision, eventually progressing to tunnel vision, where only central vision remains. This is due to the loss of photoreceptors in the peripheral retina, where rod cells predominate (see Figure 1.3), and loss of rod photoreceptor cells and function is faster than for cones, in most cases. In some unusual forms of retinitis pigmentosa called cone-rod degeneration, cone loss is more prominent than rods, leading to a loss of visual acuity and colour vision deficits (Birch et al., 1999). As the disease progresses, the fundus of the eye takes on a pigmented appearance and finally central vision is lost as cone photoreceptors begin to die. Due to the survival of central cone-mediated

vision to late stages of disease (usually 60 years), some useful vision is often retained in older patients (Berson, 2007).

Although 32 genes are known to be associated with retinitis pigmentosa, including Rhodopsin, no single mutation accounts for more than 10% of cases of these diseases, and around 60% of cases have no known genetic cause (Wang et al., 2005). The pattern of inheritance differs between cases of retinitis pigmentosa, with autosomal dominant (30-40%), autosomal recessive (50-60%) and X-linked (5-15%) patterns seen (Hartong et al., 2006).

1.4.2 Age related macular degeneration

Age related macular degeneration (AMD) is a chronic disease of the central retina, in which central vision is lost. This degeneration affects the fovea and the surrounding area: the macula. This area is specialised for its function as the area of high acuity vision, with a high density of photoreceptors and a lack of blood vessels in the underlying tissue. In particular, this area is home to a large number of cone photoreceptors and RGCs: it has been estimated that lesions in the central 2mm of retina affect 25% of the RGC population of the human retina (Penfold et al., 2001).

This condition is the most common cause of incurable blindness in the Western world. As the name implies, the risk of AMD increases with advancing age, affecting 13% of people over 85 (Smith et al., 2001). With the population in many countries increasing in average age, this disease is likely to become more important still. However, while age is an important factor, AMD has a strong genetic component, with up to 20 genes related to this condition, as well as numerous environmental factors such as obesity, smoking and nutritional deficiency (Lim et al., 2012).

AMD is often separated into two types, commonly termed ‘wet’ and ‘dry’ AMD. The degree to which these types are related is contested, with evidence that one form can progress to the other. Wet, or exudative AMD is characterised by choroidal neovascularisation, with the production of new subretinal blood vessels which tend to grow towards the fovea, extending through Bruch’s membrane. Wet AMD progresses more quickly than the dry variety, with legal blindness occurring within months of both eyes being affected, if untreated. Haemorrhage and exudation from these vessels is another cause of damage to the overlying retinal cells (de Jong, 2006).

Dry, non-exudative or atrophic AMD is more common, and involves loss of the RPE cells at the macula, as well as choroidal atrophy. Clumps of pigment are seen to form at the edge of the area of atrophy. Another characteristic symptom is the appearance of ‘drusen’, white or yellow circular patches which appear on the retina, which can be identified by ophthalmoscope. With loss of support from the RPE cells, the overlying cone photoreceptors begin to degenerate.

The main visual symptom of AMD is the loss of central vision, including detailed and colour vision in this area, as a result of the death of cone cells in the macula and fovea. Due to the importance of central vision for everyday tasks, this loss can have profound effects on the quality of life of patients with AMD. As a multi-factorial, age-related disease, AMD is not caused by a single genetic defect as is the case with several other retinal degeneration conditions. It is therefore not likely that treatments targeted at the genetic level represent an effective way of treating AMD, and the restoration of vision is only possible if the cone cells are replaced.

The ultimate aim of this thesis, as it focuses on the extension of cell therapy techniques to utilise cone photoreceptors, is to aid in the treatment of AMD and similar conditions which affect cones.

1.4.3 Treatments

Many prospects for treatment of retinal degenerative diseases, including those outlined above, exist. Many are in preclinical stages, but clinically useful interventions are also currently used, although none are currently able to restore lost photoreceptors. While this thesis will focus on the use of cell therapy as a treatment (discussed in section 1.5), I will here briefly describe other strategies.

1.4.3.1 Pharmacology

The neovascularisation that accompanies development of symptoms in wet AMD represents a target for treatment; recent attempts to suppress the function of the angiogenic vascular endothelial growth factor (VEGF) using antibody antagonists have been successful at reducing the symptoms of AMD and improving vision in some patients (Tobergte and Curtis, 2011), although limitations exist in that repeated treatment is necessary, and not all patients respond to these interventions. For dry AMD, treatment options are more limited, although disease progression is in general much slower in this variety of the condition. Increasing choroidal blood flow may be a possibility to reduce disease progression (Kruger et al., 1998). The complement immune system has been implicated in the pathogenesis of dry AMD, and interventions targeting this system may hold some promise for treatment opportunities.

In retinitis pigmentosa, vitamin A supplementation has been reported to reduce the progression of disease (Berson, 2007). A number of neurotrophic growth factors

have also been identified as showing potential for slowing disease progression, including CNTF, NGF and rod-derived cone viability factor (see Guadagni, Novelli, Piano, Gargini, & Strettoi, 2015). Targeting the inflammation that accompanies the disease may also be an avenue for treatment, as elevated levels of proinflammatory cytokines have been seen in retinitis pigmentosa patients (Yoshida et al., 2013). However, treatment of this kind would be likely only to alleviate the symptoms of disease and slow cell loss, rather than treating the root cause.

1.4.3.2 Gene therapy

Gene therapy is the introduction of genetic material into a patient in order to treat a disease. A primary variety of this approach is the replacement of a faulty, missing or mutated gene with a healthy copy, commonly referred to as gene supplementation. Most often, genes are introduced into the cells of a patient using a viral vector, of which the two major types currently in use are adeno-associated viruses (AAV) and lentiviruses. These approaches are under investigation for use for the treatment of a number of retinal diseases (see Smith et al. 2009; Tan et al. 2009). Other potential methods of transfecting target cells in the retina include electroporation and ultrasound (Matsuda and Cepko, 2004; Yamashita et al., 2007), as well as chemical methods using liposomes and polymers to introduce genetic material (Naik et al., 2009).

Recent studies have shown improvement in human vision after treatment for retinal conditions, such as the x-linked recessive disease of choroideremia (Maclaren et al., 2014), and similar trials have been carried out for Leber's Congenital Amaurosis (Bainbridge et al., 2008; Hauswirth et al., 2008; Maguire et al., 2008), with long term effects showing visual improvement in some patients (Bainbridge et al., 2015). For this treatment to be effective, however, the target gene must be well understood,

including in its transcriptional regulation, so that a healthy copy can be introduced and produced in useful quantities. Gene therapy is of most use in conditions involving the malfunction of a single gene, while diseases with multiple causes are more difficult to treat.

1.4.3.3 Retinal regeneration

The intrinsic regenerative capacity of the nervous system is very limited in higher vertebrates, particularly mammals. In amphibians and fish, however, this capacity is often sufficient to replace damaged cells in the eye, through the activation of sources of stem cells in the retina. For example, members of the newt family are able to regenerate the whole retina after its removal (see Araki, 2007). These animals use the RPE as a source of replacement cells, the cells undergoing transdifferentiation into retinal progenitor cells which divide and produce the cells of the retina.

In mammalian retina, although there is little evidence of any meaningful regeneration, some studies have suggested that populations of adult stem cells can be found in the retina, in the pigmented ciliary margin (see Tropepe et al. 2000) and that cells from this area can proliferate *in vitro* and give rise to cells specific to the retina, including rods, bipolar cells and Müller glia. Success at harnessing these cells has been limited, however, with other studies showing that these cells fail to produce photoreceptor-specific markers (Gualdoni et al., 2010). In the zebrafish, it is the Müller glia which re-enter the cell cycle and become progenitor cells, which divide to produce replacement cells after retinal damage. The possibility of activating a similar system in mammals is under investigation, with reports showing that the forced expression of Ascl1 in Müller glia allows these cells to divide, and can lead to retinal regeneration in young mice, with the production of amacrine and

bipolar cells, and photoreceptors (Brzezinski et al., 2011; Pollak et al., 2013; Ueki et al., 2015) By whichever means, the production of mature retinal cells by the activity of endogenous cell populations represents a possibility for replacing the cells of the retina.

In the next section, I will discuss a similar strategy of replacing retinal cells, this time from an exogenous source via transplantation.

1.5 Cell Therapy in the retina

Cell replacement therapy refers to the replacement of lost cells by the introduction of new ones which can restore the function of those that were lost. Replacing the cells lost in retinal degenerative diseases has the potential to restore vision. This approach is particularly attractive for those conditions where photoreceptor loss is the primary cause of vision impairment, as replacing the photoreceptors is likely to be simpler than replacing other cells. As afferent sensory neurons, photoreceptors do not receive input from other neurons and a newly introduced photoreceptor must therefore only create a single synapse in the IPL to replace one which has been lost.

One major advantage of the prospect of using cell therapy as a treatment for retinal degenerative diseases is that whereas other treatments aim to stop or slow the progression of disease, replacing cells has the potential to reverse the loss of vision. Other major advantages are that, if donor cells are derived from a normal donor, they have the potential to restore function in any condition, even if the underlying causes are unknown. This contrasts with gene therapy, which targets a specific faulty gene or other deficiency. Advances in stem cell techniques in recent years

also provide the possibility that renewable sources of cells for transplantation can be established.

Multiple methods to attempt restoration of the cells of the retina have been attempted (see Pearson 2014). Transplantation of neonatal or embryonic whole retinal sheets – the entirety of the neural retina – into the eyes of recipient animals has been shown to lead to the survival and differentiation of these grafts into more mature tissue (F. Ghosh et al., 2004). In rats with retinal degeneration, transplants of this kind have led to the recording of visual responses in the superior colliculus up to several months after transplantation (Seiler et al., 2008): retrograde synaptic tracing using pseudorabies virus indicated that connections are made that link the transplanted tissue and the superior colliculus. In human recipients with retinitis pigmentosa and AMD, there is likewise some evidence that transplanting foetal retinal sheets can improve visual acuity (Radtke et al., 2008), although the mechanism for this is unclear, and it has been suggested that effects on disease progression and growth factor release from the transplanted tissue may explain these results.

The advantage of this approach is that the internal circuitry of the retina should be intact, with synapses between retinal cells either formed at the time of transplantation or developing normally over time. On the other hand, this approach involves the severing of RGC axons, and relies on their regrowth through the remaining host retinal tissue, or on analogous connections being made with the remaining cells of the recipient retina. Transplantation of partial thickness grafts, comprising the photoreceptor layer only, may therefore be of use in the treatment of degenerating retinas which have no remaining ONL, as only connections between photoreceptors and bipolar cells will have to be made. Initial attempts of this have however not been successful as the tissue does not survive well after

transplantation (Ghosh et al., 1999) but the possibility of growing partial thickness grafts of this kind *in vitro* may allow for the expansion of this approach.

Transplantation of dissociated neural progenitor cells from the brain or retina, which have the capacity to become any cell of their source tissue, has been attempted. Retinal precursor cells are able to survive the process of being injected into the subretinal space of recipient rats and have been shown to express markers of mature photoreceptor types including rhodopsin (Klassen et al., 2004; Qiu et al., 2005). However, these cells did not appear to possess the capacity to move into the recipient tissue or make connections with recipient cells when injected into adult recipients. Using neural precursor cells from the brain, transplanting GFP expressing progenitor cells from the hippocampus into rat retina led to GFP+ cells being observed within the recipient tissue, but these cells did not show the morphologies of mature retinal cells (Young et al., 2000). Sakaguchi *et al* (Sakaguchi et al., 2003) found that the outcome of the transplantation of brain precursor cells into the retina is improved when the recipient is a developing eye, with GFP expressing murine brain precursor cells transplanted into the neonatal opossum leading to GFP+ cells observed within host retinal tissue with the positions and morphologies of a range of retinal cell types. The developing retina may therefore represent a more permissive environment for transplantation, either because it is more similar to the environment from which the progenitor cells are sourced, or for structural reasons, such as the lack of an OLM.

1.5.1 Photoreceptor precursor transplantation

A number of studies have since found that the injection of postmitotic, immature retinal precursor cells leads to the most striking results. The seminal study in this field (MacLaren et al., 2006) used several adaptations to this technique which have

become standard. They used the NrlGFP reporter mouse which uses the promoter of the rod-specific transcription factor Nrl to fluorescently label rod precursors with GFP shortly after terminal mitosis (Akimoto et al., 2006). Using fluorescence-activated cell sorting (FACS) allowed the isolation of only these cells, providing a pure population of rod precursors for injection.

Rod precursors were injected into the subretinal space of the retinas of recipient mice. After transplantation, GFP+ cells were found in the recipient ONL, indicating that the injected cells had moved into recipient tissue and matured. Examples of these cells can be found in Figure 1.6A. The authors also identified the early postnatal period as the optimal age for donor cells to be isolated, leading to the largest number of GFP+ cells in recipient retina. They showed that both retinal progenitor cells taken from the proliferating period (embryonic day E11.5) and adult cells did not lead to high numbers of GFP+ cells in the recipient ONL.

The reporter-labelled cells within the recipient retina were shown to exhibit the morphology of mature photoreceptors, with segments immunopositive for the photoreceptor proteins phosducin and rhodopsin. They also exhibited spherule synapse-like structures that stained for the synaptic marker bassoon and appeared to make physical connections with bipolar cells.

Many subsequent studies have used these methods to investigate transplantation in different contexts. Photoreceptor precursors have been shown to give rise to GFP+ cells in the recipient ONL which display outer segment formation (Eberle et al., 2012) and correctly localised photoreceptor proteins even when injected into a mouse model lacking these markers, such as the Prph2 and Rhodopsin mutant models (MacLaren et al., 2006), as shown in Figure 1.6B, and the Gnat1$^{-/-}$ model which lacks rod α-transducin (Pearson et al., 2012).

1.5.1.1 Stem cell sources of donor cells

Donor cells for transplantation of photoreceptor precursor cells have typically been taken from neonatal or embryonic donor mice. The analogous human age is around the second trimester of pregnancy. Therefore, in a clinical context, an alternative source of human cells must be used, for both ethical and logistical reasons. Considerable advances have been made in producing precursor cells from embryonic stem cells (ES cells) and induced pluripotent stem cells (IPSCs).

Mouse embryonic stem cells can be developed into 3-dimensional embryoid bodies which produce structures analogous to developing optic cups (Eiraku et al., 2011), containing stratified neural tissue, and can be stimulated into producing large numbers of photoreceptors. Lamba *et al.* (Lamba et al., 2009) showed improvement in visual function in mice after transplantation of photoreceptors derived from human ES cells. More recently, rod precursors from mouse ES cells have been isolated at a developmental stage similar to that of the postnatal cells used in the experiments described above, and transplanted into recipient mice deficient in the Gnat1 gene (Gonzalez-Cordero et al., 2013). Reporter-labelled cells were seen to correctly locate to the ONL of the recipient retina. These cells presented outer segments containing rod α-transducin, peripherin 2 (a protein involved in the production of outer segments, which is abolished in the rd2 mutant) and rhodopsin, as well as synaptic structures.

IPSCs, generated from the reprogramming of adult differentiated somatic cells (Takahashi and Yamanaka, 2006), are able to replicate and differentiate into mature adult cells. As with the ES cells, human IPSCs can be grown into 3-dimensional structures analogous to optic cups, and can develop photoreceptors that mature

A

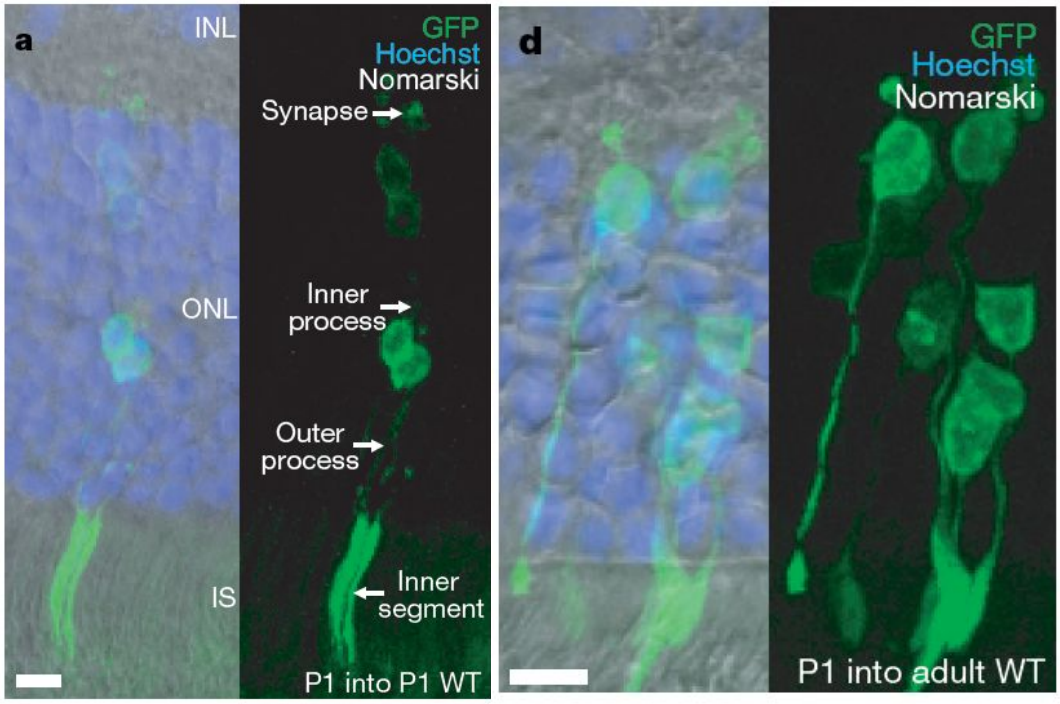
a
INL
ONL
IS
GFP
Hoechst
Nomarski
Synapse
Inner process
Outer process
Inner segment
P1 into P1 WT
d
GFP
Hoechst
Nomarski
P1 into adult WT

B

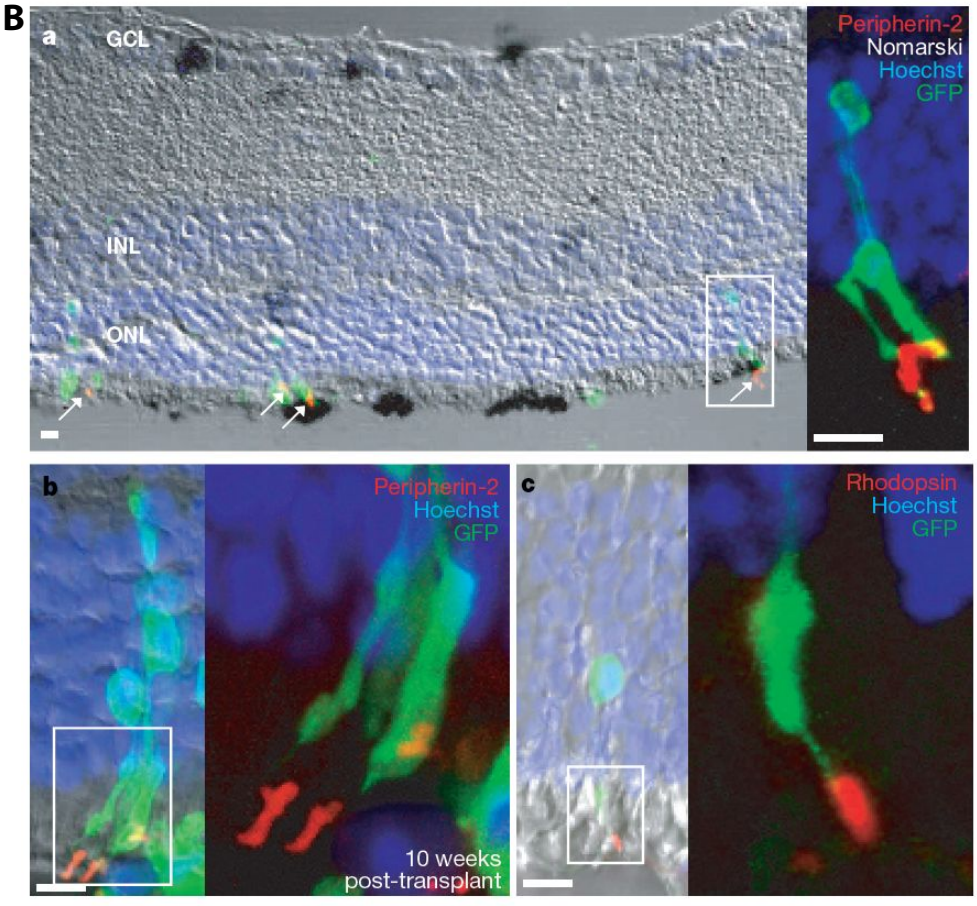
a
GCL
INL
ONL
Peripherin-2
Nomarski
Hoechst
GFP
b
Peripherin-2
Hoechst
GFP
10 weeks post-transplant
c
Rhodopsin
Hoechst
GFP

Figure 1.6 GFP+ cells in recipient retina after transplantation of GFP-expressing photoreceptor precursors into the subretinal space of recipient mice.
A P1 ubiquitous GFP- expressing cells injected into P1 (left) and adult (right) recipient retina. GFP+ cells are found in the recipient ONL and display photoreceptor morphology, including inner segments, a cell body with basal and apical processes and a synaptic terminal.

B NrlGFP rod precursor cells transplanted into the $Prph2^{rd2/rd2}$ retina (a,b) and the Rhodopsin deficient $Rho^{-/-}$ retina (c) lead to GFP+ cells in the recipient ONL which show correctly localised forms of the protein lacking in the respective recipients in short outer segments.

These images reprinted by permission from Macmillan Publishers Ltd: *Nature* (Maclaren et al 2006), copyright 2006.

sufficiently to include the elaboration of outer segments (Zhong et al., 2014). This approach is also able to generate patient-specific photoreceptors from those with particular diseases, allowing the study of the behaviour of affected cells without the need for biopsied tissue or approximate animal models (Di Foggia et al., 2016).

1.5.1.2 The effect of the retinal environment

While the above shows that, in principle, it is likely that suitable sources of cells to transplant may be available for human treatment, if retinal cell therapy is to be used to treat retinal degenerative diseases, it must be shown to be effective in environments similar to these. Despite an endpoint of the death of photoreceptor cells, degeneration is associated with many other changes in the structure and cell populations of the retina. These have been shown to affect the outcomes of the transplantation of photoreceptor cells. In particular, reactive gliosis, occurring as a result of the activation of Müller glia, has been shown to represent a barrier to transplantation outcomes (Kinouchi et al., 2003; Ma et al., 2011).

The integrity of the outer limiting membrane has also been shown to play a role in the efficiency of cell transplantation. The $Crb1^{rd8/rd8}$ mouse is a model for Leber's Congenital Amaurosis, a congenital retinal dystrophy which is associated with mutations of this gene in humans (Den Hollander et al., 2001). Crb1 is a constituent protein of the adherens junctions which make up the OLM (Gosens et al., 2008). Injections of photoreceptor precursor cells into the $Crb1^{rd8/rd8}$ model has been shown in multiple studies to lead to increased numbers of GFP+ cells seen in recipient retina (Barber et al., 2013; Lakowski et al., 2010; Pearson et al., 2010).

This is consistent with other studies, which have shown that targeted disruption of the OLM can increase the number of GFP+ cells being found within the recipient

ONL after transplantation. Treatment with α-aminoadipic acid (AAA), a toxin that affects Müller cells in the mammalian retina, has been shown to cause a transient disruption of the OLM (Ishikawa and Mine, 1983). Administration of AAA by intravitreal injection before subretinal injection of NrlGFP precursor cells led to the observation of an increased number (approximately twofold) of GFP+ cells in the recipient retina (West et al., 2008). Similarly, use of RNA interference techniques allowed transient reduction of the expression of the OLM constituent protein zona occludens 1 (ZO-1). Disruption of the OLM with the application of siRNA molecules against this gene in conjunction with the injection of NrlGFP cells led again to improved transplantation outcome in both the WT and Rhodopsin-deficient mouse (Barber et al., 2013; Pearson et al., 2010).

However, many other different mouse models of retinal degeneration exist, similar to the diversity found in human disease, and factors other than the OLM have been shown to be of importance. Investigations of the outcome of transplantation into a number of these showed a marked difference depending on the recipient model and its underlying aetiology (Barber et al., 2013). Transplantation outcome was markedly worse in the Rhodopsin knockout mouse, but much better in the $Crb1^{rd8/rd8}$ mouse, compared to WT mice.

This study also noted that the transplantation efficiency was affected by the progression, but not the severity, of degeneration. With the $Crb1^{rd8/rd8}$, $Gnat1^{-/-}$ (both relatively stationary models), and $Rho^{-/-}$ (which exhibits a moderate rate of degeneration) models, transplantation efficiency decreased with disease progression, but increased with the $Prph2^{+/\Delta 307}$ model, while no change was found over time in the (rapidly degenerating) $Pde6\beta^{rd1/rd1}$ or (moderate) $Prph2^{rd2/rd2}$ mice.

The reason for these observations is likely to be due to the changes to the retinal environment that occur in these retinal models during disease progression. These changes vary but typically include increases in the death and removal of photoreceptor cells, with consequent thinning of the ONL, and effects on other cell types, notably the Müller glia. These cells react to pathology by undergoing gliosis: a process of hypertrophy and the upregulation of cytoskeletal proteins associated with the intermediate filaments, such as GFAP and vimentin (Bringmann et al., 2006), leading to the formation of a glial scar. This may occur through communication between microglial cells and the Müller glia (Wang and Wong, 2014).

The extracellular matrix (ECM) is also affected, with changes in the deposition of cell-cell adhesion molecules such as cell-surface proteoglycans (CSPGs). Since the integration of cells requires movement past the OLM and through the ECM into the ONL, it is unsurprising that changes to these factors affect the outcome of transplantation.

Likewise, damage of other kinds to the retina has been shown to have an effect. Lesions to the retina via laser application improve the numbers of reporter-labelled cells found in recipient ONL after transplantation of retinal progenitor cells (Jiang et al., 2010), with concurrent upregulation of the matrix metalloproteinases MMP-2 and MMP-9, which degrade proteins of the ECM. Indeed, co-transplantation of MMP2 with retinal progenitor cells has also been shown to increase transplantation outcome (Yao et al., 2011). Similarly, the application of Chondroitinase ABC, an enzyme which degrades proteoglycans, has been shown to improve transplantation outcome (Barber et al., 2013; Ma et al., 2011; Suzuki et al., 2007).

These observations show that the recipient environment should always be borne in mind when assessing the outcome of transplantation. They also provide scope that the efficiency of cell transplantation can be improved by targeted interventions: by changing gliosis levels or disrupting the OLM, successful integration could be improved, and more photoreceptors restored.

1.5.2 Cell therapy using cone photoreceptors

Human vision is primarily dependent on cone photoreceptors rather than rods, and therefore the transplantation of cones specifically is likely to be the most promising application of cell replacement therapy. Cones are vital for detailed colour and daylight vision. Despite being outnumbered by rods by a factor of 30, cones are far more concentrated in the macular and foveal region of the retina and mediate high acuity vision at the centre of the visual field. Developing robust methods for cone cell transplantation is crucial to the effective treatment of retinal degenerative diseases; in later stages of retinitis pigmentosa, patients retain useful vision despite the loss of most of their rod photoreceptors, since cones degenerate more slowly in this condition (Berson, 2007). This suggests that with the successful replacement of relatively few functional cone photoreceptors, the return of useful photopic vision could be achieved.

Recently, attempts to continue this work using cone photoreceptors rather than the rod photoreceptors privileged by the methods described above. In particular, this thesis will aim to build on the work of a study which used CrxGFP labelled cells to isolate both rod and cone photoreceptors at early donor ages, when cones outnumber rods (Lakowski et al., 2010). At E15.5, 75% of Crx expressing cells were seen to express the cone-specific marker Rxrγ. This proportion fell over time until P3, at which point it approximated the cone:rod ratio found in adult retina.

Equal numbers of FACS purified CrxGFP+ cells were transplanted at ages between E12.5 and P3. GFP+ cells were found in the recipient ONL after 3 weeks for all donor ages above E14.5, with more cells found with older donor populations (median for E14.5 donors = 334 cells, for P3 donors = 5610 cells). These cells displayed morphological features of mature photoreceptors as in other studies, and a subset were also seen to express the cone markers Rxrγ and cone arrestin, as shown in Figure 1.7. These Rxrγ positive cells were always located close to the apical limit of the ONL, exhibited short inner and outer segments and showed the large pedicle characteristic of cone photoreceptors. More of these cone-like cells, as a proportion of the total number of GFP+ cells, were observed using embryonic donor cells than with postnatal donors, as predicted. However, with all ages of donor cell, at least 100 times fewer GFP+ cells were seen to express Rxrγ, compared with those that were Rxrγ negative. This is similar to the endogenous cone:rod ratio, but much lower than the percentage in the transplanted donor cell population. The highest number of GFP+ Rxrγ expressing cone cells seen in a single retina was 54, using E17.5 cells.

Looking at the mass of injected cells, which did not integrate but remained in the subretinal space, this study found many CrxGFP+ cells co-expressing Rxrγ (9.4% after transplantation of E15.5 cells), meaning that the results are not due to a failure of cone precursors to survive. Additionally, at early stages after transplantation, Rxrγ expressing GFP+ cells in the subretinal space were also seen apparently migrating towards the ONL, but seemingly could not traverse the OLM.

To investigate the effect of different retinal environments on the outcome of this transplantation, embryonic CrxGFP cells were also transplanted into the Gucy2e$^{-/-}$ mouse. This model is deficient in the guanylate cyclase 2e gene, a component of

the phototransduction cascade, and shows cone-specific dystrophy (Yang et al., 1999), with functionless cones which decline in number after 2 months of age. Similar total numbers of GFP+ cells were seen within the recipient ONL after transplantation into this model, but the number that resembled cone photoreceptors increased slightly, with 1.9% expressing Rxrγ. While this was still much lower than the equivalent proportion in the CrxGFP donor population, it indicated that the rod:cone ratio of the recipient retina has an effect on the outcomes of transplantation.

One possible explanation for these results is that rod precursors integrate much more readily than do cone precursors, enough to counteract the high cone proportion of transplanted populations at early donor ages; this would explain both the increased number of GFP+ cells seen after transplantation and the decreasing proportion of cone photoreceptors seen using later donor ages. Alternatively, it was hypothesised that some of the CrxGFP cell population originally fated to become cone photoreceptors could adopt a rod fate during the migration process, as a result of the plasticity that has been seen in postmitotic photoreceptors, described above.

However, due to the limitations of this study, distinctions could not be made between these possibilities. The presence of rod precursors in the transplanted population, even the relatively small proportion found at embryonic ages, meant that no distinction could be made between rod precursors integrating preferentially, and cone precursors undergoing a change in fate, or alternatively a failure to fully develop as cones.

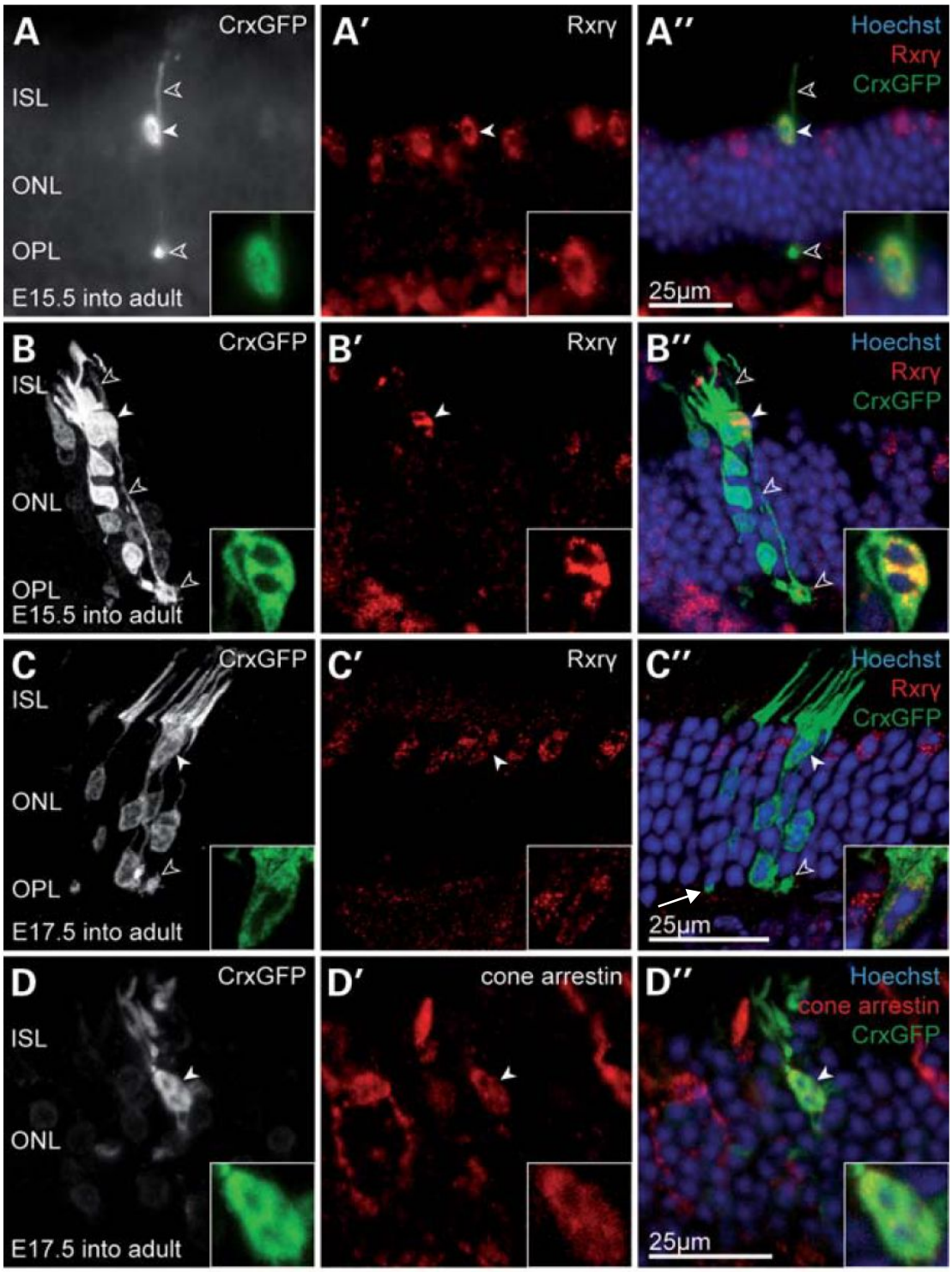
A
CrxGFP
ISL
ONL
OPL
E15.5 into adult
A′
Rxrγ
A″
Hoechst
Rxrγ
CrxGFP
25μm
B
CrxGFP
ISL
ONL
OPL
E15.5 into adult
B′
Rxrγ
B″
Hoechst
Rxrγ
CrxGFP
C
CrxGFP
ISL
ONL
OPL
E17.5 into adult
C′
Rxrγ
C″
Hoechst
Rxrγ
CrxGFP
25μm
D
CrxGFP
ISL
ONL
E17.5 into adult
D′
cone arrestin
D″
Hoechst
cone arrestin
CrxGFP
25μm

Figure 1.7 Cone-like GFP+ cells seen in recipient retina after transplantation of CrxGFP-expressing cells into the WT mouse. Fluorescence-sorted embryonic cells (A,B E15.5, C,D E17.5) were injected into the subretinal space. A small fraction of GFP+ cells seen in recipient retina were cone-like, located at the apical edge of the ONL and expressing the cone-specific markers Rxrγ (A-C) and cone-arrestin (D). They showed cone-like morphologies including multiple points of condensed heterochromatin (see particularly B) and large triangular synaptic end feet. The majority of other GFP+ cells can be seen to have a more rod-like morphology, with smaller nuclei with single points of condensed heterochromatin and smaller spherules in the OPL, e.g. C, white arrow. These cells do not stain for cone markers.

Previous studies had also shown that transplantation outcome was better using postnatal donor cells than using embryonic cells (MacLaren et al., 2006), and the improvement seen at older ages was therefore likely not only due to the increased proportion of rod cells. As described above, by the early postnatal period, the cells isolated were overwhelmingly rod photoreceptors, with cone precursors approximately 3% of the transplanted CrxGFP population, as in the adult retina. This approach, therefore, did not allow for the transplantation of significant numbers of cone precursors at postnatal ages, due to the changing rod:cone ratio in the CrxGFP population. Due to the difference in time course of the production and maturation of cone photoreceptors, it could be that the optimal time for cone integration is different to that of rods. A major aim of this study is therefore to investigate the effects of transplanting pure populations of cones at ages which this study could not address.

More recently, there have been studies that have used both true cone precursors (Smiley et al., 2016) and the cone-like cells produced by the $Nrl^{-/-}$ mouse (Santos-Ferreira et al., 2014) for transplantation experiments. As these studies did not inform the background of my project during initial stages, I shall discuss them in later chapters in the light of my own results.

1.5.3 Functional assessments of transplanted cells

The end goal of cell therapy is to restore vision by adding functional photoreceptors to the diseased recipient retina. Previous studies have used a range of techniques to assess an improvement in functional capacity after cell injection, on a variety of scales from single cells, to the retina, to the behaviour of the whole animal; and at different processing levels, including the cortex of the brain. In many cases, only a single measure of output was assessed, leading to a lack of cohesion in the

literature about the best approach (Klassen et al., 2004; Lamba et al., 2009; Tucker et al., 2011).

A paper from this group illustrates a number of these techniques (Pearson et al., 2012), which I shall discuss in detail. Mice from the Gnat1$^{-/-}$ model, deficient in rod α-transducin and lacking rod function, were transplanted with NrlGFP cells. Cells expressing GFP and rod α-transducin were subsequently found in large numbers in the recipient retina, and displayed mature rod markers and outer segment formation. Multiple techniques showed that visual function was improved in these mice after cell transplantation.

Suction-pipette recordings were used on individual GFP+ cells in the recipient ONL. This technique involves drawing the inner segment of a photoreceptor into a pipette to record cellular currents, and has been used in both rods (Chen et al., 1995) and cones (Nikonov et al., 2006) and is able to determine the sensitivity of individual cells to wavelength and light intensity. The GFP+ cells within the recipient ONL responded to dim-flash stimuli in a manner similar to WT rods recorded using the same protocol, indicating rod-like functionality at the single cell level.

ERG responses at scotopic levels were not detected in these injected mice, however, despite high numbers of GFP+ cells seen after transplantation (7,135-26,616 cells). However, the ERG is an averaged response across the whole eye and as such is a relatively insensitive, if robust and readily repeatable, measure of visual function. Accordingly, it was determined, with viral introduction of a Gnat1 transgene, that treatment of more than 100,000 cells was necessary to see a repeatable effect on the ERG measurement.

The haemodynamic responses of the brain were investigated via intrinsic imaging of the primary visual cortex, as illustrated in Figure 1.8A. This approach uses red light to determine changes in blood flow by imaging through the mouse skull (Grinvald et al., 1986). Scotopic stimulation of Gnat1$^{-/-}$ mice receiving NrlGFP cells elicited cortical activity not found in untreated animals.

The optomotor reflex was used as a behavioural assay for retinal function (Figure 1.8B). In an optomotor test, mice are shown a visual grating rotating in a certain direction. Mice will track their heads in the direction of the moving grating if it can be seen. The grating can be varied in contrast, frequency and brightness, to assess contrast sensitivity, visual acuity, and light sensitivity. As head tracking in different directions is driven by the function of different eyes (clockwise rotations are driven by the left eye, anti-clockwise rotations are driven by the right eye), functional improvements in one eye can be found relative to the contralateral eye. At scotopic luminance levels, optomotor responses were seen to be driven by eyes treated with NrlGFP cells, but not those receiving sham injections of Gnat1$^{-/-}$ cells.

A further assessment of vision sufficient to affect behavioural outcomes was a water maze (Figure 1.8C). Mice are released into a pool of water and must choose between two swimming paths, one of which contains a hidden platform marked by a visual stimulus, which would allow them to escape the deeper water (Wong and Brown, 2007). After transplantation, four out of nine treated Gnat1$^{-/-}$ animals were able to complete the task (above 70% correct responses), while all untreated Gnat1$^{-/-}$ mice performed no better than chance.

1.5.3.1 Cell recording

Recording from single photoreceptors is a powerful technique for determining the response characteristics of transplanted cells. For cell therapy to be effective, however, it is not enough for transplanted cells to respond to light, they must transmit their response to the inner retina, and subsequently the brain, for processing. This requires successful synapse formation with the bipolar cells in the recipient retina, which then transmit information to the retinal ganglion cells (RGCs). The RGCs are the only retinal neurons that fire action potentials. Due to this, they are suitable as a target for certain of the electrophysiological techniques which are used in other parts of the CNS.

Finding an improvement in the response of a RGC to light would show that transplanted photoreceptors can transmit their light response synaptically to the bipolar cells and RGCs, which are the input to the path leading to the brain. Additionally, since RGCs sample from a small area of the retina, any improvement will not be diluted by the activity of the untreated parts of the retina, as is the case with the ERG.

Multi-electrode arrays (MEA) have been used to record extracellular voltage changes from neural tissue, in a tissue or culture of cells, and allow for the comparison of different cells in proximity to one another, enabling the study of local neural networks (Buzsáki, 2004). This approach has been used in *ex vivo* retinal tissue to record from RGCs (Sodhi and Hartwick, 2014, 2016; Walch et al., 2015).

In this thesis, I will focus on MEA recordings to measure functional improvements. The multiple electrodes allow the gathering of more information than single cell recordings, yet are more sensitive to local changes than ERG measurements.

A

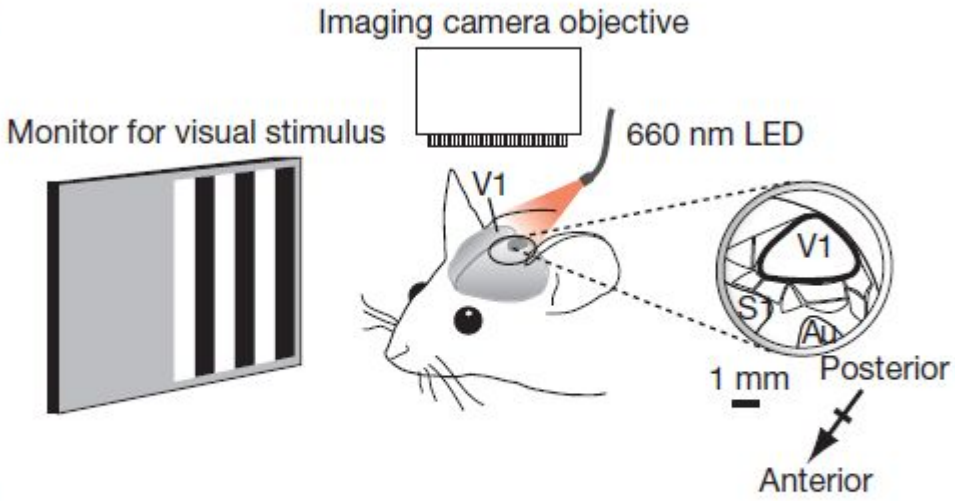
Imaging camera objective
Monitor for visual stimulus
660 nm LED
V1
V1
S1
Au
1 mm
Posterior
Anterior

B

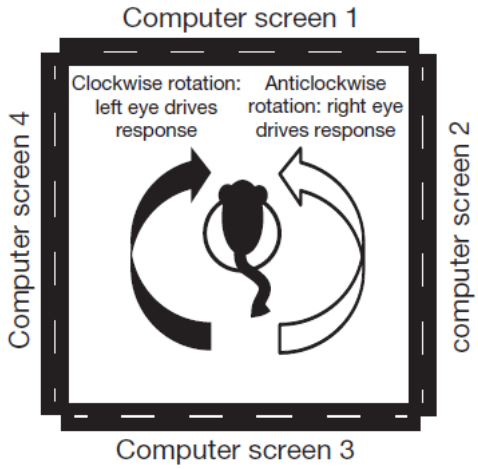
Computer screen 1
Clockwise rotation: left eye drives response
Anticlockwise rotation: right eye drives response
Computer screen 4
computer screen 2
Computer screen 3

B'

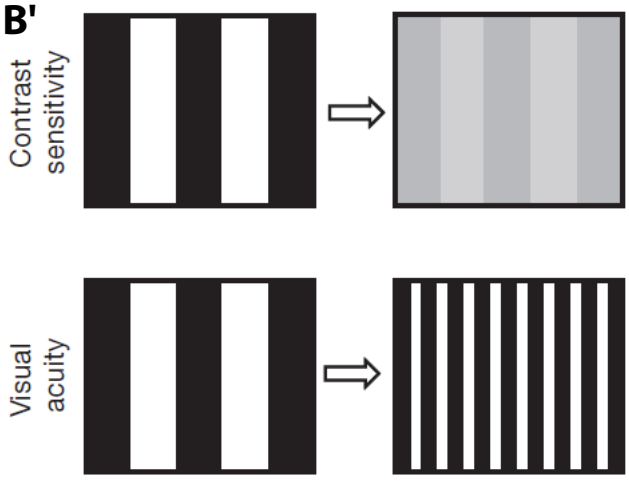
Contrast sensitivity
Visual acuity

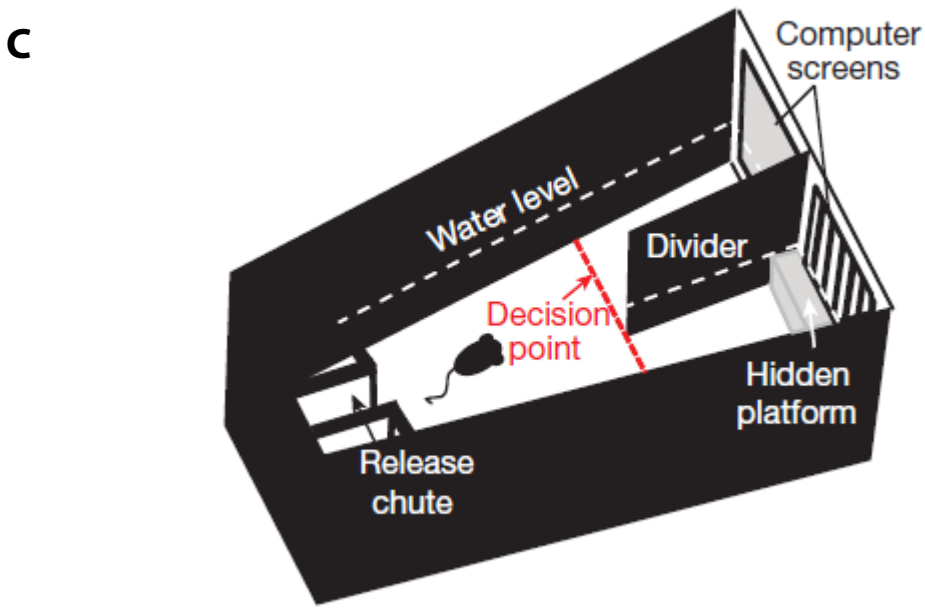

Figure 1.8 Assessments of visual function.

A Intrinsic imaging of the visual cortex of the brain. Changes in blood flow can be measured by imaging through the skull of a mouse shown visual stimuli to measure the activity of the brain if visual information is transmitted.

B The optomotor response. Mice will track the movement of a visual grating (here presented on screens on the walls of the enclosure, based on the activity of the left or right eye. This grating can be varied to test contrast sensitivity and visual acuity (B').

C The water maze test. A mouse is released into a water bath and must choose between two routes, one of which is marked by a visual stimulus and contains a hidden platform which allows escape from the water. Correct choices above chance level indicate that the mouse can see the stimulus.

Previous studies have shown that only small numbers of cone-like cells are likely to be seen after transplantation (Lakowski et al., 2010), so large scale functional rescue of vision is unlikely to be apparent in the short term. With the MEA approach, it will be possible to direct recordings to areas which have received transplanted cells, rather than attempting to measure the response of the whole retina.

1.5.3.2 Spike sorting

Recordings from extracellular electrodes such as those in a MEA, particularly in tissues with high numbers of active cells, such as the GCL, often receive input from the action potentials of more than one cell. Separating these inputs, and removing noise (electrical input from any of a range of sources not related to action potentials), is necessary to improve the signal-to-noise ratio of data gathered in this way.

While many techniques to separate these inputs exist, I will briefly discuss a method which allows the spikes obtained from recordings to be assigned to groups in a semi-automated, computerised manner, developed by Quiroga *et al* (Quiroga et al., 2004). This allows relatively large datasets to be analysed by reducing the human supervision necessary for the sorting process.

Action potentials from different cells picked up by the same electrode may vary in several features, depending on a number of factors, for example the proximity and orientation of the cell to the electrode, or the part of the responding cell giving rise to the signal. However, it is not known *a priori* on which features spikes will differ, and an automated method must be able to determine this, before sorting can take place.

Once putative spikes have been identified by the application of an amplitude threshold, removing low amplitude noise, their wavelet transforms are calculated, creating a number of Haar wavelets (scaled square-shaped functions), which each describe the shape of the spike at different time points within its progression. This means that wavelets for different spike classes will differ only for those which describe the specific part of the waveform which deviates between spike classes. Thus, by comparing the wavelets for all the spikes recorded by a single electrode, the wavelets pertaining to the parts of the spikes which differ can be identified, as they will have the highest deviation from normality, being drawn from two populations.

Superparamagnetic clustering forms the basis of subsequent spike sorting (Blatt et al., 1996). This is based on the behaviour of the spin of units in a ferromagnetic system. While a detailed discussion of the theory of this process is beyond the scope of this thesis, I will describe the key features below.

The relevant features of the spikes – those wavelet coefficients that differ the most between all spikes – are represented by plotting each spike as a point on a multidimensional space. Interaction between these points is then modelled by their proximity in this space, with the strength of interaction falling exponentially with increasing distance. Thus, spikes with similar features interact more strongly.

In the superparamagnetic model, changing one variable, the ‘temperature’ (again based on the behaviour of ferromagnets), changes the degree to which points influence each other, thus changing the groups to which strongly interacting points can be assigned. For example, at low temperatures, all spikes are sorted into one group. At high temperatures many small groups are generated with only a few very closely interacting spikes assigned. At medium temperatures (the

‘superparamagnetic’ phase), only a few clusters are generated, with only those spikes which are grouped together assigned to them. By generating the groups for a number of temperatures primarily in the superparamagnetic range, a number of possible clustering options are provided.

With these techniques, much information can be determined from the recordings of extracellular electrodes. I plan to use these approaches to investigate the outcomes of cell transplantation on the neuronal circuits of the retina.

1.6 Cell migration in retinal development

For effective transplantation, the movement of cells from the subretinal space where they are injected to the ONL where mature recipient photoreceptors are found is essential. It has been shown that efforts to change the recipient environment with developmentally relevant growth factors can enhance the efficiency of transplantation.(West et al. 2012) Since successful integration is reliant on the migration of transplanted cells, understanding this process, combined with the ability to manipulate the recipient retina, could allow greater efficiency of this therapy by encouraging migration. Investigation of the time course of transplantation has indicated that integration happens within the first week after injection, and the morphology of cells at early time points shows the progression of the migration process (Warre-Cornish et al., 2014). The cells appear to first extend a process into the ONL, and subsequently enter by nuclear translocation. Once inside the ONL, observed cell morphologies suggest that the integrating photoreceptors extend a basally directed neurite and their somata translocate basally to their final locations, with the basal process eventually terminating in the IPL in order for synapse formation to take place.

Retinal cells, including cone photoreceptors, undergo migration during normal development, including moving through the ONL to take up their final positions. As shall be seen, relatively little is known about the mechanism and purpose of this migratory activity. The success of several approaches in improving transplantation outcome by understanding the effect of the retinal environment, as seen above, suggests that by understanding the migratory process, further improvements could be made.

The numerous different cell types in the nervous system and their various target positions and functions in a mature animal mean that there are several distinct mechanisms by which these cells migrate. An appreciation of these mechanisms will be necessary to guide conclusions made about the migration of cone photoreceptors.

In this section, I will show evidence from previous studies, both in brain and retina, which detail what is known the different types of migration which occur in the nervous system, and the methods used to investigate them, in order to inform strategies for experiments to look at the migration of cones.

1.6.1 Interkinetic nuclear migration (INM)

Interkinetic nuclear migration (INM) is the term given to the distinctive fluctuation between apical and basal position exhibited by proliferating cells in the developing CNS. This migration tends to give rise to the pseudo-stratified appearance of proliferating neural tissue. As illustrated in Figure 1.9A, during proliferation, mitosis takes place only at the apical surface, but cells can be found displaced basally

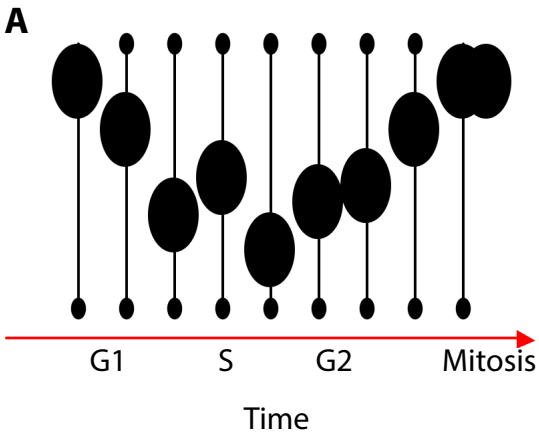

Figure 1.9 Types of neural migration.

A Schematic of Interkinetic nuclear migration (IKNM) representing one proliferating cell over time from left to right. After mitosis, cells leave the apical surface and migrate basally during the G1, S and G2 phases of the cell cycle. This migration is not smooth but includes periods of stochastic movement interspersed with periods of rapid basal progression. Cells finally move apically again to divide. The basally directed process appears to be inherited by one of the daughter cells in most cases (Saito et al. 2003).

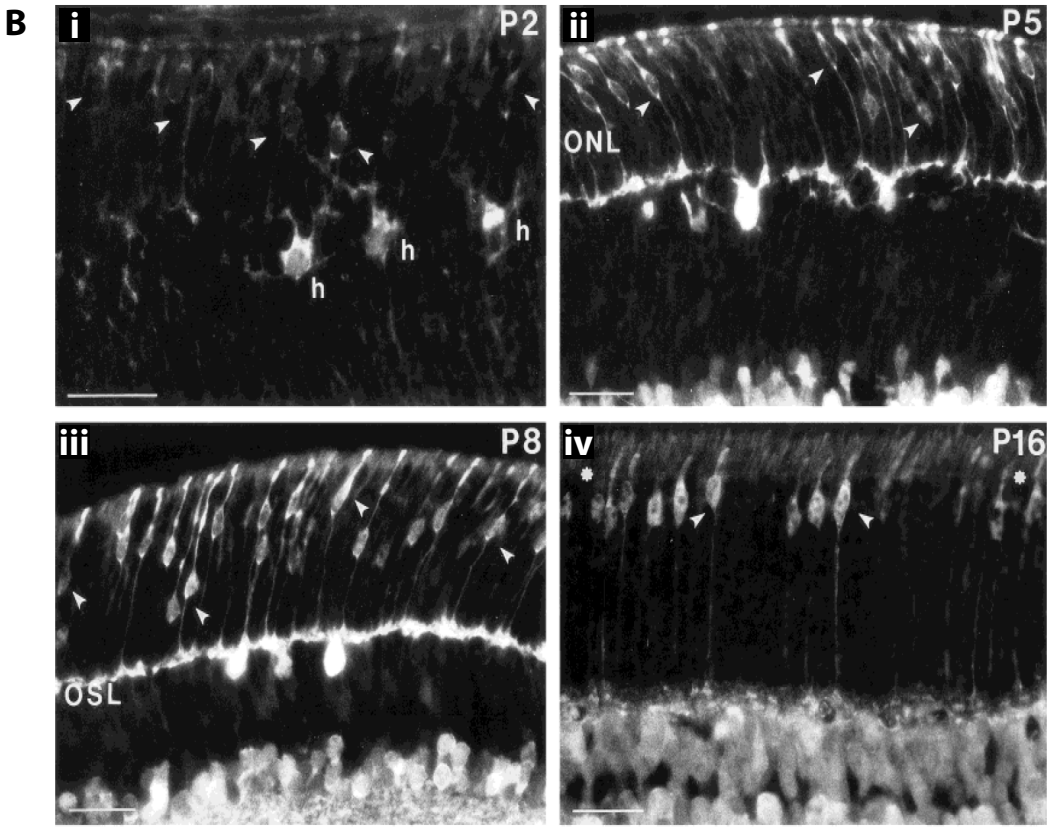

B Cone migration in the developing mouse retina. Cone precursors (white arrowheads) are labelled with an antibody to neuron-specific enolase (NSE). Scale bars 10 µm.

At P2 (i), cone cells are located in the outer portion of the retina, and their processes may interact with horizontal cells (h). At P5 (ii) and P8 (iii) cones can be found throughout the depth of the ONL, while at P16 (iv) the cells have returned and are uniformly positioned adjacent to the OLM. This image reprinted by permission from Wiley: *The Journal of Comparative Neurology* (Rich et al, 1997), copyright 1997.

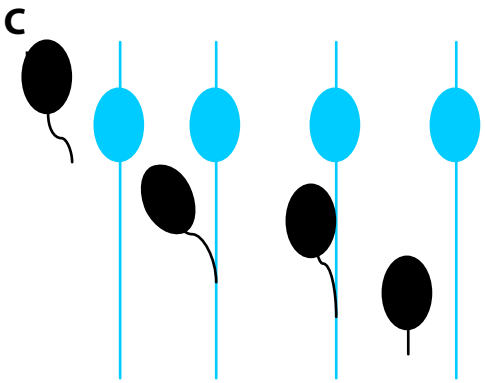

C Glial guided migration (one cell over time, left to right). Migrating cells (black) extend a highly motile leading process which contacts a glial cell fibre (blue) traversing the whole depth of the developing tissue. The whole cell soma translocates along this fibre, along with the leading and trailing processes, although the leading process is continually exhibiting autonomous movemen, yet maintaining a roughly constant length (contrast with somal translocation, C).

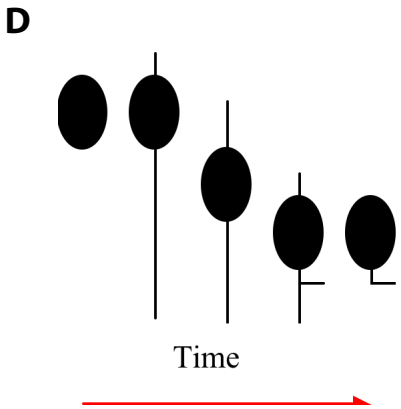

D Somal translocation (one cell over time, left to right). Cells extend a process basally and apically and the nucleus translocates along this process to the correct tissue layer. Once there the basal process is retracted while the apical process often retracts during migration. Axons and dendrites have been observed developing from the processes before migration has been completed in some cases, such as retinal bipolar cells (Morgan et al. 2006).

during the G1, G2 and DNA synthesis (S) phases of the cell cycle, before apparently moving apically once more to divide. In the immature neural retina, the whole retinal epithelium consists of proliferating cells. Retinal progenitor cells divide only at the ventricular zone, adjacent to the retinal pigmented epithelium (RPE) and between divisions can be found undergoing INM to the innermost boundary of the developing retina, the site of the inner limiting membrane (Robinson et al., 1985). This process is very similar between different parts of the CNS.

It has been shown that rather than the smooth gradual movement initially supposed for these cells, moving the full distance from the apical surface to the basal boundaries for S phase processes, and then the full distance back to the apical limits, the movement of cells during INM is instead stochastic and less directed than previously thought (Baye and Link, 2008). The movement seems to consist of a combination of at least two forms of motion (Norden et al., 2009): mostly transient periods of stochastic and seemingly random movement with frequent changes of direction, interspersed with occasional periods of persistent and rapid (directional) movement, most often in the apical direction, where change of direction is rare. The apical movement of cells undergoing INM is apparently triggered by the onset of G2 phase (Leung et al., 2012). These observations have been made with the aid of time-lapse imaging techniques which have allowed for much detailed study of the characteristics of INM (and, as shall be seen, other types of migration) by enabling the observation of the behaviour of individual cells as they develop in real time.

It has been suggested that the driving force for INM is motor proteins transporting the cell nuclei along the microtubule scaffolding which makes up a portion of the cytoskeleton (Kulikova et al., 2011). This would implicate the motor protein classes of dyneins and kinesins, which move cellular cargo towards the negative and positive ends (respectively) of the polarised microtubules, and indeed it would seem

that these are part of the picture. In zebrafish *mok* mutants where the motor protein Dynactin-1 (involved in connecting cellular cargo to the dynein motor) is disrupted, nuclei undergoing INM move more rapidly in the basal direction and more slowly to the apical side (Del Bene et al., 2008).

However, after blocking the zebrafish dynein/dynactin complex in a temporally controlled way (Vaughan et al., 2001), other evidence suggests that both the apically directed and stochastic movement components of INM continue to take place (Norden et al., 2009). Indeed, after destabilisation or even complete destruction of microtubules by the application of colcemide, the major features of INM can still be seen.

This has led to the suggestion of another cellular motor system as the driving force of INM: actomyosin, the mechanism behind certain other functions such as muscle contraction and cytokinesis. The active form of Myosin II (the primary form of myosin in the nervous system) can be found on the basal side of the nucleus in some cells, and inhibition of this protein abolishes rapid apical movement of RPCs in the zebrafish retina and greatly reduces the velocity and random walk of nuclear migration.(Norden et al., 2009; Schenk et al., 2009) Others, however, have found no effect of myosin II disruption on INM in rodent brain and concluded that the driving force of the apical movements indeed came from the actions of dynein and an unconventional form of kinesin (Tsai et al. 2010). It is unclear as yet how these contradictions are to be reconciled, although the difference in animal models used and in the organs studied could underlie some of these issues.

As might be expected, the connections of the nuclei of migrating cells with the cytoskeleton seem to be crucial for the successful migration. In particular, complexes called linkers of nucleoskeleton and cytoskeleton (LINC) comprising the

SUN-domain proteins of the inner nuclear membrane and the KASH-domain proteins of the outer membrane connect the nuclear membrane to cytoplasmic cytoskeletal components and molecular motors (Burke and Roux, 2009; Tapley and Starr, 2013; Zhang et al., 2009) and appear to be important in neural migration, including INM (Burke, 2012; Starr, 2003; Zhang et al., 2009). Evidence has been found that the KASH proteins Syne-2/Nesprin-2, and the SUN-domain containing proteins Sun1 and Sun2 link the nucleus to the dynein/dynactin and kinesin complexes, again suggesting the role of the microtubular motor proteins in this process (Yu et al., 2011).

The purpose of INM seems to be closely linked to the fact that all proliferating cells must divide at the apical surface. The process of this migration is very closely linked to the cell cycle itself: arresting zebrafish neuroepithelial cells in S phase pharmacologically (preventing progress to G2) abolishes the rapid apical movement which usually precedes mitosis. However, this lack of apical migration was also found when arresting in G2 phase (preventing progress to the mitotic phase) by addition of the Cdk1 inhibitor RO-3306.(Leung et al., 2012)

The idea that INM exists to allow other cells access to the apical region of mitosis could explain the measure of communication between cells that appears to be necessary for this movement. Gap junctional communication, widely found in the developing CNS, has been found to be a factor in the normal progression of INM in the retina, possibly by allowing the intercellular transfer of Ca^{2+}, thought to be involved in the saltatory movement of migrating cells.(Pearson et al., 2005) Interfering with gap junction formation by disrupting connexin 43 slows INM and leads to a reduction in retinal progenitor cell proliferation, suggesting a tight link between correct migration and correct amounts of proliferation.

A related hypothesis is that INM acts to expose the proliferating cells to signals that then trigger the cyclical process of division. Notch proteins are a family of transmembrane receptors that transduce signals from ligands including Delta, and plays a key role in the development of the CNS, including in the retina, by effecting lateral inhibition between neighbouring cells. Here, the Notch signalling pathway maintains cells in a proliferative state (Jadhav et al., 2006a). In the proliferating tissue, a Notch gradient can be observed: Notch mRNA is higher on the apical side, balanced by higher Delta translation at the basal limit. It is therefore hypothesised that INM acts to expose Notch expressing cells to the Notch ligand expressed by its neighbours in a controlled and cyclical way.(Del Bene et al., 2008) Disruption of retinal INM such as in the *mok* mutant described above causes early exit from the proliferative stage which is rescued by activation of the Notch pathway.

The interplay of the cell cycle and migration underpins interkinetic nuclear migration, although it is not clear which causes which, or if there is a simple causal link between the two processes at all. Migration could expose proliferating cells to the signals needed for correct progression through the cell cycle, and the appearance of new cells at the apical surface could provide some of the impetus for moving less recently produced cells in the basal direction. Whatever the mechanisms, it is clear that this process is essential for the proper development of the CNS; generating the correct number of neural precursor cells ready for the next stage of migration.

1.6.2 Post-mitotic migration

INM occurs during the proliferative stage of CNS development. After terminal mitosis, however, newly produced retinal cells must migrate to a suitable position in the retinal layers. This migratory stage is more specific to the cell type generated and a number of mechanisms are proposed for how the cells move. Cone

photoreceptors specifically appear to undergo a stage of late migration. Rich *et al.* (Rich et al., 1997) noted in the mouse that between postnatal days (P)4 and P11, cells positive for the cone marker peanut agglutinin became displaced from their position adjacent to the outer limiting membrane at P2 and were found scattered throughout the developing outer nuclear layer, as shown in Figure 1.9B. From P12 onwards, however, they were to be found once more in the outermost part of the ONL.

The different classes of cell in the retina take up places appropriate to their cell function. As cells become post-mitotic in the outermost part of the retina, adjacent to the RPE, the cell types taking up positions in the inner reaches of the retinal tissue have a greater distance to migrate. RGCs therefore have the furthest to travel, and these are the first cells to become postmitotic, although the retina does not appear to be generated in a strict outside-in or inside-out fashion as seen in other parts of the CNS (Marquardt and Gruss, 2002).

1.6.2.1 Glial guided locomotion

Early evidence that migrating neural cells might use the fibres of glial cells as a scaffold along which to migrate came from electron microscopy studies which showed the leading processes and somata of migrating neurons in the telencephalon of the brain closely apposed to these glial fibres which span the whole thickness of the developing cell layers (Misson et al., 1991; Rakic, 1972). However, this process appears to be seen only at later stages of development (Shoukimas and Hinds, 1978). Glial guided migration is implicated when migrating cells can be reliably found in close proximity to glia. Intriguingly, such observations have been made in the retina of the cichlid fish. Mack *et al.* (Mack et al., 2003) discovered rod photoreceptors migrating shortly after their birth in the retina of adult

fish (produced by a stem cell population capable of producing photoreceptors throughout adult life, unlike in mammals), which followed a path of migration from the outer part of the outer nuclear layer towards the outer plexiform layer. Many of these cells, particularly those that were spindle-shaped and radially oriented - apparently migrating through the tissue - were to be found in close proximity to the glial fibres of Müller cells. Müller glia are a good candidate for guides for retinal cell migration, spanning the entire depth of the retina from inner limiting membrane to outer limiting membrane, but these cells also become post-mitotic later in development (just before birth in the mouse) and thus cannot provide guidance to cells, which migrate prior to this. However, as shall be seen below, there are good reasons for expecting that the earlier generated cell types migrate in a glia-independent manner or delay their migration.

In mouse retina, however, there are reasons to believe that glial guided migration might be the means by which transplanted cells migrate into the retina. In previous work in this group, the processes and cell bodies of transplanted cells were often closely apposed to those of recipient Müller glia, as measured by nearest-neighbour analysis (Warre-Cornish, 2013), and some processes of transplanted cells were seen to branch away from glial fibres and reassociate with a fibre from a different glial cell. This indicated that glia are used as a pathfinding guide for these cells, although this has yet to be seen in real time.

Glial guided migration is a form of cell locomotion: movement of the entire cell, including the processes it extends ahead and behind it. An illustration of this process is shown in Figure 1.9C. Cells undergoing locomotion typically exhibit a very thin and highly motile leading process or processes which maintain a roughly constant length during migration. These processes rapidly extend and retract, advancing only on average by extending more. It is also interesting to note that the

movement of the soma behind the leading process is not synchronised with this movement. In the cortex, the movement itself has been described as saltatory, involving transient periods of rapid forward motion separated by phases where the cells are stationary (Hatten, 1987; Nadarajah et al., 2003, 2001; Nadarajah and Parnavelas, 2002). This could imply that the locomotion of the cell proper takes place sporadically when the continually moving leading process has found a route and stabilised.

In the brain, much evidence has been gathered about the components necessary for glial guided migration, even if the whole picture is not yet clear. Clearly, the process of adhering to glia is crucial and must involve cell surface molecules which recognise the target glial cells. Many putative candidates for molecules involved in this adhesion process have been identified (Solecki, 2012) including astrotactin, neuregulin and β1 integrin.

As in INM, the actin/myosin molecular motor appears to be involved in generating at least some of the force needed for the actual migration. The leading processes of neurons migrating in this way show a high turnover of F-actin, as determined by fluorescence recovery after photobleaching (Solecki et al., 2009) and are also enriched in Myosin II, indicating a large amount of remodelling of the F-actin cytoskeleton. Inhibition of Myosin II or stabilisation of the F-actin components causes somal and centrosomal movement to decrease in speed. In addition, Par6α, identified as regulating the somal and centrosomal movement in migration (Solecki et al., 2004), is present in the leading process of migrating cortical granule cells and regulates Myosin II motors by controlling the phosphorylation of myosin light chains. Disruption of actin filaments, with cytochalasin-B, in granule neurons also greatly slows glial guided migration, despite not causing the uncoupling of neuron and glial cell (Hatten and York, 1995).

The separation of the movement of the leading process and the migration of the rest of the cell has been briefly mentioned. There is evidence that the two facets of this migration could be served by different mechanisms. The effect of KASH and SUN protein disruption on migration (Razafsky et al., 2012) indicates the importance of linking the nucleus to the microtubular cytoskeleton, in particular to the microtubular motor proteins dynein and kinesin (Burke and Roux, 2009; Yu et al., 2011). It appears that both systems are required for migration; disruption of either has been shown to prevent correct movement (Schaar and McConnell, 2005; Vallee et al., 2009). It seems that the exploratory leading process might be reliant on actin/myosin complexes, while the nucleus and centrosome are transported by the continually restructuring microtubules.

1.6.2.2 Somal translocation

As mentioned above, evidence indicates that glial guided locomotion is not the main mode of migration during the earlier stages of neural development. A glia-independent mechanism of migration has been observed at these stages and dubbed somal, or perikaryal translocation. In this process, migrating cells initially extend processes to both the apical and basal surfaces. Once migration begins, the nucleus is observed to move along this process, retracting the trailing process as it goes and with the leading process connected to the basal surface becoming progressively shorter and thicker until the target position is reached, in contrast to the roughly constant dimensions of the leading process of glial-guided locomoting cells (Nadarajah et al., 2003, 2001; Nadarajah and Parnavelas, 2002). A schematic of somal translocation can be seen in Figure 1.9D. This form of migration has been characterised in the cerebral cortex as exhibiting continuous advancement at

around 60 μm per hour, faster than the glial directed migration which, given its saltatory characteristics, has an average speed of around 35 μm per hour.

Hawthorne *et al.* studied the migration of serotonergic neurons, finding that they did not colocalise with glial cells, and moved in a manner consistent with somal translocation, with a bipolar shape, leading and trailing processes, and a swelling preceding the nucleus apparently containing the centrosome and Golgi apparatus (Hawthorne et al., 2010). They attempted to investigate the molecular motors involved in this process by looking at the role of dynamin, a large GTPase implicated in endocytosis and microtubule dynamics: regulating microtubule instability and the Golgi apparatus, as well as the actin/myosin complex. Inhibitors of Myosin II and kinesin had no significant effect on the cell movement, but dynamin inhibition with dynasore slowed migration (but did not stop it entirely).

A microtubular system for somal translocation has been implicated before by evidence that the leading process of migrating cells are rich in newly assembled microtubules with their positive ends facing the growing tip and negative ends undergoing disassembly near the nucleus, in contrast with the unaligned microtubules in the trailing process (Rakic et al., 1996). This suggests that the mechanism of migration in somal translocation could be quite different from the other types discussed here, perhaps not using the actin/myosin system that is likely at least partly responsible for movement in glial guided, tangential (see below) and INM.

1.6.3 Photoreceptor migration

Both classes of photoreceptors take up positions very close to the site of their terminal mitosis and evidence for their post-mitotic migratory phases is patchy. As

mentioned above, cone photoreceptors undergo a stage of migration an unusually long time after terminal mitosis. Michalakis *et al.*(2005) found that mice with the cpfl5 mutation in the cone specific cyclic nucleotide-gated channel alpha 3 did not show normal cone migration. This model shows a complete lack of cone function and a progressive loss of ventral cone cells in the first few postnatal months.

It is not clear whether photoreceptors migrate in a glia-dependent manner or not, although in the ferret it has been found that before maturity photoreceptor cells extend processes beyond the outer plexiform layer (where they will make synapses as mature cells) all the way to the INL.(Johnson et al., 1999) Extension of processes to the basalmost boundary of the tissue is indicative of somal translocation (Nadarajah and Parnavelas, 2002). However, as mentioned above, in the zebrafish retina migrating cone cells do appear closely apposed to the glial fibres (Mack et al., 2003) although this was in the developed adult retina. Interestingly, there is evidence that it is the phylogenetically older cells that tend to use the somal translocation pathway (Nadarajah et al., 2001), which may or may not apply in the retinal tissue.

The LINC complexes discussed above in conjunction with INM which mediate connections between the nucleus and the cytoplasmic cytoskeleton are implicated in post-mitotic migration. Mutations in the KASH protein Syne-2/Nesprin-2, or in SUN-domain containing proteins Sun1 and Sun2 lead to mislocalisation of photoreceptor nuclei in the inner nuclear layer and outer plexiform layer, electroretinographic disturbances and an increase in apoptosis, as well as an abnormally thin outer nuclear layer (although this may be a result of effects on RPC proliferation, preventing expansion of the progenitor pool) (Yu et al., 2011). Visualisation of these proteins show that they are strongly expressed in the nuclear

envelope of all cells until at least postnatal day 9, after which the expression is downregulated except in the cells of the outer nuclear layer.

It appears that the cone photoreceptor migratory phase mentioned above is reliant on LINC complexes (Razafsky et al., 2012). Induced disruption of LINC complexes prevent the migration of cone precursors in the apical direction, meaning they are found in the basal parts of the ONL and even the OPL. In these disrupted retinas it also appears that the cone pedicles and outer segments are disrupted or absent, suggesting that the migratory process, or at least the localisation of cones to the apical surface, is necessary for their correct maturation and development. In addition, rod migration is affected: they can also be found mislocalised in the OPL.

1.7 Summary, and aims of this thesis

Cell replacement therapy represents a promising strategy for repairing the damage done by retinal degenerative diseases. Past work has focussed on the transplantation of rod cells, but for human vision, the replacement of cone cells has the capacity to make a much greater difference to useful sight. This thesis will therefore aim to extend the techniques of cell therapy to use cone cells, and build on previous attempts in this area to develop robust methods of observing cone transplantation.

Determine the efficacy of cone transplantation using cone photoreceptors.

I aim to identify appropriate sources of cone and cone-like donor precursor cells. This will require the identification of suitable genetic markers, specific to cone cells alone at early postnatal time points, as a target for immunohistochemistry or for a

transgenic mouse model to express fluorescent protein in cone cells. The latter would allow not only the isolation of a pure source of cone photoreceptor precursors for transplantation, but also enable the visualisation of individual developing cells in live tissue in real time. I will assess the capacity of these cells to demonstrate successful transplantation at various ages and under various conditions of recipient retinas, and compare this to previous results of rod transplantation.

Investigate the use of cone-like cells

I will determine methods for isolating cone-like cells from the $Nrl^{-/-}$ and $Nr2e3^{rd7/rd7}$ mouse lines, using fluorescent reporters. These models produce more cones than in WT retina (see section 1.3.1.1) and may therefore represent a more effective option for the provision of cone-enriched donor cell populations These will also be assessed for successful transplantation capability at a range of developmental stages and a range of recipient retina types, and compared to those using true cone cells.

Assess the effect of cone transplantation on retinal function

Depending on the outcomes seen after transplantation of cone or cone-like cells, I plan to assess for any increase in cone-based visual function, via electroretinography and cell recording techniques.

Characterise cone precursor migration in real time in postnatal development.

To further the understanding of the migratory phase of cone precursor development, I will use the tools developed for the investigation of cone transplantation to track cone precursors in the migratory phase. I will use pharmacological techniques to determine the cellular mechanisms driving this migration, and determine in what ways, if any, this migration is analogous to that of migrating transplanted cells.

Chapter 2 – Methods and Materials

2.1 Animals

Male and Female mice were housed in the animal facility at University College London. Animals were group-housed wherever possible and provided fresh bedding and nesting material daily and food and water were given ad lib. They were kept on a standard 12/12 hour light/dark cycle. Experiments were conducted in accordance with the Policies on the Use of Animals and Humans in Neuroscience Research, revised and approved by the ARVO statement for the Use of Animals in Ophthalmic and Vision Research. The following mouse models were used:

Table 2.1 Animal models used

Line name	Mutation	Origin	Description
C57 bl6/9	None (wild-type)	Harlan Laboratories, UK	
$Nrl^{-/-}$	Nrl coding region replaced with neomycin resistance cassette	Kind gift from Anand Swaroop, National Eye Institute, Bethesda, Maryland	(Daniele et al., 2005; Mears et al., 2001)
NrlGFP	3 EGFP copies driven by upstream Nrl sequence	Kind gift from Anand Swaroop, National Eye Institute, Bethesda, Maryland	(Akimoto et al., 2006)
$Nrl^{-/-}$/NrlGFP	See above	Bred on site from above	
Crx.GFP	Crx.eGFP BAC transgene	Kind gift from Constance Cepko, Harvard University, Massachusetts	(Samson, Emerson, & Cepko, 2009)
Chrnb4.eGFP	Chrnb4.eGFP BAC transgene	Mutant Mouse Regional Resource Centre (MMRRC)	(Siegert et al., 2009)

OPN1LW-eGFP	Human 5' regulatory sequence for human opsin 1, joined to eGFP	Mutant Mouse Regional Resource Centre (MMRRC)	(Y Fei & Hughes, 2001; Yijian Fei, 2003)
Nr2e3$^{rd7/rd7}$	Antisense LINE-1 insertion into exon 5	Kind gift from Anand Swaroop, National Eye Institute, Bethesda, Maryland	(Haider, Naggert, & Nishina, 2001)
Pde6c$^{cpfl1/cpfl1}$	Spontaneous 116bp insertion and 1bp deletion	Kind gift from X-Q Ding, University of Oklahoma	(Chang et al., 2009)
Ubiquitous GFP	eGFP introduced into pCAGGS expression vector (CMV enhancer and CBA promoter)	Jackson Laboratory, USA	(Okabe, Ikawa, Kominami, Nakanishi, & Nishimune, 1997)
Prph2$^{rd2/rd2}$	Insertion of 9.2kb repetitive genome element into exon 2	Kind gift from Dean Bok, Jules Stein Insitute, Los Angeles	(Ma, Norton, Allen, & Burns, 1995)
Cnga3$^{cpfl5/cpfl5}$	Exon 5 missense mutation	Kind gift from X-Q Ding, University of Oklahoma	(Pang et al., 2010)
Prph2$^{rd2/rd2}$/ Cnga3$^{cpfl5/cpfl5}$	See above	Bred on site from above	
R91W;Nrl$^{-/-}$	Knock-in of two point mutations into codon 91 of the Rpe65 gene, Nrl$^{-/-}$ as above	Kind gift from Christian Grimm, Zurich	(Samardzija et al., 2014)

2.2 Transplantation of photoreceptor precursor cells

2.2.1 Cell preparation

The neural retinas of donor mice were isolated by dissection in Earls Buffered Salt Solution (Sigma, UK). The donor ages used (+/- 1 day) were embryonic day (E)15.5, postnatal day (P)1 and P8. A single-cell suspension was obtained using papain digestion (Worthington Biochemical, Lorne Laboratories, UK). Reagents were made up according to the instructions of the manufacturer and stored at -20°C until use. They comprised papain solution (20 units of papain per ml, 1mM L-cysteine and 0.5mM EDTA, with DNase added at 100 units per ml), DNase solution (2000 units per ml) and ovomucoid inhibitor (OMI) (10mg ovomucoid inhibitor and 10 mg albumin per ml).

Figure 2.1 shows a schematic illustrating the transplantation process. Dissected neural retinas were incubated in 500µl of Papain solution (20 units of papain per ml, 1mM L-cysteine and 0.5mM EDTA, with 50 units DNase added) at 37°C, 95% O_2, 5% CO_2 for 45 minutes, with occasional gentle mixing. Samples were then gently triturated using 200µl pipette tips and passed through a 70µm nylon strainer (Falcon), to yield a single cell suspension, washing with extra EBSS to reduce cell loss. The suspension was centrifuged for 5 minutes at 200g and the resultant pellet was resuspended in EBSS with 10% OMI solution and 5% DNase solution to inhibit the papain reaction. After 5-10 minutes' incubation in this inhibitor solution, the suspension was layered on top of 500µl of neat OMI solution and centrifuged for 5 minutes at 100g to fully inhibit the dissociation reaction and separate out debris and cell membranes. After discarding the supernatant, the resultant cell pellet was resuspended in EBSS with 5% DNase, counted at between a 1:50 and 1:200 dilution using a haemocytometer chamber (Marienfeld-Superior, Germany) and

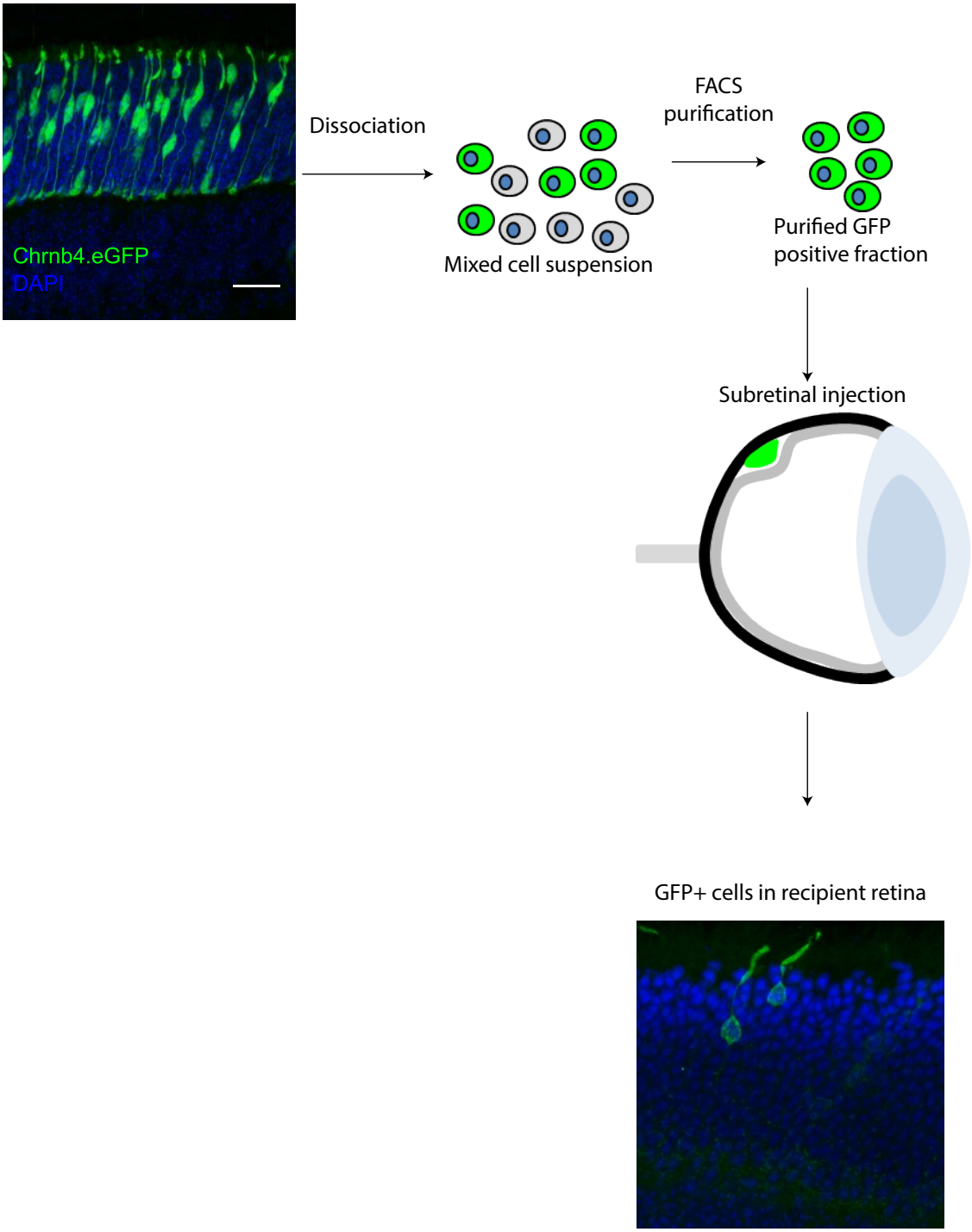

Figure 2.1 Transplantation of GFP positive cells. Neural retina from developing mice are dissociated using papain and the GFP expressing cells are purified by FACS. These cells are then injected into the subretinal space of a recipient mouse. Scale bar 10µm.

diluted in EBSS with 1% foetal calf serum (FCS) to a concentration of 10-20 million cells/ml.

Fluorescent Activated Cell Sorting (FACS) was used to purify the GFP-expressing population in cases where GFP was selectively expressed (Beckman Coulter MoFlo™XPD, BD Biosciences FACS Aria III, BD Biosciences Influx) using a sheath and sample pressure of 50 psi and 70 µm nozzle. The FACS process was carried out by Dr Robert Sampson or Dr Ayad Eddaoudi. The process aimed to isolate only single cells that were GFP positive and to this end excluded cell doublets and larger clusters, as well as cell fragments and debris. Dead cells were excluded using the live cell impermeant DNA dye Draq7 (Biostatus, UK). GFP-expressing cells were sorted into 50% EBSS, 50% FCS in 15ml Falcon tubes. Following the sort, part of the sample would be assessed by FACS for cell viability and GFP expression purity. Sorted cells were centrifuged at 150g for 18 minutes. For transplantation, pelleted cells were resuspended in EBSS and 5% DNase solution and counted using a haemocytometer, using a 1:1 dilution in trypan blue (Sigma Aldrich) to label dead and dying cells, which were then excluded from the count. Finally, the cells were centrifuged for 10 minutes at 150g and resuspended in sterile EBSS and 5% DNase at a concentration of 100,000 or 200,000 live cells / µl (see Results) and kept on ice until ready for transplantation. At least four retinas were isolated for each FACS experiment, and when cells were isolated for injection at least 6-12 retinas were used. Viability was at least 85% after sort. For injection experiments, with $Nrl^{-/-}$ NrlGFP cells eventual cell yield was at least 200,000 live cells, and with Chrnb4.eGFP cells at least 100,000 live cells.

2.2.2 Subretinal transplantation

Mice were anaesthetised via intraperitoneal injections of an anaesthetic mixture containing Dormitor (1 mg/ml medetomidine hydrochloride, Pfizer Pharmaceuticals, Kent UK), ketamine (100 mg/ml, Fort Dodge Animal Health, Southampton, UK) and sterile water in a 5:4:42 ratio were used before injections (0.01 ml per gram). Pupils were dilated using 1% topical tropicamide solution (Mimm's; Bauschand Lomb, USA) and then protected with Viscotears gel (Novartis, Switzerland).

Injections were performed under direct visual control using an operating microscope (Zeiss, UK). Injections were performed by R Pearson, and not the candidate. All injection experiments using OPN1LW-EGFP cells were carried out by Amanda Barber. Eyes were gently held in place using a pair of forceps by holding on to a segment of the conjunctiva and extraocular muscle. A glass cover slip was placed on top of the cornea over the layer of Viscotears applied earlier to facilitate visualisation of the retinal fundus through the operating microscope. The sclera was punctured at the level of the anterior chamber with the tip of a 8mm, 34-gauge hypodermic needle (Part identification: ga34/8mm/pst12; Hamilton, Switzerland) mounted on a 5 µl Hamilton syringe (Hamilton, Switzerland) to avoid excessive intraocular pressure. The same needle was then used to administer a sub-retinal injection of 1µl of cell preparation by tangential insertion through the sclera into the sub-retinal space, resulting in local retinal detachment. Unless otherwise stated, and for all experiments where counts of GFP+ cells in host ONL were subsequently carried out (see section 2.3.1), cells were introduced into the subretinal space of the superior retina by a single injection of 1µl. For some experiments – those in which transplanted retinas were assessed by multi-electrode array (see section 2.8 and

Chapter 6) – two injections were made, one into the superior and one into the inferior retina, by the same technique.

After sub-retinal detachment was confirmed by the return of visible blood vessels in the neural retina, the needle was slowly withdrawn, helping the tunnel to self-seal thereby reducing reflux of the injected volume. Eyes in which sub-retinal detachment was not observed, or in which significant levels of reflux was seen, were excluded from later analysis. Animals were allowed to recover from surgery following intra-peritoneal administration of Antisedan reversal solution dosed at 1mg/kg (Pfizer Pharmaceuticals, Kent UK). During the injection and during the first post-operation day, mice were placed on heat mats set to 33 °C to help regulate their body temperatures. Upon returning to cages, mice were placed on tissue to reduce the risk of bedding material contacting the eyes and given softened food. Table 2.2 shows a summary of the transplantation injections which were made.

Table 2.2 Summary of transplantation experiments

Donor cell	Approx. Donor cell age	Recipient (adult unless specified)	Injection Repetitions	Total Eyes injected
Chrnb4.eGFP (200,000 cells)	E15.5	WT	1	1
	P1	WT	1	2
	P8	WT	4	8
Chrnb4.eGFP (200,000 cells)	E15.5	$Nrl^{-/-}$	1	4
	P1	$Nrl^{-/-}$	1	2
	P8	$Nrl^{-/-}$	2	6
Chrnb4.eGFP (100,000 cells)	P1	WT	1	6
	P8	$Nrl^{-/-}$	3	14
	P8	$Nrl^{-/-}$	3	7
OPN1LW-EGFP (200,000 unsorted cells)	E15.5	WT (adult)	5	15
	E15.5	WT (P5)	3	10
	P7	WT	1	2
	P14	WT	1	2
$Nrl^{-/-}$NrlGFP (200,000 cells)	E15.5	WT	2	11
	P1	WT	2	17
	P8	WT	2	15
	P1	$Nrl^{-/-}$	2	10
	P8	$Nrl^{-/-}$	2	13
	P8	$Pde6c^{cpfl1/cpfl1}$	3	14
	P8	$Prph2^{rd2/rd2}$	3	15
	P8	$Nr2e3^{rd7/rd7}$	3	11
	P8	$Cnga3^{cpfl5/cpfl5}$	2	17
	P8	$Nrl^{-/-}$ (separate)	2	11
	P8	R91W;$Nrl^{-/-}$	2	18
$Nr2e3^{rd7/rd7}$CrxGFP (200,000 cells)	P8	WT	2	18
	P8	$Nrl^{-/-}$	2	9
	P8	$Nr2e3^{rd7/rd7}$	3	25
CrxGFP (200,000 cells)	P8	WT	3	20
	P8	$Nrl^{-/-}$	3	8
	P8	$Nr2e3^{rd7/rd7}$	3	12

2.3 Immunohistochemistry and microscopy

Mice were sacrificed by cervical dislocation and the eyes enucleated. These eyes were dissected to remove the cornea, lens and iris before fixation in 1% or 4% paraformaldehyde (PFA). These eyecups were cryopreserved in 20% sucrose at 4°C before freezing in Optimal Cutting Temperature (OCT) Embedding Matrix (Pyramid Innovations, UK) with isopentane (Sigma), cooled with liquid nitrogen.

Eyes were stored at -20°C until ready for sectioning. Cryosections were cut on a Bright OTF5000 cryostat (Bright Instruments Co Ltd) set to produce sections between 15 and 18μm thick). Sections were transferred to Super Frost Ultra Plus Adhesion glass slides (Thermo Scientific), dried at room temperature and subsequently stored at -20°C.

For immunohistochemistry, slides were thawed at room temperature for 30 minutes. The sections were circumscribed with a hydrophobic pen (Dako, UK) and OCT was removed with PBS for at least 10 minutes. Sections were preblocked to reduce non-specific protein binding using a solution containing 1% bovine serum albumin (Sigma Aldrich), 0.1% Triton (Sigma Aldrich), and a variable component of animal serum in PBS for one hour before incubating overnight at 4°C with primary antibodies (see Table 2.2) in block solution. For cone marker staining in Figures 3.3, 3.6, and 3.7, Dr Fabiana Di Marco sectioned, stained and imaged eyes provided by the candidate.

Table 2.3 Immunohistochemical reagents

Primary antibody target	Animal	Source	Concentration	Block	Secondary antibody (AlexaFluor)
Rxrγ	Rabbit	Abcam	1:200	10% FBS 1% BSA 0.1% Triton	Goat anti-rabbit 546
Biotinylated Peanut agglutinin (PNA)	N/A (plant lectin)	Vector Laboratories	1:500	10% FBS 1% BSA 0.1% Triton	Streptavidin 633
S-opsin (Opn1sw)	Goat	Santa Cruz	1:100	2% Normal Donkey serum 1% BSA 0.1% Triton	Donkey anti-goat 546
Prph2	Rabbit		1:500	10% FBS 1% BSA 0.1% Triton	Goat anti-rabbit 546
Rod a-transducin	Rabbit	Santa Cruz	1:500	2% Normal Donkey serum 1% BSA 0.1% Triton	Donkey anti-goat 546
Cone Arrestin	Rabbit	Millipore	1:200	2% Normal Donkey serum 1% BSA 0.1% Triton	Donkey anti-rabbit 647
Protein kinase C alpha	Mouse	Millipore	1:500	10% Normal Goat Serum 1% BSA 0.1% Triton	Goat anti-mouse 546
GFP.FITC	Goat	Abcam	1:200	10% FBS 1% BSA 0.1% Triton	N/A

Sections were subsequently rinsed with PBS (3x15 minutes) and incubated with secondary antibodies (AlexaFluor, Invitrogen, UK) for two hours at room

temperature, rinsed again with PBS (3x15 minutes) and counterstained with DAPI for 10 minutes at room temperature. Slides were mounted with sufficient Fluorescent Mounting Medium (Dako, UK) and sealed with ordinary nail polish.

Sections were viewed with an inverted fluorescence microscope (Observer Z.1, Zeiss, UK) and images taken with a confocal microscope (Leica SP2, UK), typically at a resolution of 1024x1024 and with an objective lens magnification of 40x or 63x. Unless otherwise stated, images show merged projection images of a confocal stack through the entire visible depth of a retinal section (approximately 15 to 30 μm), with each optical section approximately 1μm thick. Scale bars are 10μm unless otherwise stated.

2.3.1 Counting GFP+ cells in recipient retina after transplantation

After immunostaining for Rxrγ (see above) and enhancing GFP signal with 1:200 FITC conjugated anti-GFP goat polyclonal antibody (Abcam, UK), sections from injected eyes were viewed with a fluorescence microscope (Observer Z.1, Zeiss). Every third cryosection was viewed and all GFP+ cells with cell bodies clearly located in the recipient ONL were counted and assessed, when possible, for Rxrγ co-staining and morphology. The total number of GFP+ cells for each injected eye was calculated as three times this count. Counts were rejected if there were indications of an acute inflammatory response and immune rejection (see (West et al., 2010) and below for grading details) and/or if the subretinal mass of transplanted cells was very small (<250 cells) or entirely absent, both indicating a major reflux of the injected cells at time of transplantation, in accordance with previous work. Counts were also rejected if there was evidence that the cells had been injected into the vitreal cavity, rather than the subretinal space. Images were taken with a confocal microscope (Leica SP2). Images show merged projection

images of a confocal stack through the entire visible depth of a retinal section (approximately 15 to 30 μm), with each optical section approximately 1μm thick.

2.3.2 Assessment of inflammation

As mentioned above, previously developed criteria were used to assess evidence of acute immune rejection (West et al., 2010). The presence of macrophages was assessed by a three-level grading system, as shown in Figure 2.2. Grade 1 outcomes were characterised by no or only occasional macrophages evident in the subretinal space, at the injection site. Grade 2 outcomes showed greater numbers of macrophages, including ramified macrophages in the subretinal space, present around the subretinal cell mass and the site of injection. In Grade 3 outcomes, many amoeboid macrophages were seen in the subretinal space and retina, accompanied by a decrease in the size of the subretinal mass and/or a thinning or outright loss of the ONL. Retinas judged at Grade 2 or 3 were excluded from quantification, unless otherwise stated.

2.4 Electron microscopy

Mice were sacrificed and the eyes enucleated. The sclera was marked by a small burn to denote the superior retina. Fixation occurred in 3% glutaraldehyde / 1% PFA solution with 0.08 sodium cacodylate-HCl. The cornea and lens were removed and the remaining eye-cups were washed for 15 minutes in 2.5% glutaraldehyde, 0.1M cacodylate buffered to pH 7.4. The eyes were then osmicated in the dark for 2.5 hours using a 1% aqueous solution of osmium tetroxide, and dehydrated in 10 minute steps using increasing concentrations of ethanol, from 50% to 100%, and finishing with three changes of 100% ethanol. The eye-cups were then passed through propylene oxide and araldite for three 10 minute sessions and left for 3

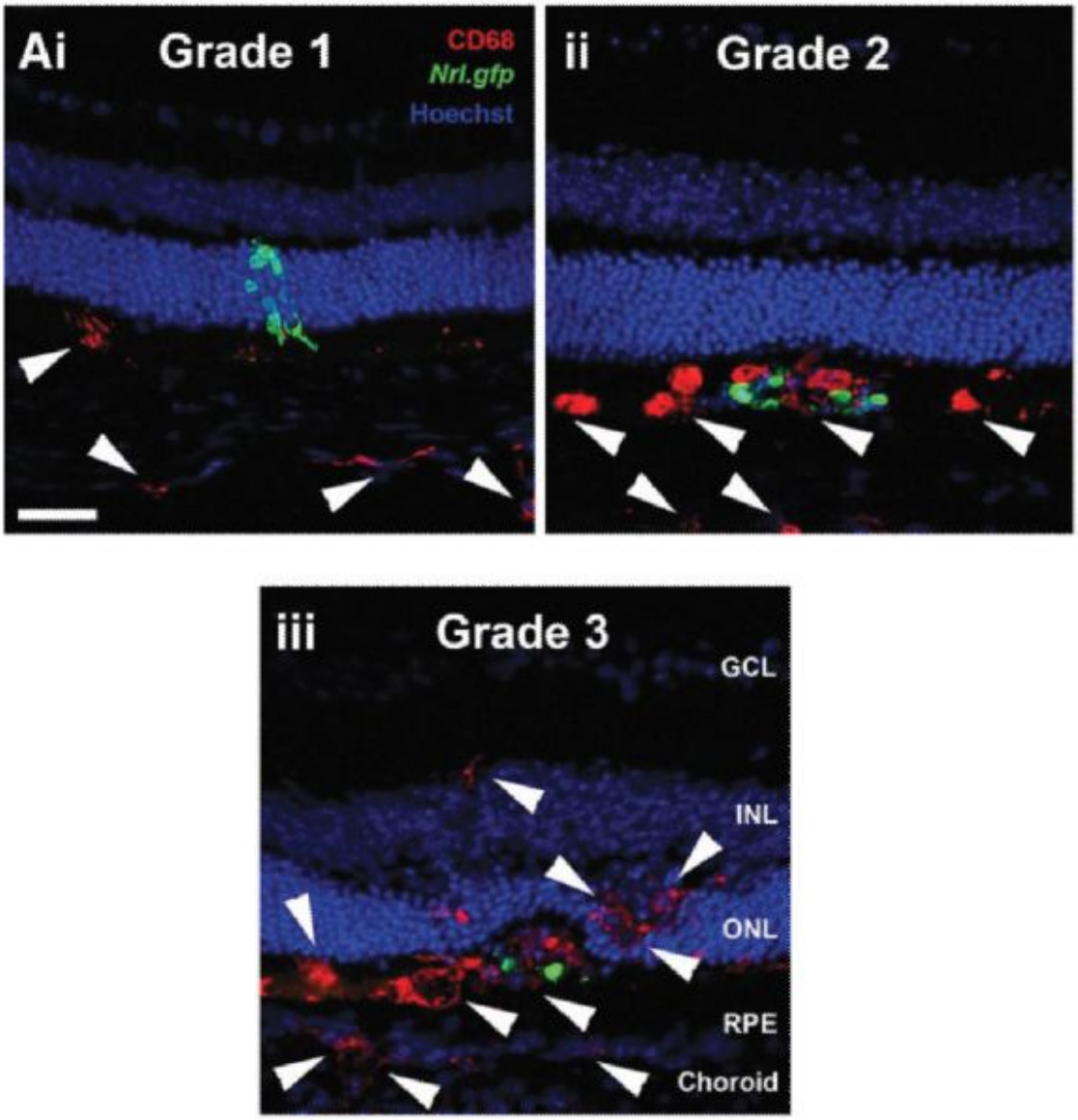

Figure 2.2 Assessment of macrophage infiltration after transplantation. Reprinted by permission from Wiley: *Stem Cells* (West et al. 2010), copyright 2010. Scale bar 50 μm.

hours with rotation in a 50:50 mixture of propylene oxide and araldite. Finally, after transferring to fresh araldite for 5 hours with rotation, the eye-cups were embedded and cured for 48 hours at 60^{o}C.

Semi-thin sections were cut at 0.7µm and ultra-thin sections at 0.07µm, using a diamond knife on a Leica Ultracut S microtome. Semi-thin sections were stained with 1% toluidine blue and imaged using a Leitz Diaplan microscope and Leica digital camera (DC 500). Ultra-thin sections were collected on 100 mesh copper grids (Agar Scientific, UK) and contrast-stained using 1% uranyl acetate and lead citrate. Images were taken using a JEOL 1010 Transmission Electron Microscope and digital camera. Electron microscopy preparation and imaging was carried out by Anna Graca (see Figure 5.6A).

2.5 Time-lapse imaging of migration in real time

2.5.1 Time-lapse imaging of cone photoreceptor precursors in neonatal retinal explants

Chrnb4.eGFP mice at various postnatal ages were sacrificed and the eyes enucleated and kept in RPMI medium (Invitrogen). These were stored on ice until dissection, typically commencing within one hour.

Chrnb4.eGFP retinas were explanted from various early postnatal animals and flat-mounted on nitrocellulose filter paper discs (Millipore). An illustration of the procedure can be found in Figure 2.3. Dissection - removing the cornea, sclera, lens and vitreous humour - was carried out in RPMI and at room temperature. Three or four radial cuts were made from the edges of the retinal cup, and the retina was subsequently flattened on a glass slide, with the RGCs upwards. A paper disc was then laid on top of the retina to mount it. These discs were affixed to the bottom of a

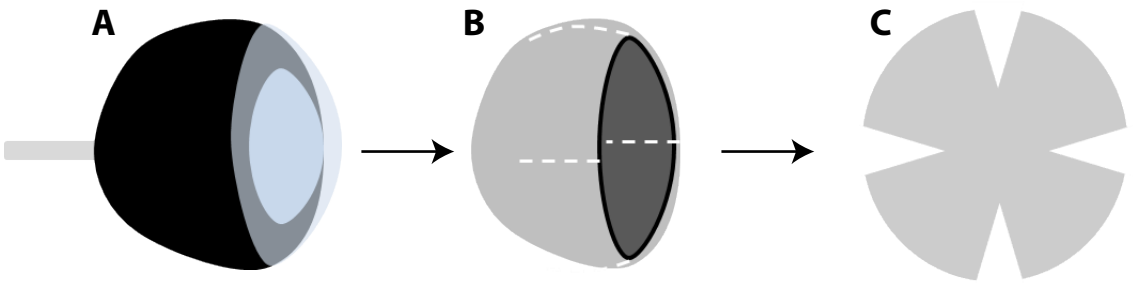

Figure 2.3 Illustration of the preparation of flatmounted retinas for live-imaging from whole eyes (A). The cornea, sclera and lens are removed and cuts are made into the neural retina (B, dashed lines). The retina is flattened and mounted on filter paper with the photoreceptors uppermost (C). This disc is affixed to the bottom of a petri dish and covered with imaging medium.

25cm petri dish, making the photoreceptor layer of the retina uppermost, using silicone grease to aid adhesion, and kept wet with RPMI at all times. The imaging medium used was 10ml $DMEM_{gfp}$-2 medium (Evrogen), a preparation of Dulbecco's Modified Eagles Medium designed to be free of substances responsible for EGFP photobleaching. Added to this medium were Rutin (Evrogen), a plant extract, which acts to further improve EGFP photostability, and 10µl Dimethyl sulphoxide (DMSO), which was added as a control in experiments where drugs were not used. Once prepared, this medium was gently added to the petri dish to cover the retinal preparations.

Imaging was carried out in an incubated chamber, and maintained at 37°C and in a 95% O_2, 5% CO_2 environment. The equipment used was a Leica TCS SP8, multi-photon microscope with integrated OPO (Optical Parametric Oscillator). Fluorescence microscopy was used to identify a retinal area without remnants of RPE, due to the efficient absorption by these pigmented cells of the wavelengths used in multiphoton microscopy. For imaging, the laser was set to 840nm and fluorescence was collected using external detectors. The objective used was a 40x ceramic water 'dipping' lens. Before commencement of time-lapse imaging, a platinum harp strung with nylon was used to improve tissue stability, and paraffin oil was added to cover the surface of the imaging medium, in order to reduce evaporation and maintain even concentration of the gases supplied to the tissue. Image stacks were taken every 10 minutes consisting of images in the xy plane repeated at depths in the z plane separated by approximately 1µm, where the z plane corresponds to the apico-basal axis of the retina. Imaging sessions were between approximately 8 and 12 hours.

In experiments where drugs were used, these were dissolved in 10 µl of DMSO and then diluted in 1ml of the imaging medium before being gently added to the

remaining imaging medium in the petri dish after at least 90 minutes of incubation and imaging without drug. Ciliobrevin D (Sigma Aldrich) was used at a final concentration of 25μM.

2.5.2 Image processing and cell tracking

After acquisition, image files were processed using ImageJ/Fiji software (Schindelin et al., 2012), with images taken beyond the extent of the fluorescent tissue discarded and the images corrected for drift of the tissue using an existing 'correct for 3D drift' plugin (Parslow, Cardona, & Bryson-Richardson, 2014).
Figure 2.4 shows examples of the images obtained, as well as stages in the analysis of these data. Spot-tracking features of IMARIS software were used to identify the coordinates of cell bodies over time. All trajectories of cells taken forward for analysis were initially generated by the software and then individually verified by visual inspection. The z-axis co-ordinate, corresponding most closely to the apico-basal dimension of the retina, was used to determine the position of cell bodies during time-lapse imaging.

Mean squared displacement (MSD) can be used to compare the position of a cell at pairs of time points, separated in time by $\Delta t = n\,\delta t$, where Δt is an integer multiple n of the smallest time difference δt between time points (i.e. the sample rate of 10 minutes). MSD measurements were calculated for the trajectory of each cell, by taking an average of the squared distance between the position of the cell separated in time by $\Delta t = n\,\delta t$ using the general formula

$$MSD(\Delta t) = \frac{1}{N-n}\sum_{i=1}^{N-n}[(p(i+n)\delta t) - p(i\delta t)]^2$$

where N is the total number of time points in the trajectory, and $p(i\,\delta t)$ is the z-axis position of the cell at time point *i* (Norden, Young, Link, & Harris, 2009). MSD values were calculated for all values of *n,* noting that as *n* increased, the number of timepoints available to be compared was reduced, so also reducing the reliability of the measurement.

Plotting the values of the instantaneous velocities (the distance moved in 10 minutes) on an inverse normal graph showed the deviation from normality. In effect, graphs of this type compare each velocity value found in the data with its equivalent value taken from a perfect normal distribution generated with the same mean and standard deviation.

The inverse normal measurement is generated by ranking the velocity values from smallest to largest, and determining the quantile of this rank:

$$quantile = \frac{rank}{n+1}$$

where n is the total number of data values. The probit of this value is then found as the value of the equivalent quantile of the standard normal distribution, described by a mean (μ) of 0 and a standard deviation (σ) of 1. Thus, the middle quantile (0.5) has a probit of 0. These values were then mapped onto the normal distribution described by the mean and standard deviation of the data. Finally, these values are plotted against the original velocity values.

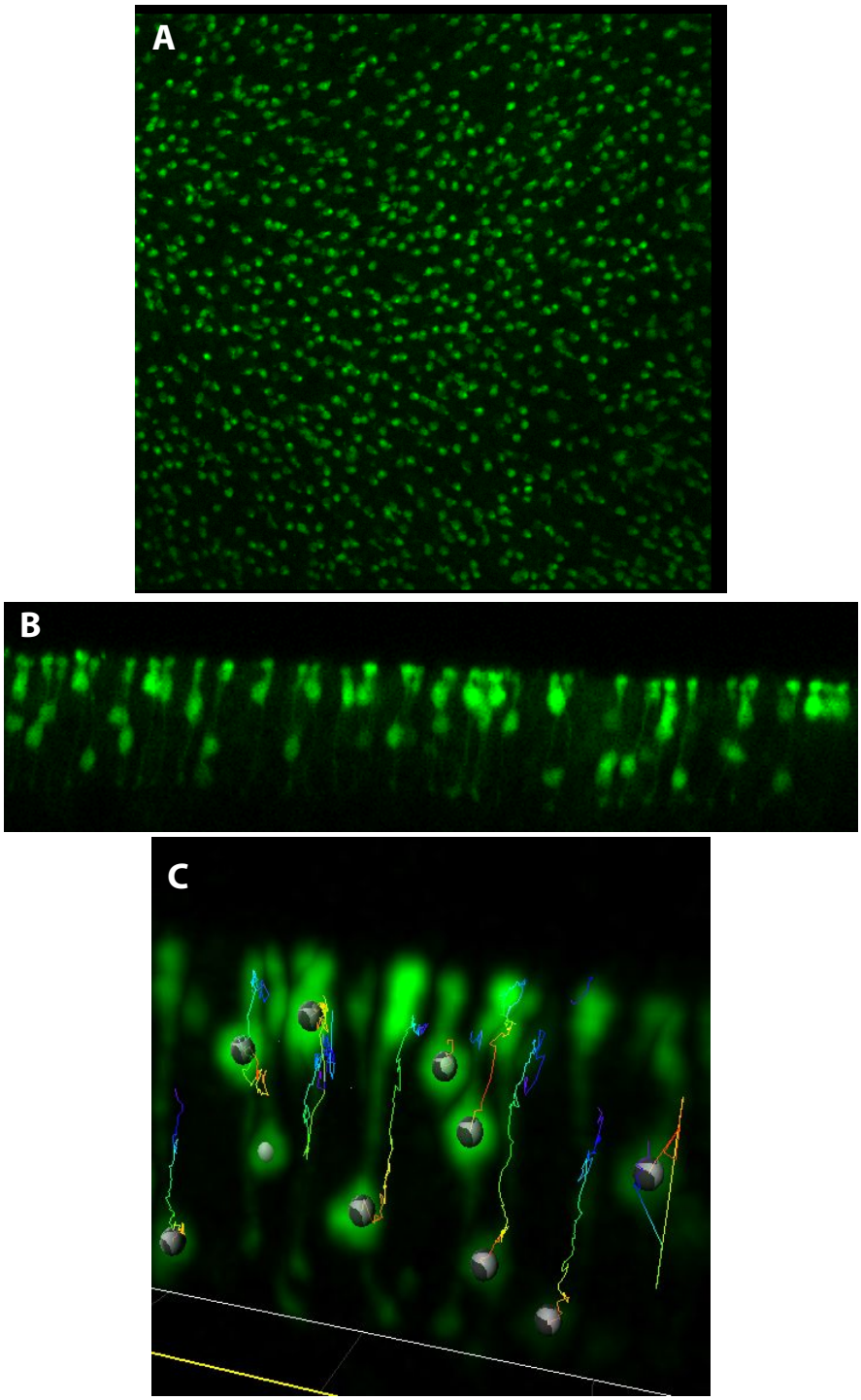

Figure 2.4 Example images from the live imaging of developmental Chrnb4.eGFP retinas. **A** Maximum projection of the stack of images taken for one time point of one P5 retina, taken with the photoreceptor layer uppermost. **B** Part of the image shown in (A), recalculated to simulate side-on vision. Cell bodies can be seen at various depths throughout the developing ONL. **C** Example image generated by IMARIS software. Grey ovoids show the position of cell bodies, identified by spot-tracking functions, and coloured lines show the position of these ovoids at time points throughout the imaging session. Each analysed cell is checked visually to ensure accurate tracking throughout. The software then generates the 3-dimensional coordinates of the cell at each time point.

2.6 PCR

2.6.1 PCR for genotyping

Genotyping, when required, was carried out on genomic DNA isolated from clips of ear tissue using Extracta DNA Prep (Quanta Biosciences, USA) to produce 100µl of genomic DNA. 1 µl of this solution was subsequently used for PCR. PCR for the eGFP sequence of Chrnb4.eGFP mice was carried out using standard protocols for the HotStar Taq Polymerase kit (Qiagen, Netherlands) and for other sequences standard protocols for the GoTaq Polymerase Master mix were used (ProMega, USA).

Band detection, when necessary (for the identification of $Nrl^{-/-}$, rd2 and eGFP genetic markers), was carried out by electrophoresis on agarose gel made with 0.5% Ultrapure TBE buffer, with 2% Ultrapure Agarose (both Invitrogen, UK) and 0.01% Safeview Nucleic acid stain (NBS Biologicals, UK). Electrophoresis was carried out using BioRad power packs and trays (BioRad, UK), against appropriate DNA ladders and with 6x Blue/Orange loading dye (both ProMega, UK), and assessed using a G Box UV imaging chamber (Syngene, UK). Appendix A shows specific conditions for each gene, including the size of band detected in the presence of each gene.

Genetic sequencing when necessary (for the identification of Cnga3, rd8 or rd1 mutations) was carried out on site with ABI DNA Sequencer 3730, using BigDye v3.1 (ThermoFisher) or externally by Beckman Coulter Genomics (Essex, UK). Gene specific information, including temperatures, conditions and primers used can be found in Appendix A.

2.6.2 Real Time quantitative PCR

Real time quantitative PCR was used to assess the presence and level of certain cone specific markers in late embryonic and early postnatal mice.

All primers (Appendix A) were designed by the online Roche Applied Science Assay design to use in conjunction with FAM-labelled probes from the Universal Probe Library. mRNA for real time qPCR was obtained (Qiagen RNeasy kit Mini/Micro) from whole neural retina dissected from the eyes of sacrificed animals or from flow-sorted fluorescent cells (see above) where specified. Whole neural retinas were frozen in 1.5ml Eppendorf tubes in liquid N_2 and stored at -80^{o}C before mRNA preparation. For flow sorted cells, samples were taken after centrifugation directly following flow sorting, and when necessary stored at -80^{o}C in lysis buffer (Qiagen kit, above).

cDNA was obtained by reverse transcription (Qiagen QuantiTect Reverse Transcription Kit) or whole genome amplification (Qiagen Whole Genome Amplification Kit). Quantitative PCR was carried out with reagents from Roche Diagnostics and used a thermal cycler (7900HT; Applied Biosciences). A final volume of 20µl was used in 96 well plates, with 1 µl cDNA preparation used per well.

The data were analysed with Sequence Detection Systems 2.2.2 (Applied Biosciences). The relative expression of each transcript was obtained through the formula $2^{\Delta\Delta Ct}$ and was normalised to B-actin expression as a housekeeping gene expressed in all cells to correct for the different number of cells used in each sample. All samples were run in duplicate and a water control for each primer pair was included.

2.7 Electroretinography

Mice selected for ERG recording were dark-adapted overnight beforehand. Mice were anaesthetised as for transplantation (above). Pupils were dilated with 1% Tropicamide and 2.5% Phenylephrine and the eyes were instilled with Viscotears liquid gel to facilitate the conductance of the electric signals to the electrodes. ERGs were recorded with an Espion E2 apparatus (Diagnosys LLC, MA, USA). Corneal wire loop electrodes were placed symmetrically on each eye, and compared with the reference electrode in the mouth of a mouse connected to a ground electrode inserted along the tail.

ERGs were measured with a scotopic 6Hz flicker paradigm using flashes ranging from -6 to 2 log.cd.s/m^2 comprising 17 steps increasing in intensity by 0.5 log.cd.s/m^2 per step. The wide range of flash intensities used allows separation and assessment of rod and cone functions. A total of 30-50 600ms second sweeps were collected and averaged for each step.

Photopic single flash responses were subsequently measured after light adaptation for 5 minutes on a rod desensitizing white background (30 cd/m^2), which was also used as the background light for the duration of photopic recordings. Forty single flash responses (100ms before to 400ms after the 4ms flash) were collected for each light intensity level and averaged. Photopic light intensities used were 0.01, 0.1, 1, 10, 31.2, and 72.5 cd.s/m^2. Adaptation time was 2 seconds before flash trains at 1 and 10 cd.s/m^2, 5 seconds before 31.2 and 72.5 cd.s/m^2, and 0 otherwise.

For the 6Hz flicker responses, amplitudes of 3 consecutive wavelets were measured and averaged for each step of light intensity. Photopic responses were assessed by

measuring the b-wave amplitude defined by the difference in electric potential between the a wave trough and b wave peak. ERG measurements derived from the two ERG protocols were compared between the treated eyes and the contralateral control eyes, which underwent control injections of EBSS.

2.8 Multi-electrode Array recording

2.8.1 Equipment

A 60pMEA100/30iR-Ti Multi-Electrode Array (MEA) (Multichannel Systems, Germany) was used, consisting of 60 Titanium Nitrite (TiN) electrodes (impedance 30-50 kOhms) with a diameter of 30um, spaced 100µm apart (centre to centre) on a 6x10 electrode grid (see Figure 2.5). The electrodes were integrated in a polyimide membrane to insulate the electrodes from each other, and this was encased in a glass housing, with a glass ring 6mm high to create a culture chamber and allow for the tissue to be surrounded by Ames' medium. The MEA membrane was also perforated with holes between 20 and 90 µm in diameter to allow for perfusion both above and below the retinal tissue, through a circular hole in the glass casing.

The MEA was used in conjunction with a Multi-Channel Systems headstage comprising an amplifier equipped with a perfusion ground plate. This apparatus was contained within a Faraday cage. The output was amplified (Gain 1200.00), and digitised (Sampling Frequency 32000Hz) and sent from the amplifier to a recording computer.

Light stimuli were delivered by various LED sources (THOR labs, Germany), specifically with wavelength peaks at 420nm, 470nm and 505nm. These were controlled in intensity using uniform neutral density filters (THOR labs) and activated using a stimulus generator (STG4002, Multi-Channel Systems) driven by a

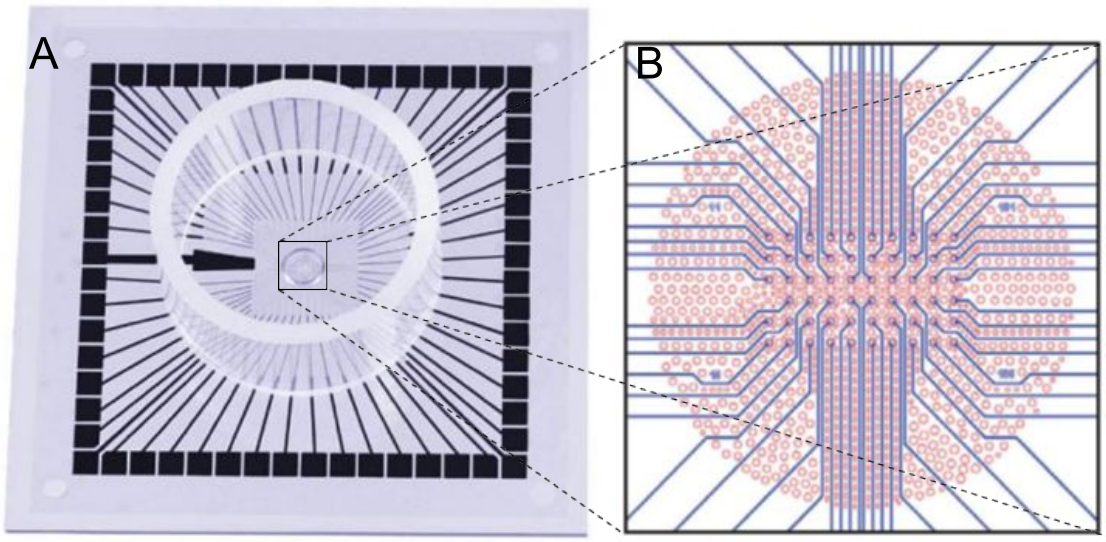
A
B

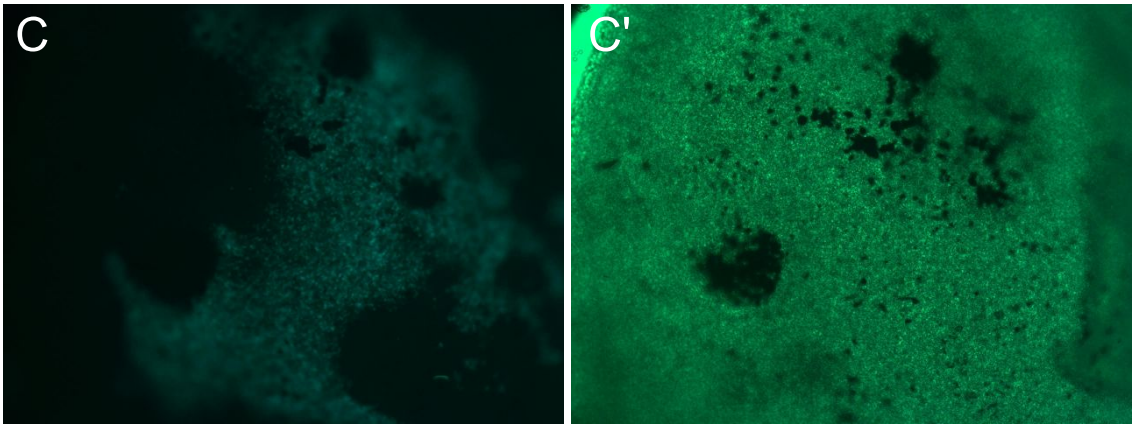
C
C'

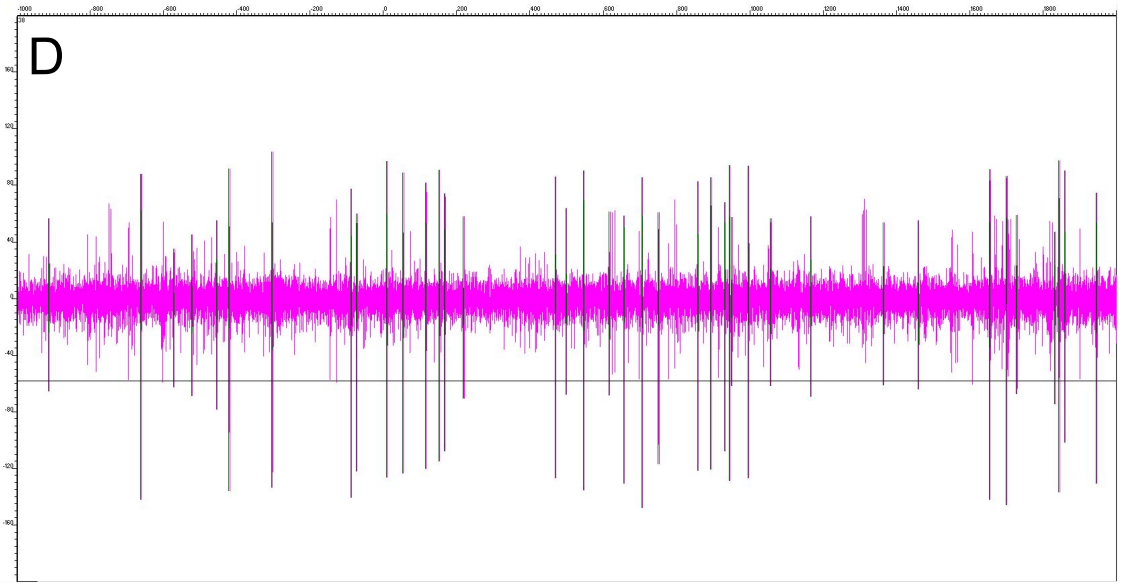
D

Figure 2.5 The Multi-electrode array apparatus and data. Images are taken from Multi-Channel Systems Manuals. **A** Glass housing for the MEA, surrounding the electrodes integrated into a polyimide membrane. Titanium/Gold tracks connect the recording electrodes in the centre with the contacts around the edge of the glass housing. The circular ring acts to create a culture chamber for perfusion medium. **B** The centre of the MEA, showing the recording electrodes in the membrane and the perforations (red circles). **C, C'** Reflected light (C) and transmitted light (C') images of a $Prph2^{rd2/rd2}Cnga3^{cpfl5/cpfl5}$ retina after transplantation and dissection. Areas of green fluorescent cells can be seen. When present, the part of the retina showing these cells is positioned on the MEA, to increase the chances of recording from an area with GFP+ cells within the recipient ONL. **D** Example data from one channel showing the voltage changes at one electrode recording (pink trace) from a $Prph2^{rd2/rd2}Cnga3^{cpfl5/cpfl5}$ mouse retina. The threshold (horizontal black line) is set at 4 standard deviations and any part of the recording which crosses it (green trace) is recorded for further analysis.

computer, via an LED driver. Light was channelled to the tissue through a fibre optic cable suspended above the MEA apparatus. An optical power-meter (THOR labs, PM100D) was used to standardise intensity before each recording session.

One litre of Ames' medium (Sigma, UK) was prepared, with 1.9g of Sodium Bicarbonate added. Carbogen (95% O_2, 5% CO_2) was continually bubbled through the Ames' medium, which constantly perfused the tissue being studied and was heated to 36^{o}C by a perfusion cannula (Multichannel Systems). Perfusion was driven by two peristaltic pumps (Gilson, France). Gentle suction was provided by slow perfusion occurring underneath the MEA via the perforations mentioned above. This acted to pull the tissue down onto the electrodes.

2.8.2 Preparation of tissue and recording

Mice were sacrificed and their eyes enucleated. The neural retina was dissected from the eyes and kept in carbogenated medium. The neural retina was cleaned of vitreous humour and cut in half, before being placed on the MEA electrodes with the photoreceptor layer upward-facing. A platinum harp strung with nylon was used to prevent the tissue moving off the electrodes. During the dissection process, an inverted fluorescence microscope (Observer Z.1, Zeiss) was used to locate any areas of GFP positive cells following injection of photoreceptor precursor cells. Control (uninjected) retinas were also screened in this way.

An initial recording was visually inspected and excessively noisy channels were disconnected, to prevent noise spreading to neighbouring channels. After a 20 minute recovery period to allow adaptation to the temperature controlled dark environment, retinas were exposed to increasing levels of light from the LED sources. Typical recordings comprised a pre-stimulus interval of 1000ms followed

by a 200ms flash, followed in turn by a 1800ms period of darkness. This pattern was repeated 20 times in total for each stimulus setting, with the inter-stimulus interval 3000ms. Recording therefore took place continually for 60 seconds. Between different stimulus settings, a recovery period of at least 3 minutes was observed.

Data were collected using MC Rack software (Multi-channel Systems, Germany). A 300Hz high pass 2nd order Butterworth filter setting was used to restrict the data collected to frequencies associated with RGC spike activity.

2.8.3 Data Processing and analysis

After acquisition, spike waveforms were extracted from the recording of each electrode channel using a threshold system. The threshold was defined as being 4 times the standard deviation of the recording. Data points were extracted in a window 1ms before and 2ms after any point at which the threshold was crossed (making 96 data values for each putative spike recorded) and aligned to their peak value. A 'censor period' of 1.5ms around a detected spike was used to prevent spikes from being detected multiple times.

SigTOOL software (a program based on MATLAB for the analysis of electrical trace data) (Lidierth, 2009) converted traces into '.kcl' format, and all traces recorded from a single channel for any given retinal sample were stitched together sequentially for analysis.

Spike sorting methods aim to separate spikes which were recorded together but are likely to come from different sources, based on their particular characteristics. The open-source spike sorting software wave_clus (Quiroga, Nadasdy, & Ben-Shaul,

2004) formed the basis for further analysis. Custom software developed in the laboratory by Ms Martha Robinson was used to co-ordinate spike sorting.

Automatic clustering transformed each spike into 96 wavelet coefficients, calculated using Haar wavelets. These represented the spike at each of its constituent data values. The 10 coefficients which deviated most from normality (using the Kolmogorov-Smirnov test) were selected, as deviation from normality indicated that a multimodal distribution might exist for that coefficient, giving different values for different units. These selected coefficients were then submitted to the superparamagnetic clustering algorithm (Quiroga et al., 2004) which generated clustering results for each of a wide range of temperature values spanning ferromagnetic, superparamagnetic and paramagnetic phases (see discussion in 1.5.3.2).

After automatic clustering, results were subjected to supervised assessment. The supervised phase of clustering involved manual selection of temperature settings, based on three-dimensional projections of the first three wavelet coefficients, and the spike waveforms themselves. Assessments of cluster quality were based on those proposed in work by Hill *et al.* (Hill, Mehta, & Kleinfeld, 2011). Plots of residuals, stationarity and spike amplitude relative to the selected threshold were assessed, with only stationary recordings, with waveforms of low variability and spike amplitudes large enough that the vast majority would be detected by the threshold, taken forward for further analysis. The spikes were also checked for refractory period violations: spikes in a single cluster occurring within 1ms of each other, indicating multiple spike origins.

2.9 General data analysis and Statistics

Data analysis, including statistical tests, data storage and graphic generation was carried out, variously, with Microsoft Excel, Graphpad Prism 5 (Graphpad Inc, La Jolla, USA), Matlab R2013a & R2014a, and Spyder (Python 2.7 environment) (Pierre Reynaut).

In general and unless otherwise stated, scale bars are 10μm and error bars show standard deviation. Data from transplantation experiments are from at least two separate and independent transplantation sessions (involving different donors, cell preparation, FACS sessions and injections). Box plots showing the number of cells seen in the recipient ONL after transplantation show the median, 25^{th} and 75^{th} percentile, and the whiskers are from the minimum to the maximum value.

Differences were assessed for significance in GraphPad Prism® software (GraphPad Software Inc.). Generally, and unless otherwise stated, the D'Agostino and Pearson test was used to assess the normality of datasets, where possible. For Student's t test, data with normal and non-normal distribution were analysed with two-tailed t test and Mann-Whitney test respectively. For ANOVA, normally and non-normally distributed datasets were subjected to One-way ANOVA (post test: Tukey if all groups were compared, Bonferroni-corrected otherwise) and Kruskal-Wallis test (post test: Dunn's) respectively. For grouped data differing in more than one variable, a two-way ANOVA (post test: Bonferroni-adjusted multiple comparisons) was used. In figures, stars indicate p-value significance where * is $p<0.05$, ** is $p<0.01$, *** is $p<0.001$ and **** is $p<0.0001$.

Chapter 3 – Generation and characterisation of donor retinas enriched in cone and cone-like cells for transplantation

3.1 Introduction

Proof of concept for the transplantation of cones came from the transplantation of a mixed photoreceptor population, marked by *Crx* expression (Lakowski et al., 2010). While reporter labelled photoreceptors positive for cone markers were found, the majority resembled rods. The mixed nature of the *Crx.GFP* population left open the question of whether this inefficiency was due to more successful integration of rod precursors or the result of plasticity in the fate of the injected immature cells.

For the further investigation of cone transplantation, therefore, it was important to secure a highly enriched source of mouse cone precursors, or to find a method of excluding rod precursors from the cells to be transplanted, at a range of developmental ages. Additionally, the ability to identify cone precursor cells as distinct from other retinal cells during development would be essential for effective assessment of the migratory behaviour of these cells. While the peak of cone genesis is around embryonic day 15.5 (Marquardt and Gruss, 2002), these cells undergo postmitotic development, and become functional several days after genesis.

Several genes, specifically restricted to cone photoreceptors, are known to be expressed in the adult retina at a level sufficient for their protein products to be used as targets for immunohistochemistry and/or for their regulatory sequences to be

used to drive fluorescent transgene reporters. It is not always apparent, however, that this expression pattern is the case throughout earlier stages of development.

Previous studies of photoreceptor transplantation (West et al. 2010; West et al. 2012; Pearson et al. 2012; MacLaren et al. 2006; Pearson et al. 2010) have used the NrlGFP reporter to label rod photoreceptor precursor cells, and exclude cone photoreceptors. The Nrl gene is a transcription factor present in all rod photoreceptors and is first expressed very soon after terminal mitosis (Akimoto et al., 2006). It acts to promote rod identity by the suppression of cone-specific genes (Oh et al., 2008). Indeed, without Nrl, rod photoreceptors follow a 'default' development pathway and develop as cone-like cells (Mears et al., 2001; Yoshida et al., 2004). There is no similarly crucial transcription factor known for cone photoreceptors that both distinguishes them from rod photoreceptors, and is present at very early stages of development. There are of course several genes which are expressed exclusively by cone photoreceptors, but it is not always clear at what point during cone development expression of these genes is sufficient that their regulatory sequences could be used to drive a reporter construct.

In this chapter, the onset of expression of cone-specific markers in WT retina was studied by analysis of the transcriptomes of developing neural retina, compared to that in adult tissue. Candidates for reporter lines based on these markers were investigated for their suitability for use both as a source of cells for transplantation and for visualisation of live cells during development.

Other sources of cone-like cells for transplantation purposes were also considered. The $Nrl^{-/-}$ and $Nr2e3^{rd7/rd7}$ mouse lines produce additional cone-like cells compared to the WT mouse and isolating some or all of these cells therefore represented a possible alternative to labelled true cones. Accordingly, these models were

investigated for the onset of cone marker expression and the production of cone-like cells, and reporter lines based on these models were also studied.

3.2 Results

3.2.1 Developmental expression of cone-specific genes

An assessment of the onset of gene expression and cone restriction of several markers was necessary to determine which markers would be appropriate for my research aims. To do this, I used quantitative PCR on cDNA obtained from whole neural WT mouse retinas to determine at what point during embryonic and postnatal development the transcripts of these genes began to rise. The expression in adult tissue was used as a comparison.

3.2.1.1 Transcriptome quantification in WT developing retina

Wild type *C57Bl/6J* mice were sacrificed at embryonic (post-conception) days 13.5 (E13.5), E15.5 and E17.5 and post-natal ages P0, P2, P4, P6, P8, P10 and P12. Their neural retinas were removed. mRNA was prepared from these whole neural retinas, and converted to cDNA by reverse transcription. Tissue for postnatal time points were gathered from pups from multiple litters, while a single litter provided tissue for multiple postnatal time points. However, since taking tissue prenatally meant that a whole litter and pregnant female needed to be sacrificed, data for embryonic time points comes from a single litter per time point. The number of individual retinas, n, for each time point used can be found in Table 3.1.

Table 3.1 Sample numbers used for qPCR assessment of whole retinas

Retinal age	n (retinas used)
E13.5	3
E15.5	3
E17.5	3
P0	4
P2	4
P4	4
P6	4
P8	5
P10	5
P12	5
Adult	3

A number of genes were selected for the assessment of expression, based on the existing literature; these genes are detailed below. Quantitative PCR primer pairs were designed online and can be found in Appendix A. Methods for qPCR are described in Chapter 2. Probe reporting activity was normalised to β-actin, as a standard for each gene, and then calculated relative to the average value of adult retina.

3.2.1.1.1 Gene selection

Genes were selected based on their perceived suitability as a cone marker: specificity to cone photoreceptors, presence in development and any reference to existing mouse models driving a reporter construct through the promoters of these genes:

Retinal cone arrestin-3 (*Arr3*), phosphodiesterase 6c (*Pde6c*) and cone transducin alpha subunit (*Gnat2*) are all components of the cone specific light transduction cascade, as described in section 1.2.2, and were therefore chosen for analysis.

Likewise, the two mouse cone opsin genes were selected for assessment. Short wavelength sensitive cone opsin (*Opn1sw*) is expressed in cone photoreceptors and a sequence upstream from the *Opn1sw* gene has been shown to drive expression exclusively in cones (Chiu et al., 1994; Chiu and Nathans, 1994), starting at birth and increasing over time.

Similarly, cone photoreceptors expressing the medium wavelength sensitive cone opsin (*Opn1mw*) have been labelled with GFP in a mouse model with a regulatory sequence taken from the human red and green opsin gene (OPN1LW) (Fei, 2003; Fei and Hughes, 2001).

Several other genes were found to be implicated in cone retinal development: *Chrnb4*, coding for a nicotinic acetylcholine receptor subunit, was used to drive GFP expression in mice by the Gene Expression Nervous System Atlas (GENSAT) project (Gong et al., 2003). In the retina, *Chrnb4* was subsequently discovered to drive GFP expression in adult cone photoreceptors (Siegert et al., 2009) but the developmental onset of expression has not been reported.

Thyroid hormone receptor beta-2 (*Thrβ2*) works with other genes to control the pattern of expression of the two types of cone opsin in cones across the retina (Ng et al., 2009). Engrailed-2 (*En2*) is a homeobox transcription factor which is involved in development, and has been found to be expressed exclusively in fluorescence sorted adult cone photoreceptors (Siegert et al., 2012).

Retinoid x receptor gamma (*Rxrγ*) is one of a family of retinoid receptors. It appears within the retina from 10.5 days after conception and is localised within cone photoreceptors, but is also expressed in RGCs (Mori et al., 2001). Its function is unknown, but it appears to be involved with *Thrβ2* in the patterning of the cone

mosaic (Azadi and Ca, 2002; Fujieda et al., 2009; Mori et al., 2001; Roberts et al., 2005).

Fibroblast growth factor receptor 4 has been indicated as an early marker of cones in macaque monkeys (Cornish et al., 2004) although it appears to be less specifically restricted in rodents (Kinkl et al., 2002).

3.2.1.1.2 Expression patterns

The results of quantitative PCR on whole retinal cDNA are shown in Figure 3.1. A number of markers showed a similar pattern of expression onset. *Arr3, En2, Gnat2, Pde6c, Opn1mw, Opn1sw* and *Thrβ2* were all seen to have very low expression levels at embryonic and early postnatal stages before a rapid increase in expression level at later postnatal stages. As many of the products of these genes are involved in the light transduction function of adult cones, it is not unexpected that their expression would occur only later in development.

The clearest exceptions included *Chrnb4*, which showed a higher level of relative expression before adulthood and, in fact, declines over the studied period, and *Rxrγ*, which showed more than 50% of adult expression level throughout much of the time period assessed. *Fgfr4* expression also appeared to be around 50% of adult during the developmental stages assessed, but due to the high variability and unknown cell type restriction in rodent it was decided to be less promising as a potential marker.

Rxrγ has been used as a marker for developing cone photoreceptors in previous studies (Roberts et al., 2005), suggesting that it would be suitable for identifying immature cones via immunohistochemistry. Due, however, to the known expression

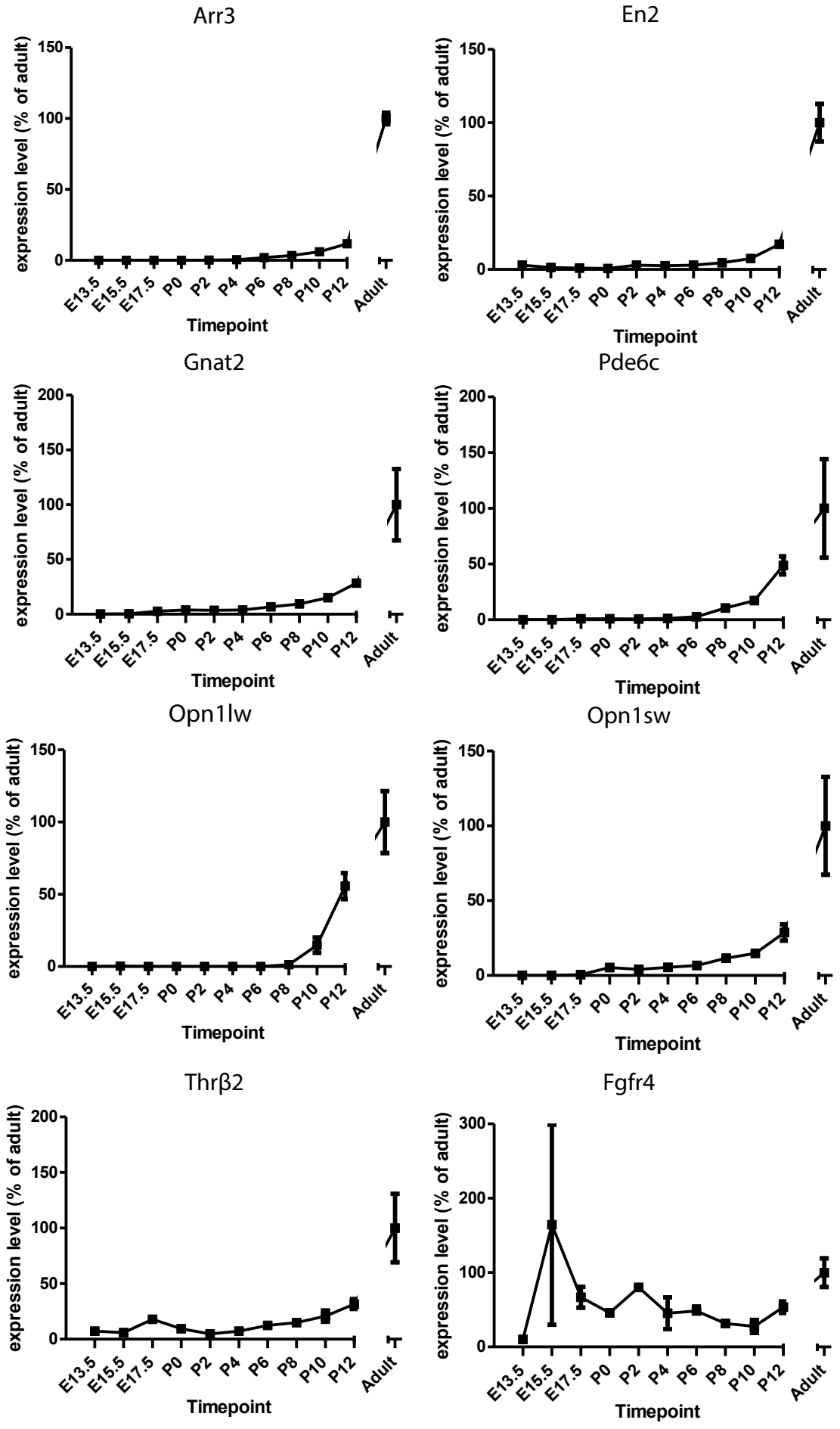
Arr3
En2
Gnat2
Pde6c
Opn1lw
Opn1sw
Thrβ2
Fgfr4
expression level (% of adult)
Timepoint
E13.5
E15.5
E17.5
P0
P2
P4
P6
P8
P10
P12
Adult

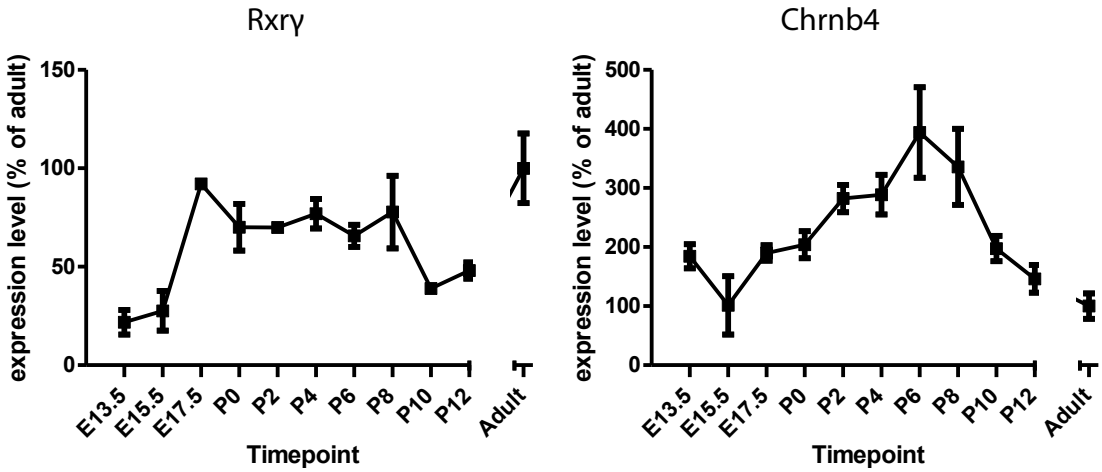

Figure 3.1 qPCR assessment of whole neural retinas taken from WT mice at various developmental ages.

Values were calculated by normalisation to the housekeeping gene β-actin. Expression levels are shown as percentages of the expression found in adult retina (6-8 weeks) on a linear scale +/- SEM. The majority of the genes assessed (Arr3, En2, Gnat2, Pde6c, Opn1lw, Opn1sw, Thrβ2) showed a similar expression pattern, with very low relative expression levels at embryonic levels before expression rises towards the end of the postnatal period assessed. In most of these, however, even at the latest stage assessed, P12, expression was still below approximately 25% of adult, although higher levels were seen for Pde6c and the cone opsins Opn1lw and Opn1sw.

Fgfr4 expression, despite high expression during the developmental period, was extremely variable in expression level, with values fluctuating both between and within cell ages, particularly in the late embryonic stage.

Rxrγ rises to between 50 and 100% of Adult expression by shortly before birth, and while variable, maintains this level throughout the postnatal period.

Chrnb4 shows higher levels of expression than found in adult retinas at all stations, with expression highest in the first week after birth.

of Rxrγ in adult RGCs, a fluorescent model based on this gene would not necessarily be optimal for isolating a pure population of cone precursor cells. Furthermore, a number of attempts to generate a mouse model expressing GFP under the control of *Rxrγ* had already been made by others in the group, as well as by other groups, without success.

In contrast, a Chrnb4.eGFP model was already known to exist (Siegert et al., 2009) and the qPCR results provided promising evidence that GFP expression would be apparent at early time points. In the next section, I investigate the suitability of this model for my specific research aims.

3.2.2 Characterisation of the Chrnb4.eGFP mouse

The GENSAT project used bacterial artificial chromosomes to generate a large number of GFP expressing mouse models. One used the Chrnb4 gene to drive GFP, and it was later found that, in the retina, GFP was expressed only in cone photoreceptors (Siegert et al., 2009).

3.2.2.1 GFP expression and immunofluorescence

To investigate the suitability of the Chrnb4.eGFP model, we acquired eyes (kind donation from Botond Roska, Friedrich Miescher Institute, Switzerland) at postnatal days 2 and 12. Confocal fluorescence microscopy showed strongly GFP+ cells which co-localised with Rxrγ at both these ages, as shown in Figure 3.2. Although no other GFP expression was seen in the P12 retina, cells weakly positive for GFP, but negative for Rxrγ were seen at P2. Furthermore, unstained pictures obtained at embryonic day 13.5 from Botond Roska's group showed GFP expression in a number of cells throughout the depth of the developing retina including notably strong expression in the presumptive GCL. The expression of GFP in cell

populations other than the cone precursors may provide an explanation for the expression level of Chrnb4 being higher in development than at adult ages, as seen in section 3.2.1.1.

On the other hand, these results implied that cone photoreceptors would be identifiable by the strength of GFP expression (high in immature cones, low in RGCs) between E13.5 and P2, with this expression thereafter persisting into the adult cones only. Since this was a significant improvement on available models such as the OPN1LW.eGFP mouse (see below), it was decided to import the model.

The model was obtained from the Mutant Mouse Regional Resource Centre. The animals delivered were the offspring of FVB/N mice bred to Swiss Webster mice and were hemizygous for the Chrnb4.eGFP transgene. Both genetic backgrounds were white mice homozygous for the $Pde6B^{rd1/rd1}$ mutation, which causes rapid retinal degeneration, and so the mice had to be outbred to the C57Bl/6J line for two generations while maintaining the reporter transgene and ensuring that the rd1 mutation was removed, which were assessed by PCR for eGFP, and PCR followed by sequencing for the rd1 mutation, as detailed in Chapter 2 (section 2.6.1) and Appendix A.

After acquisition of the Chrnb4.eGFP model, further assessment of retinal tissue at various ages of development was carried out. Figure 3.2 shows images from fixed retinal slices taken at postnatal ages P0, P4, P6, P8, P10 and Adult. These images show that GFP expression is strong in at least one population of cells at all these ages, and that all cells that are positive for Rxrγ expression also express GFP. They also show (more clearly at higher levels of exposure), however, that at earlier postnatal ages (P8 and younger) there exist other (more weakly) GFP expressing cells which are not Rxrγ positive, notably in the GCL and in the developing ONL.

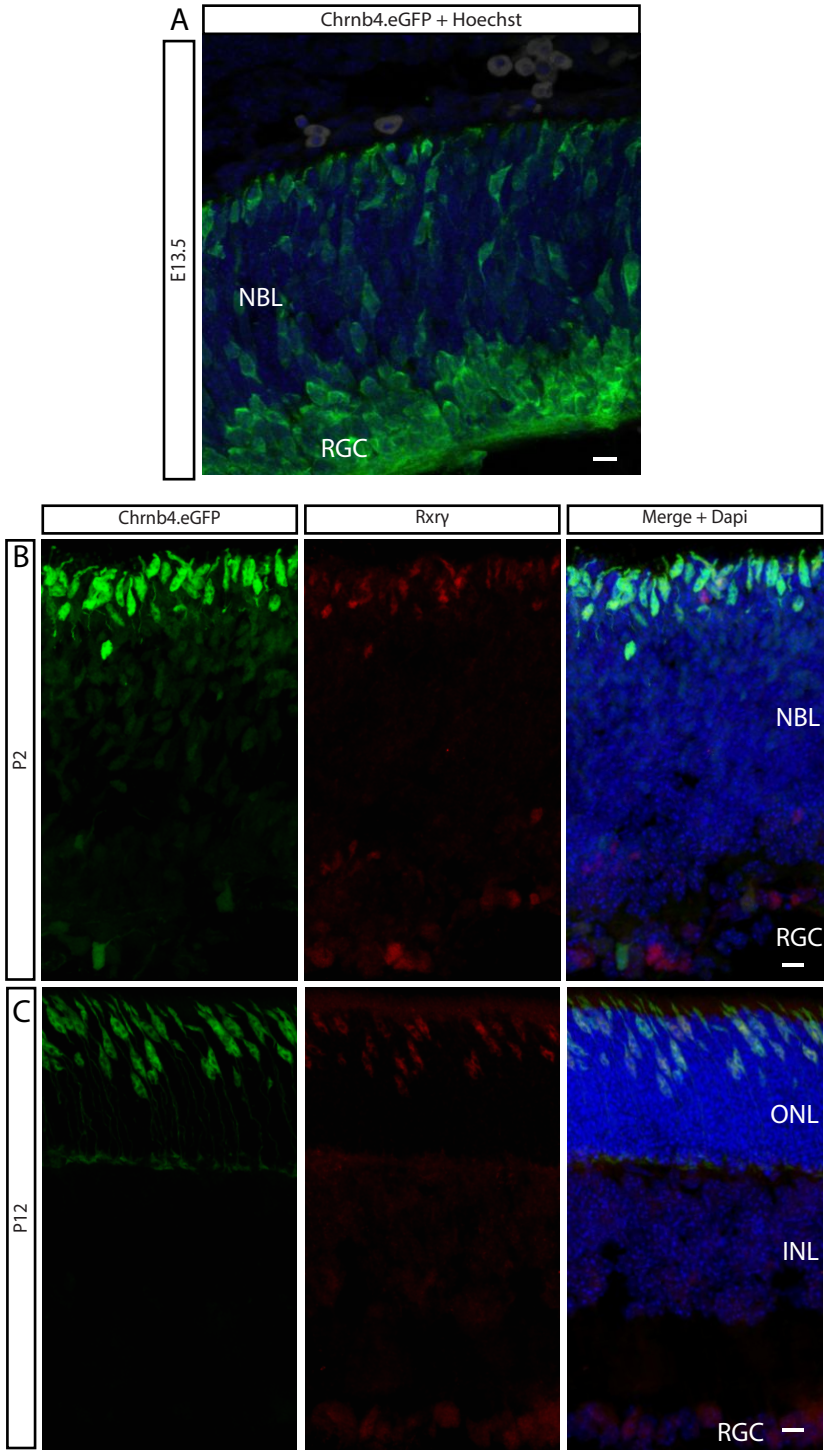

Figure 3.2 Characterisation of the Chrnb4.eGFP mouse. (**A-C**) Initially obtained tissue from Chrnb4.eGFP retinas (kind gift of B Roska) showed clearly identifiable GFP-expressing cells in the ONL at P8 (C) which colocalised with Rxrγ, indicating that these are cone precursors. At E13.5 (A, picture sent by B Roska's group) large numbers of brightly GFP expressing cells were seen, including strongly in the developing retinal ganglion cell layer. At P2 (B) despite a large number of weakly GFP expressing cells, a distinct population of bright cells were seen at the apical edge of the ONL which also colocalised with Rxrγ. Scale bars are 10µm.

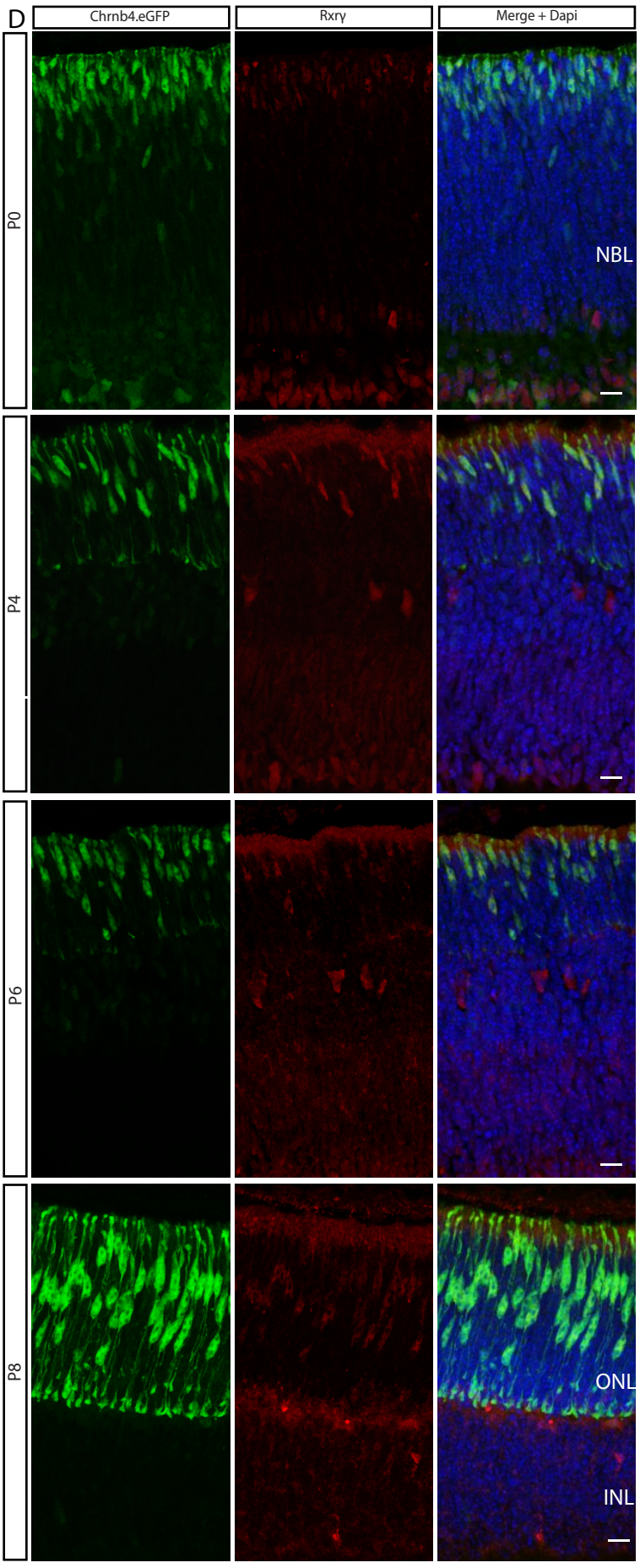

D-D' After acquisition of this model, brightly GFP expressing cells colocalising for Rxrγ were seen in the ONL (or equivalently, the neuroblastic layer) at every postnatal age, and Adult. This indicated that the Chrnb4.eGFP could be used to identify cone photoreceptors and precursors at a variety of ages. Note also the appearance of the cone photoreceptor nuclei at developing and adult stages, showing the characteristic multiple points of condensed heterochromatin. Scale bars are 10µm.

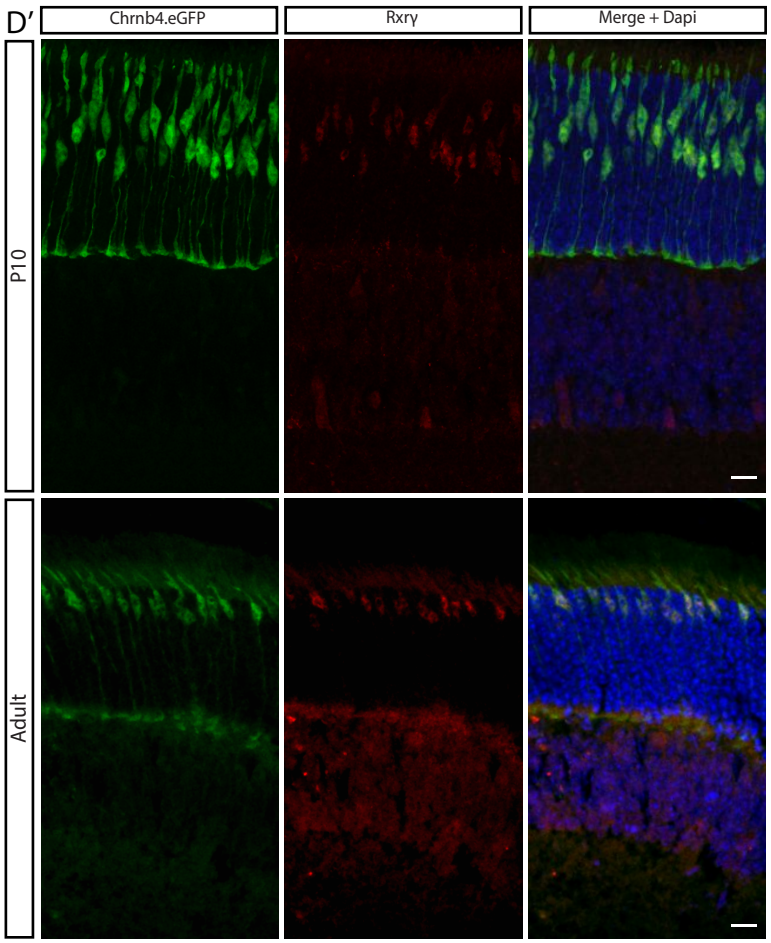

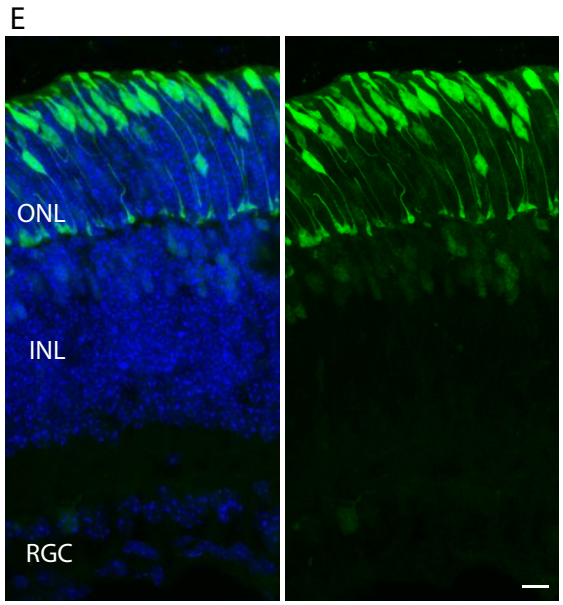

E FACS analysis of P8 Chrnb4.eGFP cells. shows a clear population of very bright GFP cell (GFP pos), as well as a population which does not express GFP. A large population of intermediate cells were found dimly labelling for GFP. These results correlate to observations made in fixed tissue from mice of this age, which have a large number of cells expressing low levels of GFP, in the ONL, INL and RGC layers. As shown in section 3.2.2.2, the brightly GFP expressing cells are the cone precursors.

FACS analysis of P8 Chrnb4.eGFP retinal tissue showed, as indicated from the histological assessments, a small population of brightly GFP+ cells, around 2% of live cells, with two other, larger populations: one weakly GFP+ and the other GFP negative (see Fig 3.2). These three populations were easily separable at this age, and were used for future purposes whenever cone photoreceptor precursors were needed.

Tissue from P8 and adult (6w) Chrnb4 eyes was taken and immunostained to assess for the presence of different cone markers: Cone arrestin, S-opsin, Gnat2 and Rxrγ (see Fig 3.3, images taken by F Di Marco). Each of these markers colocalised with the brightly GFP+ cells at both ages, although Gnat2 expression was less clear in the cone precursor cells at P8, compared to 6w.

At later adult stages (6 months), however, a reduction in GFP expression was seen (Figure 3.3), and many cells that were positive for cone markers apparently no longer expressing GFP. This difference was most apparent in the central retina nearest the optic nerve, with very few GFP+ cells remaining, while some GFP+ cells remained in the peripheral retina.

3.2.2.2 Quantitative PCR analysis of GFP-expressing populations

To further confirm that the Chrnb4.eGFP model could be used to effectively isolate cone precursor cells at developmental ages, the transcriptomes of fluorescence-sorted Chrnb4.eGFP expressing cells were assessed using quantitative PCR, as described in Chapter 2. Retinas from P8, 3 week old and adult (5-9 week old) mice were isolated and dissociated using Papain digestion into a single cell suspension. These cells were fluorescence-sorted to enrich the population which most brightly expressed GFP. mRNA was prepared from this GFP+ population, and subsequently

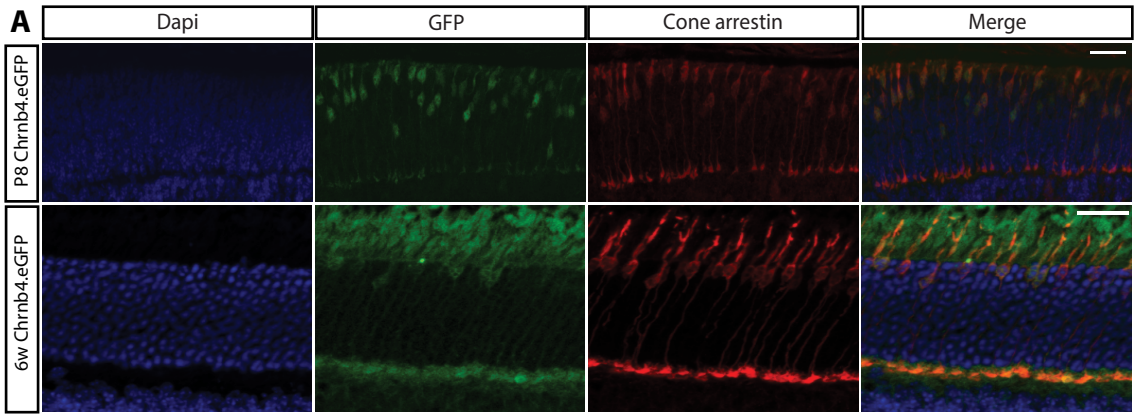
A
Dapi
GFP
Cone arrestin
Merge
P8 Chrnb4.eGFP
6w Chrnb4.eGFP

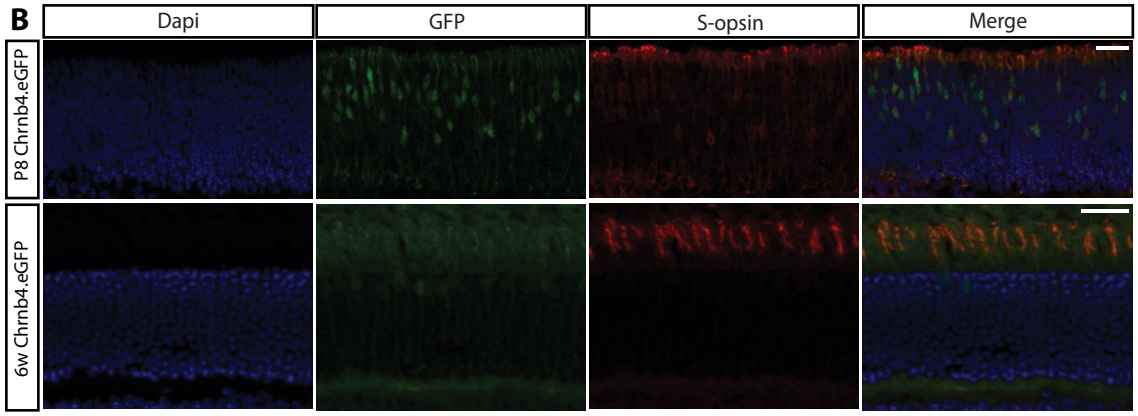
B
Dapi
GFP
S-opsin
Merge
P8 Chrnb4.eGFP
6w Chrnb4.eGFP

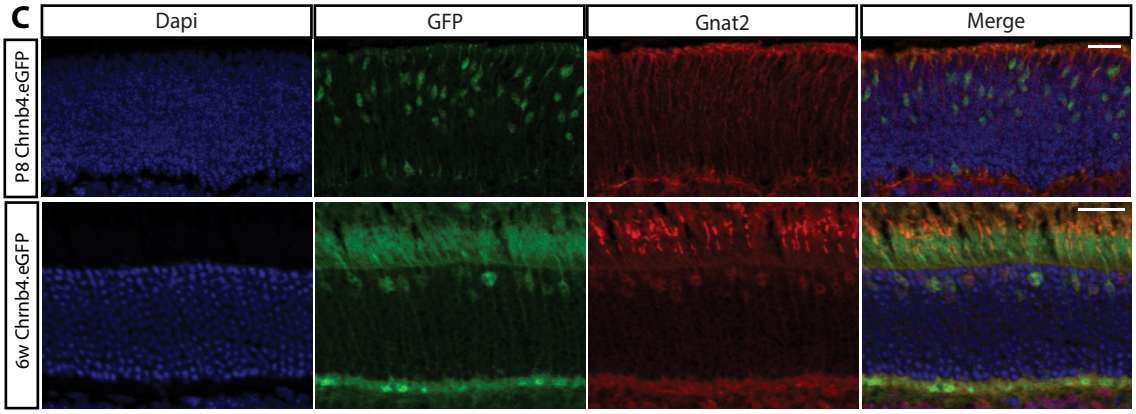
C
Dapi
GFP
Gnat2
Merge
P8 Chrnb4.eGFP
6w Chrnb4.eGFP

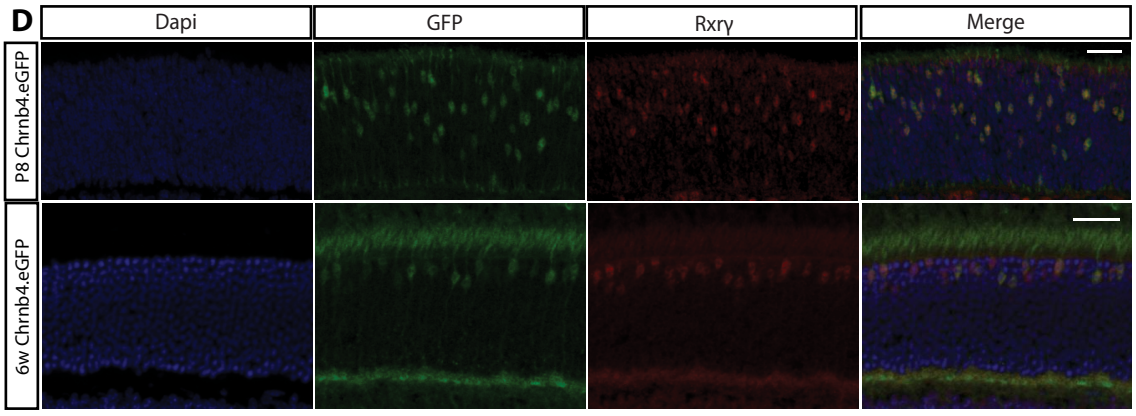
D
Dapi
GFP
Rxrγ
Merge
P8 Chrnb4.eGFP
6w Chrnb4.eGFP

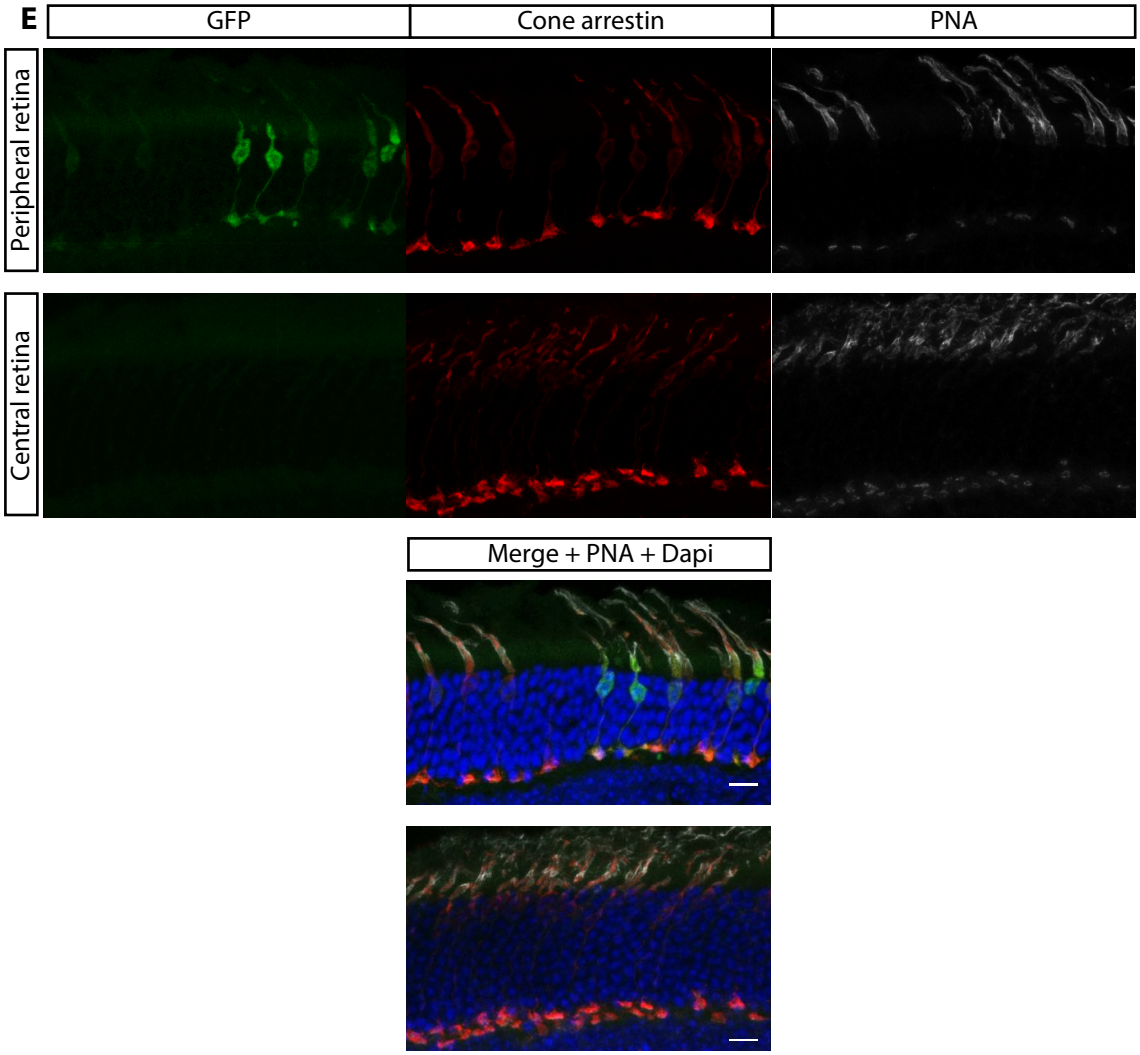

Figure 3.3 A-D Expression of various cone-specific markers in P8 and adult (6 week) Chrnb4.eGFP retina (thanks to Dr Fabiana di Marco for these images). GFP expressing cone photoreceptors can be seen stained with all markers at Adult ages. While at P8 GFP positive cells do not appear to stain clearly with Gnat2, all other markers label this cell population at this age. Scale bars are 20µm.

E Images from 6 month old adult Chrnb4.eGFP retinas show that GFP expression declines over time, with this reduction most obvious in the central retina which retains almost no GFP positive cells, but cone arrestin and PNA positive cells which are not positive for GFP can also be seen in the peripheral retina. Scale bars are 10µm.

converted to cDNA. Rod photoreceptor cDNA samples were also prepared in the same way using age-matched NrlGFP mice.

These cDNA preparations were analysed by qPCR. A number of cone-specific markers and rod-specific markers were chosen for assessment. To investigate cone identity, primers for *Rxrγ*, *Chrnb4*, *Thrβ2*, *Arr3*, *Opn1sw* and *Opn1mw* were used, as detailed above. To assess rod identity, primers for Rhodopsin (*Rho)*, and the rod-specific transcription factors *Nrl* and *Nr2e3* (Mears et al., 2001; Milam and Rose, 2002; Swaroop et al., 2010) were also designed. Primers for the cone-rod homeobox protein (*Crx*) were used as a photoreceptor marker not specific to cone or rod cells. In this, and later experiments, samples showing an expression level of less than 5% of the Crx expression found in comparable NrlGFP cell populations were disqualified as indicative of nucleic acid degeneration or a failure of reverse transcription (1 sample).

Quantification was carried out for this and subsequent experiments (see sections 3.2.4.2 and 3.2.5.2) relative to the expression of each gene analysed in NrlGFP rod photoreceptors. This includes the expression of cone genes, which, while expressed only at low levels in rod photoreceptors, could still be reliably identified in these cells, and it was decided that it was preferable to use NrlGFP cells as a control, rather than the newer cell populations assessed in these experiments, particularly as a primary aim of these experiments was to determine whether cells of different genotypes could be effectively isolated in these models.

For this analysis, different samples were collected from separate mouse litters, within which dissociated cells were pooled before sorting. Due to this, as well as the need for sorted cells for other purposes, it was not feasible to have a minimum number of more than 3 samples for all groups. Comparisons are made on the basis

of groups of genes classified *ab initio* as rod genes (*Nrl*, *Nr2e3*, *Rho*) or cone genes (*Rxrγ*, *Chrnb4*, *Thrβ2*, *Arr3*, *Opn1sw* and *Opn1mw*). Differences in the expression of these markers between cell types taken as a group are studied, using a two-way ANOVA, in which the sources of variation were the cell source used, and the gene studied. Therefore, for each comparison of either rod or cone marker genes, an effect of Cell indicated that the expression of these genes changed in the studied cell source compared to the control cells, and an effect of Gene meant that different genes were expressed at different levels. An interaction between these two meant that the change in expression due to the cell source used varied for different genes. Subsequent Bonferroni-corrected statistical tests to find individual differences on the single gene level were carried out, but it should be noted that statistical power is substantially reduced by the need to correct for multiple comparisons.

The results, along with those for different sources of cells, are shown in Figure 3.4 and will be discussed in detail below. This graph shows the data as a base-2 logarithmic fold change as calculated by the -ΔΔCt method, and these numbers were also used for statistical comparisons. Expression of each gene was normalised to β-actin, and then the average value given by the NrlGFP cells was set to zero. Differences therefore represent the fold change in expression as a power of two, with for example a value of 2 representing a four-fold increase. Using this measure has the effect of increasing the symmetry of the data, with reductions in expression given the same weight as increases, compared to using percentage values (Willems et al., 2008).

Crx, as a general photoreceptor marker gene, was compared separately from others as a control, as shown in Figure 3.4B and E. For P8 cells, Crx expression was not significantly different between Chrnb4.eGFP and NrlGFP cells $t(9) = 2.035$, $p = 0.0724$, with N = 5 samples for NrlGFP and 6 samples for Chrnb4.eGFP cells in this

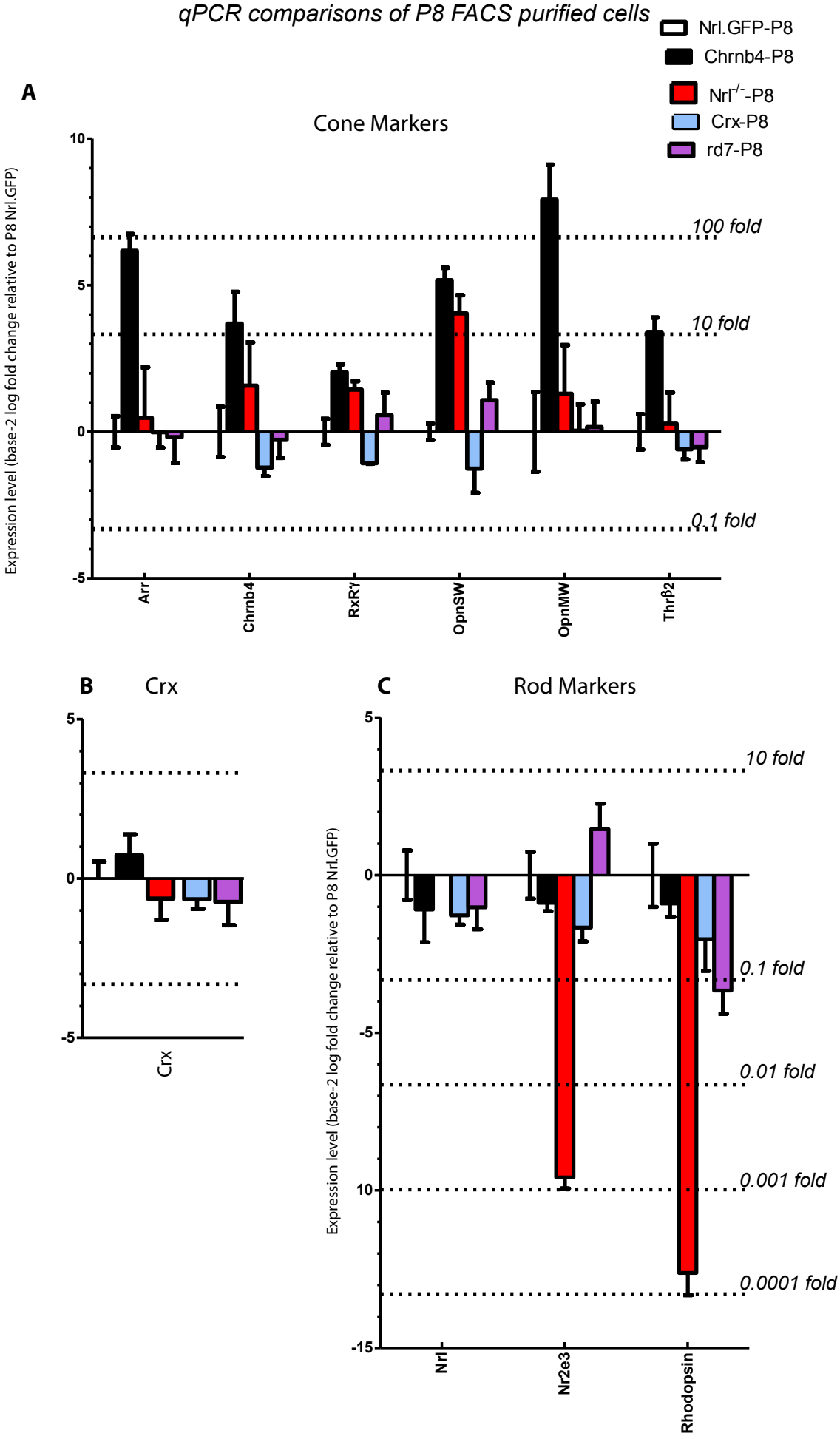
qPCR comparisons of P8 FACS purified cells
Nrl.GFP-P8
Chrnb4-P8
Nrl-/--P8
Crx-P8
rd7-P8
A
Cone Markers
Expression level (base-2 log fold change relative to P8 Nrl.GFP)
100 fold
10 fold
0.1 fold
Arr
Chrnb4
RxRγ
OpnSW
OpnMW
Thrβ2
B
Crx
Crx
C
Rod Markers
10 fold
0.1 fold
0.01 fold
0.001 fold
0.0001 fold
Nrl
Nr2e3
Rhodopsin

qPCR comparisons of 3 week and Adult FACS purified cells

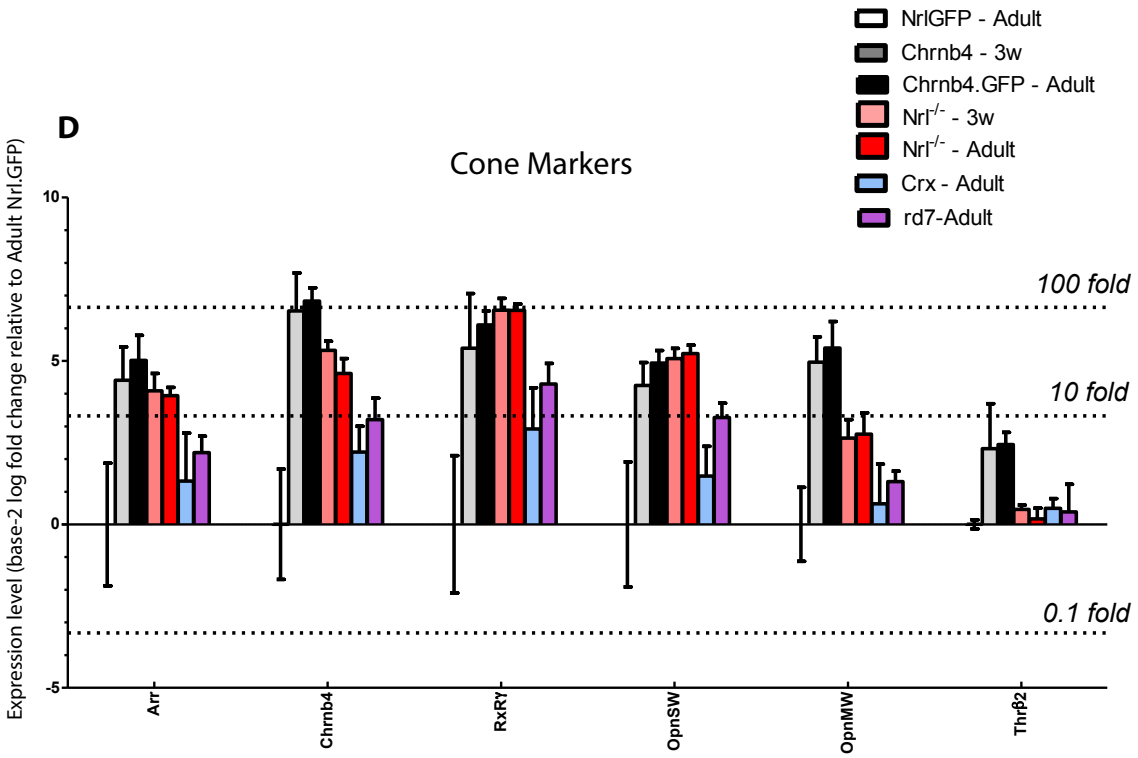

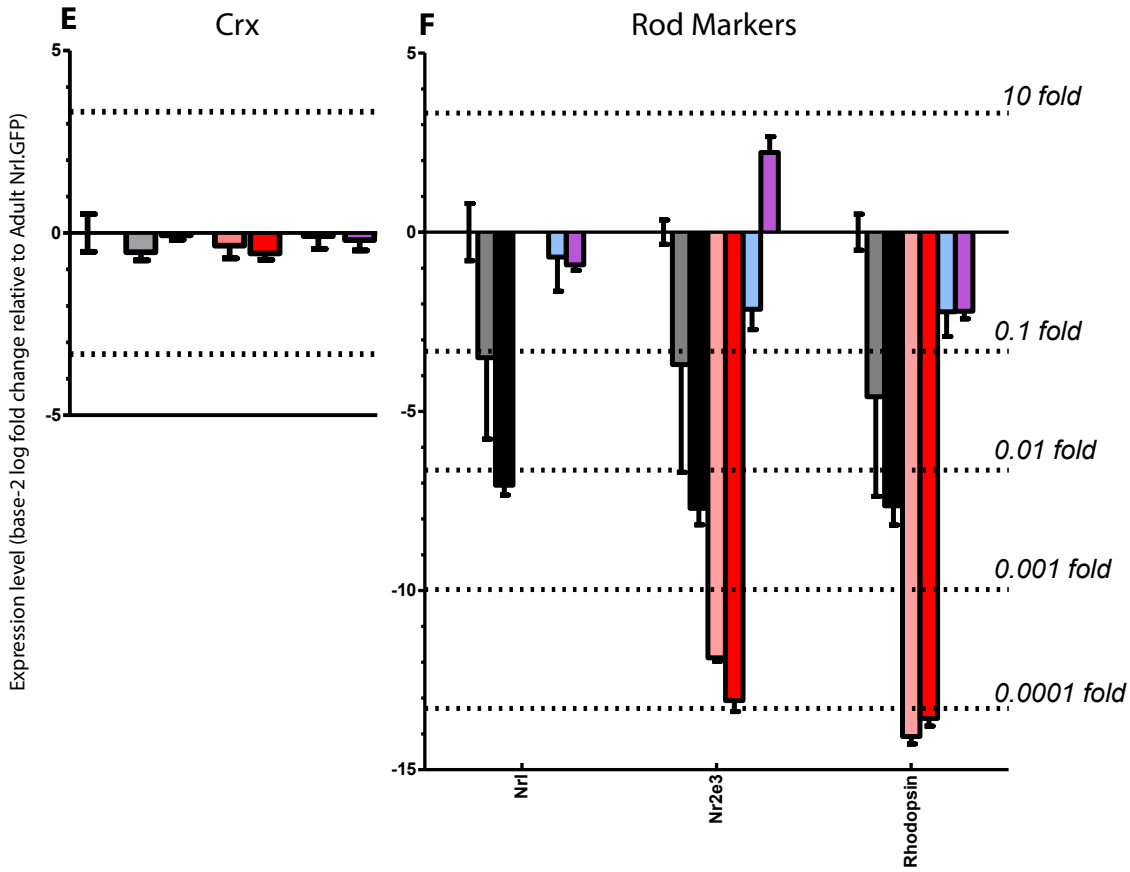

Figure 3.4

qPCR comparisons of the expression of various photoreceptor-specific marker genes in developing (P8) and Adult FACS purified cells.

Adult cells are taken from mice between 5.5 and 9 weeks old. Values given are -ΔΔCt, the difference in signal detection found for the gene and the housekeeping gene β-actin, compared to that in NrlGFP cells of similar age, set to zero. This corresponds to the base-2 log of the fold change, the scale therefore being logarithmic. For comparison, the equivalent fold change in powers of 10 has been included. Measurements were taken as the means of duplicates and the plotted values are +/- standard deviation.

Cell sources chosen for comparison are cone photoreceptors from Chrnb4.eGFP retinas (Chrnb4), cone like photoreceptors from $Nrl^{-/-}$NrlGFP ($Nrl^{-/-}$), a mixed photoreceptor population from CrxGFP (Crx) and a mixed photoreceptor population with increased numbers of cone like cells from $Nr2e3^{rd7/rd7}$CrxGFP (rd7). For Chrnb4 and $Nrl^{-/-}$ cells, 3 week old cells were also obtained and compared with Adult NrlGFP cells.

The genes assessed are separated into cone markers (A, D) and rod markers (C, F). Crx was selected as a control for its expression in all photoreceptors (B, E).

Groupwise (separated into rod and cone markers, and for P8 and older cells) and individual comparisons can be found in the main text. Separate comparisons with NrlGFP cells were made with Chrnb4, and with $Nrl^{-/-}$ cells. rd7 cells were compared with Crx cells as a closer control.

comparison and those below. In older cells, Crx expression was again not significantly different: a one way ANOVA revealed no effect of group $H(2,8) = 2.024$, $p = 0.2129$, with Dunnett's Multiple Comparison Test, comparing both ages of Chrnb4.eGFP cells with NrlGFP cells, finding no significant differences at $p = 0.05$, with $N = 3$ samples for each cell type.

Cone markers

These results are shown in Figure 3.4A and D. Statistical comparisons for P8 cells are shown in Table 3.2a, and those for older cells in Table 3.2b. For P8 cells, while the existence of an interaction makes it difficult to discern specific effects the results indicated that cone marker expression is higher in the Chrnb4.eGFP cells, and for each gene. In older cells, a similar pattern of results was found, indicating that cone markers were in general expressed at higher levels in Chrnb4.eGFP cells, with only *Thrβ2* not significantly differently expressed, likely as a result of the necessary corrections.

These results show that the cells obtained from the Chrnb4.eGFP model are enriched in the expression of cone marker genes, and it is therefore likely that they are cone photoreceptors. The data from P8 cells show that this cone marker identity is specified at postnatal ages or before.

Table 3.2a qPCR comparisons of cone marker expression between P8 Chrnb4.eGFP and P8 NrlGFP flow sorted cells

Chrnb4.eGFP - P8						
Cone markers						
Effects						
Cell		Gene		Interaction		
F(1,54)	p	F(5,54)	p	F(5,54)	p	
636.62	<0.0001 ****	21.39	<0.0001 ****	21.39	<0.0001 ****	
Post-test comparisons (Bonferroni-corrected) – significance with p values						
Arr	Chrnb4	Rxrγ	OpnSW	OpnMW	Thrβ2	
<0.0001	<0.0001	<0.001	<0.0001	<0.0001	<0.0001	

Table 3.2b qPCR comparisons of cone marker expression between 3 week and adult Chrnb4.eGFP and adult NrlGFP flow sorted cells

Chrnb4.eGFP – 3 weeks and adult							
Cone markers							
Effects							
Cell		Gene		Interaction			
F(2,36)	p	F(5,36)	p	F(10,36)	p		
100.46	<0.0001 ****	5.83	0.0005 ***	1.49	0.1840 n.s		
Post-test comparisons (Bonferroni-corrected) – significance with p values							
	Arr	Chrnb4	Rxrγ	OpnSW	OpnMW	Thrβ2	
3 weeks	<0.001	<0.0001	<0.0001	<0.01	<0.001	n.s	
Adult	<0.001	<0.0001	<0.0001	<0.001	<0.0001	n.s	

These tables show the results of two-way ANOVAs comparing Chrnb4.eGFP and NrlGFP flow sorted cells, with the effects of Cell type, Gene, and the interaction between the two, and post-test comparisons. Statistical comparisons are made with using the base-2 log of the fold change of expression, as shown in Figure 3.4.

Rod markers

Statistical comparisons for P8 cells are shown in Table 3.3a, and those for older cells in Table 3.3b. Results are also shown in Figure 3.4C and F.

Table 3.3a qPCR comparisons of rod marker expression between P8 Chrnb4.eGFP and P8 NrlGFP flow sorted cells

Chrnb4.eGFP - P8	Rod markers					
	Effects					
	Cell		Gene		Interaction	
	F(1,27)	p	F(2,27)	p	F(2,27)	p
	13.00	0.0012 **	0.06	0.9384 n.s	0.07	0.9360
	Post-test comparisons (Bonferroni-corrected) – significance with p values					
	Nrl		Nr2e3		Rhodopsin	
	n.s		n.s		n.s	

Table 3.3b qPCR comparisons of rod marker expression between 3 week and adult Chrnb4.eGFP and adult NrlGFP flow sorted cells

Chrnb4.eGFP – 3 weeks and adult	Rod markers					
	Effects					
	Cell		Gene		Interaction	
	F(2,18)	p	F(2,18)	p	F(2,18)	p
	48.11	<0.0001	0.27	0.7694	0.13	0.9679
	Post-test comparisons (Bonferroni-corrected) – significance with p values					
		Nrl		Nr2e3		Rhodopsin
	3 weeks	n.s		n.s		<0.05
	Adult	<0.001		<0.0001		<0.001

For P8 cells, the results indicated that overall, rod marker expression is lower in the Chrnb4.eGFP cells than in NrlGFP cells, and that this difference is approximately similar for each gene assessed. The lack of significant differences in post-test comparisons suggests that these differences are relatively small, but consistent when taken as a whole. With older cells, rod markers were again shown to be different in Chrnb4.eGFP cells. However, while in adult cells all rod markers were significantly reduced compared to NrlGFP cells in individual comparisons, with 3 week old cells only Rhodopsin was shown to be significantly different.

As shown here, the expression levels in P8 Chrnb4.eGFP+ cells of the rod-specific markers *Rho, Nrl* and *Nr2e3* were unexpectedly relatively high at approximately 50% of the expression shown in P8 NrlGFP+ cells for all markers studied. This compares with approximate increases in the expression of cone marker genes of between 4- and 300-fold (see Figure 3.4A). Furthermore, these results suggest that even at 3 weeks of age, when the retina is formed and fully functional, the expression of rod markers in the Chrnb4.eGFP+ population was reduced compared to NrlGFP+ cells, but still relatively high. By later adult ages, however, the expression of these rod markers had declined.

3.2.3 Characterisation of the OPN1LW-eGFP mouse

As mentioned above, a transgenic mouse model has been developed taht labels M-opsin expressing cone photoreceptors by the action of a 5' regulatory sequence taken from the human red and green visual pigment genes (OPN1LW). This model had been previously acquired and was therefore investigated for suitability for the experiments proposed for this thesis.

3.2.3.1 GFP expression and immunofluorescence

As detailed above, developmental qPCR data indicated that the onset of Opn1mw expression occurred in the murine retina at around P12, with expression levels very low before this. Eyes were taken from mice of this model at postnatal days 2, 4, 6, 8, 10 and 12, and adult age P21, fixed with PFA and immunostained for GFP in a different wavelength to ascertain whether there were cells expressing GFP too weakly to be seen (using a rabbit polyclonal antibody subsequently labelled with a secondary fluorescent antibody, see Chapter 2.3 and Table 2.2). Histological analysis of these eyes, consistent with the qPCR data, from the OPN1LW-eGFP

model showed that fluorescent cells before postnatal day 4 (P4) could not be seen, and even after this were very few in number until P12, as can be seen in Figure 3.5, and the cells which could be seen were primarily restricted to the dorsal retina. This corresponds to the qPCR data shown in section 3.2.1.1, which showed that the onset of *Opn1mw* expression occurs late, with expression levels very low until approximately P8.

These data were gathered historically, and the OPN1LW-eGFP mouse line was subsequently lost from the facility after the experiments detailed above and in Section 4.2.2.

3.2.4 Characterisation of the Nrl$^{-/-}$.NrlGFP mouse

It was not possible, due to animal facility limitations, to use the CrxGFP reporter gene to label photoreceptor precursor cells for these, and following, experiments. The NrlGFP reporter gene used in previous transplantation experiments concerning rod photoreceptor precursors (MacLaren et al. 2006; Pearson et al. 2012; West et al. 2012; Warre-Cornish et al. 2014) was selected for use instead. The NrlGFP mouse was cross-bred with the Nrl$^{-/-}$ model onsite (thanks to Dr Claire Hippert who cross-bred these models).

3.2.4.1 GFP expression and Immunofluorescence

In the NrlGFP mouse, GFP has been shown to be expressed very shortly after terminal mitosis (Akimoto et al., 2006). GFP+ populations were found by FACS in Nrl$^{-/-}$NrlGFP populations as early as E15.5, and this population made up 3-5% of the total population of single cells at this age. At P1, this proportion was approximately 12% and by P8, approximately 50%.

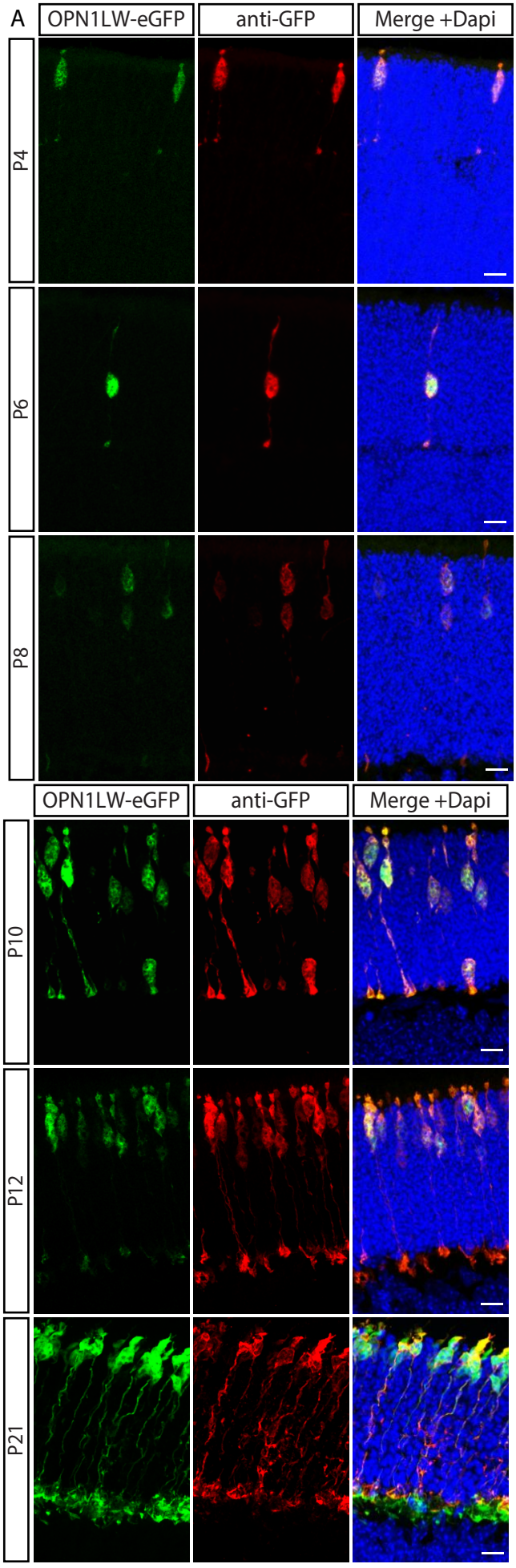
A
OPN1LW-eGFP
anti-GFP
Merge +Dapi
P4
P6
P8
OPN1LW-eGFP
anti-GFP
Merge +Dapi
P10
P12
P21

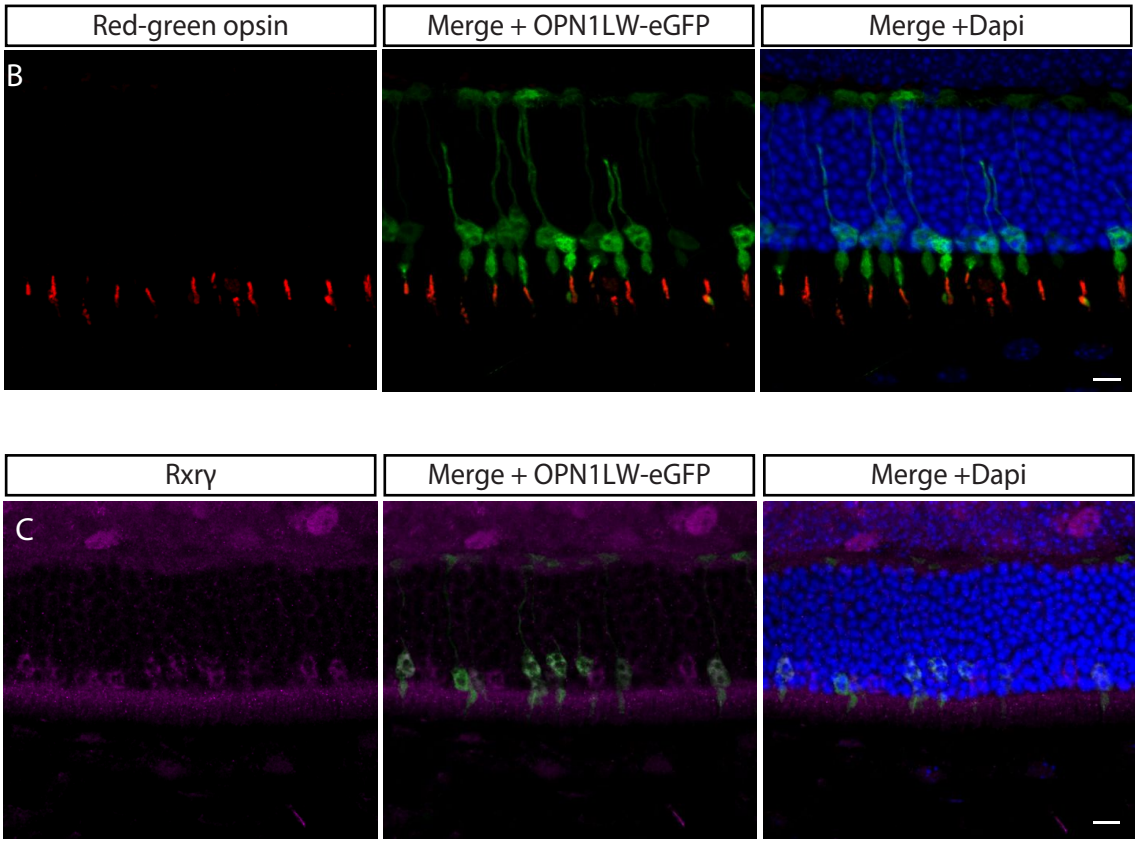

Figure 3.5 The OPN1LW-eGFP line. **A** Images from the retina of these mice taken at various postnatal ages show that at early stages very few GFP-expressing cone precursors can be seen in the ONL, with none seen prior to postnatal day 4. Immunostaining for GFP did not indicate that there were cells expressing GFP too weakly to be seen. At later stages cone photoreceptors were seen to express GFP in higher numbers. Scale bars are 10μm (approx). **B-C** Images of adult OPN1LW-eGFP retinas show colocalisation with cone markers. These figures from Dr A Barber.

Although the majority of GFP expressing cone cells are positive for the red green mouse opsin (B), some do not appear to colocalise with this protein, and similarly not all labelled outer segments are associated with a GFP expressing cell. However, as weakly GFP-expressing synaptic end feets can be seen opposite segments labelled for this protein, it may be the case that these cells lose GFP fluorescence over time.

Staining for Rxrγ (C) further shows that not all cone cells labelled with this protein express GFP.

Isolation of the cone-like cells only by use of the NrlGFP reporter gene allowed exclusion of the true cones, which also exist in the $Nrl^{-/-}$ model. However, some evidence of a loss of GFP signal was seen in the $Nrl^{-/-}$/NrlGFP model over time. Images taken from older retinas (10 months old) show a reduction in GFP expression (Figure 3.6E), with some bright GFP+ cells remaining but many others showing a low or absent fluorescent signal. In particular, images taken from the central retina, near the optic nerve, showed a more marked decline in fluorescence compared to images from the peripheral retina. This could be due to repression of the Nrl promoter in these cells as they become fully mature and more strongly committed to a cone-like fate, as this decline in GFP expression does not happen so noticeably in the NrlGFP model. For this reason, however, a termination time of 2 weeks post-transplantation was chosen for use in future transplantation experiments. Previous studies have shown no difference in transplantation outcome with a post-injection interval of 2 weeks, compared to 3 weeks (Warre-Cornish et al., 2014).

Tissue from P8 and adult (6w) $Nrl^{-/-}$/NrlGFP eyes was taken and immunostained to assess for the presence of different cone markers: Cone arrestin, S-opsin, Gnat2 and Rxrγ (see Fig 3.6, these images taken by F Di Marco). Cone marker expression can be seen at very high levels at adult stages, for all markers chosen, and the shorter outer segments characteristic of this model can be clearly seen (Daniele et al., 2005). In P8 tissue, while S-opsin and Gnat2 are clearly visible, and Rxrγ labels the whole of the ONL, Cone arrestin appears to primarily label a discrete population of cells, most likely representing the remaining true cones in this model, as they do not appear to be positive for NrlGFP expression, while the cone-like cells have presumably not yet reached the necessary stage of cone development, as the expression of cone arrestin was widespread in the adult. Attempts to measure the

extent to which cone-like cells differ from true cones are addressed in the next section.

3.2.4.2 Quantitative PCR analysis of GFP-expressing populations

The developmental progression of Nrl$^{-/-}$ photoreceptors, as cells which would otherwise develop as rods except for an inability to produce Nrl, is not wholly clear. In the normal retina, rod and cone photoreceptors are produced at different times, and mature at different rates, as evidenced by the difference in their onset of a migratory phase.

The transcriptome of the Nrl$^{-/-}$ mouse has been studied before using whole retinal preparations (Yoshida et al., 2004), finding 161 genes differentially expressed from wild type retina. However, another study (Akimoto et al., 2006) used fluorescence-sorted cells from the Nrl$^{-/-}$/NrlGFP mouse and compared them to rod cells from the NrlGFP mouse. They found significantly more genes to be differentially expressed in these purified populations than in whole retinal samples. Genes such as *Opn1sw*, *Gnb3*, and *Elovl2* had increased expression in the Nrl$^{-/-}$ cells, whereas the expression of *Rho*, *Nr2e3*, *Pde6b* and *Nrl* were reduced relative to NrlGFP rods. This study also looked at several developmental ages and found that these differences generally arose between P2 and P6.

For the purposes of this project, it was decided to verify the expression levels of the cone-specific genes examined in section 3.

The transcriptomes of P8, 3 week old and adult (5-9 week old) fluorescence-sorted Nrl$^{-/-}$NrlGFP expressing cells were assessed using quantitative PCR, using the same methods as described in section 3.2.2.2 and likewise compared to NrlGFP

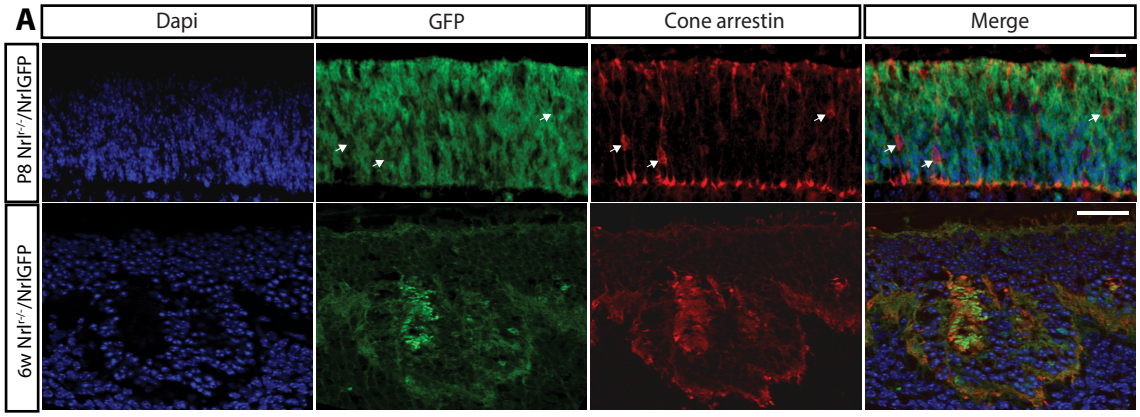
A
Dapi
GFP
Cone arrestin
Merge
P8 Nrl-/-/NrlGFP
6w Nrl-/-/NrlGFP

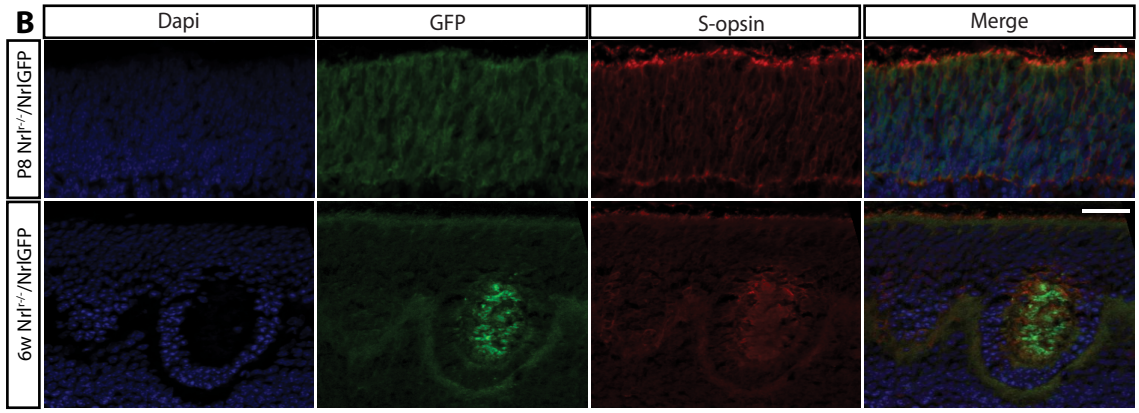
B
Dapi
GFP
S-opsin
Merge
P8 Nrl-/-/NrlGFP
6w Nrl-/-/NrlGFP

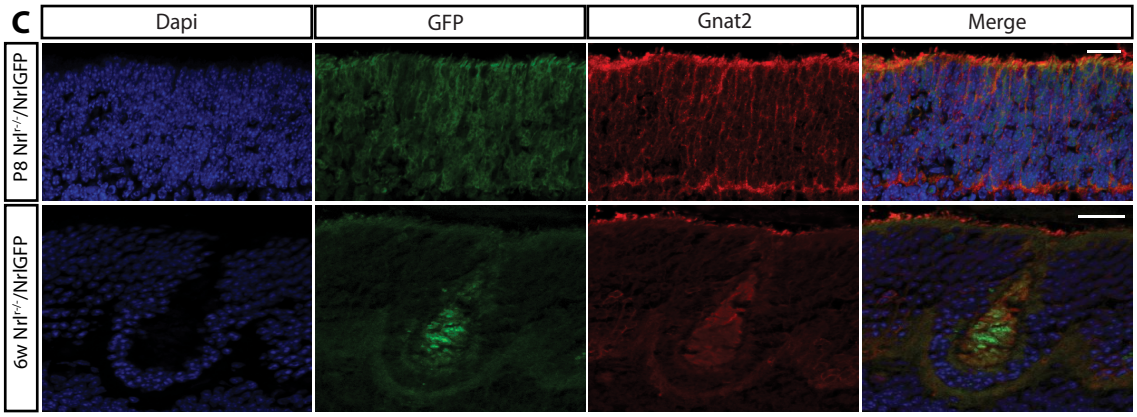
C
Dapi
GFP
Gnat2
Merge
P8 Nrl-/-/NrlGFP
6w Nrl-/-/NrlGFP

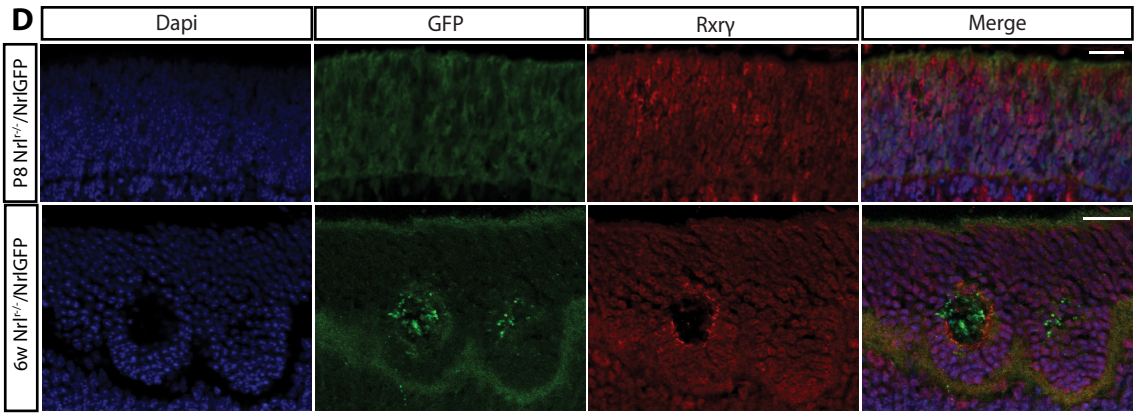
D
Dapi
GFP
Rxrγ
Merge
P8 Nrl-/-/NrlGFP
6w Nrl-/-/NrlGFP

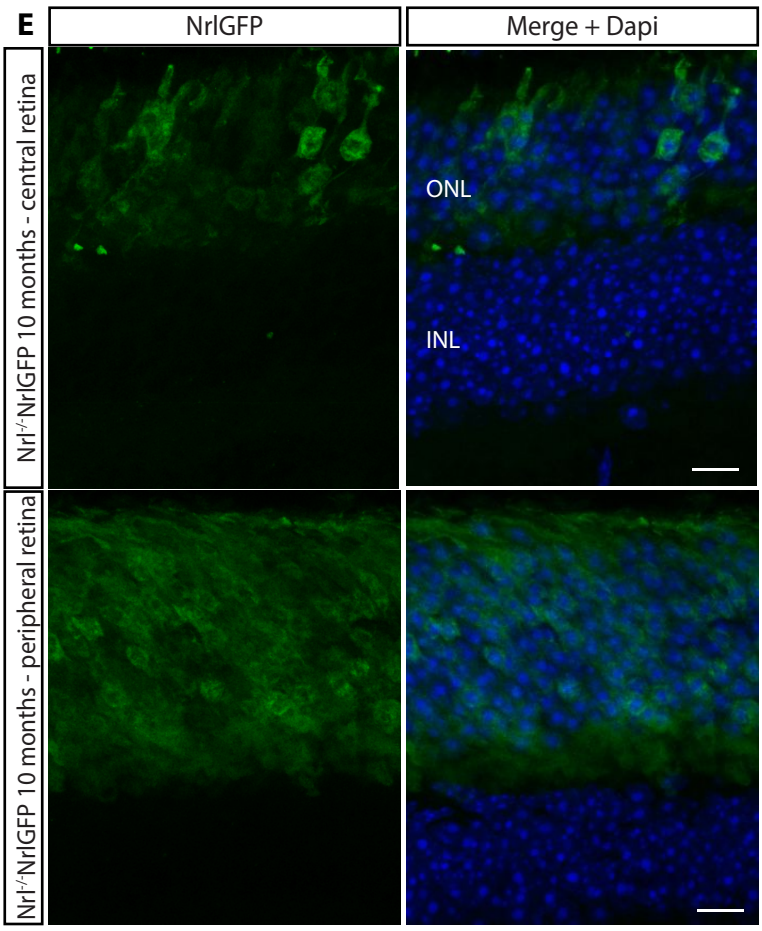

Figure 3.6 A-D Expression of various cone-specific markers in P8 and adult (6 week) $Nrl^{-/-}$Nrl-GFP retina (thanks to Dr Fabiana di Marco for these images).

At P8, cone arrestin (A) labels only a subset of the cells in the ONL, most likely the true cones remaining in this model, as they do not appear to express NrlGFP (white arrows). S-opsin (B) and Gnat2 (C) are clearly visible at this age, while Rxrγ (D) labels the whole of the ONL in P8 tissue. In adult retina, cone markers are ubiquitous in and around the ONL (compare with Figure 3.3).

Rosettes typical of this model can also be seen in these retinas, with GFP and cone marker signal visible inside. Scale bars are 20µm.

E $Nrl^{-/-}$NrlGFP retinas at later ages show a decline in the expression of GFP. At 10 months GFP signal is reduced in many cells and absent in others in the ONL of the central retina, although cells clearly labelling with GFP remain. Expression is maintained more strongly in the peripheral retina, with the majority seen to express GFP. Scale bars are 10µm.

sorted cells of the same age. Expression levels are shown together with those for the other cell types analysed in this chapter in Figure 3.4.

Expression of Crx was not significantly different between P8 Nrl$^{-/-}$NrlGFP cells and P8 NrlGFP cells $t(7) = 1.586$, $p = 0.1567$, with N = 5 samples for NrlGFP and 4 samples for Nrl$^{-/-}$NrlGFP cells in this comparison and those below. In older cells, Crx expression was again not significantly different: a one way ANOVA revealed no effect of group $H(2,8) = 1.472$, $p = 0.3019$, with Dunnett's Multiple Comparison Test, comparing both ages of Nrl$^{-/-}$NrlGFP cells with NrlGFP cells, finding no significant differences at $p = 0.05$, with N = 3 samples for each cell type.

Cone markers

These results are shown in Figure 3.4A and D. Statistical comparisons for P8 cells are shown in Table 3.4a, and those for older cells in Table 3.4b.

Table 3.4a qPCR comparisons of cone marker expression between P8 Nrl$^{-/-}$NrlGFP and P8 NrlGFP flow sorted cells

Nrl$^{-/-}$NrlGFP - P8	**Cone markers**					
	Effects					
	Cell		Gene		Interaction	
	F(1,42)	p	F(5,42)	p	F(5,42)	P
	30.37	<0.0001	3.97	<0.0049	3.97	0.0049
	Post-test comparisons (Bonferroni-corrected) – significance with p values					
	Arr	Chrnb4	Rxrγ	OpnSW	OpnMW	Thrβ2
	n.s	n.s	n.s	<0.0001	n.s	n.s

Table 3.4b qPCR comparisons of cone marker expression between 3 week and adult Nrl$^{-/-}$NrlGFP and adult NrlGFP flow sorted cells

Nrl$^{-/-}$NrlGFP – 3 weeks and adult	**Cone markers**						
	Effects						
	Cell		Gene		Interaction		
	F(2,36)	p	F(5,36)	p	F(10,36)	p	
	95.81	<0.0001 ****	19.67	<0.0001 ****	5.00	0.0002 ***	
	Post-test comparisons (Bonferroni-corrected) – significance with p values						
		Arr	Chrnb4	Rxrγ	OpnSW	OpnMW	Thrβ2
	3 weeks	<0.001	<0.0001	<0.0001	<0.0001	<0.05	n.s
	Adult	<0.001	<0.0001	<0.0001	<0.0001	<0.05	n.s

For P8, the results show that overall, cone marker expression is higher in Nrl$^{-/-}$ NrlGFP cells than in NrlGFP cells, but that most individual comparisons are not significant. In older cells, expression is again overall higher in Nrl$^{-/-}$NrlGFP cells than in NrlGFP cells. However, for both ages of older Nrl$^{-/-}$NrlGFP cell, *Thrβ* expression was not significantly increased relative to NrlGFP cells, according to individual comparisons. While these results are subject to the same caveats regarding the power of corrected comparisons as others, it makes sense that this gene would not be upregulated in the Nrl$^{-/-}$ mouse, as the cone-like cells produced by this model are primarily S-opsin expressing, and Thrβ is thought to be involved with the induction of M-opsin expression (Ng et al., 2009). M-opsin, while upregulated in the Nrl$^{-/-}$ cells, similarly did not seem to be increased to the same extent as was seen in Chrnb4.eGFP cells.

Rod markers

NB. For these genes, Nrl was not detected at all in the majority of preparations of Nrl$^{-/-}$ cells (2 out of 4 for P8 cells, 2 out of 3 for 3 week cells, 3 out of 3 Adult cells), and when a signal could be found it was at negligible levels, most likely due to very low levels of contamination and/or non-specific amplification. These values were between -14 and -18, which would represent fold reductions of approximately 18000

and 250000. Given this, it was concluded that Nrl was not truly present in these samples, and Nrl was excluded from further analysis and not given a value in Figure 3.4C and F, noting that this changes the comparisons relative to other cell types.

Figure 3.4C and F shows the results of these experiments. Statistical comparisons for P8 cells are shown in Table 3.5a, and those for older cells in Table 3.5b.

Table 3.5a qPCR comparisons of rod marker expression between P8 Nrl$^{-/-}$NrlGFP and P8 NrlGFP flow sorted cells

Nrl$^{-/-}$NrlGFP - P8	Rod markers					
	Effects					
	Cell		Gene		Interaction	
	F(1,14)	p	F(1,14)	p	F(1,14)	p
	943.69	<0.0001 ****	17.57	0.0009 ***	17.57	0.0009 ***
	Post-test comparisons (Bonferroni-corrected) – significance with p values					
	Nrl		Nr2e3		Rhodopsin	
	excluded		<0.0001		<0.0001	

Table 3.5b qPCR comparisons of rod marker expression between 3 week and adult Nrl$^{-/-}$NrlGFP and adult NrlGFP flow sorted cells

Nrl$^{-/-}$NrlGFP – 3 weeks and adult	Rod markers					
	Effects					
	Cell		Gene		Interaction	
	F(2,12)	p	F(1,12)	p	F(2,12)	p
	2204.85	<0.0001 ****	23.18	0.0004 ***	12.68	0.0011 **
	Post-test comparisons (Bonferroni-corrected) – significance with p values					
		Nrl	Nr2e3		Rhodopsin	
	3 weeks	*excluded*	<0.0001		<0.0001	
	Adult	*excluded*	<0.0001		<0.0001	

In P8 cells, the results showed that rod marker expression was reduced in Nrl-/-NrlGFP cells compared to NrlGFP cells for all rod marker genes. This pattern was also seen in older cells. These results can be easily seen in the graph shown in

Figure 3.4C,F, where both rod genes are much reduced in both 3 week and adult Nrl$^{-/-}$NrlGFP cells, while Nrl is negligible.

Summary

These data show that for cone-related genes, Nrl$^{-/-}$NrlGFP cells show a similar expression profile to Chrnb4.eGFP true cone cells, that is, an increase in expression relative to NrlGFP rod photoreceptors. The results suggest, however, that consistent with the S-opsin expressing phenotype of the cone-like cells produced by this model, the expression of *Opn1mw* and *Thrβ* genes are not increased to the same level. At P8, the increase in expression does not appear to be of the same magnitude as found in Chrnb4.eGFP cells of the same age, which suggests that the cone-like cells of the Nrl$^{-/-}$ model are not as developmentally advanced at this age.

With rod related genes, the Nrl deficient cells show a near total absence of expression at all ages, in contrast with the true cone cells, in which expression of rod markers was found, declining only towards later adulthood. This lack of expression includes Nr2e3, the downstream target of Nrl, and the functional rod protein Rhodopsin. These data together show that the Nrl$^{-/-}$NrlGFP model does allow for isolation of successfully developmentally interrupted rod photoreceptors.

3.2.5 Characterisation of the Nr2e3$^{rd7/rd7}$CrxGFP mouse

Crx is a homeobox gene in the *Otx* family and is involved in the specification of photoreceptor fate, activating the transcription of photoreceptor specific genes (Chen et al., 1997; Furukawa et al., 1997), Its expression is apparent from E12.5, and reporter genes based on Crx expression have been shown to label all photoreceptors from early stages of development (Samson et al., 2009). Cells isolated from the CrxGFP model have been used for transplantation purposes (Lakowski et al., 2010).

3.2.5.1 GFP expression and Immunofluorescence

Eyes were taken from P8 and Adult Nr2e3$^{rd7/rd7}$CrxGFP and CrxGFP mice, fixed with PFA and immunostained for Rxrγ, Cone arrestin, Gnat2 and S-opsin. Images (taken from the ventral retina) can be seen in Figure 3.7 (images by Dr Fabiana Di Marco). CrxGFP expression can be seen in the whole of the ONL in both models.

Supernumerary and mislocalised cones are particularly evident in the adult retina, with all cone markers indicating an increase in the overall numbers of cone photoreceptors, with many seen to be located throughout the depth of the ONL. In P8 tissue, the additional cones can only be clearly seen after Rxrγ staining, in accordance with the early onset of this gene compared with other cone markers (as shown in section 3.2.1.1, and in Figures 3.3 and 3.6).

3.2.5.2 Quantitative PCR analysis of GFP-expressing populations

As with Chrnb4.eGFP and Nrl$^{-/-}$NrlGFP cells above, the transcriptomes of P8 and adult (5-9 week old) fluorescence-sorted Nr2e3$^{rd7/rd7}$CrxGFP+ cells were assessed using quantitative PCR, using the same methods as described in section 3.2.2.2. For analysis, while base-2 logarithmic expression was again normalised to that of NrlGFP cells of similar age, for statistical purposes these cells were compared to P8 and adult cells taken from CrxGFP retina as a closer control.

Expression levels can be seen in Figure 3.4, alongside those from other cell sources for comparison. Crx expression was not significantly different between P8 CrxGFP and Nr2e3$^{rd7/rd7}$CrxGFP, $t(4) = 0.1013$, $p = 0.9242$, nor between adult CrxGFP and Nr2e3$^{rd7/rd7}$CrxGFP cells $t(4) = 0.2390$, $p = 0.8228$.

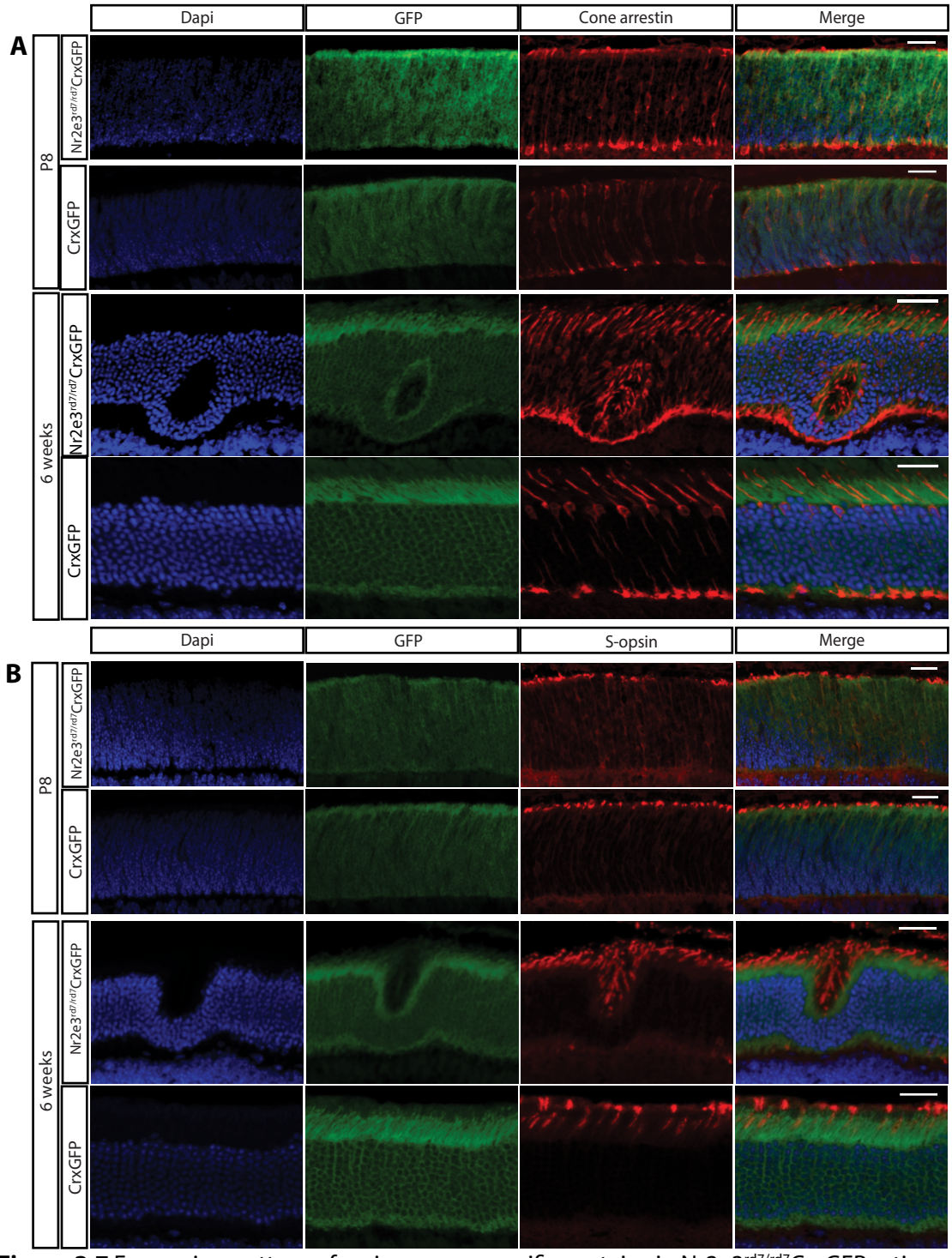

Figure 3.7 Expression pattern of various cone specific proteins in Nr2e3$^{rd7/rd7}$CrxGFP retina compared to CrxGFP (thanks to Dr Fabiana di Marco for these images). Both models show widespread GFP expression at both P8 and adult (6 week) ages. Scale bars are 20µm. **A** Cone arrestin expression shows an increase in cone cell bodies in adult Nr2e3$^{rd7/rd7}$CrxGFP tissue. These cones can also be seen to be mislocalised at various depths through the ONL rather than aligned at the apical edge as in the CrxGFP retina. A rosette, characteristic of this model can also be seen in this image, with cone arrestin expression visible inside. **B** Increased levels of s-opsin express-ing segments can be clearly seen in adult tissue in the inferior/ventral retina, but it is not clear if more cells are labelled at P8 with this protein.

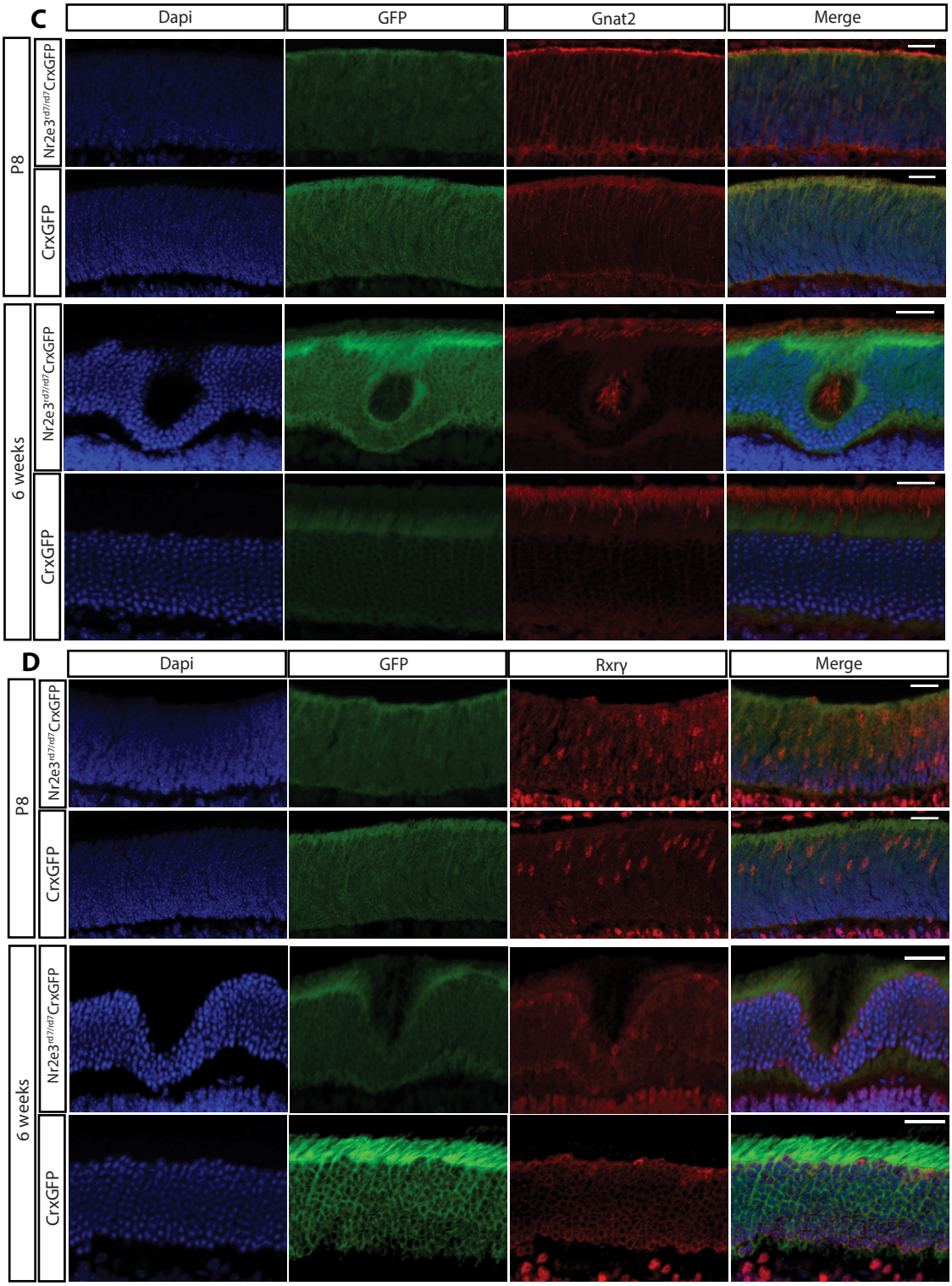

C Gnat2 expression can be seen in P8 tissue but does not obviously show an increase in cone number at this stage. Gnat2 can be seen expressed in more cone cells in adult tissue, as well as within the rosette visible in this image.

D Rxrγ staining shows the increase in cone precursors even at P8, with extra cell bodies clearly visible throughout the ONL. This can also be seen in adult tissue, with some mislocalised cone cells also visible.

Cone markers

Statistical comparisons for P8 cells are shown in Table 3.6a, and those for adult cells in Table 3.6b.

Table 3.6a qPCR comparisons of cone marker expression between P8 Nr2e3$^{rd7/rd7}$CrxGFP and P8 CrxGFP flow sorted cells

Nr2e3$^{rd7/rd7}$CrxGFP - P8	**Cone markers**					
	Effects					
	Cell		Gene		Interaction	
	F(1,24)	p	F(5,24)	p	F(5,24)	p
	4.81	0.0382 *	0.49	0.7837 n.s	1.18	0.3494 n.s
	Post-test comparisons (Bonferroni-corrected) – significance with p values					
	Arr	Chrnb4	Rxrγ	OpnSW	OpnMW	Thrβ2
	n.s	n.s	n.s	n.s	n.s	n.s

Table 3.6b qPCR comparisons of cone marker expression between adult Nr2e3$^{rd7/rd7}$CrxGFP and CrxGFP flow sorted cells

Nr2e3$^{rd7/rd7}$CrxGFP – adult	**Cone markers**						
	Effects						
	Cell		Gene		Interaction		
	F(1,24)	p	F(5,24)	p	F(5,24)	p	
	10.64	0.0033 **	11.05	<0.0001 ****	0.85	0.5271 n.s	
	Post-test comparisons (Bonferroni-corrected) – significance with p values						
		Arr	Chrnb4	Rxrγ	OpnSW	OpnMW	Thrβ2
	Adult	n.s	n.s	n.s	n.s	n.s	n.s

For P8 cells, the results showed that overall, the expression of cone markers was increased in Nr2e3$^{rd7/rd7}$CrxGFP cells relative to CrxGFP. The lack of significant post-test comparisons indicates that the differences are relatively small, but consistent when taken as a whole. Similarly, for adult ages, expression of cone markers is generally increased for Nr2e3$^{rd7/rd7}$CrxGFP cells, with this difference being small but consistent.

Rod markers

Statistical comparisons for P8 cells are shown in Table 3.7a, and those for adult cells in Table 3.7b.

Table 3.7a qPCR comparisons of rod marker expression between P8 Nr2e3$^{rd7/rd7}$CrxGFP and P8 CrxGFP flow sorted cells

Nr2e3$^{rd7/rd7}$CrxGFP - P8						
Rod markers						
Effects						
Cell		Gene		Interaction		
F(1,12)	p	F(2,12)	p	F(2,18)	p	
1.03	0.3292 n.s	7.75	0.0069 **	5.77	0.0175 *	
Post-test comparisons (Bonferroni-corrected) – significance with p values						
Nrl		Nr2e3		Rhodopsin		
n.s		<0.05		n.s		

Table 3.7b qPCR comparisons of rod marker expression between adult Nr2e3$^{rd7/rd7}$CrxGFP and CrxGFP flow sorted cells

Nr2e3$^{rd7/rd7}$CrxGFP – adult						
Rod markers						
Effects						
Cell		Gene		Interaction		
F(1,12)	p	F(2,12)	p	F(2,12)	p	
8.75	0.0120 *	7.82	0.0067 **	10.12	0.0027 **	
Post-test comparisons (Bonferroni-corrected) – significance with p values						
	Nrl		Nr2e3		Rhodopsin	
Adult	n.s		<0.001		n.s	

For P8 cells, no overall difference in rod marker expression was found, but the expression of Nr2e3 was significantly increased in P8 Nr2e3$^{rd7/rd7}$CrxGFP cells. The presence of an interaction makes these data difficult to interpret, but looking at the data and taking this difference into account, the likely explanation is that the increase in Nr2e3 expression in Nr2e3$^{rd7/rd7}$CrxGFP cells accounts for both the effect of Gene and the interaction, with the other genes not significantly different in expression.

Similarly, with adult cells, the results indicated that expression of rod markers differs between Nr2e3$^{rd7/rd7}$CrxGFP and CrxGFP cells. Post-test comparisons found again that only the expression of Nr2e3 was increased in the Adult Nr2e3$^{rd7/rd7}$CrxGFP cell population. As with the younger cells, a likely explanation is that Nr2e3 expression is elevated in Nr2e3$^{rd7/rd7}$CrxGFP cells compared to CrxGFP. It should be noted that of course due to the rd7 mutation that a functional protein is not produced from these transcripts.

Summary

The above data indicate that the cell population obtained by sorting for GFP fluorescence in Nr2e3$^{rd7/rd7}$CrxGFP tissue is somewhat enhanced in its expression of cone-specific markers at adult ages, and likely also at earlier postnatal ages. This is consistent with the increased population of cones in the Nr2e3$^{rd7/rd7}$ model, but as the cone-like cell population still makes up a relatively small proportion of the population, the increases are relatively modest.

Interestingly, Nr2e3 itself was seen to be upregulated in the Nr2e3$^{rd7/rd7}$CrxGFP cells, as seen in previous studies (Corbo and Cepko, 2005), implying that this gene may be involved in its own downregulation, or that transcription of this gene is upregulated when its downstream effects do not occur.

This shows that using this model, a population of cells which have an increased number of cone-like cells can be successfully isolated.

3.3 Discussion

These experiments detail the development of the tools and resources needed for the major aims of this thesis; specifically robust methods for visualising cones in

developing retinal tissue and for isolating pure populations of cone and cone-like cells for transplantation purposes.

Rxrγ appears to be a suitable marker for immunohistochemically labelling cone and cone-like photoreceptors in fixed developing retina, in particular due to its nature as a nuclear marker making it easy to identify cell bodies, compared with other cone specific proteins which are more often found in the segments. However, due to previous unsuccessful attempts at using this gene to drive reporter expression, and the expression of this protein in RGCs, I decided that the Chrnb4.eGFP model was more suitable as a transgenic line for investigating live developing cells and as a source of cells for transplantation.

The data presented here show that the Chrnb4.eGFP model labelled cone photoreceptors at developing ages, and that cells isolated from this model at developmental and adult ages show a distinctive pattern of expression compared to rod cells, indicating that they are indeed cone photoreceptors.

The cone-like cells produced by the $Nrl^{-/-}$ and $Nr2e3^{rd7/rd7}$ models were also assessed. Models to isolate these cells for transplantation purposes were obtained: the $Nrl^{-/-}$/NrlGFP and $Nr2e3^{rd7/rd7}$CrxGFP mice. Immunostaining of these models showed that the production of extra cones in these models was clear. I also found that it was possible to use these reporter models in order to isolate cells that were enriched in the expression of cone markers, compared to rod cells.

3.3.1 Differences between cone-like and true cone cells

The expression levels of genes in Chrnb4.eGFP true cone cells and $Nrl^{-/-}$NrlGFP cone-like cells showed some differences in their comparisons with NrlGFP rod cells.

Notably the expression of rod marker genes was very low or negligible in all ages of $Nrl^{-/-}$ cells whereas P8 and 3 week old Chrnb4.eGFP cells showed surprisingly high levels of rod marker expression, with levels declining in adult cells.

With cone markers, although $Nrl^{-/-}$ cells did in general express high levels of these genes, at younger ages the increase relative to NrlGFP rod cells did not appear to be as marked as was found in Chrnb4.eGFP cells, indicating that in some ways these cone-like cells might not develop at the same rate as true cones. Additionally, at older ages, while for most cone markers expression was similar between cone and cone-like cells, M-opsin and Thrβ2 expression is not increased to the same extent in the $Nrl^{-/-}$ cells, as in the Chrnb4.eGFP cells, as may be explained by the cone-like cells being primarily S-opsin expressing (Ng et al., 2009).

These results indicated that while $Nrl^{-/-}$ cone-like cells are a good source of cells which are much like cones, there are some differences in developmental progression, gene expression and response characteristics which should be borne in mind. However, the results also indicate possible issues with these tools and resources which could cause problems in subsequent experiments.

3.3.2 Limitations of the models used

The Chrnb4.eGFP mouse allows isolation of cone photoreceptor precursors from the developing retina. However, although at postnatal ages cone precursors can be isolated due to the strength of GFP expression, at embryonic time points strong GFP expression is also seen in other cell types, meaning that isolation of a pure cell population may not be possible at these stages. Additionally, a reduction of GFP expression is seen at older adult ages of this model, raising the possibility that cells

may lose their fluorescence after transplantation and thus fail to be identified in the recipient tissue.

The presence of relatively high levels of expression of the Nrl, Nr2e3 and Rhodopsin genes in P8 and young adult cone photoreceptors compared to rod photoreceptors of the same age was unexpected. Since previous reports (Lakowski et al., 2010) had hypothesised that transplanted cone photoreceptors might follow a more rod-like fate in the adult WT retina, these transcription patterns raised the possibility that photoreceptor fate is perhaps less fixed at earlier timepoints than generally thought.

A recent study reported the use of a different model for the fluorescent identification of cone cells (Smiley et al., 2016). A gene trap insertion of GFP into the Coiled-coil Domain Containing 136 (ccdc136) locus led to cone photoreceptors and their precursors being fluorescently labelled from prenatal ages. This line was successfully crossed with the $Nrl^{-/-}$ mouse where it similarly labelled cone-like cells. However, this model shows relatively weak GFP expression in M-opsin expressing cones, and furthermore GFP was found in bipolar cells. As a result, cells from this model, while excluding rod photoreceptors, do not constitute a completely pure population of all cone photoreceptors.

Despite these issues, the Chrnb4 model represented a significant improvement over previously used sources for cone photoreceptors, and the model was taken forward for use in subsequent experiments.

The OPN1LW-eGFP mouse showed very few positive cells at earlier developmental time points, consistent with the late onset of the *Opn1mw* gene. For purposes such as tracking the migration of developing cone cells, this represents an obstacle for

seeing the onset of movement at around P2. It should be noted that *Opn1mw* is present only in a subset of all retinal cones, primarily in the dorsal retina, meaning that not all cones would be able to be isolated from this model. Since the extra cones produced by the $Nrl^{-/-}$ and $Nr2e3^{rd7/rd7}$ models are primarily s-opsin expressing, this reporter gene is also not suitable for crossing into these models.

A further complication with this model is the development of a degenerative phenotype, with a loss of all types of cone photoreceptors over time (Lipinski et al., 2011). The reasons for the degeneration in this model are not fully understood, but seem to be linked to the insertion site for the transgene being proximal to genetic loci associated with the retinal diseases North Carolina Macular Degeneration and Progressive bifocal chorioretinal atrophy. This degeneration reduces the suitability of this model for further experimental purposes.

Historical data for the transplantation of OPN1LW-eGFP cells can be found in Chapter 4. Due to the above mentioned limitations and the subsequent loss of the model, further use of this model for tracking migration was not attempted.

The other models chosen for use present other potential limitations. The use of the CrxGFP marker, which labels all photoreceptor types, means that a pure population of the supernumerary cone-like photoreceptors produced by the $Nr2e3^{rd7/rd7}$ mice cannot be isolated, meaning that for the gene expression experiments above and for subsequent transplantation purposes, cells isolated from the $Nr2e3^{rd7/rd7}$.CrxGFP model represent a mixture between cone-like cells and the hybrid cells produced by this model (Cheng et al., 2011). The line as it exists, however, represents a good starting point for exploratory experiments using this model, and the Chrnb4.eGFP gene represents a good candidate for labelling the cone-like cells of this model, if it becomes desirable to do so.

The NrlGFP marker used in combination with the knockout of the Nrl coding region has the advantage of labelling only the cells affected by the mutation, preventing contamination of isolated cell populations by true cone photoreceptors, but has issues similar to those of the Chrnb4.eGFP model regarding a reduction of GFP expression at later time points. Since true cones in this model comprise a small percentage of the total photoreceptor population (as they do in WT mice), it is unlikely to represent a large effect on the efficiency of this cell source, and would also, by the same token not significantly increase the number of cones isolated from this line. The advantages of the purer population are that results from the use of this mouse line in transplantation can be more reliably attributed to the cone-like cells, without the chance of contaminations from the true cones.

Conclusion

The tools and models developed in this chapter, despite some limitations, represent a good compromise between specificity and practicality. Bearing this information in mind will inform the conclusions that can be made from the results of future experiments.

Chapter 4 – Transplantation of early and late cone cells

4.1 Introduction

Previous work has shown that rod photoreceptor precursors can be transplanted into adult mouse retinas by subretinal injection. Cells from transgenic NrlGFP mice, which fluorescently label all rod photoreceptor cells from soon after terminal mitosis (Akimoto et al., 2006), are purified with FACS methods and injected into the subretinal space of recipient mice. After injection, GFP+ cells can be found in the ONL of the recipient mice. These cells express photoreceptor-specific proteins and exhibit characteristic photoreceptor morphology (MacLaren et al., 2006).

More recently, attempts have been made to extend this principle by transplanting cone photoreceptor precursor cells. The CrxGFP marker was used to label all photoreceptor cells and donor cells were isolated and transplanted at early stages before all rod photoreceptor precursors had been produced, so that they would be primarily cones (Lakowski et al., 2010). Although GFP+ cells were found within the recipient ONL, the majority of them had rod-like morphology, with an average of less than 1% of GFP+ cells in WT recipient retinas co-expressing Rxrγ, even when cells were taken from embryonic donors at a stage where more than 75% would have been cone precursor cells.

Given that this was a mixed cell population, the reason why this occurred was not clear and possible explanations were proposed. It could be the case that the portion of the injected cells that were rod precursors were integrating more easily and in higher numbers than the cone precursors. Another explanation was that the cells transplanted were not fully committed to their eventual fate and could go through a

process of changing fate to become rod photoreceptors rather than cones. The fate of photoreceptor cells is known to be malleable, at least to an extent, as shown by the Nr2e3$^{rd7/rd7}$ and Nrl$^{-/-}$ mice, in which the developmental pathway for rods is disrupted, and rod precursors instead develop as cone-like cells (Haider et al., 2000; Yoshida et al., 2004). Similarly, the introduction of Nrl into cone cells has been shown to promote a rod fate in *Xenopus* and mouse (McIlvain and Knox, 2007; Oh et al., 2007). In addition, since the population of rod photoreceptors in the mouse retina rises to become the vast majority of all photoreceptors soon after birth (Brzezinski and Reh, 2015; Marquardt and Gruss, 2002), the above study did not allow for investigation of the transplantation of cone cells from donors older than postnatal day 3.

For the further investigation of the possibility of transplanting cone photoreceptors, therefore, it was necessary to isolate a purer population of cone photoreceptor precursor cells, at a range of developmental ages, with minimal contamination from rod precursors, in order to determine firstly whether cone cells integrate less efficiently than rods, and whether the cells retain their cone appearance after integration.

In Chapter 3, I identified the Chrnb4.eGFP model as a promising line for identifying cone cells in adult and developing tissue. Although the expression of GFP in this model is not wholly restricted to the cone photoreceptors at embryonic stages, before P8 cone photoreceptors can be isolated based on their high levels of GFP expression. This makes the Chrnb4.eGFP model suitable as a source for cone photoreceptor precursor cells. Other methods of the fluorescent labelling of cone photoreceptors exist, and were mentioned in Chapter 3. The OPN1LW-eGFP model has GFP expression in M-opsin expressing cones and has also been used as a source of cone precursor cells for transplantation.

In this Chapter, I will look at the results of injecting Chrnb4.eGFP cells into recipient mouse retinas, as well as using cells derived from the OPN1LW-eGFP model.

4.2 Results

Previous studies have shown that the age of donor cells has a marked effect on the success of transplantation (MacLaren et al., 2006), with postnatal day 8 having been identified as the optimum age for NrlGFP rod precursor cells (Pearson et al., 2012). However, the development of cone photoreceptors differs to that in rods, with one major difference being the time of birth; the majority of cone precursors become post-mitotic around E15.5, well before the peak of rod genesis at around P1 (Brzezinski and Reh, 2015; Marquardt and Gruss, 2002).

Due to this, it was not assumed that cone precursors would demonstrate optimal transplantation outcome at P8, and I investigated a range of ages: E15.5, the age of peak cone genesis, P8, the peak of transplantation outcome using rod cells, and P1, an intermediate age, which is also the peak of rod genesis. FACS analysis of Chrnb4.eGFP retinal cells at these ages showed that at P0/1 a bright GFP+ population corresponding to cone precursors could be identified, distinct from the dimly GFP+ cells also seen in these retinas (see section 3.2.2.1), however the difference was not as distinct as had been seen in P8. At E15.5, a distinction could not be made, and therefore for this age the cell population obtained for transplantation consisted of the entirety of the GFP+ group, and should be considered a mixed population of cells. These observations are summarised in Figure 4.1.

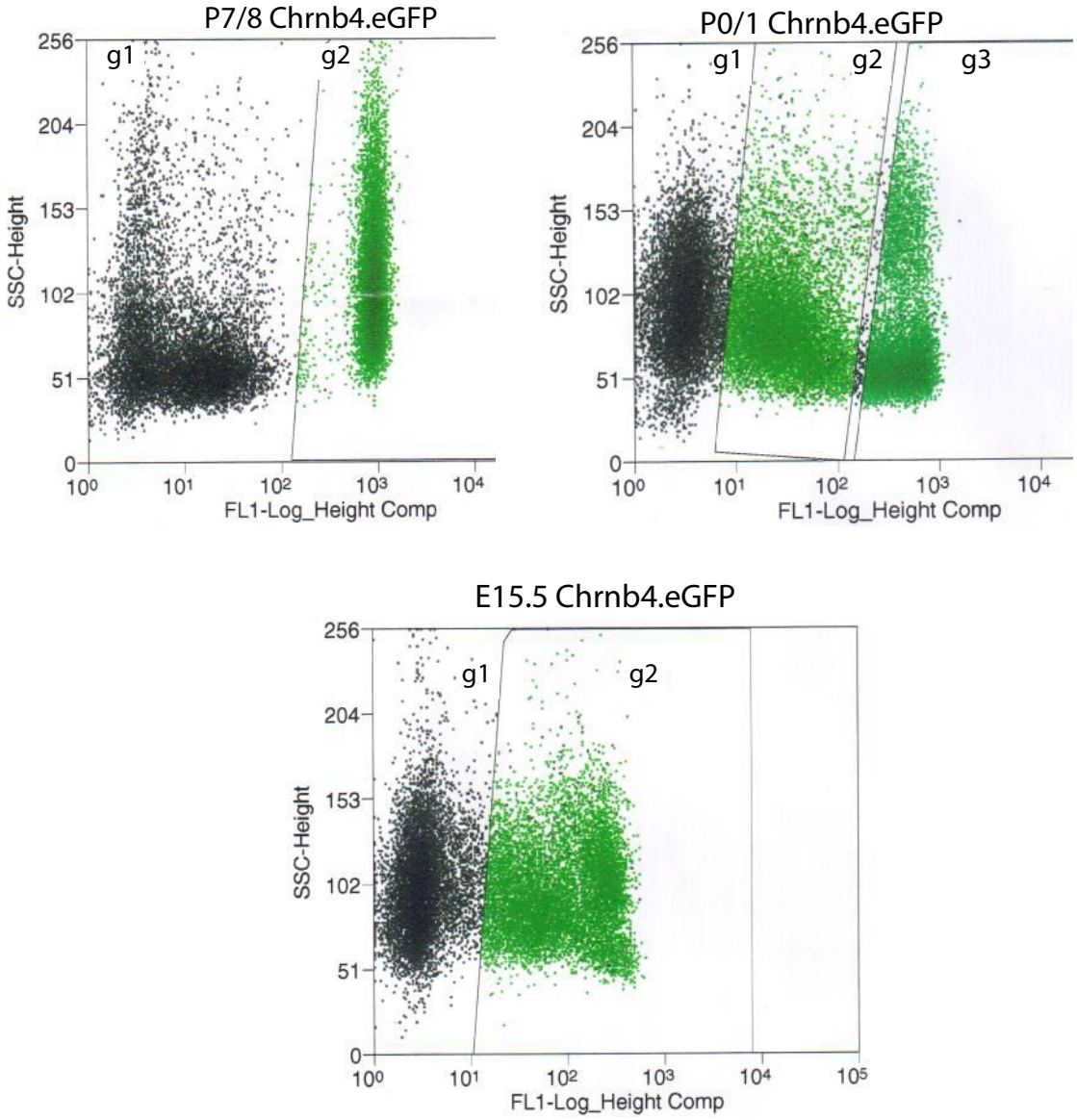

Figure 4.1 FACS plots of embryonic and postnatal Chrnb4.eGFP cells, showing live single cells. Values for the side-scatter measurement of these cells are plotted against GFP fluorescence on the x-axis. Compared to data from P8 cells (see also Figure 3.2E), bright and dim GFP expressing populations are more difficult to isolate at younger ages, although both can be distinguished from GFP negative cells (g1 in all cases). In P0/1 and P7/8 cells, the populations can be separated as shown, with a bright population of approximately 6% (P0/1, g3) and 2.5% (P7/8, g2) of live single cells, with the dimmer cells separate from these cells (eg. P0/1 cells, g2 where they comprise 42.5% of the total). In E15.5 cells, these populations cannot be reliably distinguished and for subsequent experiments the entirety of the GFP expressing population (g2) was used (approximately 22% of the total).

Previous studies have shown the effect of recipient environment on photoreceptor transplantation outcomes, with injections into some degenerative models showing an increase, and in others a decrease, in the occurrence of GFP+ cells in the recipient ONL, compared to that found in WT (Barber et al., 2013). Previous attempts to transplant CrxGFP+ cone precursor donor cells into the WT retina resulted in a much greater number of GFP+ rods in the recipient ONL, compared to GFP+ cones (Lakowski et al., 2010), suggesting either that cones do not integrate as readily as rod photoreceptors or that those that do switch to a rod-like fate. During development, cones are born into a rod-less environment. However, the adult WT ONL is comprised, predominantly, of rods and the small percentage of cones present are restricted to the apical edge of the ONL. The $Nrl^{-/-}$ retina, in contrast, is able to maintain an ONL consisting almost entirely of cone-like cells, despite a degree of cell loss and the formation of rosettes (Roger et al., 2012). Because of this, I used this model as another recipient to investigate whether the cone rich $Nrl^{-/-}$ represented a more permissive environment for cone transplantation, or whether the rod-like outcome of previous transplantation attempts is related to the rod-rich environment of the WT retina.

4.2.1 Transplantation of Chrnb4.eGFP donor cells

Cells for transplantation were obtained by dissociation of Chrnb4.eGFP neural retina, and fluorescence sorting to isolate GFP+ cells, as detailed in Chapter 2. Initially, transplantations of 200,000 FACS-purified Chrnb4.eGFP cells at E15.5, P1 and P8 cells (+/- 1 day) were made into the subretinal space of adult WT and $Nrl^{-/-}$ recipient mice. The recipient mice were sacrificed 2 weeks after transplantation (see section 3.2.2.1), fixed with 4% PFA, frozen in OCT and cryosectioned between 15-18µm. Eyes were stained for Rxrγ, PNA and GFP.

Table 4.1 Recipients of 200,000 Chrnb4.eGFP cells

Recipient genotype	Age of donor cells	Mean	SD	SEM	Analysed injected eyes	Rejected
WT	E15.5	N/A	N/A	N/A	0	1
	P1	N/A	N/A	N/A	0	2
	P8	369	394.6	279.0	2	6
$Nrl^{-/-}$	E15.5	60.75	42.66	21.33	4	0
	P1	672	513.4	363.0	2	0
	P8	860.3	810.4	405.2	4	2

This table shows the mean number of GFP+ cells found in the adult recipient retina 2 weeks after transplantation, as well as the standard deviation (SD) and standard error of the mean (SEM). Rejections are based on criteria described in section 2.3.1.

In contrast to previous reports and results presented elsewhere in this thesis (see Chapter 5), surprisingly few successful transplantation outcomes were observed with the WT recipient. In general, donor cell masses were absent from the sub retinal space (an indicator of successful transplantation), or if present, below the 250 cell criteria for acceptance (see section 2.3.1), but, in contrast to what has been seen previously in instances of acute rejection of rod donor cells (Warre-Cornish et al., 2014; West et al., 2010), there was no particular evidence of acute inflammation, such as autofluorescent debris or activated macrophages. This could be due to a number of factors, most likely with the problems associated with acquiring enough viable cone cells for injection. Further, due to the low number of cone photoreceptors (approximately 180,000 compared to 6.4 million rods (Jeon et al., 1998)) in the wild type mouse retina, and the fact that the Chrnb4.eGFP model had to be maintained as hemizygotic animals, the yield of GFP+ cells that could be isolated from a single litter was very low, allowing for only a very low number of injections to be made from each preparation of cells for transplantation. Indeed, on occasion not enough cells could be isolated to make any injections of 200,000 cells, in particular with the cells from embryonic ages (E15.5).

Together, these meant that the variability associated with the number of cells injected was higher, and the number of transplantations that reached our normal acceptance criteria (West et al. 2010, see also section 2.3.1) was lower, in these experiments, compared to those previously reported for rod transplantation and elsewhere in this thesis (Chapter 5). The results obtained are summarised in Table 4.1.

No successful transplantations were achieved into the WT retina with E15.5 or P1 Chrnb4.eGFP donor cells, however with the above in mind, it is not clear if this recipient represents a specific barrier to transplantation. More successful results were obtained with with the $Nrl^{-/-}$ recipient, however the number of successful repeats were still too few in number to conclude at this stage that this recipient represents a more permissive environment for cone transplantation.

In the absence of data in WT retina, the Kruskal-Wallis test was used to compare the number of GFP+ cells seen in $Nrl^{-/-}$ recipient ONL after transplantation. No effect of donor age was seen $H(2,7) = 5.543$, $p = 0.0626$.

Given the significant difficulties in obtaining sufficient numbers of donor cells, it was decided to reduce injection amounts to 100,000 cells, to permit an increase in the number of injected eyes per cell preparation. Injection amounts lower than 100,000 cells per eye have been shown in previous studies to much reduce the number of GFP+ cells within the recipient ONL (Pearson et al., 2012). Even with this reduction in donor cell number, however, the number of possible injections was still small. Given this, it was not possible to obtain N numbers sufficient for normality tests to be applied to the data.

Given the absence of any clear association between transplantation outcome and developmental age of the Chrnb4.eGFP donor cells, together with the relative ease of isolating the bright cone precursor population from older retina, I chose to focus on the P8 donor stage in the remaining experiments. Specifically, I aimed to repeat the above experiments, injecting cone precursors into WT and $Nrl^{-/-}$ retinas to determine the outcome of transplantation.

Adult WT or $Nrl^{-/-}$ mice received injections of 100,000 P7/8 Chrnb4.eGFP cells into the superior subretinal space. Additionally, adult WT mice received injections of 100,000 P1 Chrnb4.eGFP cells. The recipient mice were sacrificed 2 weeks after transplantation, fixed with 4% PFA, frozen in OCT and cryosectioned between 15-18µm. Eyes were stained for GFP and the cone markers Rxrγ and PNA.

With these injections, more reliable success could be seen, with unintegrated masses of more than 250 cells observed in the subretinal space in accepted eyes, and the eyes that were rejected exhibited the features more typical of acute rejection. GFP+ cells were found in the ONL of recipient retinas after 2 weeks, the numbers of which can be seen in Table 4.2.

Table 4.2 Recipients of 100,000 Chrnb4.eGFP cells

Recipient genotype	Age of donor cells	Mean	SD	SEM	Analysed injected eyes	Rejected
WT	P1	306	60.2	34.8	3	3
	P8	352.1	317.1	112.3	8	6
$Nrl^{-/-}$	P8	343.5	255.3	104.2	6	1

Figure 4.2(A,B,E) shows representative images of GFP+ cells found after transplantation. Examples of photoreceptor morphology can be seen in these images, including apical and basal processes from the cell bodies, synaptic end feet

and segments. However, in the WT recipient the overall morphological features of these cells was more in keeping with that of rod, rather than cone, photoreceptors although immunostaining to determine rod marker expression was inconclusive due to the high number of rods in the WT retina (Figure 4.2D).

Notably, in the WT recipient, the vast majority of GFP+ cells within the recipient ONL did not express Rxrγ, cone arrestin, s-opsin or PNA (Figure 4.2 A,B). Moreover, the synaptic terminals, when visible, were small and more closely resembled the button-like structures of rod synapses, rather than the larger triangular ribbons characteristic of cone cells. While adult cone cells in the WT retina are invariably located at the apical edge of the ONL, the GFP+ cells were located in various places throughout the depth of the ONL. Nuclear morphology was also more rod-like than cone-like, with GFP expressing cells exhibiting small nuclei with a single point of condensed heterochromatin rather than the larger nuclei with multiple points of heterochromatin found in cone cells (see also section 1.2.1, Figures 1.2, 1.6 and 3.2, and Lakowski et al., 2010 for examples of GFP+ rod-like and cone-like cells).

Interestingly, the mass of injected, but non-integrated, cells remaining in the subretinal space did express cone markers, as seen in Figure 4.2C, and had cone-like nuclei, although this pattern of heterochromatin is also similar to that of progenitor cells in the developing ONL (see, for example, Figure 3.2) and could therefore indicate the immaturity of these cells.

In the $Nrl^{-/-}$ recipient, however, the GFP+ cells resembled cones more closely, in nuclear, morphological and immunohistochemical features (Figure 4.2 E).

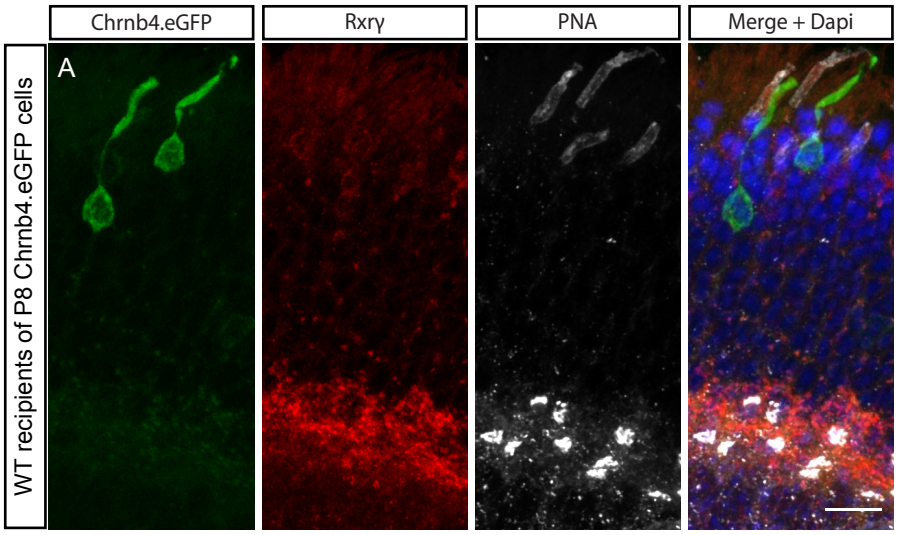
Chrnb4.eGFP
Rxrγ
PNA
Merge + Dapi
A
WT recipients of P8 Chrnb4.eGFP cells

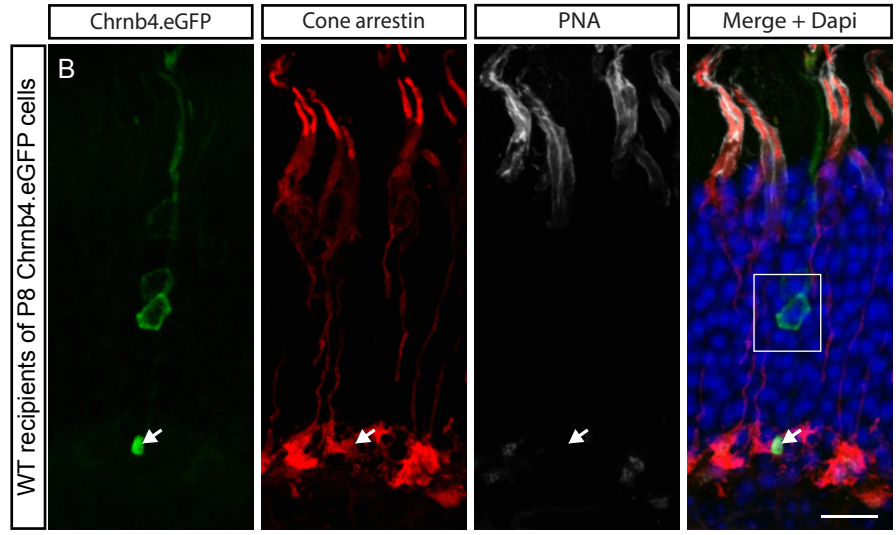
Chrnb4.eGFP
Cone arrestin
PNA
Merge + Dapi
B
WT recipients of P8 Chrnb4.eGFP cells

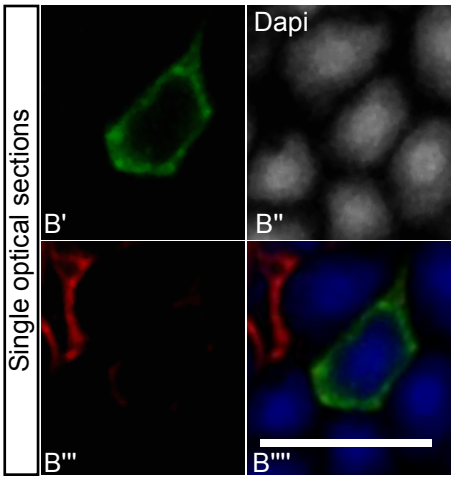
Dapi
B'
B''
B'''
B''''
Single optical sections

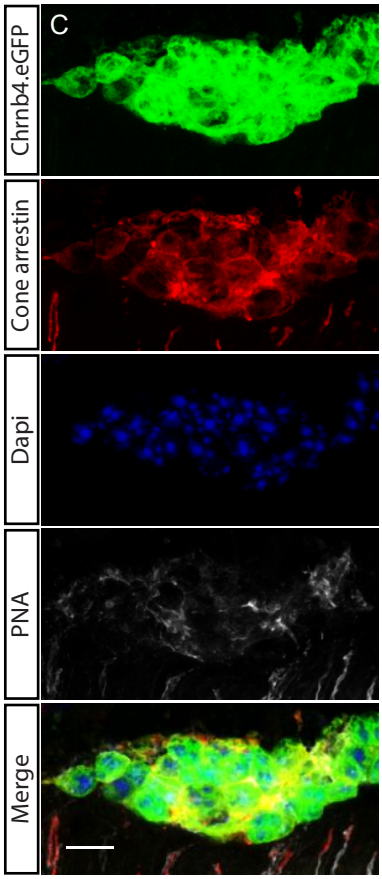
C
Chrnb4.eGFP
Cone arrestin
Dapi
PNA
Merge

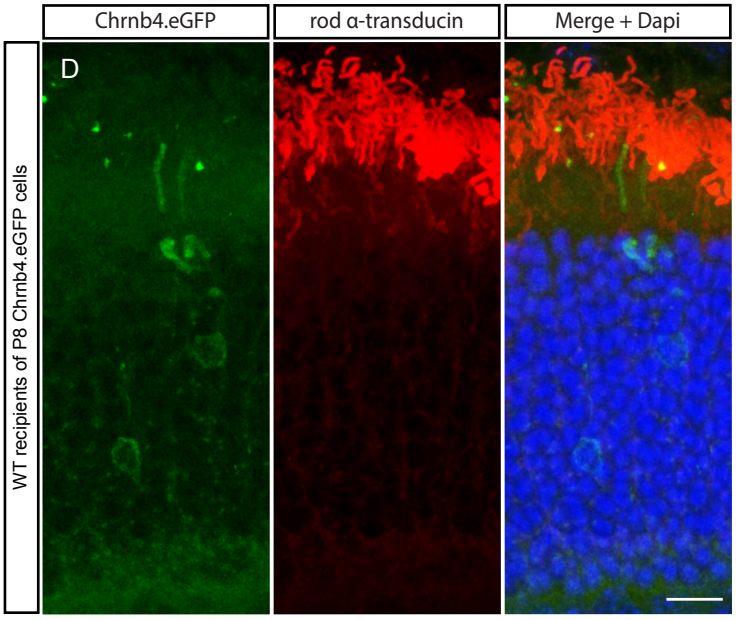
Chrnb4.eGFP
rod α-transducin
Merge + Dapi
D
WT recipients of P8 Chrnb4.eGFP cells

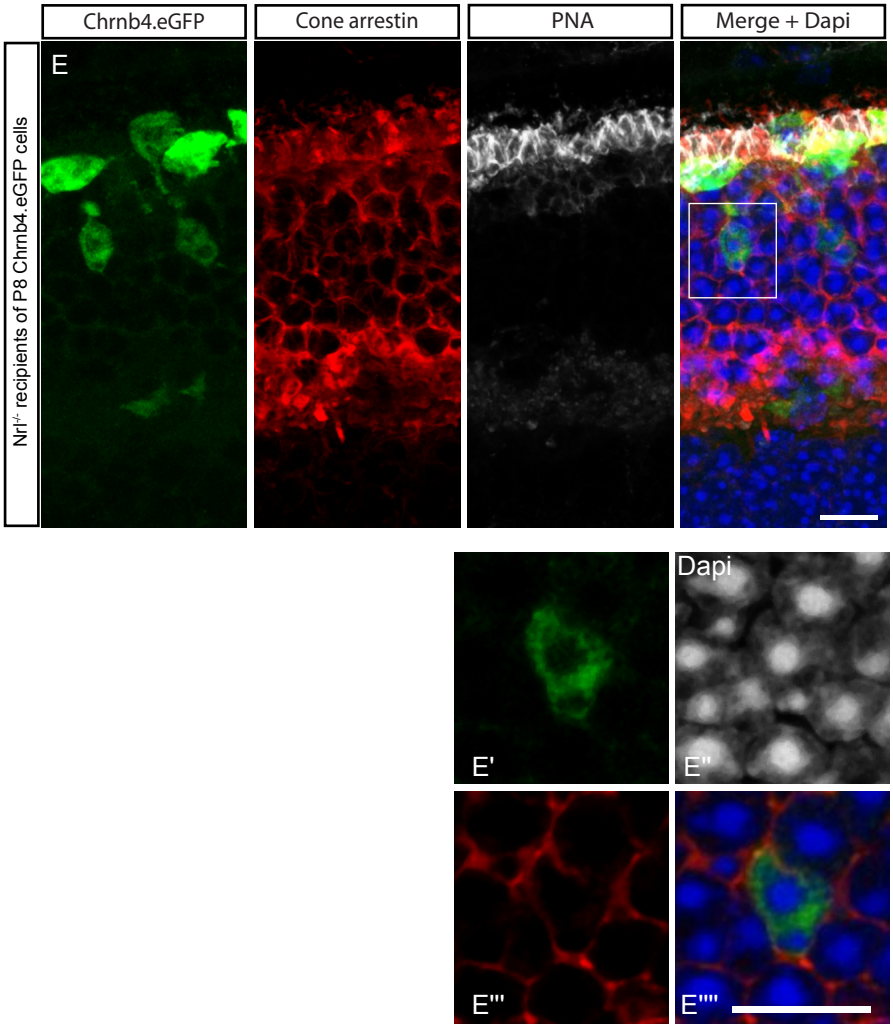
Chrnb4.eGFP
Cone arrestin
PNA
Merge + Dapi
E
Nrl-/- recipients of P8 Chrnb4.eGFP cells
Dapi
E'
E''
E'''
E''''

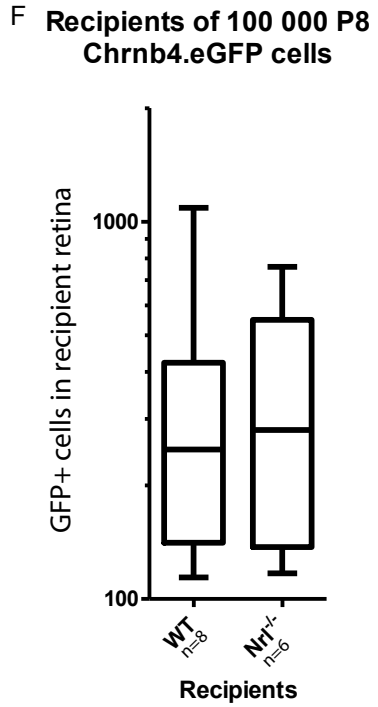

Figure 4.2 Transplantation of Chrnb4.eGFP cells into WT and Nrl$^{-/-}$ recipients. Adult recipient mice received a subretinal injection of 100,000 GFP positive Chrnb4.eGFP cells isolated from P8 donors. Scale bars are 10µm.

(**A-B**) GFP+ cells were found in the WT host ONL after transplantation. The majority of these cells resembled rod photoreceptors, with small cell bodies showing a single point of condensed heterochromatin and small synaptic terminals (B, arrow). The cells additionally were not seen to express the cone photoreceptor markers Rxrγ, PNA or cone arrestin. B'-'''' are single optical sections of the boxed area, showing the rod-like nuclei of GFP+ cells.

(**C**) Subretinal masses of unintegrated cells were seen to express cone markers cone arrestin and PNA.

(**D**) Attempts to find expression of rod markers (here rod α-transducin) were inconclusive due to the high density of rod photoreceptors in the WT retina.

(**E**) In the Nrl$^{-/-}$ recipient, GFP+ cells were also seen. These cells exhibited larger cell bodies with nuclei showing multiple points of condensed heterochromatin, and larger synaptic terminals. Single optical sections of the boxed area (E'-'''') indicate that these cells express the cone marker cone arrestin and display characteristic cone-like nuclei.

(**F**) Number of GFP+ cells found in recipients 2 weeks after injection. No significant difference was seen in integration number between WT and Nrl$^{-/-}$ recipients.

The mean number of GFP+ cells within the recipient retinas is shown in Figure 4.2F, and Table 4.2. These numbers are noticeably lower than have been seen in previous studies after the transplantation of NrlGFP rod photoreceptors, where P8 donor cells typically result in more than 6000 GFP+ cells in the recipient ONL (Warre-Cornish et al., 2014).

No significant difference was found between the number of GFP+ cells within the ONL of $Nrl^{-/-}$ and WT recipients: $U(12) = 23.00$, $p = 0.9497$. Similarly, no difference was found between transplanting P1 and P8 cells into WT recipients $U(9) = 10.00$, $p = 0.7758$.

Despite the difficulties encountered in these transplantations, and the surprisingly rod-like appearance of the cells resulting from injections, these results indicate that true cones can survive transplantation and a proportion integrate into the recipient ONL in a manner similar to rod photoreceptors.

4.2.2 Transplantation of OPN1LW-eGFP donor cells

A mouse model using a regulatory sequence upstream of the human red and green cone opsin gene to drive GFP expression has been previously described (Fei, 2003; Fei and Hughes, 2001). As discussed in 3.2.3, this model labels some cone photoreceptors, predominantly in the superior/dorsal retina, which express the medium-wave opsin gene. These mice were used as a source of mature cone cells for transplantation. (N.B. these data were collected historically by Dr Amanda Barber, and the line was not subsequently retained at this facility.)

Since GFP expression in this model is very low before birth, 200,000 cells from unsorted populations of neural retinal cells, taken from E15.5 OPN1LW-eGFP donor

mice were transplanted into the subretinal space of adult or P5 WT recipients. Purified OPN1LW-eGFP+ cells were isolated from P8 and P14 donor OPN1LW-eGFP mice and also transplanted into the subretinal space of WT recipient mice, injecting 100,000 cells per eye.

With adult recipients, 3 weeks after transplantation of E15.5 cells, very small numbers of in GFP+ cells were found within the recipient ONL (mean = 3 cells, SD = 3.1, with n = 15 eyes). P5 WT recipients of E15.5 cells showed similarly low numbers of GFP+ cells within the recipient ONL (mean = 8 cells, SD = 9.4, n=10 eyes).

Slightly higher numbers of GFP+ cells were found using postnatal donor cells; 38 and 105 cells (n = 2 eyes) were found using P8 cells, and with P14 cells 0 and 9 cells (n = 2 eyes) were seen. Regardless, these data indicate that cone precursor cells at later stages of development do not integrate effectively.

Examples of the appearance of these cells can be seen in Figure 4.3. Similar to the results with Chrnb4.eGFP, the GFP+ cells seen in these cases showed a rod-like morphology, with cell bodies occupying various positions in the depth of the ONL, and small nuclei with a single point of condensed heterochromatin. Occasionally, cells were seen that presented with a more cone-like nuclear morphology, with larger nuclei possessing more than one focal point of condensed heterochromatin, as shown in Figure 4.3C.

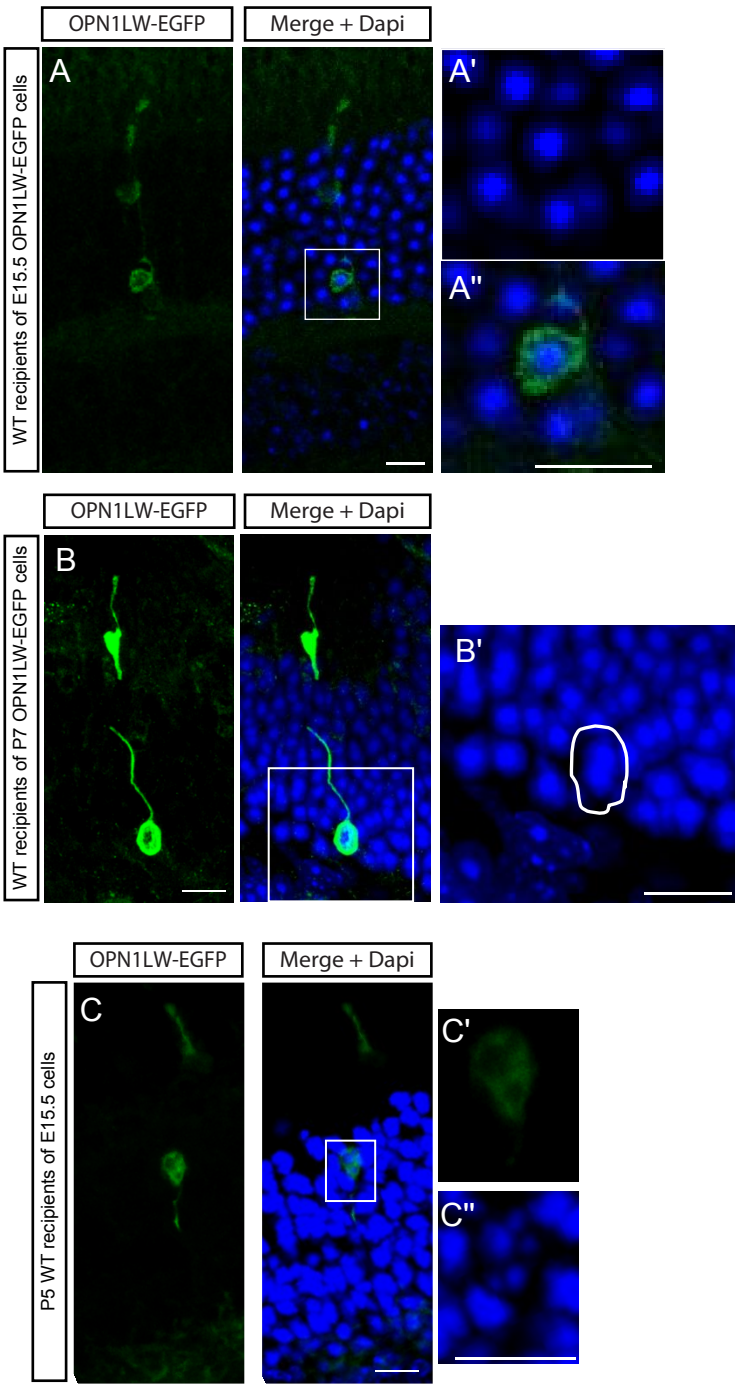
OPN1LW-EGFP
Merge + Dapi
WT recipients of E15.5 OPN1LW-EGFP cells
A
A'
A"
OPN1LW-EGFP
Merge + Dapi
WT recipients of P7 OPN1LW-EGFP cells
B
B'
OPN1LW-EGFP
Merge + Dapi
P5 WT recipients of E15.5 cells
C
C'
C"

Figure 4.3 Transplantation of OPN1LW-EGFP cells into WT recipients. These experiments and images carried out by Dr A Barber. The numbers of GFP+ cells seen in recipient ONL after transplantation can be found in the main text. Scale bars are 10μm (approx).
(**A**) Adult WT mice received injections of 200,000 unsorted cells from E15.5 donor mice. GFP+ cells were found in the host ONL after transplantation. The majority of these cells resembled rod photoreceptors, with small cell bodies showing a single point of condensed heterochromatin (A', A'' show enlarged views of the white box).
(**B**) Adult WT mice received injections of 200,000 sorted cells from P7 donor mice. GFP+ cells were also seen in the host ONL after transplantation, again resembling rod photoreceptors with small cell bodies with a single point of condensed heterochromatin (B' shows an enlarged view of the white box).
(**C**) Early postnatal (P5) mice also received injections of 200,000 unsorted cells from E15.5 donor mice. Most GFP+ cells in the host ONL after injection again resembled rod photoreceptors but very occasional cells with cone-like nuclear morphology were seen, (C', C'' showing enlarged views of the white box).

The lack of success encountered with transplantation of cells from this source could have a number of explanations. As I noted in Chapter 3, there are several problems with the OPN1LW-eGFP as a source of cone photoreceptors, most notably the late onset of GFP expression, the exclusion of cone photoreceptors which do not express M-opsin, and in particular the degenerative phenotype shown by this model (Lipinski et al., 2011) – cone photoreceptors degenerate over time, irrespective of GFP expression.

4.3 Discussion

In this chapter, I provide evidence to indicate that cone photoreceptors derived from the Chrnb4.eGFP cells can be successfully transplanted into the recipient retina. GFP+ cells take up positions in the ONL and elaborate the morphological features of mature photoreceptor cells. Although the number of GFP+ cells was significantly lower than has been seen in previous studies using NrlGFP rod precursors, a small number of cells was always seen, even with a range of different donor ages.

Transplantation outcome following the injection of GFP+ donor cells taken from the OPN1LW-eGFP mouse was poorer, both in terms of survival of the transplanted donor cell mass and the number of GFP+ cells within the recipient ONL, but otherwise showed similar results to those cells taken from the Chrnb4.eGFP model. Due to the poor outcomes and the problems that this model exhibits, the OPN1LW-eGFP model was not used further.

The poor transplantation efficiencies seen could be due to a number of factors. Many things have been shown to affect the efficiency of transplantation, of which the most important are the age of the donor cells injected (MacLaren et al., 2006), and the aetiology of the recipient retina (Barber et al., 2013; Warre-Cornish et al.,

2014). The very low yield of cone photoreceptor donor cells meant that few injections could be made, and a conclusive answer of which donor cell age was best was not able to be found, although embryonic cells appeared to lead to the poorest outcome. Injections of fewer cells at P1 and P8 met with more success, and GFP+ cells were seen within the recipient ONL with some reliability. The restricted number of donor cell ages used in these experiments means that it is possible that an alternative intermediate age of donor cell may be more effective than those used here, and that a number of mouse mutant retinal models exist which could be more permissive for cone integration. A simpler explanation would be that cone photoreceptors are less able to integrate than rods in general, perhaps lacking the migratory machinery necessary to move into the recipient ONL.

4.3.1 Chrnb4.eGFP+ cells within the recipient ONL resemble rod photoreceptors

After transplantation of Chrnb4.eGFP donor cells into WT retina, the GFP+ cells located within the recipient did not typically exhibit characteristics of cone photoreceptors and, in most respects, resembled rods. They were not seen to express cone-specific markers such as Rxrγ or PNA, were located throughout the depth of the ONL, had small button-like synaptic end feet when these could be seen, and had nuclear morphologies with a single focal point of heterochromatin, rather than the multiple points which would be expected in a cone photoreceptor. These observations were limited to the reporter-labelled cells within the ONL, however, as the cells remaining in the subretinal space continued to differentiate towards the cone fate and produce mature cone proteins, despite not showing photoreceptor morphology. Conversely, when transplanted into $Nrl^{-/-}$ recipient retinas, the GFP+ cells within the recipient ONL did morphologically resemble cones and expressed cone markers. In the WT retina, rods make up the overwhelming

majority of photoreceptors in the ONL, and likewise the vast majority of segments in the retina are rod segments. As a result, it is extremely difficult to ascertain whether the GFP+ cells were in fact expressing rod proteins, as might be predicted by their morphology.

These observations are in keeping with those seen in previous studies looking at the transplantation of mixed photoreceptor populations labelled with GFP under the control of the cone-rod homeobox transcription factor, Crx (Lakowski et al., 2010). Here, even at developmental ages when the transplanted population was predicted to be >75% cone photoreceptors, the overwhelming majority (at least a hundred-fold) of GFP+ cells in the recipient ONL resembled rod photoreceptors.

The above results are also comparable to those reported in a recently published paper (Smiley et al., 2016). In this study, a different promoter for GFP expression was used to label developing cones, using the ccdc136 locus. Injections of 10 000 fluorescent cells from E17 donors of this model were made into the subretinal space of adult WT recipient mice, and between 40 and 170 GFP+ cells were subsequently seen in the recipient ONL. These cells were described by the authors as undifferentiated, as although they exhibited polarised morphology including processes and outer segments, these cells failed to display cone arrestin expression.

The results of this chapter and the work of other groups indicate that even with the use of a purified population of true cones, the majority of GFP+ cells in the recipient ONL resemble rod photoreceptors.

4.3.2 Fate switching towards rod identity

qPCR evidence, as presented in Chapter 3, suggests that at developmental time points and young adult stages, Chrnb4.eGFP cone precursor cells show a surprisingly high level of expression of rod-specific transcripts, in comparison to the negligible expression levels shown by fate-restricted $Nrl^{-/-}$ cells. Previous studies have shown that cone photoreceptors can be converted to rod-like function with a relatively low level of ectopic Nrl expression (McIlvain and Knox, 2007; Oh et al., 2007). It could be, therefore, that something about the change of environment associated with transplantation into the rod-dominant adult WT recipient retina that allows these potentially plastic cells to respond to rod developmental genes and/or environmental cues that are instructive for rod differentiation.

Arguing against this is the fact that, in normal development, WT cone photoreceptors mature successfully while surrounded by large numbers of rod photoreceptors. While the adult retina of the recipients used in these experiments might provide distinct environmental cues from the developing retina, previous attempts to transplant cone photoreceptors into immature retinas did not lead to an increased proportion of GFP+ cells in the recipient ONL which resembled cone photoreceptors (Lakowski et al., 2010).

For cell fate plasticity to account for these results, therefore, one can propose that there must be an external environmental cue present in the rod-rich WT retinas, but not in the rod-lacking $Nrl^{-/-}$ recipients, that causes only transplanted cone precursors to move towards a rod fate.

The possibility that external factors might influence the fate of photoreceptor precursor cells is supported by many previous studies. For example, adding

exogenous developmental transcription factors to retinal cultures *in vivo* has effects on the production of rod photoreceptors. Similar approaches have been used in more recent successful attempts to encourage the production of photoreceptors in cultures of embryonic and induced pluripotent stem cells (Osakada et al., 2008). Taurine and retinoic acid have been shown to increase the production of rod photoreceptors in cell cultures taken from the dissociated retinas of embryonic rats (Altshuler et al., 1993; Kelley et al., 1994) with a concomitant decrease in amacrine cell numbers, although these effects appeared only to affect progenitor cells before terminal mitosis. Conversely, addition of ciliary neurotrophic factor (CNTF) on retinal explants taken from postnatal rats resulted in a marked reduction in the production of rods in these retinas (Ezzeddine et al., 1997), with these cells apparently differentiating into bipolar cells instead, even after terminal mitosis.

Perhaps more relevantly, the Notch pathway, an intercellular signalling pathway which plays a major role in neurogenesis, has been shown to be important in retinal development. Conditional ablation of Notch1 in early progenitor cells led to the enhanced production of cone photoreceptor cells, while later ablation encouraged the production of rod photoreceptors (Jadhav et al., 2006b; Yaron et al., 2006). These cell types appeared to be produced at the expense of numbers of the other component cells of the retina. On the other hand, the ability of Notch mechanisms to affect cell fate appear to decline over time as retinal development becomes more complete (Silva et al., 2003). Interference with Notch expression using antisense nucleotides allowed genesis of RGCs beyond the time when it would usually cease, but only for a brief period after this. Such temporal restrictions on the activity of this system, and others like it, could explain why cone cells can develop under normal circumstances, but fail to mature fully after transplantation.

A primary reason for these observations, however, appears to be due to effects of the timing of exit of cells from the cell cycle, privileging early-born rather than late-born cells or *vice versa*. Evidence of an ability to affect the fate of neural cells after terminal mitosis, when differentiation has begun to take place, without artificially induced genetic alterations, is rarer in the literature.

Studies have shown that some types of cell in the nervous system can respond to injury with marked changes to their appearance, transcriptional profile and function, indicating that phenotypic plasticity is not unknown in neural tissue. Astrocytes have been shown to be able to produce new neuronal cells in response to injury, by a process of dedifferentiation to a proliferative neuroblast state, followed by cell division and the production of neural precursors (Shen et al., 2015). In the retina of lower vertebrates, it is the RPE cells and in fish, chicks and rodents, the Müller glia which can be stimulated to de-differentiate to produce proliferating progenitor cells for the replacement of retinal neurons (reviewed in Gallina, Todd, & Fischer, 2014). This process of reversion to an earlier proliferative stage is not, however, apparent in the photoreceptor precursor cells injected in this or previous studies (MacLaren et al. 2006; Pearson et al. 2012; West et al. 2012).

Indeed, while attempts to reprogramme cells *in vivo* to generate neurons have attempted primarily to convert astroblasts into proliferative neuroblasts, it has been shown that cortical glia can be induced to become functional neurons directly by the induction of SOX2 or NEUROD1 expression, and more relevantly, that the subtype of developing neurons could be changed (Smith et al., 2016). For example, a study found that postmitotic callosal projection neurons of layer II/III in the mouse neocortex can be converted into layer V/VI corticofugal projection neurons by inducing expression of the FezF2 transcription factor (Rouaux and Arlotta, 2013). While the ability to cause this change was limited to embryonic and early postnatal

time points, this compares with the age range of the cells transplanted in retinal photoreceptor cell replacement therapy in this and other studies.

A closer parallel in the retina, as mentioned above, are studies showing that postmitotic cone photoreceptor precursors can be converted to rod-like function with the induction of a low level of Nrl expression in *Xenopus* and mouse (McIlvain and Knox, 2007; Oh et al., 2007). Also, by expressing Nr2e3 in developing cone precursors under the S-opsin promoter WT cones have been shown to transform into cells which are partially rod-like in their nuclear morphology and expression of rhodopsin (Cheng et al., 2006). Similarly, rod photoreceptors can be reprogrammed to become cone-like, and maintain function, even in the adult retina (Montana et al., 2013), through the induced inactivation of Nrl expression. This last study shows that prolonged production of specific transcription factors appears to be necessary for the maintenance as well as the specification of a particular photoreceptor fate.

However, in contrast to the developmental effects of cell-cell communication, for example via Notch, or secreted factors such as retinoic acid, the examples provided above all involve intervention at a cell-internal level, primarily through artificial supply or a change in regulation of cell type-specific transcription factors using inducible genetic modification, viruses, transfection or electroporation. It is not clear how similar effects – the changing of a cone cell to a rod fate - might take place in the context of transplanted cells at ages well past terminal mitosis, as suggested by my results, purely as an effect of a recipient environment with no obvious internal supply of Nrl. With this in mind, the possibility that my injected cells might undergo a change in fate required careful further investigation.

4.3.3 Alternative approaches

From a clinical point of view, the possibility that injected cone photoreceptor cells might change their developmental fate and mature into more rod-like cells presents a problem for the utility of the transplantation approach. Since cone-mediated vision is necessary for colour, high light and high acuity vision, these cells are more important for human sight. If injected cone photoreceptors are not, in the main, able to maintain a cone fate, it may not be possible to restore significant cone vision with this method.

It is important to note, however, that the specific environment of the human retina is different to that of the mouse. Cone photoreceptors are concentrated in the central retina, with rod cells absent in this area, making the environment more similar in some ways to that of the cone-only $Nrl^{-/-}$ mouse. The pathology of AMD is also focussed on this area (see section 1.4.2) and cell therapy to treat this part of the retina might therefore be better represented by transplantation into the $Nrl^{-/-}$ model.

Mouse retinal models that have disrupted pathways leading to the production of rod photoreceptors (for example, the $Nrl^{-/-}$ and $Nr2e3^{rd7/rd7}$ mice discussed in Chapters 1 and 3), provide an interesting way to test the hypothesis that transplanted cone precursors can change in fate to become more rod-like. It would be expected that cone photoreceptors isolated from these models would be unable to change their developmental fate in this way and might therefore represent a superior source of cells for transplantation.

Previous studies have shown the effect of different recipient retinal environments on the outcomes of transplanting cells (Barber et al., 2013). In particular, previous attempts to transplant cone precursor cells found that cone-like phenotypes were

more common after transplantation into the cone-functionless Gucy2e$^{-/-}$ model (Lakowski et al., 2010). However, due to the inefficient nature of transplanting true cone cells, and difficulty in obtaining enough cells to do sufficient numbers of injections, it was decided that it would not be feasible to follow a similar line of investigation with Chrnb4.eGFP donor cells to a satisfactory degree.

Similarly, since previous studies of the restoration of function after the transplantation of photoreceptor cells has shown that the many thousands of GFP+ cells in the recipient ONL of a functionless model are needed after transplantation to find evidence of large scale functional capacity (Pearson et al., 2012) , the results found so far with Chrnb4.eGFP cells suggest that a more effective combination of donor and recipient will be necessary to have realistic prospects of impacting upon visual function.

Instead, in Chapter 5, I will focus on the use of alternative sources of cone-like cells for the exploration of transplantation: the Nrl$^{-/-}$ and Nr2e3$^{rd7/rd7}$ mouse models. The Chrnb4.eGFP model was however again used for investigations into the migratory behaviour of developing cone photoreceptors, as shown in Chapter 7.

Chapter 5 – Transplantation of cone-like cells

5.1 Introduction

The Chrnb4.eGFP line represents a useful source of cone photoreceptor precursors for use in the investigation of cell replacement therapy in the retina, as shown in section 3.2.2. However, cone photoreceptors comprise just 3% of the total photoreceptor numbers in the mouse, around 180,000 cells in each adult retina (Jeon et al., 1998), not all of which will be successfully obtained by the fluorescence sorting methods described. Additionally, I showed in Chapter 4 that the majority of transplanted Chrnb4.eGFP+ cells in the host ONL do not resemble mature cone photoreceptors morphologically or in their patterns of protein expression. This is similar to the results seen after transplantation of CrxGFP cells (Lakowski et al., 2010) where even with donor cells cells taken from developmental stages at which they should have been overwhelmingly cone photoreceptor precursors, the majority of labelled cells within the recipient retina resembled rod photoreceptors.

The $Nrl^{-/-}$ mouse does not produce rod photoreceptors, lacking as it does the Nrl transcription factor which acts through its target, Nr2e3, to suppress cone identity (Oh et al., 2008). Instead, the retina is composed of a large amount of photoreceptors which resemble cones in their morphology, protein production and light response (Yoshida et al., 2004). If the rod-like appearance of GFP+ cells in recipient retina after the transplantation of Chrnb4.eGFP cells is due to the donor cells integrating into the recipient and undergoing a change of cell fate, it might be predicted that the $Nrl^{-/-}$ model would be unable to change fate in this way.

In practical terms, too, the high number of cone-like cells produced by the $Nrl^{-/-}$ retina represents a more efficient source of cells for transplantation than the true cones produced by the Chrnb4.eGFP mouse.

Another enriched source of fate-restricted cone-like cells is provided by the $Nr2e3^{rd7/rd7}$ mouse. Nr2e3, as the target of Nrl, is involved in the promotion of rod identity at the expense of cone photoreceptors. As a result, this model produces supernumerary S-opsin expressing cones primarily in the ventral retina (Haider et al., 2001, 2000). Unlike the $Nrl^{-/-}$ model, however, it also produces photoreceptors that are more similar to rods: the majority of the photoreceptors in this model being hybrid cells expressing all expected rod marker genes but, additionally, many cone markers, including *Pde6c* and *Gnat2*.

In this chapter, I test the hypothesis that $Nrl^{-/-}$ and $Nr2e3^{rd7/rd7}$ cone like cells can integrate into recipient retinas after transplantation, and develop into mature cells. Given the results of the transplantation of Chrnb4.eGFP cells, I will be looking particularly at the appearance of these cells after transplantation, and attempting to characterise their pattern of protein expression.

For cell replacement therapy to be of use in a clinical context, it must be able to occur in not only the healthy retina but also the diseased retinal environment.

The changes to the retinal environment that occur in retinal degeneration vary considerably depending upon the initiating cause, and are discussed in section 1.5.1.2. They often include the death and removal of photoreceptor cells, ONL thinning, and the process of gliosis in the Müller glia. Effects on the ECM cause changes in the deposition of cell-cell adhesion molecules. Since for donor cells to

integrate into recipient ONL they must move past the OLM and through the ECM, the role of these factors is likely to be important for transplantation outcome.

Several mouse lines exist that aim to model different retinal diseases, degenerations and conditions, and while differences exist between these models and human conditions, they represent an essential point of progression towards clinical applications. Previous studies have found that while reporter labelled cells are found in the recipient retina of most mouse models assessed after transplantation, the outcome of cell injection varies significantly between models. In particular, the number of reporter-labelled cells in the recipient ONL has been seen to increase relative to wild-type in some models, and decrease in others (Barber et al., 2013).

To assess the ability of cone photoreceptor replacement therapy to restore functional qualities of the recipient retina in future experiments, it is also desirable to identify a recipient type in which transplantation outcome is good but which has minimal functional capacity of its own, so that the function of transplanted cells can be seen.

In this chapter I also look at the effect of degenerating retinal environments on the transplantation of cone-like cells.

5.2 Results

5.2.1 Transplantation of Nrl$^{-/-}$/NrlGFP donor cells into WT recipients

In order to assess the transplantation capacity of these cells, it was necessary to first inject them into wild-type mice, in accordance with previous work.

Previous work has shown that the age of donor cells affects the outcome of rod photoreceptor transplantation (Decembrini et al., 2011; Gonzalez-Cordero et al., 2013; MacLaren et al., 2014), and that the best outcome of transplantation using rod photoreceptor precursors is when the cells are isolated at postnatal day 8 (Pearson et al., 2012). Rod and cone photoreceptors develop differently in several ways, notably in the time of birth and of migration. Although the Nrl$^{-/-}$ cone-like photoreceptor resembles a cone cell in most ways, it seems likely that they might differ most at the earliest stages of development; Nrl$^{-/-}$ photoreceptors are born at the same time as rod photoreceptor precursors, and although Nrl can be seen to be active within hours of terminal rod mitosis (Akimoto et al., 2006) it is not clear at what point the absence of Nrl causes a change in photoreceptor development and fate.

As shown by the qPCR and IHC data presented in Chapter 3 (see section 3.2.4), at P8, while expression of rod specific markers is very low, the Nrl$^{-/-}$NrlGFP cells do not have the same expression profile of cone specific markers as the Chrnb4.eGFP cells. Furthermore, the low numbers of GFP+ cells seen in host retina after transplantation of Chrnb4.eGFP cells at each of the time points chosen for injection did not provide strong evidence for an optimum age for transplantation.

Therefore, a number of ages of donor cells were selected for transplantation: P8, the age at which the transplantation of NrlGFP rod precursors is most efficient; P1, the age of peak rod genesis, and E15.5, the age of peak cone genesis. Adult WT mice received injections of 200,000 GFP positive cells from P8, P1 or E15.5 (+/- 1 day) $Nrl^{-/-}$/NrlGFP mice into the superior subretinal space. The recipient mice were sacrificed 2 weeks after transplantation. Eyes were stained for Rxrγ and GFP.

Figure 5.1 shows representative pictures of GFP+ cells in the ONL of recipient retinas. All injected eyes examined and not rejected due to inflammation or insufficient subretinal mass presented with GFP+ cells within the recipient ONL. The majority of the GFP+ cells had unambiguous photoreceptor morphology, including processes from the cell soma, inner and outer segments, and synaptic end feet, although not all cells showed all of these features, most likely due to sectioning or imaging artefacts.

Figure 5.1E shows the number of GFP+ cells seen in the ONL of recipient eyes (based on a tripling of the count of every third section taken). It should be noted that the counts for the use of E15.5 donor mice were not held to the same exclusion criteria as the other donor ages. In all 11 injected eyes, the sizes of the observed subretinal masses were below the level usually taken to represent a successful transplantation. However, macrophage activity was observed in 4 and autofluorescent debris in the presumed area of injection, often with damage to the ONL seen, was observed a further 5 times, suggesting a general failure of the transplanted cells to survive over short periods. Due to this, and the very low numbers of GFP+ cells available at this developmental stage for isolation and injection (fewer total cells for sorting were obtained from the smaller retinas, and the FACS yield for E15.5 cells was also typically around 3-5%), it was decided that it would be impractical to pursue the transplantation of E15.5 cells further. From the

data obtained – that is, the counts from all 6 retinas where GFP+ cells could be seen in the recipient retina, regardless of exclusion criteria – are included for comparative purposes, although all E15.5 data were excluded from statistical evaluation.

No difference was seen between the number of GFP+ cells within the recipient ONL using either P1 or P8 donor cells ($t(16) = 0.1827$, $p=0.8573$). The mean number of GFP+ cells in the recipient ONL using P8 donor cells was 242 (SD = 195, SEM = 62, n=10 injected eyes with 5 rejected) and using P1 cells was 257 (SD = 122, SEM = 43, n=8 injected eyes with 9 rejected). Notably, these cells were comparable to the numbers seen after transplantation of Chrnb4.eGFP cells (see 4.2.1), but much lower than previous work using NrlGFP rod photoreceptor precursors where an average number of more than 6000 GFP+ cells has often been achieved (Warre-Cornish et al., 2014). This is despite the fact that these cells can be easily isolated from donor tissue (in contrast to Chrnb4.eGFP cells) and could thus be injected in the usual numbers (200,000 / eye). This indicates a difference in the integration capacity of cone and cone-like precursor cells, compared to NrlGFP rod precursors. The reason for this is not clear, although due to the size and appearance of the subretinal masses of donor cells, it did not appear to involve a failure to survive post-transplantation.

Notably, and similarly to results obtained with the transplantation of Chrnb4.eGFP cells, many aspects of the GFP+ cells in the recipient retina resembled rod photoreceptors rather than cones, as shown in Figure 5.1A. Cells were found located throughout the whole width of the ONL, and their nuclei were typically small and with single points of condensed chromatin, while when segments could be seen they mostly resembled those of rod photoreceptors. In addition, the vast majority of the GFP+ cells did not express the cone marker, Rxrγ.

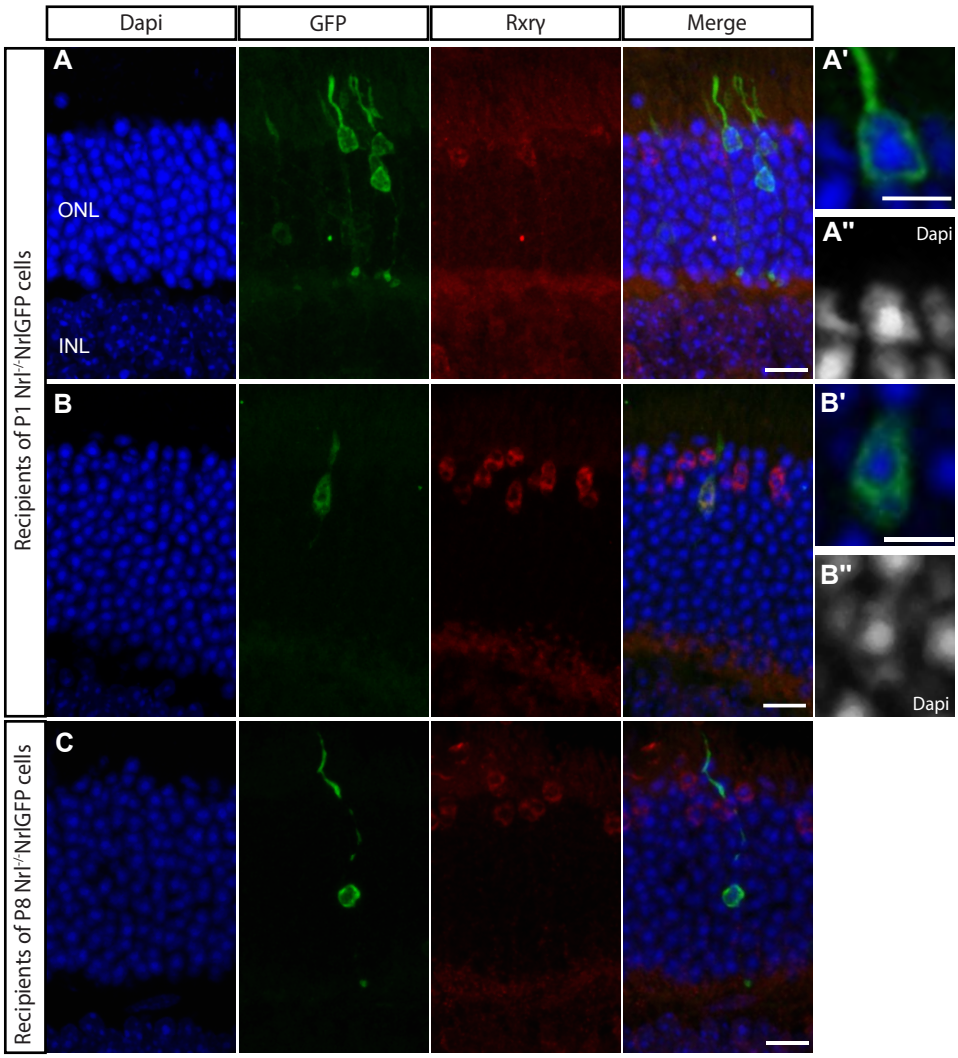

Figure 5.1 Transplantation of Nrl$^{-/-}$ cells .

(**A-D**) Adult WT mice received transplantation of 200,000 GFP positive Nrl$^{-/-}$NrlGFP cells isolated from E15.5, P1 or P8 donors. GFP positive cells were found in the host ONL after transplantation of P1 (A,B) and P8 (C,D) cells. The majority of GFP+ cells resembled rod photoreceptors (A,C), with small cell bodies showing a single point of condensed chromatin (A', single optical section), and small synaptic terminals. A small minority of cells (B) were found which expressed Rxrγ, were located in the outer part of the ONL and had multiple visible points of condensed chromatin (B', single optical section). Another minority of cells expressed different cone markers such as cone arrestin (D, arrows, this image from an eye which was taken 4 weeks after cell injection) despite being located away from the apical limit of the ONL (lower arrow) and with condensed, rod-like nuclei.
Scale bars 5µm in A', B', 10µm otherwise.

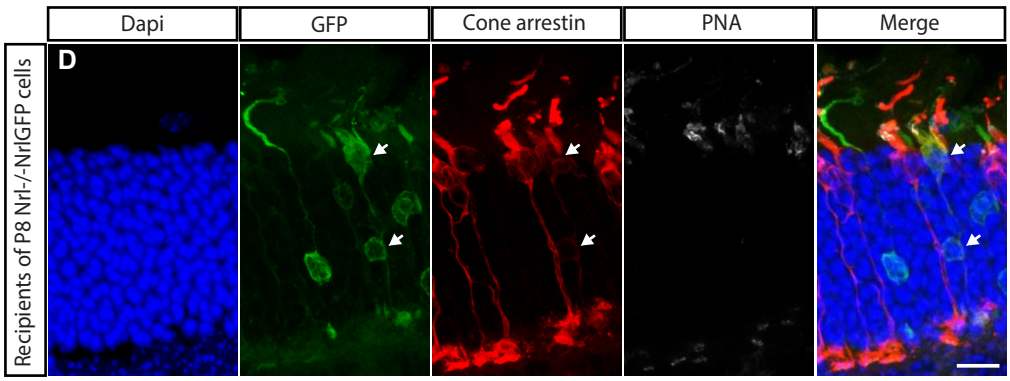

E Wild-type recipients of 200 000 Nrl$^{-/-}$/NrlGFP cells

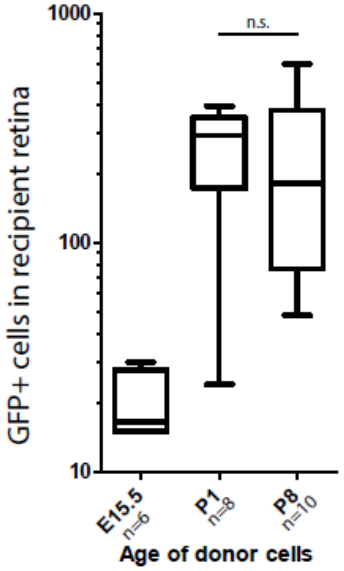

(**E**) Number of GFP+ cells found in WT recipients 2 weeks after injection. Range and quartiles are shown. Numbers for P1 and P8 cells are not significantly different from each other, while those from E15.5 cells are excluded from statistical analysis (see main text).

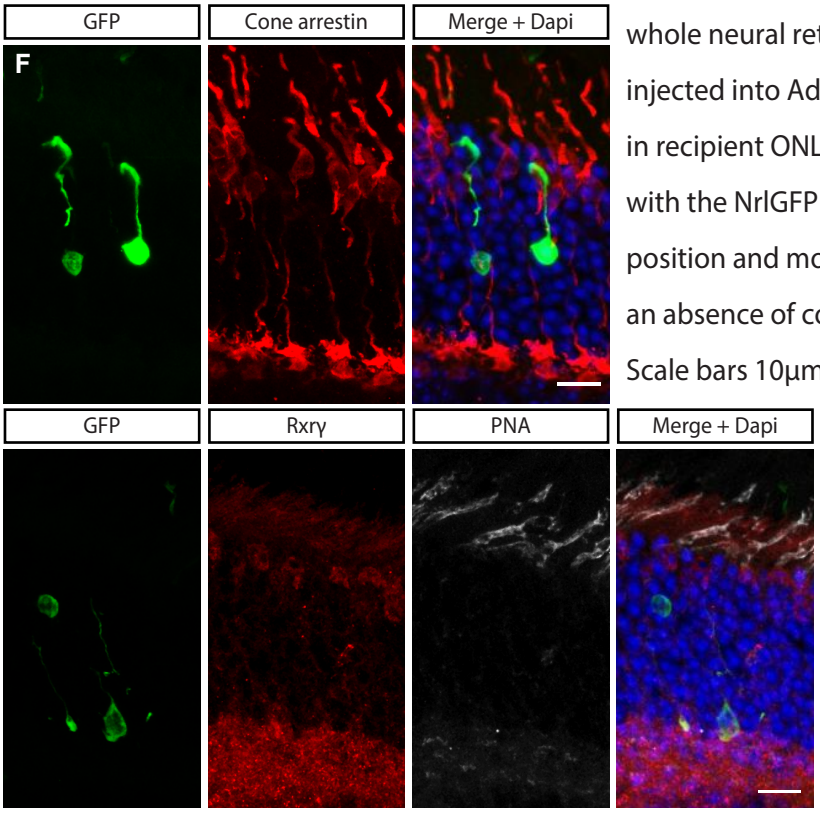

(**F,G**) Transplantation of ubiquitously GFP-expressing Nrl$^{-/-}$ cells into WT recipients. 200,000 cells isolated from whole neural retinal preparations were injected into Adult WT mice. GFP+ cells in recipient ONL resembled those found with the NrlGFP reporter, with their position and morphology rod-like, and an absence of cone-marker expression. Scale bars 10µm.

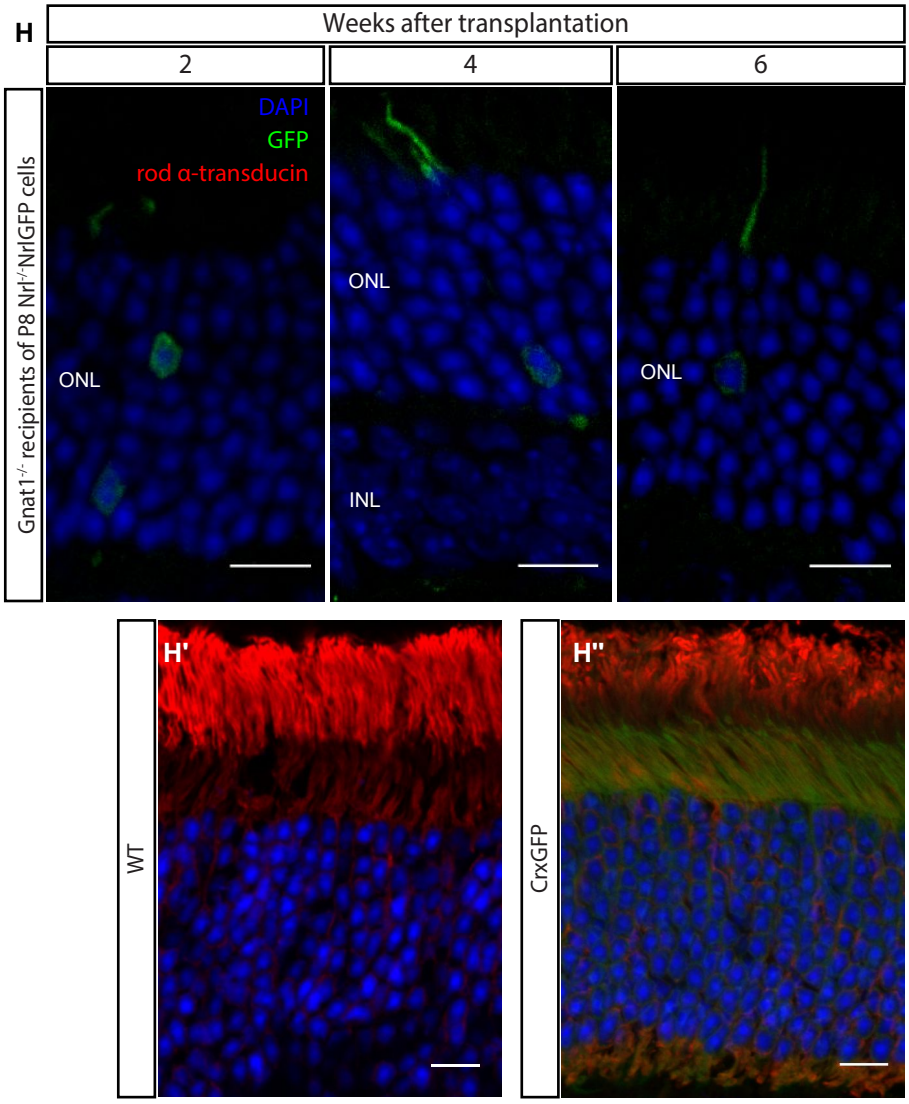

H Transplantation of 200,000 P8 Nrl$^{-/-}$NrlGFP cells into Gnat1$^{-/-}$ recipients. At 2, 4 and 6 weeks after transplantation, despite rodlike appearances of the GFP^{+} cells in the recipient ONL, neither these cells nor those of the recipients expressed Gnat1 (rod α-transducin). Rod α-transducin staining is evident in the WT (H') and CrxGFP (H'') control retinas, particularly in the photoreceptor segments. Scale bars 10μm. Thanks to Dr F Di Marco for these images.

Some exceptions could be found, however. Figure 5.1B shows an example of a GFP+ cell following transplantation of P1 donor cells which resembles a cone photoreceptor in position, Rxrγ expression and nuclear appearance. Although few examples of cells with these characteristics could be positively identified (fewer than 10 in each injected eye), it is notable that all those cells found that expressed Rxrγ were also located near to the apical margin of the ONL and showed the multiple points of condensed chromatin typical of cone photoreceptors.

Previous work has shown that transplanted cells (both those within the recipient ONL and those subretinal space) are more likely to express markers of mature functional photoreceptors with increased time after transplantation (Warre-Cornish et al., 2014). Some eyes of WT mice injected with $Nrl^{-/-}$/NrlGFP cells were left for 4 weeks after transplantation to investigate the effect of increased time post-transplantation on apparent cell fate. As shown in Figure 5.1D, immunostaining for cone arrestin and PNA revealed that although the majority of GFP+ cells located within the recipient ONL still did not express either of these markers, several could be seen which did. Notably, and in contrast to the Rxrγ positive cells seen above, which were almost always cone-like in appearance, a proportion of these GFP+/cone arrestin+ and GFP+/PNA+ cells had an appearance that more closely resembled rods, with smaller cell bodies that were located in the ONL away from the OLM and small rod-like nuclei.

As shown in Chapter 3, the $Nrl^{-/-}$/NrlGFP model shows a decline in GFP expression over time. The relatively short interval between transplantation and analysis of injected eyes, and the use of an antibody to enhance GFP signal was an attempt to reduce the impact of this decline on the visibility of transplanted cells. However, the observation that transplantation of $Nrl^{-/-}$ donor cells led to the appearance of GFP+ cells that more closely resembled rod photoreceptors, rather than cones, raised a

possibility that the Nrl promoter may be less active in cone-like cells, compared to rod-like cells, and we might therefore miss cone-like cells with weak GFP expression.

To investigate this, I crossed the $Nrl^{-/-}$ mouse with a mouse model that ubiquitously expresses GFP under the control of a CBA promoter and CMV enhancer (see Table 2.1). Neural retinal tissue from P8 mice resulting from this cross was dissociated using a papain kit into a single cell solution, but not sorted by FACS. 200,000 cells of this kind were injected into the subretinal space of adult WT mice. The animals were sacrificed two weeks after transplantation.

Figure 5.1F and G show GFP+ cells in the ONL of recipient mice. Similar results to those found after transplantation of $Nrl^{-/-}$/NrlGFP cells, specifically that the vast majority of GFP+ cells in recipient retina resembled rod photoreceptors rather than cones and did not stain positively for Rxrγ, cone arrestin or PNA. Due to the injected cells consisting of the whole cell population of the neural retina rather than a purified population, quantitative comparisons of the number of GFP+ cells in the recipient ONL were not attempted. However, based on these results, it did not appear that a reduction in GFP expression is the reason for the ambiguous appearance of Nrl-/-/NrlGFP cells within the recipient retina.

To investigate whether these cells were undergoing a change in fate and becoming rod-like photoreceptors, 200,000 $Nrl^{-/-}$NrlGFP cells were purified by FACS and injected into the subretinal space of rod α-transducin deficient ($Gnat1^{-/-}$) mice which have functionless rod photoreceptors. At 2, 4 or 6 weeks after transplantation, no rod α-transducin expression was found either in recipient cells or GFP+ cells in the recipient retina (Figure 5.1H, Dr Fabiana Di Marco sectioned, stained and imaged injected eyes provided by the candidate for these images) indicating that if donor

cells do become rod-like, they are not able to produce adult rod proteins. This is in contrast to NrlGFP rod photoreceptor precursor donors, which have been repeatedly shown to lead to robust rod α-transducin expression in GFP+ cells in recipient retina after transplantation (Barber et al., 2013; Pearson et al., 2012; Warre-Cornish et al., 2014).

5.2.2 Transplantation of $Nrl^{-/-}$/NrlGFP donor cells into $Nrl^{-/-}$ recipients

The low efficiency and ambiguous cell fate seen after the transplantation of $Nrl^{-/-}$ cells into WT retina, while similar to using Chrnb4.eGFP cells (Chapter 4), showed differences from the outcome of transplantation of rod photoreceptor precursors reported in previous work (Barber et al., 2013; Bartsch et al., 2008; Eberle et al., 2012; MacLaren et al., 2006; Pearson et al., 2012). To investigate the reasons for this, I assessed the outcomes of injecting these cells into a different environment.

Previous studies have shown strong effects both of the recipient retinal environment on the outcome of transplantation (Barber et al., 2013), and also the rod-cone balance of the recipient retina (Lakowski et al., 2010). To investigate the influence of the rod-cone ratio of the recipient retina on the transplantation of $Nrl^{-/-}$NrlGFP cells, I used the cone-only $Nrl^{-/-}$ retina as a recipient, representing the same environment as that from which donor cells were taken.

Adult $Nrl^{-/-}$ mice received injections of 200,000 GFP+ cells from P8 or P1 (+/- 1 day) $Nrl^{-/-}$/NrlGFP mice into the superior subretinal space. Recipient mice were sacrificed 2 weeks after transplantation. Eyes were stained for Rxrγ and GFP. In all analysed recipient retinas GFP+ cells could be seen in the ONL. Fig 5.2 shows representative pictures of GFP+ cells in the outer nuclear layer of recipient retinas. Again,

examples of photoreceptor morphology were apparent in GFP+ cells. Areas of a very high density of GFP+ cells could be seen, for example Fig 5.2C.

Figure 5.2 D shows the number of GFP+ cells seen in the recipient retinas after transplantation. A significant difference was seen between P1 or P8 donor cells $t(19) = 3.260$, $p=0.0041$. The mean number of GFP+ cells using P8 donor cells was 6251 (SD = 4642, SEM = 1400, n=11 injected eyes with 2 rejected) and using P1 cells was 1362 (SD = 967.8, SEM = 306, n=10 injected eyes with none rejected).

For each age of donor cell, the number of GFP+ cells per retina were strikingly higher in $Nrl^{-/-}$ recipients than WT mice (P1 - $t(16) = 3.190$, $p=0.0057$; P8 - $t(19) = 4.08$, $p = 0.0006$) using the results above.

Morphological assessment of the GFP+ cells within the recipient ONL indicated that they resembled cone photoreceptors, or at least the cone-like photoreceptors that are the predominant photoreceptor type in both the recipient and donor retinas, and that these cone-like cells were far more numerous than was seen after transplantation into WT retina. Given that the entirety of the recipient ONL expresses Rxrγ, it was difficult to determine with certainty whether the GFP+ cells also expressed this marker. Single confocal optical sections (Figure 5.2A'-A"") indicate that Rxrγ and cone arrestin are indeed found in most, if not all, observed GFP+ cells and that these cells have large nuclei with multiple points of condensed chromatin visible. Where segments could be seen, they appeared to be of a similar length to those of the recipient photoreceptors, suggesting maintenance of a 'cone-like' rather than 'true cone' phenotype, although it should be noted that GFP is expressed only weakly by outer segments, making these structures difficult to assess.

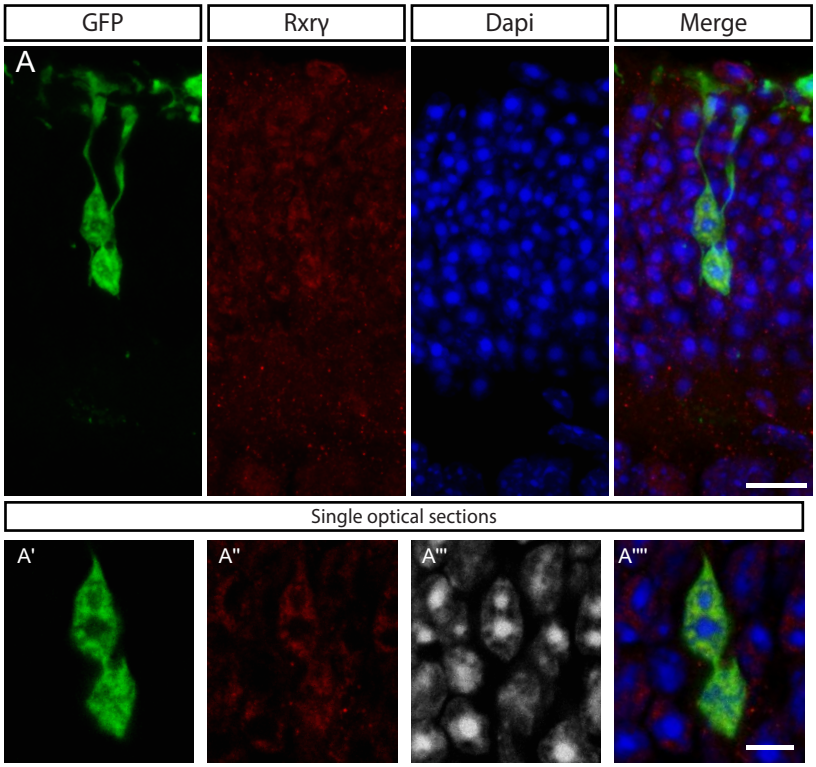
GFP
Rxrγ
Dapi
Merge
A
Single optical sections
A'
A''
A'''
A''''

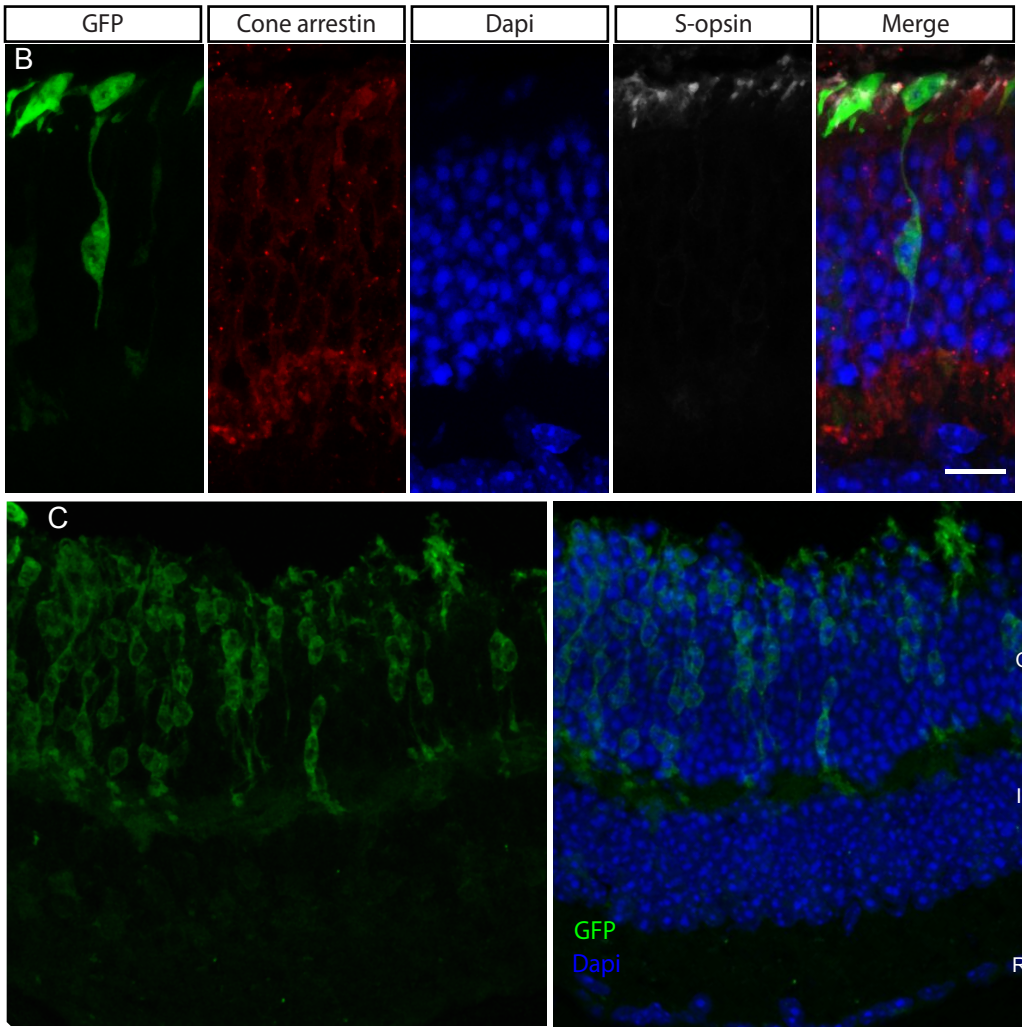
GFP
Cone arrestin
Dapi
S-opsin
Merge
B
C
ONL
INL
GFP
Dapi
RGC

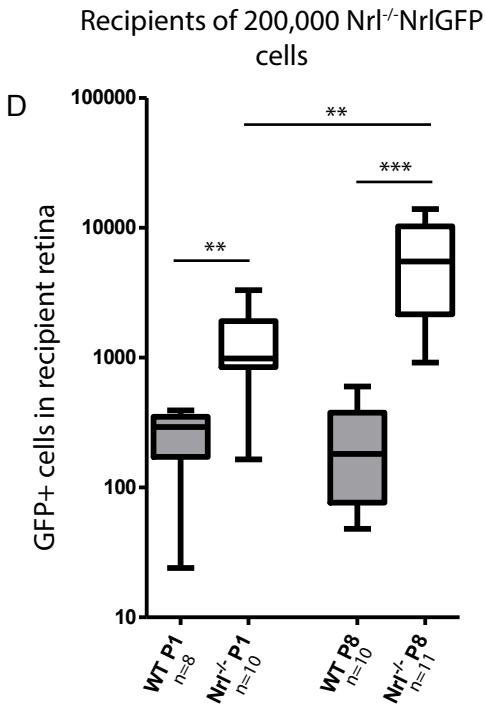

Figure 5.2 Transplantation of Nrl$^{-/-}$NrlGFP cells into Nrl $^{-/-}$ recipients. Adult Nrl$^{-/-}$ mice received transplantation of 200,000 GFP positive Nrl$^{-/-}$NrlGFP cells isolated from P1 or P8 donors. Scale bars 10μm, in A'''' 5μm.

(**A-B**) GFP+ cells were found in the host ONL after transplantation.

Single optical sections (A'-A'''', scale bar 5μm) showed the presence of Rxrγ in these cells, as well as nuclei resembling those of cones/cone-like cells, with large nuclei containing multiple points of condensed chromatin.

(**C**) Areas of very high numbers of GFP+ cells were seen in some parts of the recipient retina of this model.

(**D**) Number of GFP+ cells found in Nrl$^{-/-}$ recipients 2 weeks after injection (white) compared to WT recipients (grey, from Fig 5.1). Significantly more cells were seen using P8 donor cells than P1. Additionally, more cells were seen in Nrl$^{-/-}$ recipients than in WT, for both donor ages (separate comparisons).

5.2.3 Transplantation of $Nrl^{-/-}$/NrlGFP donor cells into degenerating recipients

Given the striking effect of the $Nrl^{-/-}$ recipient environment on both the efficiency of transplantation and the morphology of GFP+ cells, it was decided to investigate transplantation into a number of other retinal degeneration models including both rod and cone dystrophies, which represent a range of degeneration speeds and rod to cone ratios and functionality. The strains selected for transplantation are listed below, while genetic details can be found in Table 2.1.

The $Pde6c^{cpfl1/cpfl1}$ mouse is a cone-depleted model. It has a mutation in the cone-specific phosphodiesterase gene. The model shows a complete lack of cone function as well as rapid cone degeneration, with very few left by five months of age (Chang et al., 2009).

The $Prph2^{rd2/rd2}$ mouse is deficient in Peripherin 2, a membrane glycoprotein. The photoreceptors of this mouse fail to produce outer segments, and show degeneration from birth. This mouse is used as a model of (relatively) slow retinal degeneration, and presents an almost complete loss of rod photoreceptors by 3 months, while cone photoreceptors appear to survive for longer, on average (Ma et al., 1995).

The $Cnga3^{cpfl5/cpfl5}$ mouse provides a cone-functionless environment. This model has a missense mutation affecting the cone cyclic nucleotide gated channel and exhibits mislocalised, non-functional cones, with cone photoreceptors degenerating over several weeks after birth. This degeneration is particularly seen in the ventral and nasal retina, with an 57% reduction in these areas at 4 weeks after birth, compared

with a reduction of around 25% in dorsal and temporal parts of the retina at this stage (Michalakis et al., 2005; Pang et al., 2010).

The Nr2e3$^{rd7/rd7}$ model was also used as an alternative cone-enriched model. As mentioned above, the rd7 mutation disrupts the development of rod photoreceptors, and leads to a retina with increased numbers of S-opsin expressing cone photoreceptors, but with a milder phenotype than the Nrl$^{-/-}$ mouse, in that the resulting hybrid cells are more similar to rods and still comprise the majority of the photoreceptor populations.

To provide an approximately similar level of degeneration between recipients, these mice were injected between 7 and 9 weeks of age.

Given that P8 Nrl$^{-/-}$ donors yielded the best transplantation outcome, this donor age was used for the experiments described below. This also brings the work into line with previous studies looking at transplantation into different retinal models (Barber et al., 2013).

Adult Pde6c$^{cpfl1/cpfl1}$, Cnga3$^{cpfl5/cpfl5}$, Nr2e3$^{rd7/rd7}$ and Prph2$^{rd2/rd2}$ mice received injections of 200,000 GFP+ cells from P8 (+/- 1 day) Nrl$^{-/-}$/NrlGFP mice into the superior subretinal space. The recipient mice were sacrificed 2 weeks after transplantation. Eyes were stained for Rxrγ and GFP. Fig 5.3 shows representative pictures of GFP+ cells in the outer nuclear layer of recipient retinas. The vast majority of cells presented with morphology typical of photoreceptor cells.

A Kruskal-Wallis test (analysing all 6 recipient types together, including WT and Nrl$^{-/-}$) showed a significant effect of group: $H(5) = 45.36$, $p < 0.0001$, with Dunn's Multiple Comparison Test (comparing all recipient types with the control WT values). These

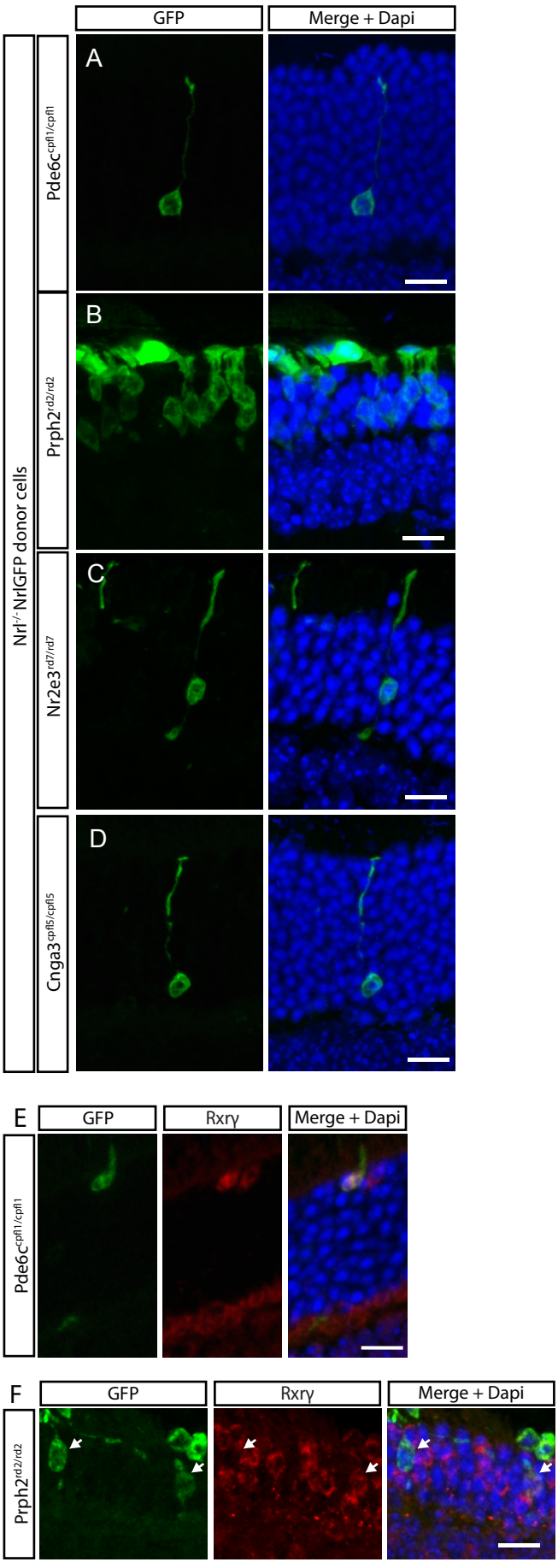
GFP
Merge + Dapi
A
B
C
D
Nrl-/- NrlGFP donor cells
Pde6ccpfl1/cpfl1
Prph2rd2/rd2
Nr2e3rd7/rd7
Cnga3cpfl5/cpfl5
E
GFP
Rxrγ
Merge + Dapi
Pde6cpfl1/cpfl1
F
GFP
Rxrγ
Merge + Dapi
Prph2rd2/rd2

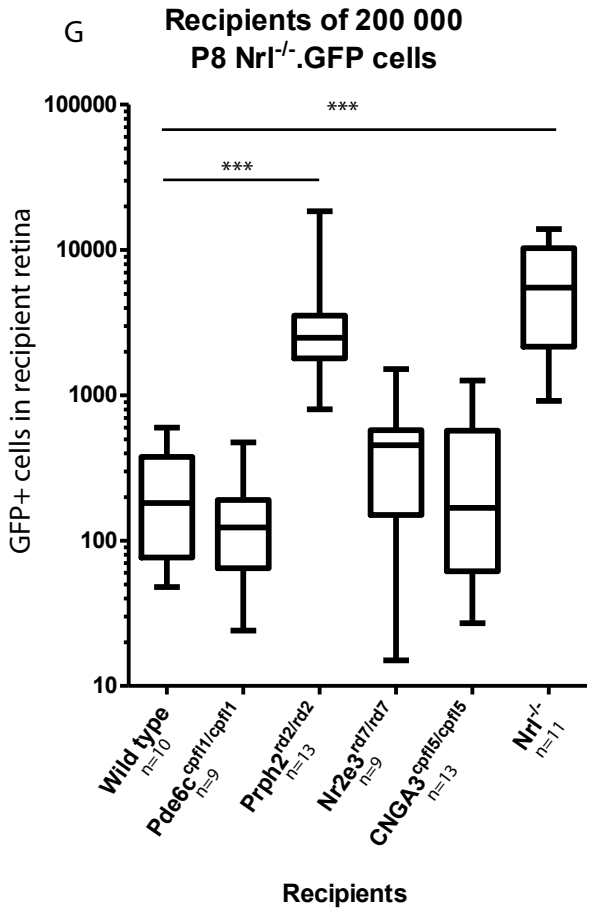

Figure 5.3 Transplantation of Nrl$^{-/-}$NrlGFP cells into various mouse degenerating recipients. Adult mice received transplantation of 200,000 P8 GFP positive Nrl$^{-/-}$NrlGFP cells.

(**A-F**) GFP+ cells were found in the host ONL of all recipient genotypes after transplantation. Areas of very high numbers of GFP+ cells were seen in the Prph2$^{rd2/rd2}$ recipient (B). In general, these cells resembled those found after transplantation into WT recipients (A-D, left arrow in F), with small, rodlike nuclei and synaptic terminals, and located away from the apical limit of the ONL. Rare exceptions which expressed cone markers such as Rxrγ , had larger conelike nuclei with several points of condensed chromatin and were located at the apical edge of the ONL were seen (E, F (right arrow), these examples in a Pde6c$^{cpfl1/cpfl1}$ and Prph2$^{rd2/rd2}$ recipient respectively). Scale bars are 10μm.

(**G**) Number of GFP+ cells found in recipients 2 weeks after injection, including WT and Nrl$^{-/-}$ recipients (previous experiments). Comparing to WT, significantly more cells were found in the Nrl$^{-/-}$ and Prph2$^{rd2/rd2}$ models, with other comparisons not significant.

data indicate that significantly more GFP+ cells were found in host retina after transplantation into both the $Nrl^{-/-}$ and the $Prph2^{rd2rd2}$ retinas ($p<0.05$ for both), compared to WT. Conversely, numbers in the $Pde6c^{cpfl1/cpfl1}$, $Cnga3^{cpfl5/cpfl5}$ and $Nr2e3^{rd7/rd7}$ mice were similar to WT. Table 5.1 shows the mean number of GFP+ cells within the different models.

Table 5.1 GFP+ cells found in recipient ONL after the transplantation of $Nrl^{-/-}$/NrlGFP cells into various recipients

Recipient genotype	Mean	SD	SEM	Analysed Injected eyes	Rejected
WT	242.4	195	61.66	10	5
$Nrl^{-/-}$	6251	4642	1400	11	2
$Pde6c^{cpfl1/cpfl1}$	149	135.3	45.09	9	5
$Prph2^{rd2/rd2}$	3780	4562	1265	13	2
$Nr2e3^{rd7/rd7}$	475.7	440.7	146.9	9	2
$Cnga3^{cpfl5/cpfl5}$	354.5	387.9	107.6	13	4

This table shows the mean number of GFP+ cells found in the recipient retina 2 weeks after transplantation, as well as the standard deviation (SD) and standard error of the mean (SEM). Rejections are based on criteria described in section 2.3.1.

GFP+ cells in the $Pde6c^{cpfl1/cpfl1}$, $Cnga3^{cpfl5/cpfl5}$ and $Nr2e3^{rd7/rd7}$ recipient retinas showed morphological profiles similar to those seen in WT recipient retina, in addition to similar efficiency. Both rod-like and cone-like morphologies were observed, although the vast majority of GFP+ cells resembled rod photoreceptors in morphology and position, and did not express Rxrγ. No obvious increases in the incidence of GFP+ cells resembling cone photoreceptors was seen in any of these models, including the $Pde6c^{cpfl1/cpfl1}$ and $Cnga3^{cpfl5/cpfl5}$ retinas, although due to the

very low number of this type of cell, this cannot be formally excluded. Rare exceptions were seen where correctly located GFP+ cells were Rxrγ positive and had nuclei resembling those of cone photoreceptors, as shown in Figure 5.3E.

In the Prph2$^{rd2/rd2}$ model, much higher numbers of GFP+ cells were seen in the recipient ONL and the cells showed a variety of nuclear and immunohistochemical profiles with a number of cells showing clear colocalisation of Rxrγ and locations at the outer edge of the ONL among the recipient cone cells, while the majority of GFP positive cells resembled rods, being Rxrγ negative and found away from the apical edge of the ONL.

The majority of recipient models, therefore, behaved similarly to the WT environment, with the reduction in cone presence evident in both the cone-functionless Cnga3$^{cpfl5/cpfl5}$ or cone-depleted Pde6c$^{cpfl1/cpfl1}$ models not seen to lead to obvious differences in transplantation results. The behaviour of the Prph2$^{rd2/rd2}$ model however suggests that some kinds of disease models support better transplantation outcomes, similar to the Nrl$^{-/-}$ model, and this will be explored in a later section.

5.2.4 Transplantation of Nr2e3$^{rd7/rd7}$/CrxGFP donor cells into WT and degenerating recipients

The Nr2e3$^{rd7/rd7}$ model was selected as an alternative enriched source of fate restricted cone-like cells. As explained above, this model produces extra S-cone like cells in the ventral retina, while the majority of photoreceptors are hybrid cells, expressing some cone markers in addition to their rod identity. This model was crossed with the CrxGFP model as a fluorescent reporter.

qPCR data on P8 and adult CrxGFP and Nr2e3$^{rd7/rd7}$/CrxGFP flow-sorted cells (see Chapter 3) suggested that the expression of photoreceptor-specific markers in both of these populations is similar to NrlGFP rods of the same ages, with an increase in cone marker expression in both cell types and particularly the Nr2e3$^{rd7/rd7}$/CrxGFP cells, as would be expected from a mixed population.

To investigate the optimum age of transplantation for these cells, adult WT mice received injections of 200,000 GFP+ cells from Nr2e3$^{rd7/rd7}$/CrxGFP mice of various ages (E15.5-E18.5, P0-P3 and P6-8) into the superior subretinal space. As a control, adult WT mice received injections of 200,000 GFP+ cells from CrxGFP mice of various ages (P0-P3 and P4-8). These experiments were carried out historically by Dr Giulia Grimaldi.

Numbers of GFP+ cells found in the ONL of each recipient type can be seen in Table 5.2. Looking at Nr2e3$^{rd7/rd7}$/CrxGFP cells after injection into WT recipients, a significant difference effect of group was found between donor ages ($H(2) = 9.988$. $p = 0.0068$), and Dunn's post-test, comparing all donor ages, finding significantly more GFP+ cells after transplantation using P0-3 donor cells than using E15.5-E18.5 cells ($p<0.05$) and P6-8 cells ($p<0.05$). With CrxGFP donor cells, there appeared to be a trend towards higher numbers of GFP+ cells seen in the recipient after the injection of P8 compared to P3 donor cells. While it is not clear why such a difference would exist, it is broadly similar to other findings of a variable effect of donor cell age, such as shown in Figure 5.2D, where a better result is seen using

P8 donor cells in the $Nrl^{-/-}$ recipient, but not the WT recipient. This may be due to the relatively overall variability of transplantation outcome.

Table 5.2 GFP+ cells found in recipient retina after the transplantation of $Nr2e3^{rd7/rd7}$/CrxGFP and CrxGFP cells of various ages into WT recipients (G Grimaldi)

Donor cell genotype	Age of donor cells	Mean	SD	SEM	Analysed injected eyes	Rejected
$Nr2e3^{rd7/rd7}$/CrxGFP	E15.5-E18.5	37	24.23	8.08	9	20
	P0-3	389	765.4	191.4	16	20
	P6-8	70.86	75.32	20.13	14	5
CrxGFP	P0-3	155.5	265.1	93.73	8	7
	P6-8	381.4	597.6	159.7	14	11

I subsequently attempted to investigate the effect of the recipient retinal environment on transplantation as I had with $Nrl^{-/-}$ donor cells. To this end, adult WT, $Nrl^{-/-}$ and $Nr2e3^{rd7/rd7}$ mice received injections of 200,000 GFP+ cells from P8 (+/- 1 day) $Nr2e3^{rd7/rd7}$/CrxGFP mice or CrxGFP mice into the superior subretinal space. The recipient mice were sacrificed 2 weeks after transplantation. Eyes were stained for Rxrγ or cone arrestin, PNA and GFP. Fig 5.4 shows representative pictures of GFP+ cells in the outer nuclear layer of recipient retinas and the majority presented morphologies typical of photoreceptors.

Table 5.3 GFP+ cells found in recipient retina after the transplantation of P7-8 Nr2e3$^{rd7/rd7}$/CrxGFP and CrxGFP cells into various recipients

Donor cell genotype	Recipient genotype	Age of donor cells	Mean	SD	SEM	Analysed injected eyes	Rejected
Nr2e3$^{rd7/rd7}$ /CrxGFP	WT	P7-8	502.7	432.0	144.0	9	9
	Nrl$^{-/-}$	P7-8	9690	7325	2442	9	0
	Nr2e3$^{rd7/rd7}$	P7-8	2085	2575	1051	6	19
CrxGFP	WT	P7-8	558.9	482.9	152.7	10	10
	Nrl$^{-/-}$	P7-8	2069	3424	1211	8	0
	Nr2e3$^{rd7/rd7}$	P7-8	1922	1453	513.8	8	4

As shown in Fig 5.4, the majority of GFP+ cells in the WT and Nr2e3$^{rd7/rd7}$ recipient models resembled rod photoreceptors both in position, and in cell and nuclear morphology. The majority also failed to express Rxrγ or Cone Arrestin (Fig 5.4 A,B), similar to results from the transplantation of Chrnb4.eGFP and Nrl$^{-/-}$/NrlGFP donor cells into these recipients. Again similarly, rare examples of cells expressing cone-specific markers were also seen (Fig. 5.4B).

As with previous attempts to transplant cells into the Nrl-/- recipient, the GFP+ cells within the retina of this model more closely resembled cone photoreceptors, both in position and morphology, and could be seen to express cone specific markers (Fig. 5.4C).

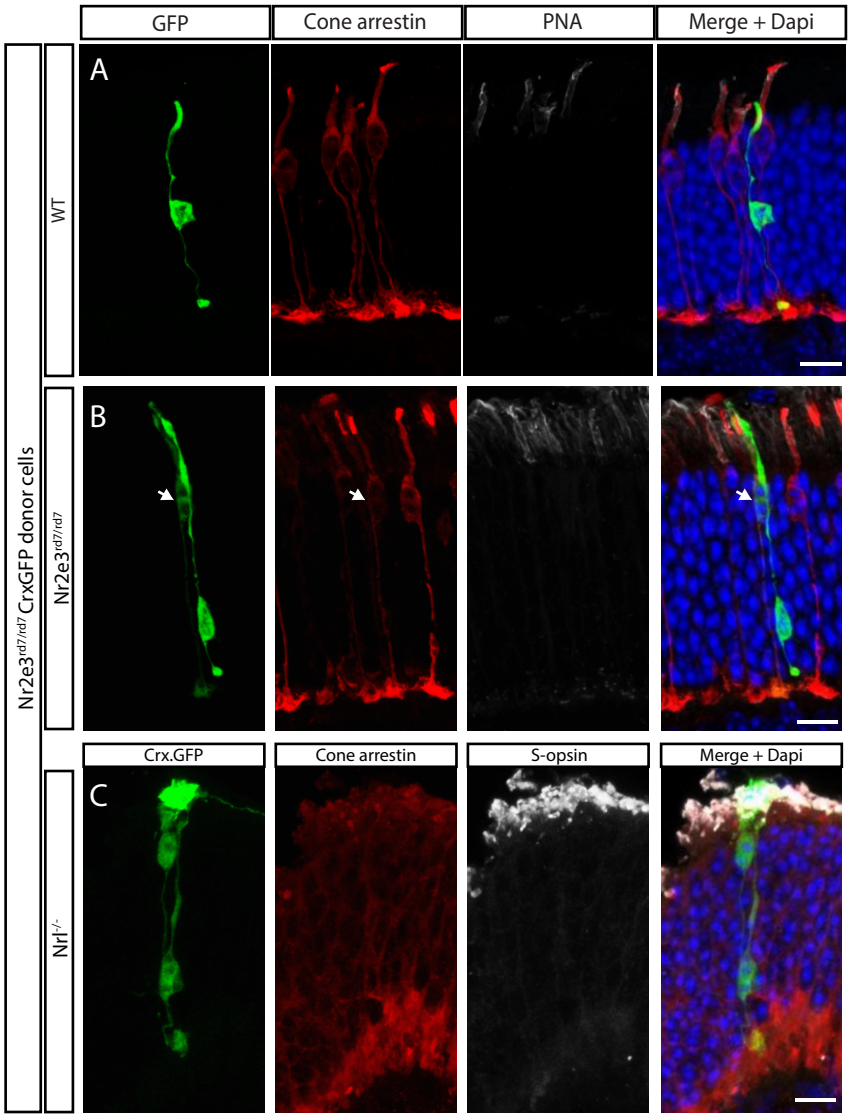

Figure 5.4 Transplantation of Nr2e3$^{rd7/rd7}$CrxGFP cells into WT, Nr2e3$^{rd7/rd7}$ and Nrl$^{-/-}$ recipients. Adult mice received transplantation of 200,000 P8 GFP positive Nr2e3$^{rd7/rd7}$CrxGFP cells.

(**A-C**) GFP+ cells were found in the host ONL of all recipient genotypes after transplantation. In general, these cells resembled those found after transplantation of Nrl$^{-/-}$ cells into WT recipients, showing small, rodlike nuclei and synaptic terminals, and located away from the apical limit of the ONL. Rare exceptions which expressed cone arrestin, had larger conelike nuclei with several points of condensed chromatin and were located at the apical edge of the ONL were seen (B, arrows). Scale bars are 10μm.

D

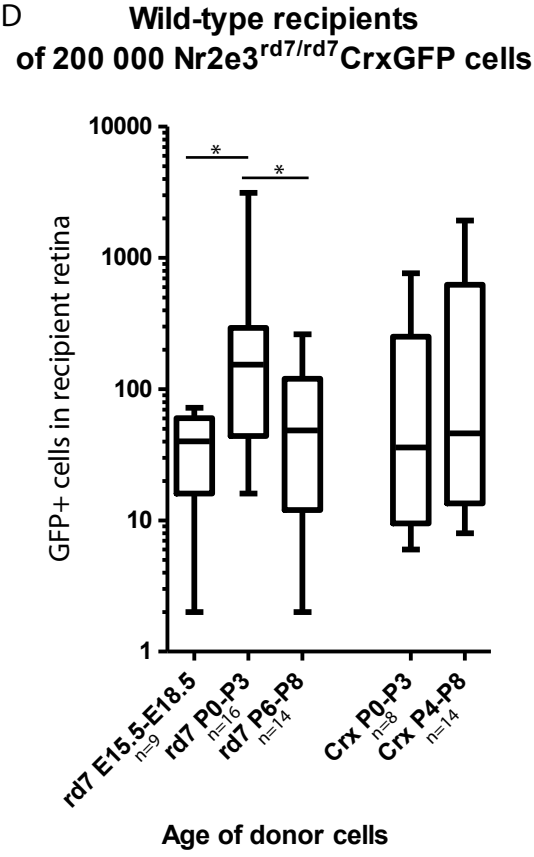

E

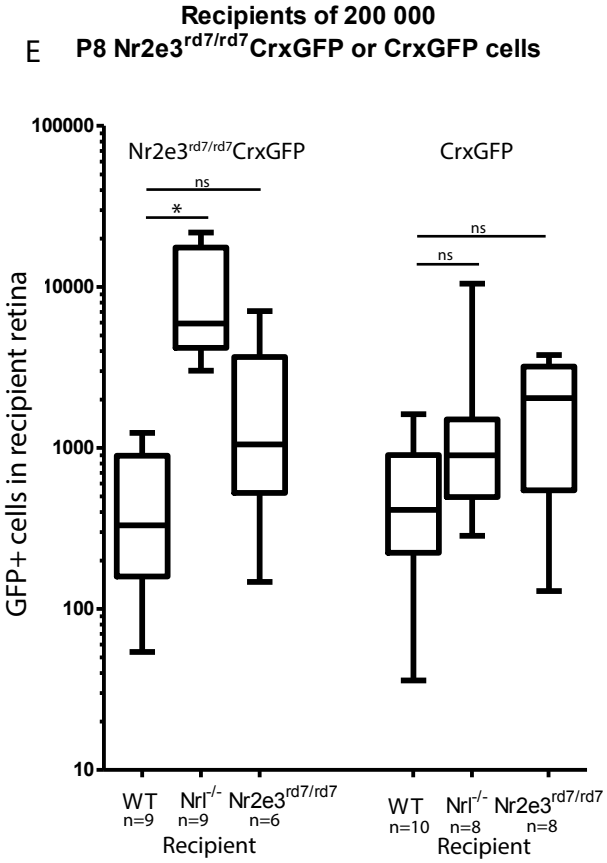

(**D,E**) Number of GFP+ cells found in recipients after injection of Nr2e3$^{rd7/rd7}$CrxGFP (left) or CrxGFP cells (right) at various donor ages (D, these data collected by G Grimaldi) or into various recipient retinas (E). (**E**) Significant effects of Recipient and Donor were found, as well as an interaction, but only Nrl-/- recipients of Nr2e3$^{rd7/rd7}$CrxGFP cells showed significantly more GFP+ cells than WT recipients of these cells, with other comparisons to WT not significant.

Acceptance rates of eyes from the Nr2e3$^{rd7/rd7}$ recipient injected with Nr2e3$^{rd7/rd7}$CrxGFP cells were surprisingly low, with only 6 out of a total of 25 eyes inspected accepted. The rejected eyes exhibited extremely low numbers of donor cells in the subretinal space, and these were often accompanied by evidence of acute inflammation and a thinning of the ONL. Given that this high level of rejection was seen even after experiments in which both other recipient types (WT and Nrl$^{-/-}$) were injected with the same preparation of donor cells, it is unlikely to be due to contamination of specific cell preparations, or repeated surgical damage. The Nr2e3$^{rd7/rd7}$ recipient has also been used with Nrl$^{-/-}$/NrlGFP donor cells (see 5.2.3) and CrxGFP cells here, without noticeably higher levels of rejection, while Nr2e3$^{rd7/rd7}$CrxGFP donor cells have variable levels of rejection after transplantation into WT and Nrl$^{-/-}$ recipients. Indeed, the Nrl$^{-/-}$ recipient appears to show lower levels of rejection than other models as rule, regardless of donor cell type. The reasons underlying this are unclear, however, the few Nr2e3$^{rd7/rd7}$CrxGFP into Nr2e3$^{rd7/rd7}$ eyes that were accepted may represent an abnormal outcome, rather than the norm, and comparisons using these data should be treated with caution.

A two-way ANOVA showed a significant effect of Recipient ($F(2,44) = 10.43$, $p = 0.0002$), Donor cell type ($F(1,44) = 6.32$, $p = 0.0157$), and an interaction between the two ($F(2,44) = 6.27$, $p = 0.004$). To summarise, these effects mean that transplantation outcome was better using Nr2e3$^{rd7/rd7}$CrxGFP cells than CrxGFP donors, and that transplantation outcome was significantly affected by the recipient retina.

To investigate the effect of recipient retina, however, Bonferroni-corrected post-test comparisons, comparing to WT, showed that the only significant difference was between Nr2e3$^{rd7/rd7}$CrxGFP into Nrl$^{-/-}$ recipients ($t(16) = 5.449$, $p < 0.0001$), and all other groups, with other comparisons not significant (although there was a non-

significant trend for better outcome in the Nr2e3$^{rd7/rd7}$ recipient, with both types of donor cell). This means that this single significant difference could be the cause of all of the significant ANOVA effects described above. Surprisingly, the improvement in transplantation outcome into the Nrl$^{-/-}$ recipient was not seen when using CrxGFP donor cells. It is not clear why this effect was not seen with CrxGFP cells, when it has been clearly seen on multiple occasions with other cells, specifically Nr2e3$^{rd7/rd7}$ and Nrl$^{-/-}$ cells (above, but see also 5.2.6 below) and NrlGFP rod cells (5.2.7, below), although notably not with Chrnb4.eGFP cone precursor cells (Chapter 4). With this in mind, it cannot be assumed that transplantation outcome is better when using Nr2e3$^{rd7/rd7}$CrxGFP donor cells than when using CrxGFP cells.

The numbers for both donor cell types into WT recipients reported above are lower than have been found using CrxGFP donor cells in previous studies (Lakowski et al., 2010) where the median number of P3 CrxGFP+ cells in recipient ONL was 5610, and also lower than previous studies looking at pure rod NrlGFP+ cell transplantation (Warre-Cornish et al., 2014).

These results are the more surprising considering that the combination of model and reporter in the Nr2e3$^{rd7/rd7}$CrxGFP mouse means that the cells transplanted would be a combination of true cones and supernumerary cones, together with a majority of hybrid cells which are primarily rod-like. Since transplantation outcome using cone donor cells (Chapter 4 and section 5.2.1) appears to be poorer than previous attempts using rod donor cells (Barber et al., 2013; MacLaren et al., 2006; Pearson et al., 2012; Warre-Cornish et al., 2014) (see also section 5.2.5 below), it would be predicted that the more rod-like population of the Nr2e3$^{rd7/rd7}$CrxGFP would have better outcome than purer cone populations. This applies even more to the CrxGFP cell populations. The Crx reporter does not allow for entirely precise isolation of photoreceptor cells only, as this model also weakly labels bipolar cells

(Lakowski et al., 2010; Samson et al., 2009), which could reduce numbers of GFP+ cells seen in the recipient ONL as eligible photoreceptor precursor cells would therefore make up a lower percentage of injected cells. However, the effect of this would not be expected to be great, as photoreceptor cells would still comprise the majority of injected cells. Indeed, unpurified ubiquitously GFP+ cells from the whole neural retina have been apparently successfully injected both in this work (see 5.2.1) and previous studies (MacLaren et al., 2006), implying that a lack of complete cell purity should not have a drastic effect.

Broadly, the results of injecting Nr2e3$^{rd7/rd7}$ donor cells are similar to those obtained using Nrl$^{-/-}$ donor cells in terms of transplantation efficiency and the appearance of transplanted cells. Similar to previous experiments, for both donor cell types, more GFP+ cells were found in the Nrl$^{-/-}$ recipient retina than into WT or Nr2e3$^{rd7/rd7}$ retina. With the exception of the Nrl$^{-/-}$ recipient, most rates of rejection were higher with Nr2e3$^{rd7/rd7}$CrxGFP transplants than encountered in previous experiments, with transplants into Nr2e3$^{rd7/rd7}$ recipients particularly high, reducing the suitability of these cells for future experiments.

5.2.5 Transplantation of NrlGFP donor cells into WT and Nrl$^{-/-}$ recipients

In 5.2.3, I examined the outcome of transplanting Nrl$^{-/-}$ photoreceptor cells into various retinal models. Two models supported much higher levels of GFP+ cells than WT recipients: the Nrl$^{-/-}$ and Prph2$^{rd2/rd2}$ mice. These models are significantly different to WT with respect to their rod:cone ratio, with a higher number of cones compared to rods. I thus considered the possibility that the better transplantation outcomes following transplantation of cone-like cells into these recipients might be enabled by the more cone-like environment of the recipient retina.

To investigate whether rod photoreceptor precursors react in a similar way, that is, if transplantation is more efficient in retinas with large numbers of rods rather than cones, I decided to transplant NrlGFP+ cells (rod photoreceptors) into rod rich WT and cone-only $Nrl^{-/-}$ retinas.

Adult WT and $Nrl^{-/-}$ mice received injections of 200,000 GFP+ cells from P8 (+/- 1 day) NrlGFP mice into the superior subretinal space. For this experiment, for each preparation of cells, both Nrl and WT mice were injected. The recipient mice were sacrificed 2 weeks after transplantation. Eyes were stained for Rxrγ, PNA and GFP. Fig 5.5 shows representative pictures of GFP+ cells in the outer nuclear layer of recipient retinas, which were correctly located within the recipient ONL and typically displated morphologies characteristic of photoreceptor morphology.

Numbers of GFP+ cells found within each recipient retina are shown in in Figure 5.5. The mean number of GFP+ cells found in $Nrl^{-/-}$ retinas was 4679 (SD = 2657, SEM = 594.2, n=20 injected eyes with 3 rejected) and into WT retinas was 1338 (SD = 1422, SEM = 410.4, n=12 injected eyes with 9 rejected). Significantly more GFP+ cells were found in the $Nrl^{-/-}$ model than in WT retinas: $U(30) = 23.00$, $p = 0.0002$

Although cell counts following transplantation of NrlGFP cells into WT retinas were lower than has been seen in previous publications (Warre-Cornish et al., 2014), they were significantly higher than those seen following the transplantation of $Nrl^{-/-}$ NrlGFP cells into WT, described above (see section 5.2.1): $t(20) = 2.409$, $p= 0.0257$.

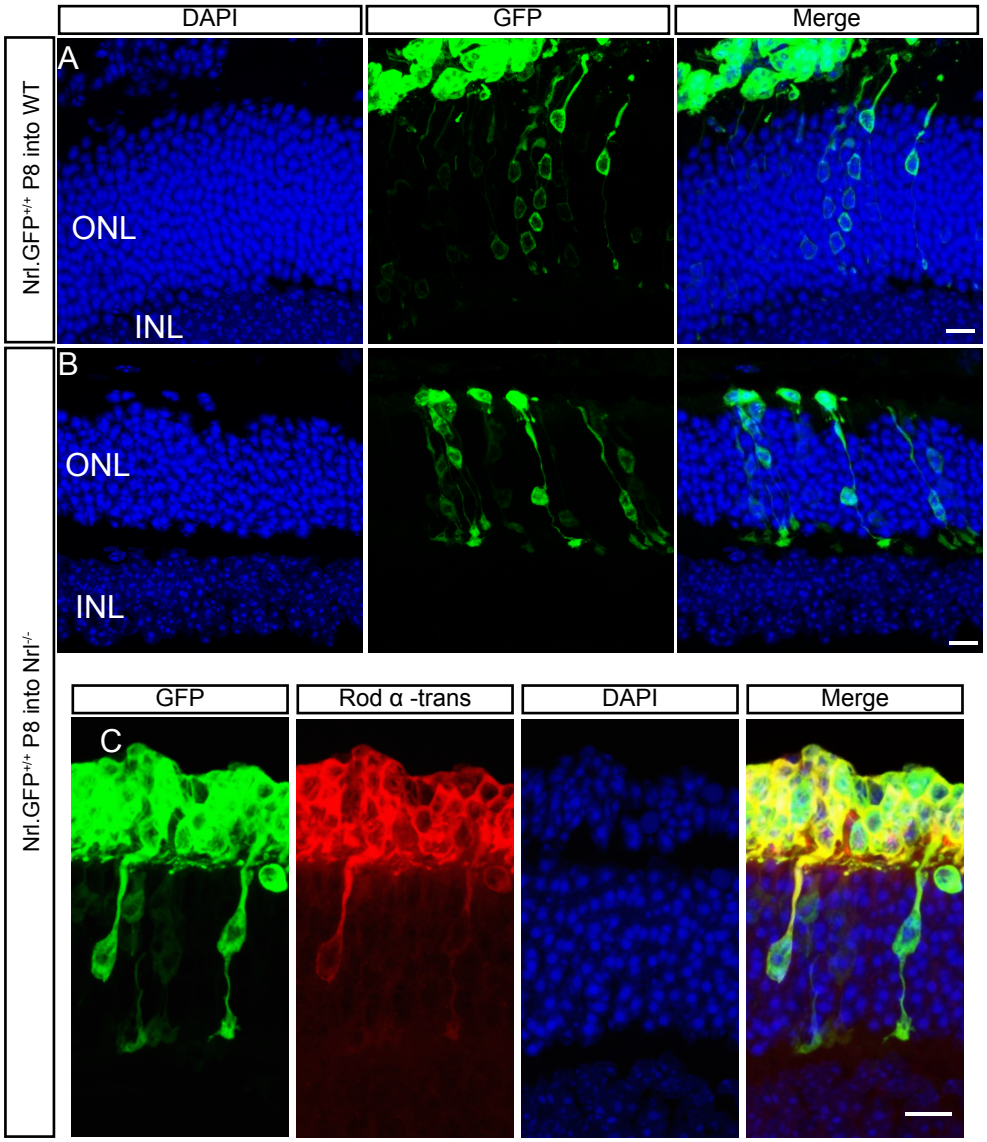

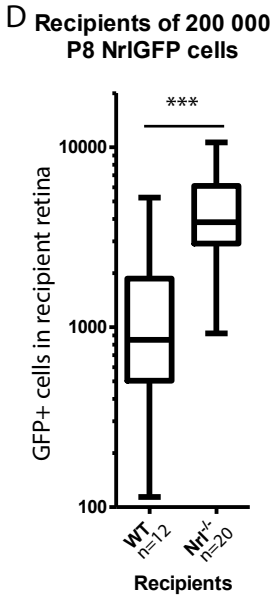

Figure 5.5 Transplantation of rod photoreceptor precursor cells into WT and Nrl$^{-/-}$ recipients. Adult mice received transplantation of 200,000 P8 GFP positive NrlGFP cells. Scale bars 10µm.

(**A,B**) GFP+ cells were found in the host ONL of both recipient genotypes after transplantation.

(**C**) Unintegrated GFP+ cells in the subretinal space, and some in the recipient retina, expressed variable amounts of rod α-transducin (not present in the recipient retina), with some strong expression seen. This protein seemed to be mislocalised to a degree, present in the soma and apical process, rather than the segments only.

(**D**) Number of GFP+ cells found in recipients 2 weeks after injection. Significantly more GFP+ cells were found in the Nrl$^{-/-}$ retina than in WT.

Further to these observations, transplanted $Nrl^{-/-}$ recipient retinas were immunostained for rod α-transducin (Gnat1); expression was clearly seen in the subretinal mass of unintegrated NrlGFP donor cells, as well as many GFP positive cells within the $Nrl^{-/-}$ recipient retina (Figure 5.5C). Expression in the GFP positive cells within the recipient retinas was variable, but was very high in some cells. Interestingly, the pattern of expression was not primarily restricted to the segments of the GFP positive photoreceptors, as would be expected in mature rods, and instead was found throughout the soma and in the apical processes.

That significantly higher numbers of GFP positive cell were seen following transplantation of NrlGFP rod donor cells into the $Nrl^{-/-}$ recipient, compared to WT recipients, indicates that, for these cells at least, the ratio of rods to cones does not underlie the improved transplantation outcome in this model.

5.2.6 Transplantation of $Nrl^{-/-}$/NrlGFP donor cells into cone-only, non-degenerating recipients

I further investigated the reasons behind increased numbers of GFP+ cells found in $Nrl^{-/-}$ and $Prph2^{rd2/rd2}$ mice after transplantation. As well as the change to the ratios of rod and cone photoreceptors seen in these models, both are also degenerative, with The $Prph2^{rd2/rd2}$ model shows no outer segment production, and loss of photoreceptors over time, with rod photoreceptors almost absent by 3 months (Barber et al., 2013; Hippert et al., 2015; Ma et al., 1995), while the $Nrl^{-/-}$ retina exhibits cell loss, reduced outer segment size, a disrupted OLM and the formation of rosettes (Roger et al., 2012). OLM integrity has previously been shown to affect transplantation outcome, with disruptions to the membrane with pharmacological agents or RNA interference methods leading to improved transplantation outcome and higher numbers of GFP+ cells within in the recipient ONL (Pearson et al., 2010;

West et al., 2008). Transplantation of NrlGFP cells into Nrl$^{-/-}$, as described above, showed that outcome is not worsened when rod photoreceptors are transplanted into an environment of cell types different to their own.

To investigate the contribution of both of these possibilities to transplantation outcome, I made use of the R91W;Nrl$^{-/-}$ mouse (Samardzija et al., 2014, 2008). In addition to the absence of Nrl, this model has a mutation in the Rpe65 gene, which is involved in the production of 11-cis retinal. 11-cis retinal is essential for the function of Nrl$^{-/-}$ cone-like photoreceptors but also appears necessary for rosette formation in this model (Kunchithapautham et al., 2009; Wenzel et al., 2007). The R91W mutation is a hypomorphic Rpe65 allele, leading to reduced levels of 11-cis retinal. When combined with the Nrl$^{-/-}$ mutation, it leads to a functional, stable all-cone retina with only very slow age-related degeneration, an intact OLM and an absence of rosettes (Samardzija et al., 2014).

To further characterise the cytoarchitecture of the recipient models, eyes were taken from adult WT, Nrl$^{-/-}$, Prph2^{rd2rd2} and R91W;Nrl$^{-/-}$ mice and prepared for confocal and electron microscopy. Cryoslices were immunostained for Crb1 and Zo-1, both components of the OLM tight junctions, by Anna Graca, from sections provided by the candidate. For electron microscopy, both semithin and ultrathin slices were prepared.

Figure 5.6 shows representative images from these retinas. It can be seen that the integrity of the OLM is disrupted in the Nrl$^{-/-}$ and Prph2$^{rd2/rd2}$ retinas, with discontinuous and fragmented patterns of Crb1 and Zo-1 staining in the confocal images, and misaligned junctions at the ultrastructural level. Examples of nuclei having 'dropped out' of the ONL and located at the level of the OLM or beyond the OLM in the interphotoreceptor matrix can be seen in both models. In contrast, the

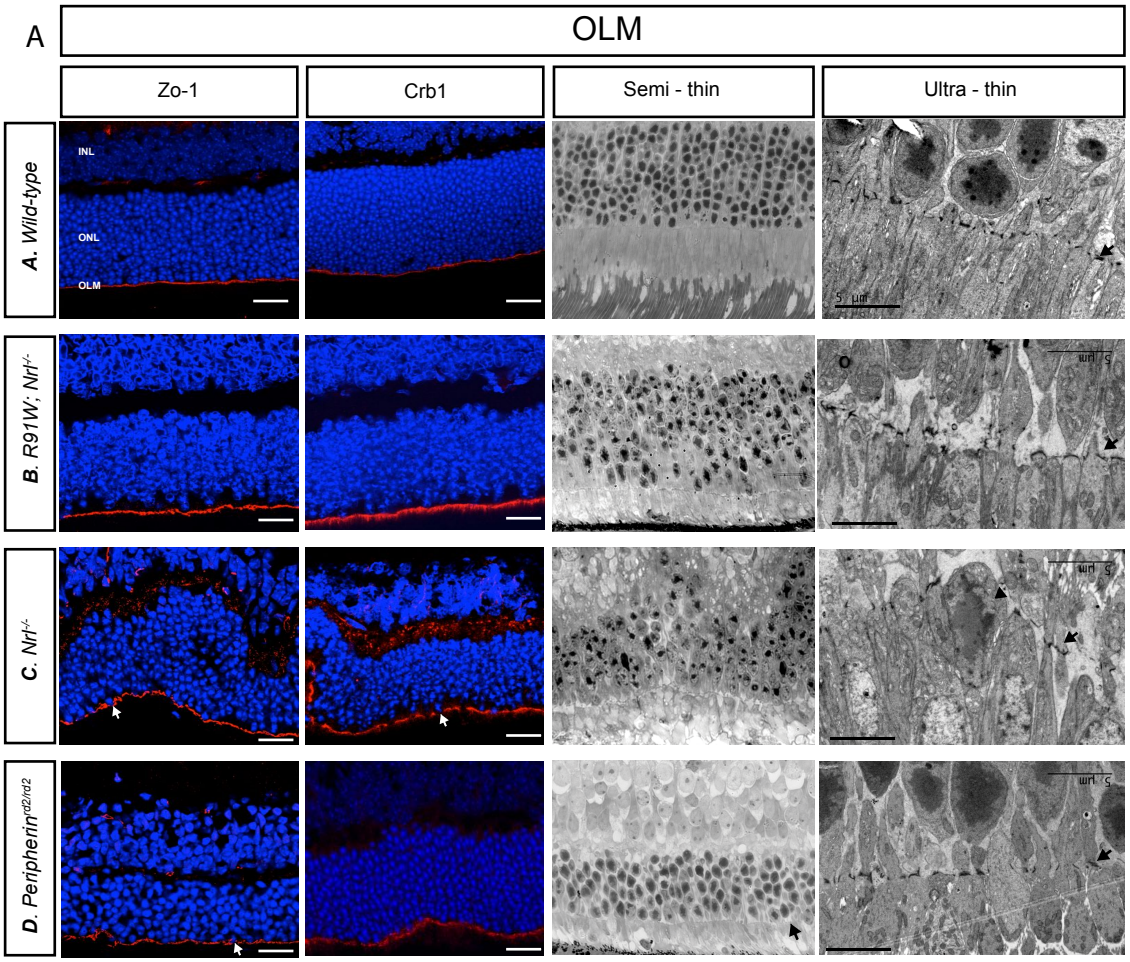
A
OLM
Zo-1
Crb1
Semi - thin
Ultra - thin
A. Wild-type
B. R91W; Nrl-/-
C. Nrl-/-
D. Peripherinrd2/rd2
INL
ONL
OLM
5 µm

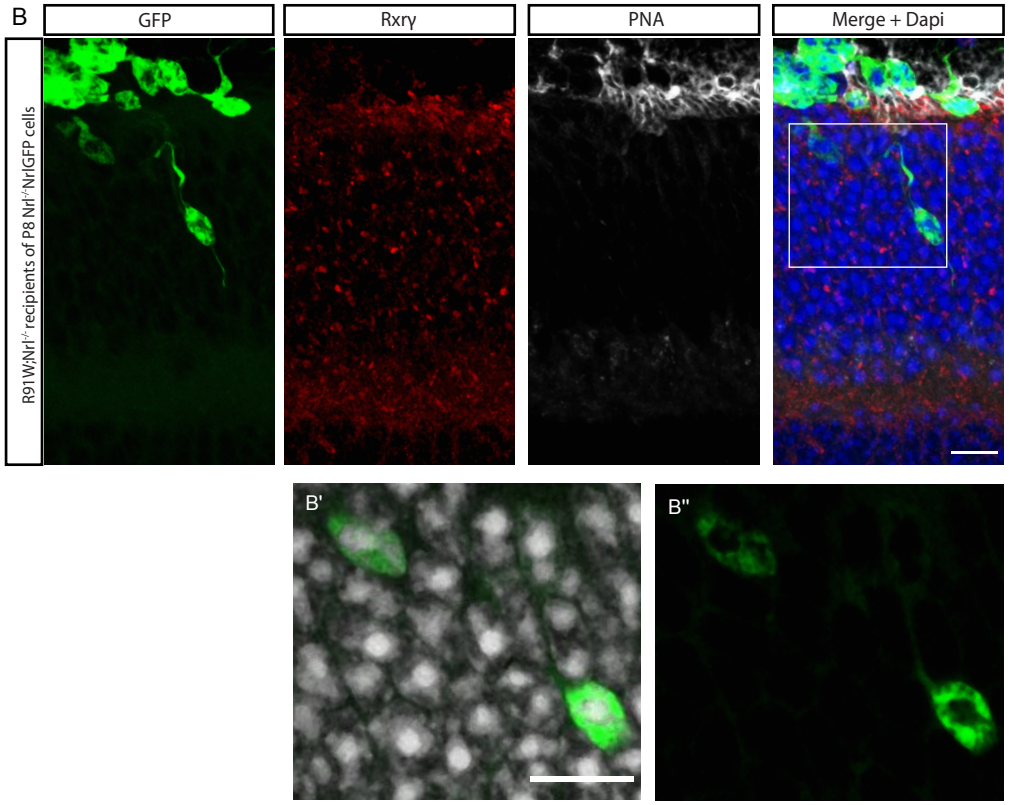
B
GFP
Rxrγ
PNA
Merge + Dapi
R91W;Nrl-/- recipients of P8 Nrl-/-NrlGFP cells
B'
B''

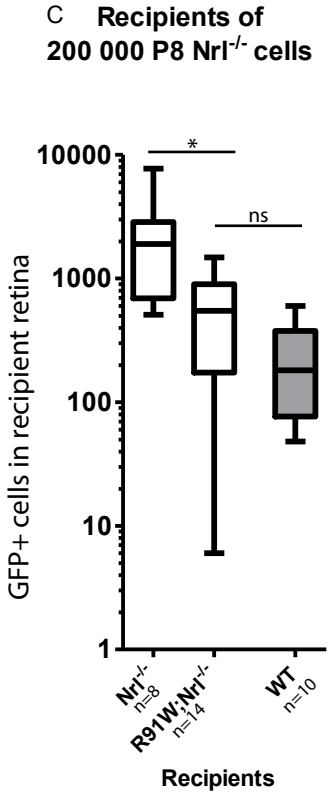

Figure 5.6 $Nrl^{-/-}$NrlGFP cells into $Nrl^{-/-}$ and R91W;$Nrl^{-/-}$ recipient retinas.

(**A**) The structure of the outer limiting membrane (OLM) in various mouse models (these images contribued by Anna Graca). Zo-1 and Crb1 staining shows a continuous line in the WT and R91W;$Nrl^{-/-}$ models, while in the $Nrl^{-/-}$ and $Prph2^{rd2/rd2}$ models these proteins form a fragmented, discontinuous line even away from obvious rosette structures. In these models, occasional nuclei can be seen transgressing the line of the OLM (white arrows).

The OLM is visible in semi-thin EM sections in all models, (arrows).

Ultra-thin EM sections (scale bars 5µm) show the tight junctions (dark spots, examples marked by arrows) form a regular spaced pattern in the WT and R91W;$Nrl^{-/-}$ models. In the $Nrl^{-/-}$ retina, these are dispersed and do not form a line, and a nucleus from the ONL can be seen disrupting the membrane (arrowhead).

Adult mice received transplantation of 200,000 P8 GFP positive $Nrl^{-/-}$NrlGFP cells.

(**B**) GFP+ cells were found in the host ONL of both recipient genotypes after transplantation. Single optical sections of the boxed area (B'-") show that these cells in the R91W;$Nrl^{-/-}$ recipient resemble cones in their nuclear morphology, with relatively large nuclei containing multiple focal points of chromatin. Scale bars are 10µm.

(**C**) Number of GFP+ cells found in recipients 2 weeks after injection. Significantly more GFP+ cells were found in the $Nrl^{-/-}$ recipient compared to the R91W;$Nrl^{-/-}$ recipient. The number of GFP+ cells in WT (previous experiments) were not significantly different to the R91W;$Nrl^{-/-}$ recipient.

OLM of the R91W;Nrl$^{-/-}$ retina is relatively intact and ordered, and large-scale disruptions such as rosettes were not seen.

Adult R91W;Nrl$^{-/-}$ and Nrl$^{-/-}$ mice received injections of 200,000 GFP+ cells from P8 (+/- 1 day) NrlGFP mice into the superior subretinal space. For this experiment, both R91W;Nrl$^{-/-}$ and Nrl$^{-/-}$ mice were injected with each preparation of donor cells. The recipient mice were sacrificed 2 weeks after transplantation. Eyes were stained for Rxrγ, PNA and GFP. Fig 5.6 shows representative pictures of GFP+ cells in the ONL of recipient retinas, which typically exhibited photoreceptor morphology similar to the cone-like photoreceptors that make up this model, displaying larger nuclei with several points of condensed chromatin, and positive staining for the cone markers previously described (Figure 5.6B).

Comparisons between the number of GFP+ cells seen in the recipient ONL after transplantation, as can be seen in Figure 5.6, show a significant difference between recipients (Figure 5.6C): $U(20) = 17.50$, $p=0.0095$. Nrl$^{-/-}$ recipients showed higher numbers of GFP+ cells, with a mean of 2403 (SD = 2332, SEM = 824.6, n = 8 injected eyes with 3 rejected) than were seen in the R91W;Nrl$^{-/-}$ recipients, with a mean of 584 (SD = 435, SEM = 116, n= 14 injected eyes with 4 rejected).

Since the R91W;Nrl$^{-/-}$ mouse also has an all-cone retina, these data suggest that it is the degenerative properties of the Nrl$^{-/-}$ retina, most likely including the disrupted OLM, which is responsible for the higher numbers of GFP+ cells seen in this model after transplantation.

5.2.7 Investigation of material transfer between recipient and donor-derived cells

To address the data presented in this thesis and other data that did not fit readily with a model of transplantation where donor cells migrate from the subretinal space into the retina migration/integration, several experiments were carried out by the group in order to find the relative contributions of integration and alternative methods of donor-recipient interaction to the results seen after transplantation – that is, to determine if there were other ways in which GFP+ cells in recipient retina could come about. The reasons for these experiments are explained in more detail in section 5.3.2, below. Appendix B shows the results of these experiments (Pearson et al., 2016), and a summary of this paper follows. The majority of these experiments were not carried out by the candidate, but by the other authors of Pearson et al. 2016, with the exception of the experiments depicted in Figure B8.

Real-time time-lapse imaging of transplanted NrlGFP+ precursor cells into the $Prph2^{rd2/rd2}$ mouse showed that GFP+ cells could be found in a subretinal position and could also be seen to move into the host ONL, through the OLM, and remained positioned in the tissue, despite a gradual loss of GFP signal (Figure B1). This indicated that true integration of cell bodies can indeed occur after cell transplantation, as had been indicated by the existence of donor-derived nuclei in BrdU-labelling experiments in previous studies (MacLaren et al., 2006).

To reinvestigate the possibility of cell-cell fusion involving nuclear transfer, immunostaining for Lamin B was used to label the nuclear envelopes of retinas which had received injections of NrlGFP cells (Figure B2 a-c). This showed that GFP+ cells in the ONL only ever contained a single nucleus. Y-chromosome FISH

labelling was also used after injecting cells from male NrlGFP donors into female recipients. Y-chromosome staining was observed in the majority of donor cells in the subretinal space, indicating success in labelling male donor-derived cells, but was not seen in the large majority of GFP+ cells found within the recipient ONL, although examples did occur (Figure B2 d,e). This showed that most GFP+ cells in recipient retina resulted from neither true integration events with donor cells entering the ONL, nor from nuclear fusion events. With incomplete penetrance of the FISH stain, and the low numbers of cells which could be counted, it was not possible to determine accurate proportions from this experiment alone.

3-dimensional reconstruction of GFP+ cells in the recipient ONL demonstrated that there were no clear examples of a visible connection between GFP expressing cells in the recipient ONL, and donor cells in the subretinal space (Figure B2 f,g).. Additionally, although GFP+ cells were often located close to a subretinal cell mass of injected cells, on many occasions GFP+ cells in the recipient ONL could be found away from any subretinal GFP+ donor-derived cells.

A number of experiments next attempted to determine the degree to which GFP+ cells in recipient retina after transplantation are due to transfer of material between cells without such fusion events. GFP positive donor cells from the NrlGFP mouse were injected into DsRed-expressing recipient mice, and assessment was made of green and red fluorescence levels across different parts of the cell of GFP+ cells in the recipient ONL, specifically the cell body containing the nucleus, and the inner segment (Figure B3). These parts were chosen as very little cytoplasm is present around the nucleus, while the inner segment contains more. The results, as determined by two independent assessors, indicated that 35-40% of GFP+ inner segments showed a lack of colocalisation, and therefore that this proportion at least might not arise from material transfer processes. With this approach, it should be

remembered that the classification of fluorescence levels requires a degree of subjective input, with the ubiquitous fluorescence of the recipient cells meaning that judging colocalisation is a question of a decrease or increase of this signal relative to that of the neighbouring cells.

FACS analysis of the retinas of DsRed-expressing mice injected with NrlGFP cells was also carried out (Figure B4). Retinas were dissociated and sorted for green and red fluorescence. Cells expressing both DsRed and GFP were identified, as well as cells expressing DsRed only (the majority of recipient cells) and GFP only. Of the cells expressing GFP, the majority (mean 80%, median 95% approx.) also expressed DsRed, with the remaining proportion representing possible events of true integration. However, although every effort was made during dissection to remove the subretinal mass of injected cells before dissociation for FACS, a proportion of the cells identified as expressing only GFP could have originated from this mass, rather than from an integrated cell.

Cells were taken from GFP+ donors and DsRed positive donors, purified by MACS separation of CD73 positive cells, mixed together and injected into recipient retinas (Figure B5). Concordant columns of fluorescent cells all of one colour were only rarely seen in the recipient ONL, and examples of mixed columns and individual cells were seen. Unexpectedly, however, rare cells positive for both ds-Red and GFP were found both in the recipient ONL (1.9% of observed cell bodies and/or segments) and in the subretinal space (6.0% of observed cells).

To further examine the extent to which cell contents can pass between recipient and subretinal donor cells, CrxGFP-labelled donor cells derived from a mouse embryonic stem cell line, transduced with a virus to cause Cre expression (ShH10 virus with Cre under the control of a CMV promoter) were transplanted into a

recipient mouse with a floxed tdTomato reporter (Figure B6). After transplantation, a number of cells were found expressing both GFP and tdTomato, indicating that both GFP and Cre had passed from injected cells into a recipient cell. Notably, a large number of cells expressing only tdTomato were observed in the recipient ONL, far outnumbering (by more than 10-fold) both the cells expressing only GFP and those co-expressing both GFP and tdTomato. To determine whether this was due to carry-over of virus in the injection, the cell-free supernatant from the final stage of preparation of cells was injected, resulting in only very few tdTomato expressing cells in the recipient retina.

To see if recipient cells could take up free protein from the environment, recombinant eGFP protein was injected into the subretinal space of recipient mice (Figure B7 a-e). The mice were then analysed for GFP+ cells in the ONL at various post-injection time points. Only at the shortest delay examined - 48 hours – were any GFP+ cells seen in the recipient ONL, and these were very few in number (<60) and only visible after immunostaining for GFP. At all other time points no GFP+ cells were seen. In order to investigate to what extent the nature of the transplanted cell population affects material transfer, GFP expressing Mouse Embryonic Fibroblast cells (MEFs) were injected into the subretinal space of recipient mice (Figure B7 f,h). All inspected eyes showed rejection of donor cells, with no GFP+ cells in the recipient ONL. Similar to previous investigations (MacLaren et al., 2006), injecting GFP+ Retinal Progenitor Cells (RPCs) did lead to small masses of injected cells persisting in the subretinal space, but only 3 GFP+ cells were seen in the recipient ONL, and only in one eye (Figure B7 g,i).

Preliminary experiments were recently carried out to extend this analysis to $Nrl^{-/-}$ cone-like donor cells. Similarly to the above experiments, 200 000 GFP+ $Nrl^{-/-}$ NrlGFP cells were injected into the subretinal space of adult DsRed mice (n=5

injected eyes, on two separate injection occasions). 2 weeks after transplantation, the retinas were dissociated and underwent FACS analysis. Between 82% and 99.5% (median 89.6%) of GFP+ cells identified by FACS also co-expressed DsRed, indicating that fluorescent marker proteins or their respective nucleic acids are transferred between host and recipient cells. An example from these results is shown in Figure B8.

5.3 Discussion

Here, I have shown that $Nrl^{-/-}$ and $Nr2e3^{rd7/rd7}$ cells have the capability to survive after transplantation and apparently integrate into the retina of adult recipient mice. This capability was observed in WT, $Nrl^{-/-}$, $Pde6c^{cpfl1/cpfl1}$, $Cnga3^{cpfl5/cpfl5}$, $Nr2e3^{rd7/rd7}$ and $Prph2^{rd2/rd2}$ recipient mice.

During the time in which these experiments were being carried out, similar work was published by other groups, also looking at the transplantation of $Nrl^{-/-}$ cells (Santos-Ferreira et al., 2014; Smiley et al., 2016). My results show several similarities with those found in these studies, but some differences were also apparent. In this discussion, I will compare the results of the above experiments to these studies.

5.3.1 GFP+ cells within the recipient WT retina usually resemble rod photoreceptors

The appearance of the majority of reporter-labelled cells within the neural retinas of many of these models was surprising: morphologically, many resembled rod photoreceptors rather than the cone or cone-like cells of their origin. Moreover, they rarely expressed cone-specific proteins. This was the case in almost all recipient retinal types, except for the cone-only $Nrl^{-/-}$ recipient, in which the reporter-labelled cells did resemble cones.

Difficulties in characterisation

Despite attempts to fully characterise the rod/cone identity and expression patterns exhibited by the apparently integrated GFP+ cells, the ambiguity in photoreceptor morphology and the difficulty involved with distinguishing expression (or the lack thereof) in a GFP+ cell from that in its neighbours has made drawing definitive conclusions very difficult. The fact that the cells used are, by their nature, atypical photoreceptors further complicates this. For example, the $Nrl^{-/-}$ cone-like photoreceptors develop markedly shorter outer segments (7.3 μm) than do WT cones (13.4μm) and WT rods (23.6 μm) (Daniele et al., 2005).

There was also evidence of a different hybrid phenotype among the GFP+ cells in the recipient retina, particularly with respect to the staining pattern of cone arrestin, which was found in a number of cells that otherwise resembled rods. The possibility is raised that the morphology of the GFP+ cells may be incidental to their functional identity, and that they are indeed still capable of the production of cone specific markers. Similarly, with NrlGFP rod photoreceptor precursor transplantation into $Nrl^{-/-}$ mice, strong maintenance of rod marker expression, including rod □-transducin, was often seen despite these cells resembling the cone-like cells of the recipient retina.

Conversely, GFP positive cells located within the $Gnat1^{-/-}$ recipient retina after transplantation of $Nrl^{-/-}$NrlGFP donors do not express rod specific markers that the recipient retina cannot and therefore if they do undergo a change in fate to become rod-like, they do not develop fully.

These observations are comparable with another recent study which also looked at the transplantation of $Nrl^{-/-}$ cells into WT and $Pde6c^{cpfl1/cpfl1}$ recipients (Santos-

Ferreira et al., 2014). They noted that several features of the GFP+ cells seen in the recipient retina after transplantation, such as synaptic terminals, resembled those of rod photoreceptors rather than cones, but found cone arrestin and s-opsin expression in the majority of ONL-located GFP+ cells after transplantation into the Pde6c$^{cpfl1/cpfl1}$ recipient, rather than a small minority as I found in the current study. In another study (Smiley et al., 2016), the investigators transplanted wild-type cones and Nrl$^{-/-}$ cells into WT, Crx$^{-/-}$ and triple knockout mice (TKO, with the mutations Gnat1$^{-/-}$ Cnga3$^{-/-}$ and Opn4$^{-/-}$) , and reported that the GFP+ cells found in recipient ONL had a rod-like morphology and did not express cone-markers.

Other possibilities for characterisation

The inconsistencies between these two published studies and the data presented here may be due to the technical difficulties in assessment. All three have relied on the use on immunohistochemistry in the recipient retina to establish the identity of the reporter-labelled cells in the recipient retina after transplantation. However, alternatives to these methods have their own complications. FACS could be used on retinas which have received an injection of cells to isolate the GFP+ cells, which could then be screened individually for protein expression or have their transcriptomes analysed by qPCR or other methods. Similarly, flow analysis could be used in conjunction with fluorescent antibodies for rod or cone markers to look for co-localisation with GFP+ cells on an automated, cell by cell basis. However, survival rates for fully differentiated adult cells undergoing the dissociation process – even if the cells are fixed after dissociation – are far lower than for developing retinas, which would greatly reduce the numbers available for analysis. With low numbers of apparently integrated cells seen in most recipients, and even lower numbers of those cells observed to resemble cones, this problem could be prohibitive.

Furthermore, in almost all cases, the number of GFP+ cells within the recipient ONL is far exceeded by the number of cells remaining in the subretinal space. Possible contamination from these cells, even in the case of perfect FACS collection of all GFP+ cells would make conclusions about the expression patterns of those GFP+ cells located in the recipient ONL difficult to draw.

Laser capture microdissection has been used to isolate areas of interest, and even single cells from tissue samples, for RNA analysis (Keays et al., 2005; Taylor et al., 2002), including in retinal tissue (Chung et al., 2013; Craig et al., 2008). While this would in theory allow exclusion of cells in the subretinal mass, to get a usable sample would require the isolation of most or all of an identified GFP+ photoreceptor, due to the significant amount of cytoplasm, ribosomes and transcriptional activity in areas of the photoreceptor beyond the soma, such as the inner segment. The risk of contamination from recipient tissue would be high in this situation. Further, this approach would again require the manual identification of individual GFP+ cells before isolation could occur, meaning the speed of analysis would be prohibitively slow.

It seems clear, however, that apart from in the $Nrl^{-/-}$ retina, the GFP-labelled cells located within the recipient ONL, after transplantation of Nrl-/- donors, in the most part do not resemble either wild-type cones or even cone-like cells. This is very similar to the outcomes seen after transplantation of Chrnb4.eGFP cone precursors (see Chapter 3). In that chapter, I discussed the possibility that the transplanted cone cells could be switching away from their developmental fate and towards that of a rod-like cell.

In this case, however, the explanation that something about the recipient retinal environment triggers the transplanted cell to develop as a rod is more difficult to justify: the genetic path for an $Nrl^{-/-}$ precursor cell to become a rod is explicitly blocked by the absence of Nrl. While photoreceptor cells are notably plastic, with evidence that post-mitotic rod photoreceptors can be reprogrammed to become cone-like, even in the adult retina (Montana et al., 2013), and that post-mitotic cone precursors can be transformed towards the rod fate in *Xenopus* and mouse (Cheng et al., 2011; McIlvain and Knox, 2007; Oh et al., 2007) in all of these cases genetic intervention was used at an internal cellular level, rather than an effect of the wider environment.

The existence of rod-like hybrid cells in the $Nr2e3^{rd7/rd7}$ model implies that there is some redundancy in the pathway, with cells able to follow a rod-like fate even with a major transcription factor nullified. However, this does not appear to be the case with Nrl as in its absence, at least within the intact retina, no rods are produced.

Attempts to rescue the cone-enriched phenotype of the $Nrl^{-/-}$ model confirm this. Ectopic expression of Nr2e3 in the $Nrl^{-/-}$ model under the control of the Crx or Nrl promoter led to partial transformation of the morphology of photoreceptor cells from cone-like to apparently rod-like appearance, including the expression of rhodopsin, but these cells were functionless (Cheng et al., 2011, 2006). In contrast, this ectopic expression of Nr2e3 was able to completely restore WT phenotype in the $Nr2e3^{rd7/rd7}$ model. The authors conclude that Nr2e3 is a potent suppressor of cone gene expression, but that it activates only a subset of rod genes, and that Nrl activity beyond its effect on Nr2e3 is necessary for rod photoreceptors to fully develop.

Therefore, it seems that for $Nrl^{-/-}$ cells to develop rod photoreceptor photoreceptor morphology in all tested recipient retina types except the cone-only $Nrl^{-/-}$ recipient,

they would need either to bypass the function of Nrl in the pathway that leads to rod development, or take up Nrl, Nr2e3, or another rod developmental transcription from the environment in some way. In the absence of any evidence of how this uptake might take place, alternative explanations will be considered.

The use of the NrlGFP reporter gene for labelling the cone-like cells, being specific to rod photoreceptors under normal circumstances, raises an alternative possibility that integrated GFP+ cells retaining a true cone fate could downregulate the activity of the reporter and so not be seen after transplantation. The existence of rare GFP+ cells that did resemble true cones shows that this does not happen in every case, however. Moreover, use of a ubiquitous GFP reporter gene showed very similar results to those using the NrlGFP reporter, indicating that a failure of the reporter gene is not likely to be the cause of these results.

The difficulties in providing conclusive and consistent evidence, as demonstrated by the published reports (Santos-Ferreira et al., 2014; Smiley et al., 2016) and the data presented here, regarding the expression profile of the apparently integrated cells, means that it is not clear whether the morphological appearance of these cells accurately represents their true cell identity, as would be expected from their connections and functional output. Even so, explaining these results within the existing framework of donor cell migration and integration is difficult, even with the possible explanation of cell fate plasticity, and leads to some inconsistencies, as discussed above. In the next section I will discuss a competing explanation for the results seen, which has some advantages over those already proposed.

5.3.2 Material transfer

5.3.2.1 Cell fusion as an explanation

Recently, evidence both from this lab, and others, has been proposed for an entirely different and novel mechanism to explain the results seen after the transplantation of cells. Instead of cell integration by the movement of donor cells from the subretinal space into the ONL, it has been proposed that some or all of the GFP+ cells in the recipient ONL are the result of existing recipient cells fusing with transplanted cells which remain in the subretinal space. The recipient cells subsequently receive material from the transplanted cells, most obviously GFP, but potentially other donor specific proteins, without the transplanted cell moving into the recipient ONL.

Cell-cell fusion as an explanation for the occurrence of apparently mature cells resulting from transplantation of immature cells into various tissues has been proposed for some time in other fields. For example, in investigating the apparent differentiation potential of bone marrow cells, co-cultures of multipotent brain progenitor cells expressing Cre-recombinase with bone marrow stromal cells containing the LacZ reporter gene (flanked by lox P sites or floxed, and thereby conditionally expressed in the presence of Cre), led to multinucleate, LacZ-expressing cells apparently produced by fusion (Alvarez-Dolado et al., 2003). Similarly, after grafting GFP- and Cre-expressing bone marrow into lethally irradiated recipient mice again containing Cre-dependent LacZ, multinucleate cells expressing both GFP and LacZ were found in brain, heart and liver. In the cerebellum, these double labelled cells displayed the location and morphology typical of Purkinje cells, and again contained two nuclei. Other studies also suggested that tetraploid hybrids arise after co-culture of embryonic stem cells and

bone marrow cells (Terada et al., 2002) or fetal brain cells taken from neurospheres (Ying et al., 2002).

Early studies in the field of retinal cell transplantation therefore attempted to rule out the possibility of cell fusion as an explanation for the results seen (MacLaren et al., 2006). Confocal assessment of GFP+ cells transplanted into a recipient mouse with ubiquitous expression of cyan fluorescent protein (CFP) showed examples of GFP+ cells within the recipient retina in which CFP was absent. Multinucleate cells were not seen among the GFP+ cells in the recipient ONL, and bromodeoxyuridine (BrdU) labelling of a proportion of donor cell nuclei prior to transplantation led to BrdU positive nuclei being seen in some GFP+ cells in the recipient ONL. Quantification of these techniques, however, was not carried out at the time. These observations, together with the absence of any mechanism proposed for fusion without the presence of multinucleate cells, led to the conclusion that integration of whole transplanted cells was the most likely explanation for transplantation outcomes.

5.3.2.2 Investigation by the group

Several experiments were carried out by the group in order to find the relative contributions of integration and alternative methods of donor-recipient interaction to the results seen after transplantation, as described in section 5.2.7.

Observations of real-time time-lapse imaging of transplanted NrlGFP+ precursor cells, the nuclei of GFP+ cells in the ONL and 3-d reconstructions of these cells, and Y-chromosome labelling in female recipients of male-derived cells indicated that true integration events do not happen at high frequency, but also that cell fusion

including nuclear fusion or the production of multinucleate cells is unlikely to occur, and therefore that material must be transferred through other means.

Use of more than one fluorescent marker allowed more insight into material transfer events. GFP positive donor cells injected into DsRed-expressing recipient mice led to a large proportion of dual-labelled cells in the recipient ONL seen by microscopy and FACS analysis. However, injection of cells taken from GFP+ donors and DsRed positive donors also led to (rare) dual-labelled cells both in the recipient ONL and in the subretinal space. This indicated one of several possibilities: that cells in the subretinal space might undergo material transfer with one another, before either integrating into the ONL or even undergoing a second material transfer with a recipient cell, or that a recipient cell might receive material from more than one subretinal donor cell, causing mixture between these cells by proxy.

GFP+ donor cells, virally induced to express Cre, and transplanted into a recipient mouse with a floxed tdTomato reporter, led to a number of cells expressing both GFP and tdTomato in the recipient ONL, but also approximately 10 times this number of cells expressing only tdTomato. Although it is possible that more residual Cre-inducing virus was present in the injected cell population, it would not be expected that any residuum would be able to transduce recipient cells in these numbers, as the virus is not able to replicate in recipient cells. A more plausible explanation is that these cells engaged in material transfer with the injected cells at some point post-transplantation and received sufficient Cre for recombination and subsequent irreversible production of tdTomato to occur, but not enough for sustained expression of GFP to be reliably seen, or alternatively that these events might be frequent but transient, with enough Cre being transferred to effect permanent tdTomato expression in a recipient cell, but enough GFP only for a

temporary green fluorescent signal. Either explanation would imply that material transfer events may be common, but limited by magnitude and/or longevity.

In summary, however, these lines of enquiry all indicate that more than one mechanism is in play, which results in the presence of GFP+ cells within the recipient retina. What is not clear from these experiments is the degree to which material transfer and donor cell integration each contribute to the results of transplantation. Possible estimates for the contribution of true integration of injected cells therefore vary from <5%, as suggested by Y-chromosome staining techniques, to 20% as suggested by FACS analysis of injected retina, to 35% or more as suggested by the colocalisation experiments detailed above.

Possible mechanisms by which material transfer might occur were also investigated. Recipient cells did not seem to be able to take up free GFP in the environment in the amounts necessary to explain these results, and injection of GFP+ MEFs or RPCs also did not reliably lead to GFP+ cells in recipient retina. With a method based on material transfer, it is not clear why the nature of the transplanted cell population should be as important as implied by these resuls, particularly if it occurs without permanent cell-cell contact, as suggested by previous experiments. It follows that material transfer events are likely to be caused by the activity of the injected cells rather than or in addition to that of the recipient photoreceptors.

5.3.2.3 Material transfer in this thesis

These experiments were carried out using rods and mixed photoreceptor populations, rather than the cone and cone-like cells used in my experiments, due to the need to develop the protocols on which they were based. However, preliminary experiments using FACS analysis on DsRed-expressing recipient mice

injected with GFP+ Nrl$^{-/-}$ donor cells showed very similar results to the above; that is, with a large proportion of dual-labelled cells.

Given these results, it appears very likely that a system based on material transfer is responsible for the results of my experiments, and this would explain several aspects of my observations. That the majority of GFP+ cells in the recipient ONL resemble rod photoreceptors regardless of the fate restriction of Nrl$^{-/-}$ cells after transplantation, is therefore due to the majority of cells in most recipient models used being rod photoreceptors themselves. In the Nrl$^{-/-}$ recipient, the cone-like appearance of GFP+ cells is likewise due to this being the appearance of the recipient cells in this model.

The minority of GFP positive cells in most types of recipient retina that do morphologically resemble cone photoreceptors and are located close to the OLM can now be explained either by the endogenous cones being less numerous and/or being less able to engage in material transfer. The differing pattern of cone marker expression among GFP expressing cells can also be explained in this way. Rxrγ, as a nuclear receptor, would not be expected to be found in a recipient cell after transfer of proteins alone, unless the cell was already expressing it (i.e. if it were already a cone), explaining why GFP+ cells also expressing Rxrγ were almost invariably found close to the OLM. Other cone markers, such as cone arrestin, were occasionally found in GFP+ cells that were deeper in the ONL and morphologically resembled rods. Similarly, rod α-transducin was found in GFP+ cells after injection of NrlGFP rod precursors into the Nrl$^{-/-}$ retina. A process of material transfer would explain this as take-up of cone arrestin or rod α-transducin or their RNA transcripts directly from a transplanted cell in the subretinal mass, perhaps with varying efficiency. The same was not seen in Nrl$^{-/-}$ transplantation into Gnat1$^{-/-}$ retina, as neither cell type was capable of producing rod α-transducin.

On the other hand, the Pde6c$^{cpfl1/cpfl1}$ mouse which has almost total cone photoreceptor loss also exhibits rare GFP+ cells that appear to be cone-like and express Rxrγ, such as in Figure 5.3E. However, rare cone photoreceptors do still exist in this model at the ages used for transplantation, which could be the cells engaging in material transfer. Since the number of endogenous cones is very low in this model, it could be expected that GFP+ cells resembling cones would therefore be correspondingly much rarer after transplantation into this model. However, the numbers of positively identifiable cells of this type in any recipient retina were very low, making it hard to determine any meaningful differences. In any case, it could instead be that these cells represent relatively rare occasions of true integration, with material transfer processes accounting for some or all of the other cells. Similar arguments apply to previous studies looking at transplantation of CrxGFP cells into the cone-functionless Gucy2e$^{-/-}$ retina (Lakowski et al., 2010).

In summary, given the recent evidence that material transfer is very likely to account for the majority of rescued cells following rod transplantation, and preliminary evidence that the same applies for the transplantation of cone-like cells, it is reasonable to propose that the rod-like appearance of cells seen in the recipient ONL following injection of cone-like cells is explained by a similar process. The mechanism of material transfer is however unclear.

5.3.2.4 Mechanism of material transfer

The mechanisms underlying material transfer must explain a wide array of experimental observations made over the past decade of study into photoreceptor transplantation. GFP+ cells in the recipient ONL have been detected as long as one year after transplantation. This persistence of GFP, as well as other donor-derived

proteins apparently transferred, means that transcription of donor-cell derived proteins must continue after material is transferred (wild-type GFP has a half-life of approximately 26 hours), which requires either a maintained connection between the recipient and donor cells, with the GFP produced by the donor, or the permanent movement of genetic material from the donor to the recipient, to allow GFP production in the recipient cell. Alternatively, as suggested by the Cre-lox experiments above, material transfer events may be relatively frequent and transient, with GFP+ cells seen in analysis only those which have engaged in material transfer recently. Donor-derived proteins unable to be produced by recipient tissue, such as rod α-transducin expression after transplantation into the Gnat1$^{-/-}$ mouse would additionally have to be targeted to the correct place in recipient cells, as well as being transferred in sufficient amounts to restore the phototransduction cascade on the level of single cells, such that photosensitivity can be assessed using single-cell recordings, as has been shown to happen (Pearson et al., 2012).

Over time, the number of GFP+ cells in recipient ONL has been seen to decline, suggesting the action of a delayed immune response to foreign tissue. Even at longer time points after transplantation (up to one year), when GFP+ cells are still seen in the recipient ONL, subretinal cells are still present, allowing for the possibility that a connection between the two is still active. Alternatively, with a system of frequent transfer events, this decline could be due to a loss or quiescence of the transplanted subretinal cells over time. In this case, a Cre-lox based investigation as described above would be expected to lead to a higher total number of cells expressing the floxed reporter over time as more cells undergo recombination.

The high number of recipient cells expressing only tdTomato after the transplantation of GFP- and Cre-expressing cells into recipient mice with a floxed tdTomato gene suggests however that material transfer into recipient cells may happen at high frequency, but not to the degree which allows detectable presence of GFP or other proteins. Assuming that the same mechanism underlies both observations, it must be explained why some connections are apparently transient while others appear to be permanent, allowing many times more material to be passed on.

An alternative explanation is that transient, discrete material transfer events involving approximately similar amounts of cell contents happen sporadically over time via short-lived connections between recipient cells and donor cells in the subretinal space. After this kind of connection, the recipient cell would appear to express GFP and other donor-derived proteins, but over time these proteins would be lost and not replaced. In this case, GFP+ cells observed after transplantation in most cases would be only those which had received a transfer of donor material recently. In the case of Cre-expressing donors, however, although the GFP would be lost over time, the recombination allowing tdTomato production in recipient cells would be permanent.

The donor cells in the subretinal space are in close proximity with the outer segments of the recipient photoreceptors. An alternative possibility, therefore, is that some sort of incomplete cell-cell fusion via the outer segments occurs. Events involving the fusion of cell membranes are of course common in photoreceptors, with the formation and shedding of photopigment-containing discs happening constantly in both rods and cones. However, this proposal is unlikely for a number of reasons. The outer segments of photoreceptors are subject to acute photo-oxidative stress, and the constant shedding of photoreceptor discs is necessary to

prevent the toxic effects of a build-up of photo-oxidative by-products (Kevany and Palczewski, 2010). A prolonged connection to this part of the photoreceptor cell would therefore be expected to quickly lead to the death of the subretinal cell.

Observations of GFP+ cells in the ONL of Prph2$^{rd2/rd2}$ retinas after transplantation also indicate that a mechanism involving fusion with the outer segments of recipient photoreceptors is unlikely, as outer segments do not form in this model, but instead only stumps lacking disc structures (Pearring et al., 2013). In fact, Prph2 is implicated in the process of membrane fusion in healthy photoreceptors, with the failure of this process thought to be an important cause of the degeneration seen in the Prph2$^{rd2/rd2}$ model (Boesze-Battaglia, 2000; Boesze-Battaglia et al., 2003, 1997). Despite this, large numbers of GFP+ cells are seen after transplantation into Prph2$^{rd2/rd2}$ mice, more in fact than into many other models. This also indicates that any mechanism of material transfer is unlikely to involve similar processes to the generation of photopigment discs, as Prph2 is essential for this process.

If connections were alternatively made with recipient cell somata, it might be expected that more GFP+ cells might be found in the outer parts of the ONL, closer to the injected cells, but this does not appear to be the case. Connections could instead arise between donor cells and recipient inner segments. The inner segments contain much of the cytoplasm and organelles of a photoreceptor, and might therefore be an effective place to receive material from donor cells. Clear connections from donor cells to recipient inner segments are not clearly seen in injected eyes.

Some evidence from the experiments described above suggested firstly that a prolonged connection between recipient and donor cell was not always apparent, but also that a recipient cell can receive material from more than one injected cell. In

other systems, it has been suggested that exosomes – cell-derived microvesicles, which are released by some cell types and can contain proteins and nucleic acids – might represent a mechanism by which cells can communicate with one another without physical cell-cell contact (Stoorvogel et al., 2002). Exosomes are present in the retina (Hajrasouliha et al., 2013) and preliminary data from our group indicates that particles of a size equivalent to exosomes can be isolated from cultures of purified postnatal precursor cells (Kalagyrou, Pers comm) but it is not yet known if these are exosomes and whether or not they can mediate the process of material transfer.

The more random transfer of material from injected to recipient cells suggested by this system would however explain some aspects of the results seen, such as the high variability in GFP content of recipient cells and recipient cells receiving material from multiple injected cells. However, it might be expected that under such a system, a recipient cell receiving material from more than one donor cell would be common, rather than a rare occurrence. In fact, it appears from the results of the transplantation of both red and green fluorescent cells that this happened only very rarely.

No currently known methods of cell fusion adequately explain all the observations of cell injected retinas. Future efforts will focus on determining both the relative contributions made by integration and material transfer to the results seen after transplantation, and on the mechanism by which transfer occurs. Again, however, despite the absence of a mechanism, the process of material transfer provides a plausible explanation for many of the results of my experiments.

5.3.3 Transplantation outcome in different degenerative models

Although robust numbers of GFP+ cells were seen after transplantation of $Nrl^{-/-}$ /NrlGFP cells into all recipient models used, significantly better results were seen in two models, the $Nrl^{-/-}$ and $Prph2^{rd2/rd2}$ mice, with the numbers of GFP+ cells in $Pde6c^{cpfl1/cpfl1}$(cone-less), $Cnga3^{cpfl5/cpfl5}$ (cone functionless) and $Nr2e3^{rd7/rd7}$ (cone enriched) recipient ONL after transplantation not significantly different to WT.

This compares with a similar study (Santos-Ferreira et al., 2014) in which $Nrl^{-/-}$ donor cells were also transplanted into $Pde6c^{cpfl1/cpfl1}$ and $Nrl^{-/-}$ recipients, and a significant increase in GFP+ cells was found after transplantation into the latter model. Another recent study (Smiley et al., 2016) again using $Nrl^{-/-}$ cells as donors, used a recipient model lacking all light perception through the combination of rod transducin (Gnat1), Cnga3 and melanopsin (Opn4) mutations, as well as a Crx knockout model, with no significant increase in transplantation outcome in either mutant model.

Previously, the two major reasons proposed for the increased numbers of GFP+ cells seen in the $Nrl^{-/-}$ recipients were based on a change in the ability of donor cells to migrate and integrate into the recipient ONL. The high cone to rod ratio seen in these models leads to an environment of cells more similar to those being transplanted, which may provide a more permissive environment for the integration of other cone-like cells. This would also explain the relatively low integration efficiency exhibited by cone cells, relative to NrlGFP rods, into wildtype retina. Alternatively, disease-specific disruptions in the retinal cytoarchitecture caused by degeneration could permit increased integration, as has been seen in previous studies (Barber et al., 2013; Pearson et al., 2010).

However, given the recent evidence that the majority of GFP+ cells in recipient ONL after transplantation are due to material transfer events, these integration-based hypotheses are unlikely to represent the true reason for the increase in transplantation outcome seen in some models. Since the mechanism of material transfer is not currently clear, it is not possible to determine how these processes would be specifically affected by the degenerating retinal environment. Nevertheless, there clearly exist effects of different retinal environments and the two parameters described above – the cone: rod ratio and the cytoarchitectural disruptions caused by degeneration – are still valid as qualities which may affect transplantation outcome.

In the current study, NrlGFP rod photoreceptor precursors were injected into WT and $Nrl^{-/-}$ retinas, and higher numbers of GFP+ cells were seen in the $Nrl^{-/-}$ recipient ONL, indicating that rod photoreceptors are not impeded in transplantation by a cone-rich environment, indeed quite the opposite.

Since the R91W;$Nrl^{-/-}$ shows a cone-only phenotype similar to the $Nrl^{-/-}$, but shows minimal degeneration, an absence of rosettes and an intact OLM, it allowed a way to separate the relative contributions of the cone enriched environment and the degeneration seen in the $Nrl^{-/-}$ to the improved outcome of transplantation. Significantly fewer GFP+ cells were seen after $Nrl^{-/-}$ cells were transplanted into the R91W;$Nrl^{-/-}$ mouse than into the $Nrl^{-/-}$ recipient. These results indicate that it is the specifics of degeneration and/or the integrity of the OLM in these models, rather than the cone-enriched environment, which explains the increased numbers of GFP+ cells in the recipient ONL.

This is also supported by the observation that the $Nrl^{-/-}$ recipient supports higher numbers of GFP+ cells after the transplantation of NrlGFP rod photoreceptor

precursor cells than seen in the wild-type retina. Moreover, previous work showed that more GFP+ cells are seen in recipient ONL after transplantation into the $Crb1^{rd8/rd8}$ retina (Barber et al., 2013), a model that has a severely disrupted OLM, and after disruption of proteins associated with the OLM (Pearson et al., 2010) or pharmacological disruption (West et al., 2008). Even gross damage caused by laser injury has been shown to increase transplantation outcome (Jiang et al., 2010).

The $Nr2e3^{rd7/rd7}$ retina also exhibits some retinal disruption, in particular rosette formation, but transplantation outcome was not significantly increased into this model, relative to WT retina. It is possible that the milder phenotype shown by the model relative to the $Nrl^{-/-}$ is responsible for this discrepancy, or alternatively this disruption is most prevalent in the ventral or inferior retina, where the greatest number of supernumerary cones are seen, while injections were made into the dorsal or superior retina, where the tissue is comparatively more similar to WT. Comparing the outcomes of superior vs inferior transplantations into this model would show whether this is likely to be the case.

Injections of $Nr2e3^{rd7/rd7}$CrxGFP cells into the $Nr2e3^{rd7/rd7}$ recipient encountered a striking increase in the frequency of rejection compared with other combinations of donor and recipient model, most notably the $Nrl^{-/-}$ recipient, which showed very low levels of rejection. While the reason for this difference is unclear, it indicates that the $Nr2e3^{rd7/rd7}$ environment is different in at least some ways to the $Nrl^{-/-}$ retina, which could be another explanation for the lack of an increase in transplantation outcome.

Research continues into the reasons behind the differing efficiency of transplantation into different degenerative environments (Graca, 2016, Thesis in preparation), seen in these and other studies (Barber et al., 2013). While the integrity of the OLM is often implicated, other aspects of the degenerating retina

may be important, in particular the processes of gliosis, and the formation of glial scarring.

Changes occurring in the extracellular matrix (ECM) during these processes vary according to the specific model. The Prph2$^{rd2/rd2}$ model, for example, has a relatively slow progression of degeneration, and exhibits atypical gliosis compared to more rapidly degenerating models (Iandiev et al., 2006) including a lack of impairment in the uptake or metabolism of glutamate. The deposition of CSPG molecules was seen to decrease over time (Hippert et al., 2015), and in my experiments this model shows increased numbers of GFP+ cells in the recipient retina after receiving transplanted cells. In the Rhodopsin knockout mouse (Rho$^{-/-}$) in contrast, GFP+ cell number after transplantation is decreased, and CSPG deposition increases over time in this model. In general, it appears that transplantation leads to fewer GFP+ cells as gliosis increases (Barber et al., 2013).

Consistent with this, disruption of components of the glial scar using Chondroitinase ABC has been shown to improve the efficiency of transplantation in retina (Barber et al., 2013; Ma et al., 2011; Suzuki et al., 2007) while matrix metalloproteases which also degrade cell adhesion molecules such as CD44 and neurocan, are implicated in the migration of neuroblast cells into brain tissue after stroke (Lee et al., 2006) and have also been shown to increase the efficiency of transplantation into the retina (Suzuki et al., 2006; Yao et al., 2011).

Understanding the reasons behind these differences could be key to developing techniques to improve the efficiency of cell transplantation, particularly by disrupting the OLM, or by reducing the effects of gliosis. These experiments show that the transplantation of cone-like cells is subject to similar restraints to the transplantation of NrlGFP rod cells. In light of the above discussion (see 5.3.2) showing that

material transfer is very likely to explain the majority of results of cell injection experiments, how the effects of different retinal environments on the efficiency and outcome of cell transplantation (and hence material transfer) must be carefully reconsidered. Until we understand the cellular mechanisms underlying material transfer, attempts to explain why this process is more efficient in some recipient models than others remain speculative.

That said, it is still plausible that the disruption to the integrity of the OLM present in models like the $Nrl^{-/-}$ would allow for increased possibility of material transfer events occurring, or indeed of more instances of true cell integration. Using the techniques described above to determine the balance of integration and material transfer events after transplantation into models such as the $Nrl^{-/-}$ would allow insight into which of these processes benefit from these environmental changes.

5.3.4 Conclusion

This chapter has shown the results of using fate-restricted cone-like cells as a donor cell source for cone transplantations. Transplantation outcome varied between different types of recipient retina, and the possibility was raised that disruption of the OLM might increase the efficiency of integration, as has been seen with rod transplantation.

The unexpected observation that the majority of GFP+ cells within WT retinas resembled rod photoreceptors more closely than cones, despite their restricted fate is difficult to reconcile with the existing theories of donor cell migration and integration after transplantation. Recent evidence indicating that the majority of donor derived protein (including, but not limited to, GFP) present within the cells in

the recipient retina arises via a process of material transfer might go some way to explaining these results.

However, even in the extreme case that no transplanted cells at all enter the retina by migration and truly integrate, the possibility exists that functional activity might still be restored by methods of material transfer, in accordance with previous studies. Following the transplantation of rod precursors in the Gnat1$^{-/-}$ recipient retina, more than 85% of GFP+ cells within the recipient retina also expressed rod α-transducin and were light responsive (Pearson et al., 2012) and other recipient rods were observed to express rod -transducin, even in the absence of GFP (Pearson et al. 2016, in press).

In the next chapter, I investigate the functional capabilities of retinas which have received cells transplanted in these ways.

Chapter 6 – The functional capacity of transplanted cells

6.1 Introduction

In Chapters 4 and 5, I showed how the transplantation of fluorescent cone and cone-like cells into the subretinal space of adult mouse retinas leads to GFP expressing cells being found in the ONL of recipient retinas.

These cells generally resembled rod photoreceptors and only rarely cone photoreceptors, although some evidence of cone specific proteins in these cells was found, in keeping with reports from other groups (Santos-Ferreira et al., 2014; Smiley et al., 2016). Evidence that the presence of these proteins in the host retina arise as a result of material transfer between donor cells injected in the subretinal space and photoreceptor cells in the recipient ONL was shown and discussed in Chapter 5. As such, I drew the conclusion that this process is likely to underlie at least the majority of my results described thus far. While this has highly significant implications for our understanding of the cellular mechanisms underlying functional rescue following cell transplantation, the possibility remains that by delivering RNA and/or protein from relatively healthy injected cells into degenerating, mutant or otherwise functionless recipient cells, the function of these recipient cells could be restored and cell death averted.

Methods to determine the functionality of retinal cells range in scale from examination of the responses of single photoreceptor cells by patching or suction cup methods, to recording from the RGCs in a small area of retina, to whole retinal approaches such as electroretinogram recordings (ERG). At a whole animal scale,

various behavioural assays exist which measure the response of a treated mouse to light, including water maze navigation, light and stimulus aversion tests, optomotor responses to a moving visual grate, and conditioned fear responses. These are described in section 1.5.3. Methods of these kinds have been used to show functional restoration in previous studies using cell transplantation methods, at several scales of response (Pearson et al., 2012). An increase in functional capacity is most apparent in an animal with a lack of any light sensitivity, and also where cell injection has been most successful, as measured by GFP+ cells located in the recipient ONL.

This chapter will focus on the use of electrophysiological techniques to determine the effects of the injection of cone-like cells into recipient mice. These techniques aim to record the electrical activity caused by cells affected by cell therapy. While the ERG technique allows for the assessment of a global retinal response, it is not necessarily a practical choice for determining functional improvements after cell injection. In previous studies, NrlGFP cell injection into Gnat1$^{-/-}$ recipients has not shown an improvement in ERG response, and the viral transduction of more than 100,000 cells with a Gnat transgene was necessary for a gene therapy approach to affect the ERG (Pearson et al., 2012). Without a similarly high level of cells treated with cell injection methods, it is unlikely that ERG improvements will be found.

The retinal ganglion cells (RGCs) are the only neurons in the retina which fire action potentials. They receive input from the bipolar cells and their axons extend to the visual cortex of the brain, through the optic nerve. Cell recordings have been made from RGCs for many years (Hartline, 1969). In the context of retinal therapy, recording from the RGCs makes it possible to determine whether the photoreceptors affected by the therapy used are both improved in their ability to

respond to light and also able to communicate their response to the bipolar cells and so through the pathway leading to the brain.

In this chapter, I will discuss experiments involving extracellular recordings from the retinas of mice treated with injections of cone-like cells, to determine whether any increase in light response can be found.

6.2 Results

6.2.1 Selection of a recipient model

Previous work has shown the necessity for high numbers of GFP+ cells to be found in recipient ONLs for functional restoration to be seen on scales larger than single cells (Barnea-Cramer et al., 2016; Pearson et al., 2012).

The relatively low levels of GFP+ cells seen in the recipient ONL after transplantation of $Nrl^{-/-}$ cells suggested that it was unlikely that large-scale functional improvements would be seen after transplantation into most recipient types. For example, although neither the $Cnga3^{cpfl5/cpfl5}$ and $Pde6c^{cpfl1/cpfl1}$ models exhibit cone function, and would therefore be a good baseline for detecting the effect of transplanting cone-like cells, these models only ever supported the presence of a few hundred GFP+ cells after transplantation with $Nrl^{-/-}$ cells (see Chapter 5.2.4), not enough to expect a noticeable effect on most measurements of function at scales above those of a single cell.

Additionally, due to the continuing uncertainty regarding the rod or cone identity of affected cells, it was unclear whether the reporter-labelled cells arising from cone-like cell transplantation would respond specifically or only at cone-specific light intensity or wavelengths. The optimal model for detecting the activity of transplanted

cells would therefore be one in which high numbers of GFP+ cells had been seen after transplantation, but which shows no more than a very low level of endogenous activity, so that any small increases in function can be seen.

The Prph2$^{rd2/rd2}$ model was therefore chosen as a suitable candidate for investigating the function of transplanted cells. The model does not produce outer segments, and previous studies have indicated that retinal function as measured by electroretinogram (ERG) recordings declines to undetectable levels by two months of age (Ali et al., 2000).

ERG recordings were performed to assess the degree of function remaining in these animals using the ERG set ups available in our lab. Note that these were not subjected to full formal quantitative analysis, but were assessed qualitatively to determine thresholds for light responsiveness.

Surprisingly, and in contrast to previous reports (Ali et al., 2000), uninjected, dark-adapted Prph2$^{rd2/rd2}$ mice displayed a noticeable level of electrical activity, even at 12 weeks of age as shown in Figure 6.1. This activity appeared only at very high light intensities, corresponding to the range of activity of cone photoreceptors. Since the degeneration of the Prph2$^{rd2/rd2}$ model affects the rod photoreceptors during early stages, it was conjectured that this activity was the result of residual cone function. This compares to a previous study which crossed this line with the Nrl$^{-/-}$ model, and showed that cone viability and function in the Prph2$^{rd2/rd2}$ model are somewhat preserved, relative to that of rods, and that the cone-like cells can maintain atypical outer segments in this model (Farjo et al., 2006).

To remove this activity it was decided to cross the Prph2$^{rd2/rd2}$ line with the Cnga3$^{cpfl5/cpfl5}$ mutant, which lacks cone function (Michalakis et al., 2005; Pang et al.,

2010). This was done over two generations, with the presence of the cpfl5 mutation assessed by PCR and sequencing, and the rd2 mutation by PCR and band detection (see Chapter 2.6).

ERG recordings from this double mutant at young ages (4.5 weeks) under dark adaptation also revealed a baseline of activity, however (Figure 6.1 D-E), indicating that some residual rod activity exists in the young mice of this double mutant, but is sensitive only to a much higher level of light intensity (approximately -2.5 log.scot.cd.s/m^2 and higher) than in WT retina (approximately -4.5 log.scot.cd.s/m^2 and higher). This activity was low enough that it was decided to use this double mutant model for the assessment of functional improvement after cell injection.

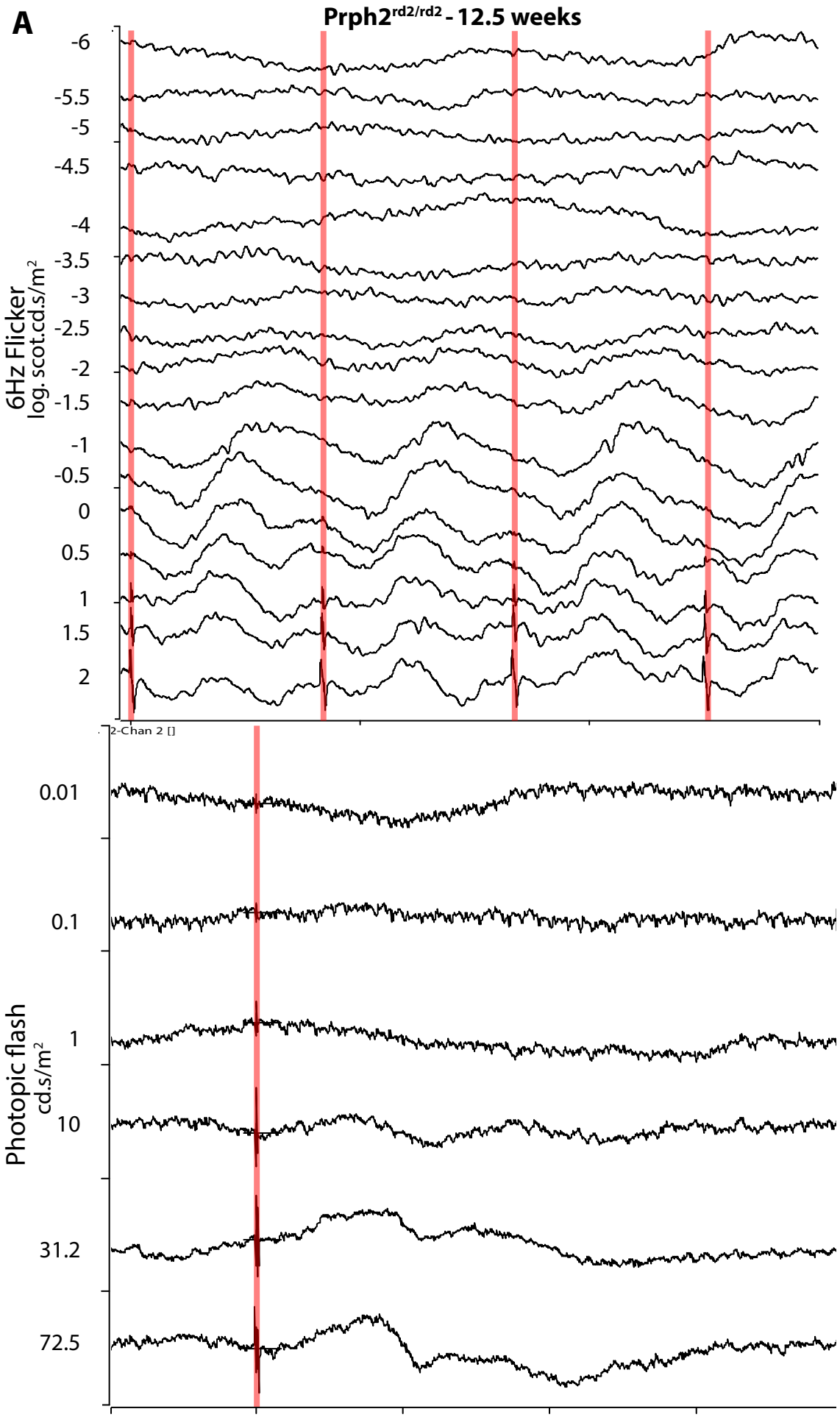
A
Prph2rd2/rd2 - 12.5 weeks
6Hz Flicker
log. scot.cd.s/m2
-6
-5.5
-5
-4.5
-4
-3.5
-3
-2.5
-2
-1.5
-1
-0.5
0
0.5
1
1.5
2
2-Chan 2 []
Photopic flash
cd.s/m2
0.01
0.1
1
10
31.2
72.5

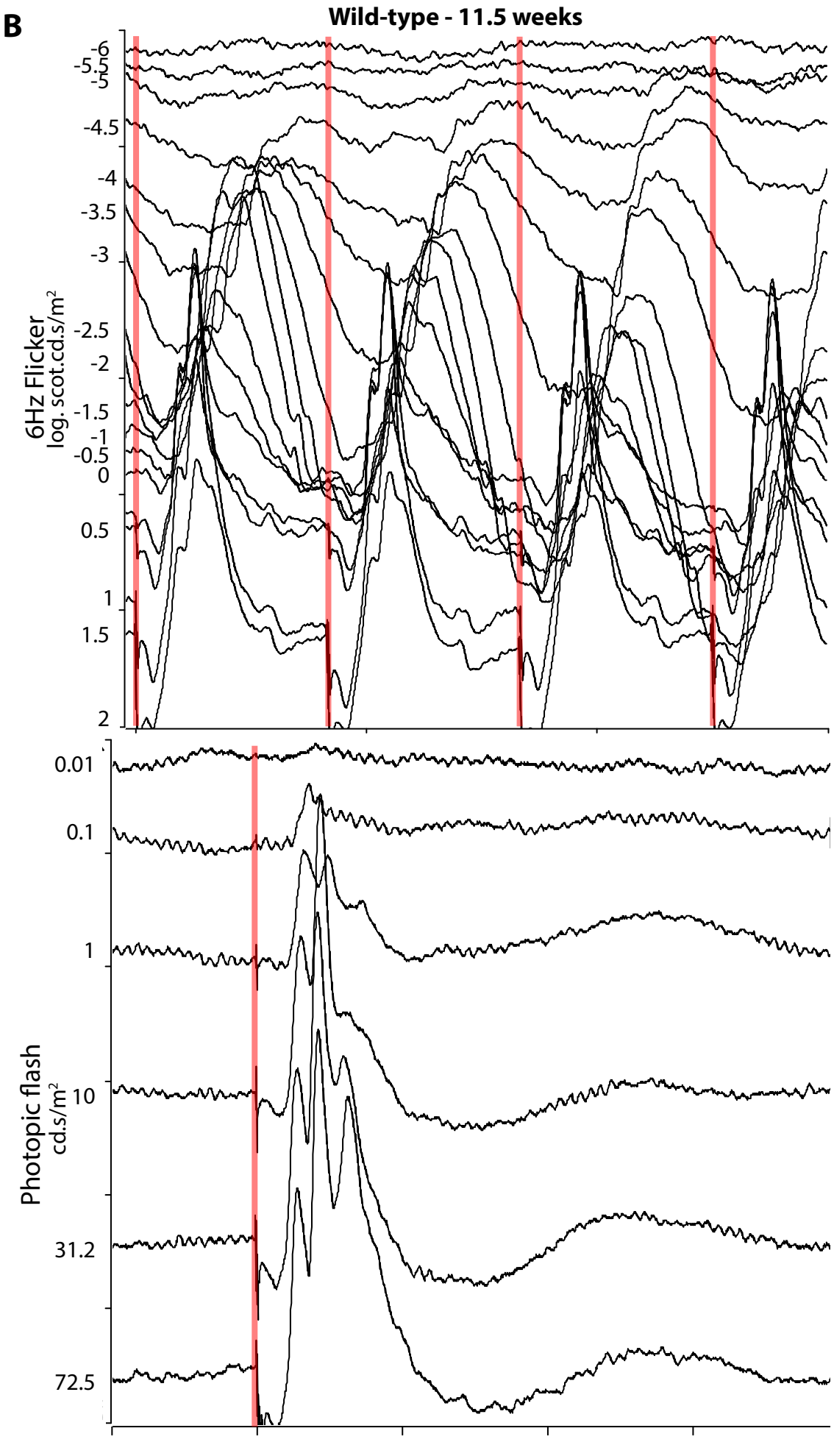
B
Wild-type - 11.5 weeks
6Hz Flicker
log. scot.cd.s/m²
-6
-5.5
-5
-4.5
-4
-3.5
-3
-2.5
-2
-1.5
-1
-0.5
0
0.5
1
1.5
2
Photopic flash
cd.s/m²
0.01
0.1
1
10
31.2
72.5

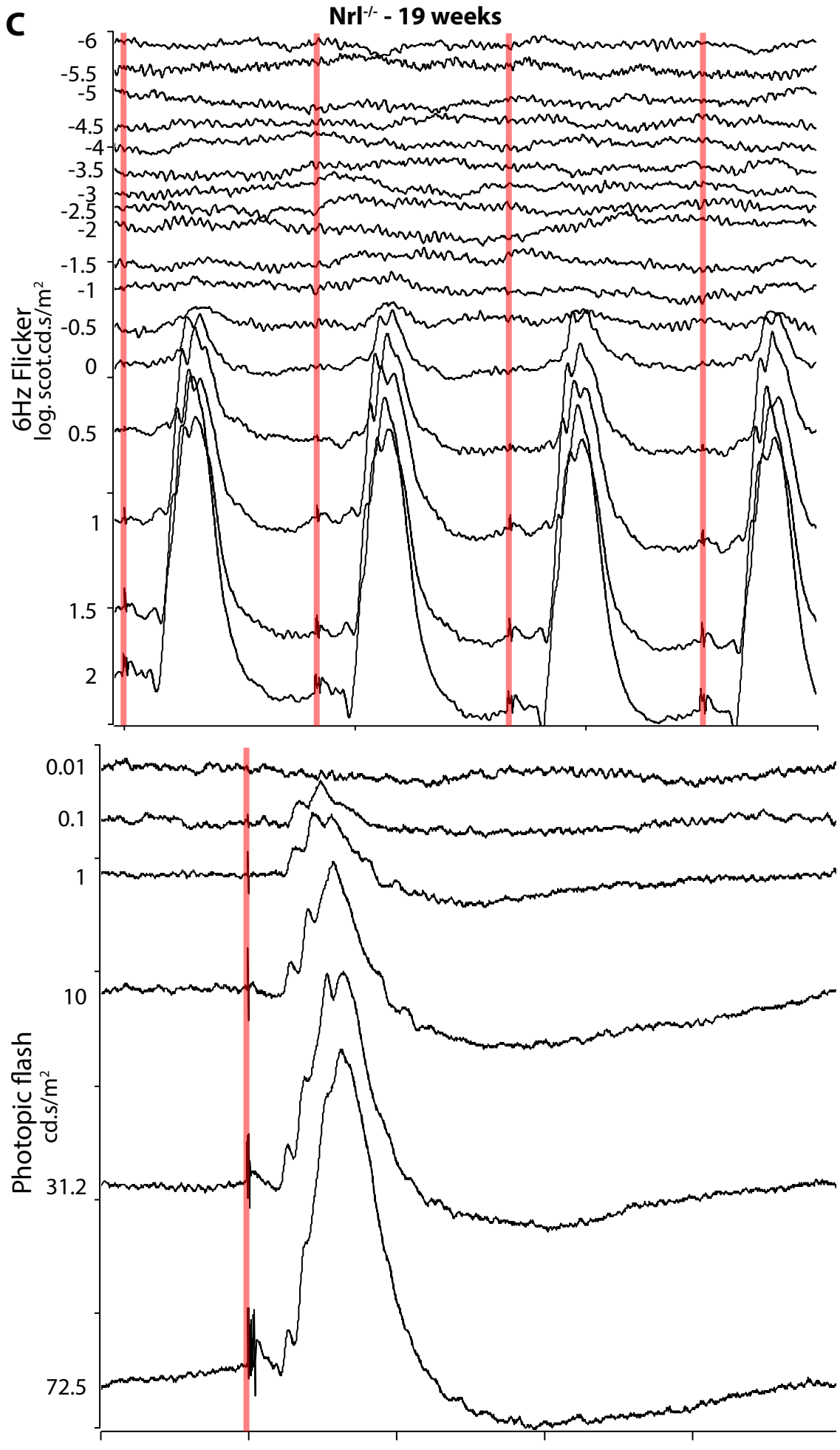
C
Nrl-/- - 19 weeks
6Hz Flicker
log. scot.cd.s/m2
-6
-5.5
-5
-4.5
-4
-3.5
-3
-2.5
-2
-1.5
-1
-0.5
0
0.5
1
1.5
2
Photopic flash
cd.s/m2
0.01
0.1
1
10
31.2
72.5

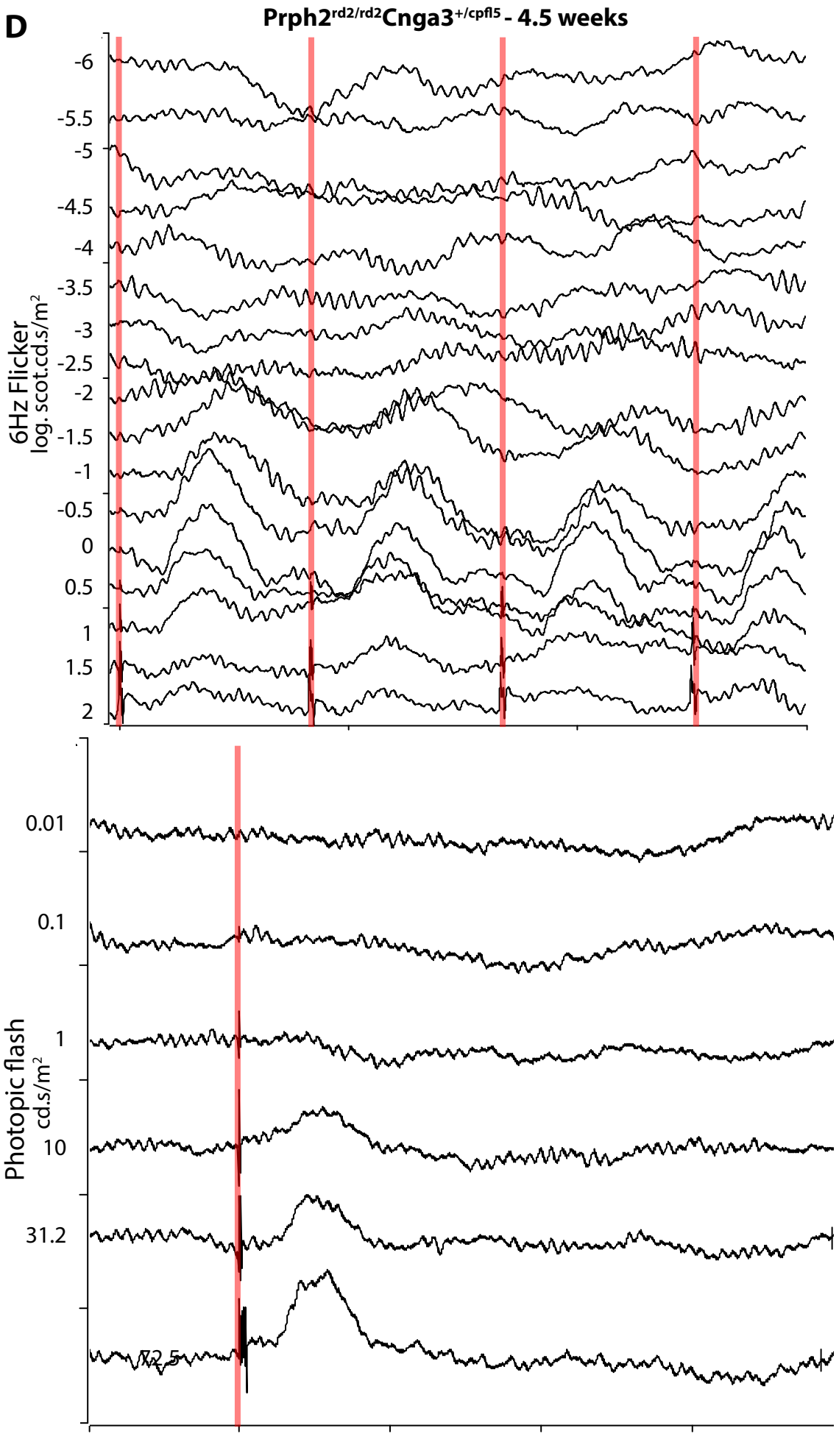
D
Prph2rd2/rd2Cnga3+/cpfl5 - 4.5 weeks
6Hz Flicker
log. scot.cd.s/m2
-6
-5.5
-5
-4.5
-4
-3.5
-3
-2.5
-2
-1.5
-1
-0.5
0
0.5
1
1.5
2
Photopic flash
cd.s/m2
0.01
0.1
1
10
31.2
72.5
260

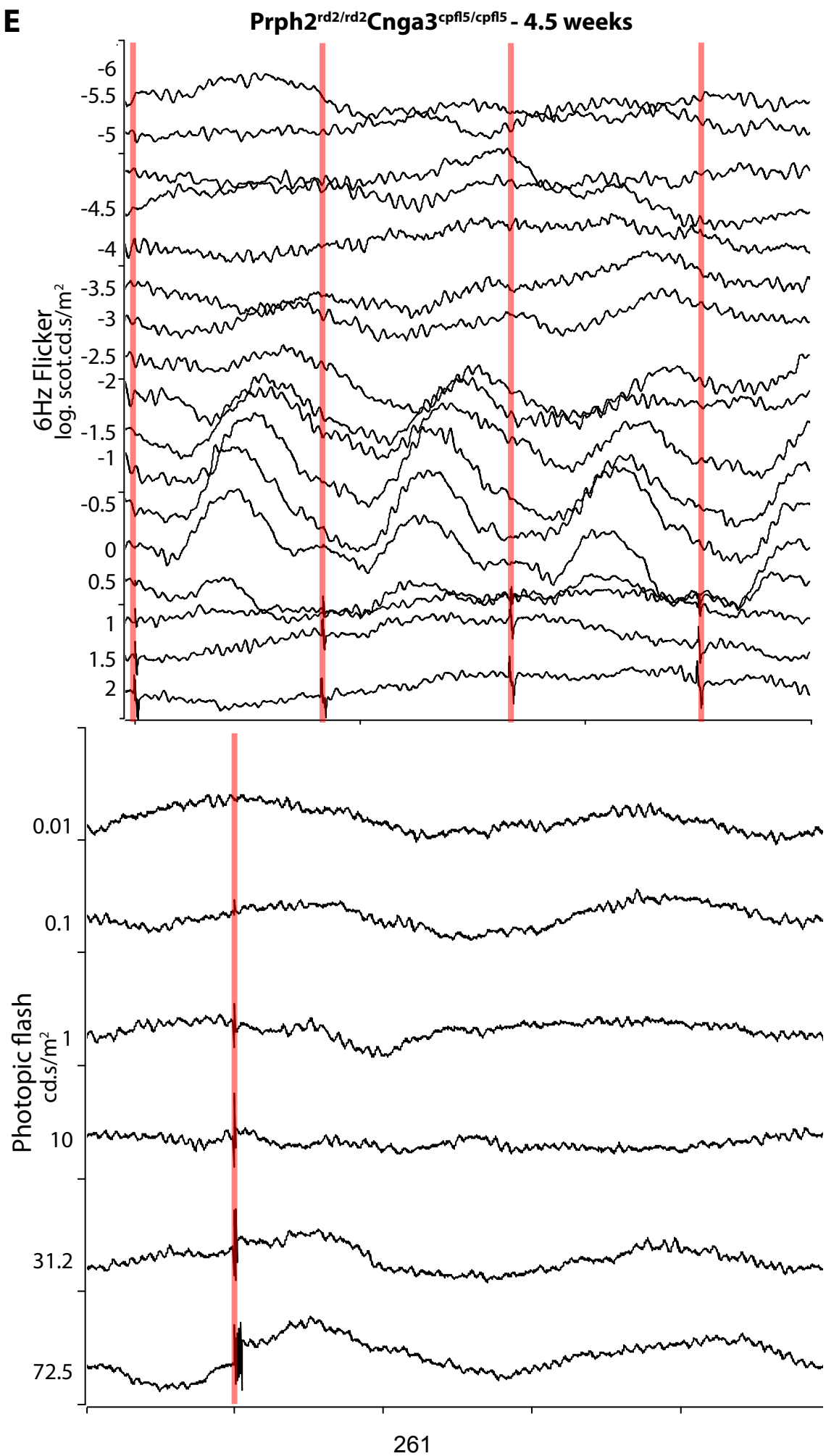
E
Prph2rd2/rd2Cnga3cpfl5/cpfl5 - 4.5 weeks
6Hz Flicker
log. scot.cd.s/m2
-6
-5.5
-5
-4.5
-4
-3.5
-3
-2.5
-2
-1.5
-1
-0.5
0
0.5
1
1.5
2
Photopic flash
cd.s/m2
0.01
0.1
1
10
31.2
72.5
261

Figure 6.1 Example ERG plots showing recorded voltage over time, separated by light intensity level.

Upper plots show a 6Hz flicker paradigm, ranging between -6 and 2 log cd.s/m^2, presented on a dark background. Ticks are 50µV on the y-axis, 200ms on the x-axis.

Lower plots are a photopic single flash paradigm ranging between 0.01 and 72.5 cd.s/m^2, with flashes on a light background of 30 cd/m^2. Ticks are 50µV on the y-axis, 100ms on the x-axis.

Red bars show onset but not duration of light stimulus presentation. Each plot for each mouse genotype are shown on the same axis scale for ease of comparison.

A The Prph2$^{rd2/rd2}$ mouse was chosen due to the high number of GFP+ cells it supported after transplantation and supposed negligible response to light by later adult ages . However, in the flicker paradigm, responses are small in amplitude, but clear by -1 log cd.s/m^2 and are maintained to the highest intensities. Similarly some evidence of response in the photopic flash condition was seen at 31.5 cd.s/m^2 upwards.

B In the WT mouse, for the flicker condition, responses are evident at low intensities (-4.5 log cd.s/m^2) and continue with high amplitudes to the highest intensities used indicating both rod and cone function. The photopic flash ERG shows responses from 0.1 cd.s/m^2.

C In the rod-deficient, cone enriched Nrl$^{-/-}$ model, in the flicker paradigm, responses begin at higher light intensities than in WT equivalents, at -0.5 log cd.s/m^2, and are maintained at the highest intensities, indicating a loss of rod function and preservation of that of cones. Accordingly, responses in the photopic flash ERG are similar to those in WT.

D-E The Prph2$^{rd2/rd2}$ model was crossed with the Cnga3$^{cpfl5/cpfl5}$ line to remove the activity shown, apparently from surviving cone photoreceptors. To determine the effect of this, ERG responses were compared between mice homozygous for the rds mutation, and either heterozygous or homozygous for the cpfl5 mutation at young adult ages.

In the Prph2$^{rd2/rd2}$Cnga3$^{+/cpfl5}$ (heterozygous) mouse (D), responses of low amplitudes begin at approximately -2.5 in the flicker paradigm, of a similar amplitude to those found in the Prph2$^{rd2/rd2}$ mouse and appear to weaken with higher amplitudes. Weak photopic responses compared to the WT and Nrl$^{-/-}$ mice are evident from 10 cd.s/m^2 in the flash ERG.

In the full double mutant Prph2$^{rd2/rd2}$Cnga3$^{cpfl5/cpfl5}$(E), responses are still seen in the flicker paradigm from approximately -2 log cd.s/m^2, but appear to be reduced, if not gone entirely at the highest intensities and in the photopic flash ERG.

6.2.2 MEA recordings from cell-injected retinas

Next, I used multi-electrode array (MEA) recordings to determine the electrical activity of RGCs in these retinas, as described in section 2.8. Since only a small region of the explanted retina can be placed on the MEA, it was first necessary to ascertain the approximate area of the retina where injection took place. This necessitated viewing the dissected neural retina under a fluorescence microscope to locate the GFP signal of the transplanted cells. Due to this, it was not possible to maintain the retina in conditions of darkness throughout preparation. The mice providing the retinas used in this experiment were therefore not dark-adapted before being sacrificed, and dissection was carried out under light conditions. As light exposure exhausts the response capacity of rods more readily than cones, this was also expected to have the beneficial effect of reducing the baseline residual rod response of the $Prph2^{rd2/rd2}Cnga3^{cpfl5/cpfl5}$ retina, allowing the responses of the cone-like cells that were transplanted to be more clearly seen.

Similarly, the retinas were not perfused with 9-cis-retinal during recording, which would otherwise act to regenerate the retinal chromophore in the photoreceptors in the place of the RPE which is mostly removed in the MEA experiments. While both rods and cones require the regeneration of their chromophore molecules, cone photoreceptors maintain their response even at high light levels by using a distinct regeneration mechanism not found in rods (Arshavsky, 2002), which involves the Müller glia, and are therefore less reliant on an external chromophore supply *ex vivo*.

To increase the chances of recording from an area of retina close to the site of transplantation, where GFP+ cells would be located in the recipient ONL, recipient mice received two injections into one eye, in the superior/dorsal, and inferior/ventral

retina. These injections were made only into one eye, to allow for the possibility of taking ERG measurements from these mice, with the uninjected eye acting as an uninjected matched control. NB. Retina from uninjected eyes was not used as a control for the MEA, as because only one piece of retinal tissue could be recorded from at any one time, the contralateral eye would have been used several hours after removing the eye from the animal, and could therefore have begun to lose viability. Instead, retinas from age-matched controls were used in separate experiments.

Adult 4-5 week old $Prph2^{rd2/rd2}Cnga3^{cpfl5/cpfl5}$ double mutant mice (treated) received two injections of 200,000 GFP+ cells isolated from P8 $Nrl^{-/-}$NrlGFP donor mice into one eye (pseudorandomised between recipients). Animals were sacrificed 7-8 weeks after injection (therefore at 11-12.5 weeks of age). Uninjected (untreated) $Prph2^{rd2/rd2}Cnga3^{cpfl5/cpfl5}$ double mutant mice were sacrificed at 10.5-12 weeks. As a positive control, Adult $Nrl^{-/-}$ mice were sacrificed at 13-14 weeks.

Neural retinas were dissected, assessed for GFP regardless of origin with fluorescence microscopy and prepared for MEA recording as detailed in Section 2.8. Before the first stimulus exposure, retinas were allowed to adapt to dark conditions for 20 minutes, and thereafter only exposed to stimulus flashes and dim red light. They underwent 200ms flashes of LED light at increasing intensities, controlled by the imposition of neutral density (ND) filters on the light path, and at three wavelengths: 420 nm, 505nm and 470nm, at each intensity level. ND filters impede light in approximate factors of 10: a filter value of 3 will allow approximately 10 times more light through than a value of 4, but approximately 10 times less than a value of 2. Since the ND filters were the control mechanism for the light intensity, common between different experiments and LED wavelengths, the filter level will be

given throughout this section when referring to the light stimulus intensity. All stimulus flashes were made on a background of darkness.

The common stimulus series was as follows:

1000ms pre-flash darkness → 200ms flash → 1800ms post flash darkness (20 repetitions)

3 minutes post-stimulus set recovery

The light stimuli used for the flash in each set are shown in order in Table 6.1. Multiple wavelengths were used for the higher light levels, to investigate the spectral sensitivity of the cells of each retina.

Table 6.1 Light stimuli for MEA recordings

Light level (μW optical power at 420nm)	ND filter used	Number of recordings at this level	LED wavelengths used, in order
0.0002	8	1	420 nm only
0.0005	7	1	420 nm only
0.0033	6	1	420 nm only
0.045	5	3	420 nm, 505nm, 470nm
1	4	3	420 nm, 505nm, 470nm
10.1	3	3	420 nm, 505nm, 470nm
147	2	3	420 nm, 505nm, 470nm
1340	1	3	420 nm, 505nm, 470nm

6.2.2.1 Data analysis and spike sorting

Putative spikes were extracted from the data by setting a threshold of 4 times the standard deviation of the filtered recordings for each electrode, and recording the trace from 1ms before to 2ms after each threshold crossing to create a ‘spike’.

These spikes then underwent automated spike sorting, which used the wavelet coefficients of these spikes to separate them into putative ‘clusters’ or groups of spikes which were similar in these properties. This process aimed to isolate the

contributions of true RGCs from background noise, and also to determine whether each electrode was receiving input from one or more RGC, and, if more than one, to isolate the response from each cell. The algorithm used gave a range of options for clustering the spikes.

Manual assessment of these clusters of spikes was then necessary, in order to determine which of the generated clusters were most likely to describe the true nature of the electrode input, and to make sure that these clusters contained all of the spikes in these groups. Clusters were chosen to contain all the spikes judged to be likely to come from the same cell.

The manual assessment process also aimed to exclude incomplete clusters, those with inputs from more than one source, and clusters consisting of background noise rather than RGC input. Noise was identified by a combination of factors. These included symmetrical spike shapes (indicating a lack of separate depolarisation and hyperpolarisation phases as would be found in an action potential event); spikes occurring too close together (a neuron would require a refractory period, preventing very rapid spiking) as measured by an interspike interval; and high variability of the waveform.

To exclude incomplete samples of the responses of cells, spike groups were also excluded if their amplitudes were small enough and variable enough that it was likely that a significant proportion would not have passed the threshold for detection.

These assessments of cluster quality were carried out by manual judgement. Due to the aims of the study: to determine whether an increase in cells responding to light could be found after the injection of cells, further exclusion of clusters by computer assessment on similar criteria was not carried out.

After injection and data processing, the 3 recordings made at the filter level of 2ND were used for the most detailed analysis – this was the level at which the strongest responses could be seen in the $Nrl^{-/-}$ control retinas, using 420nm light, and also the level where the largest number of responsive cells were found in cell-injected $Prph2^{rd2/rd2}Cnga3^{cpfl5/cpfl5}$ retinas (see section 6.2.2.4).

Example plots for cells in $Nrl^{-/-}$ retina at these levels are shown in Figure 6.2. Raster plots for these cells show a vertical line for each action potential. The onset of a response in these cells is clear at a short delay from the presentation of the stimulus at t=0. Examples of likely ON, OFF, and ON-OFF type responses are shown (Nelson, 2001), although it should be noted that classification of these response types can only be putative, without pharmacological verification.

Peristimulus time histograms (PSTHs) are also shown, which display the mean impulses in every 20ms window, by comparing across the time windows of all 20 repeated stimulus presentations.

The cumulative sum control plots shown display the cumulative deviation of the average spike frequency per ms from the average baseline value given by the prestimulus window of 1000ms before stimulus presentation. Cells were counted as responding to the stimulus if their cumulative spike rate in any given time bin of 1ms rose above, or fell below, 3 times the standard deviation of the spike rate given by the pre-stimulus interval, for more than 8 ms. The variance for this standard deviation was given by the formula

$$V = n\left[\frac{c^2 t}{m} + \frac{1}{6} - \frac{c^4}{6} + \frac{(ct)^2}{um}\right]$$

where *c* is the coefficient of variation and *m* the mean interval between spikes in *n* trials. (Davey et al., 1986) This threshold diverges over time due to the cumulative nature of the measurement.

Clusters with extremely low total numbers of spikes (fewer than two in every one of the 20 intervals of 1000 ms recorded before the onset of stimulation in each trial) were excluded from analysis in this way, as this made the calculation of an interval between spikes in the prestimulus period impossible. The number of clusters which fell into this category varied considerably between retinas (from 0 to 13), and the numbers are included in the relevant sections below. This exclusion raises the possibility that true inputs from cells with a very low baseline spiking rate might be excluded. Only one cluster of this magnitude was identified by visual inspection as showing a response to light, in a treated (cell-injected) $Prph2^{rd2/rd2}Cnga3^{cpfl5/cpfl5}$ retina, as shown in Figure 6.2F.

Table 6.2 summarises the retinas analysed and the number of cells which were identified by the above methods, for one set of wavelength and intensity values.

Table 6.2 Summary of MEA experiments

	Retinas analysed	Cells identified (420 nm, 2ND)				
$Prph2^{rd2/rd2}Cnga3^{cpfl5/cpfl5}$ (treated)	5	54	95	59	57	66
$Prph2^{rd2/rd2}Cnga3^{cpfl5/cpfl5}$ (untreated)	5	73	18	52	72	41
$Nrl^{-/-}$	3	52	58	40		

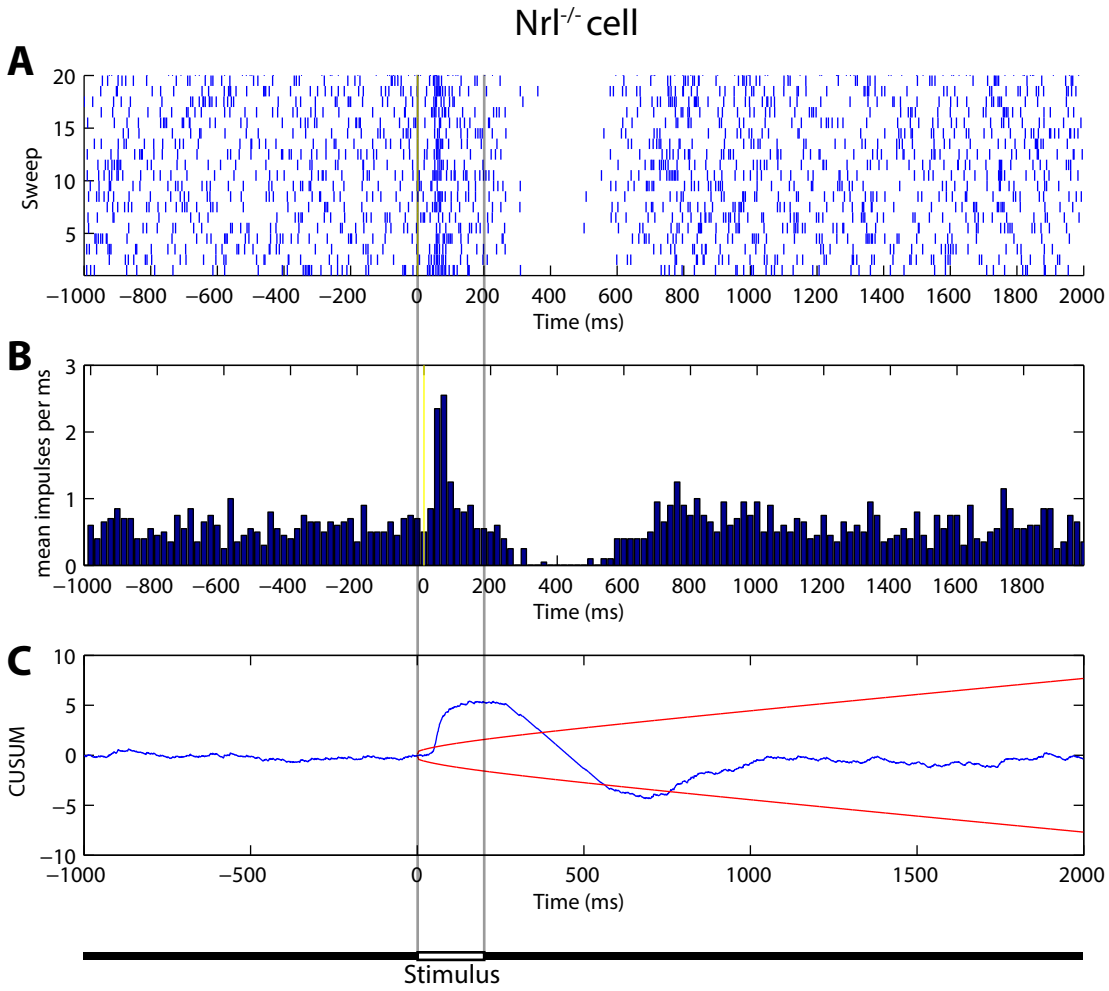

Figure 6.2 Plots showing the response of a cell from an Nrl$^{-/-}$ retina, identified by spike sorting, to 200ms flash (within the grey lines) of 420nm light at 2ND of neutral density impedance.

A A raster plot of spikes from this cell. A vertical line represents a spike occuring at a given time during a sweep, and all 20 sweeps are shown on a different line. The baseline firing rate is shown for 1000ms before stimulus presentation at 0 (yellow line). In each sweep, the firing rate increases sharply but temporarily after stimulus presentation (an ON response), returning to baseline levels while the stimulus is maintained, and subsequently decreases (relative to baseline) at around t = 300ms, most likely in response to the switching off of the stimulus.

B A peristimulus time histogram (PSTH) showing the mean impulses per millisecond in each 20ms time window during the sweeps. A higher spike rate can be seen shortly after stimulus presentation, and a lower one after the stimulus is removed at t=200.

C A cumulative sum plot showing the cumulative deviation of the spike rate in each ms time window from the average spike rate set by the 1000ms prestimulus window. Thus it rises when the spike rate exceeds the prestimulus average (such as here approximately t=20-100ms) and falls only when the spike rate is reduced compared to the prestimulus average (here between approximately t=280 and 500 ms). The limits (red lines) are set to detect any violation in the spike rate of 3 times the standard deviation of the spike rate of the 1000ms pre-stimulus period. A cell crossing this for more than 8 time points is classed as responding to the light stimulus.

Different cells from the same $Nrl^{-/-}$ retina show other modes of response.

D A putative OFF response, showing an increase in spike rate on stimulus loss.

E A putative ON-OFF response, showing an increase in spike rate both at stimulus presentation and loss.

F Cells with a very low pre-stimulus spike rate (fewer than two spikes in every prestimulus interval) were excluded from standard analysis due to the inability to determine appropriate thresholds for response. In one case (F), a cell from a $Prph2^{rd2/rd2}Cnga3^{cpfl5/cpfl5}$ retina excluded on these grounds appeared to show a response to light, with spikes occurring only in the post-stimulus interval, at a range of stimulus wavelengths (420, 470 and 505nm).

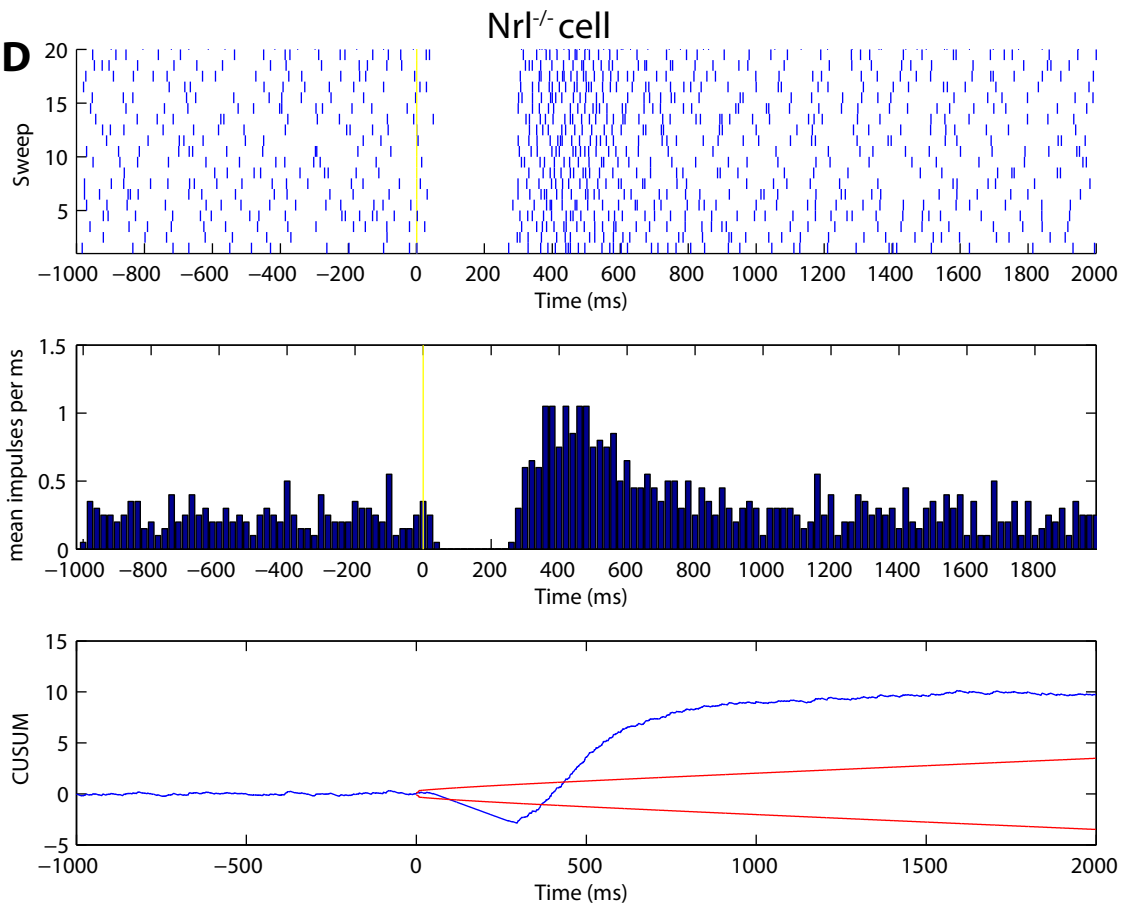

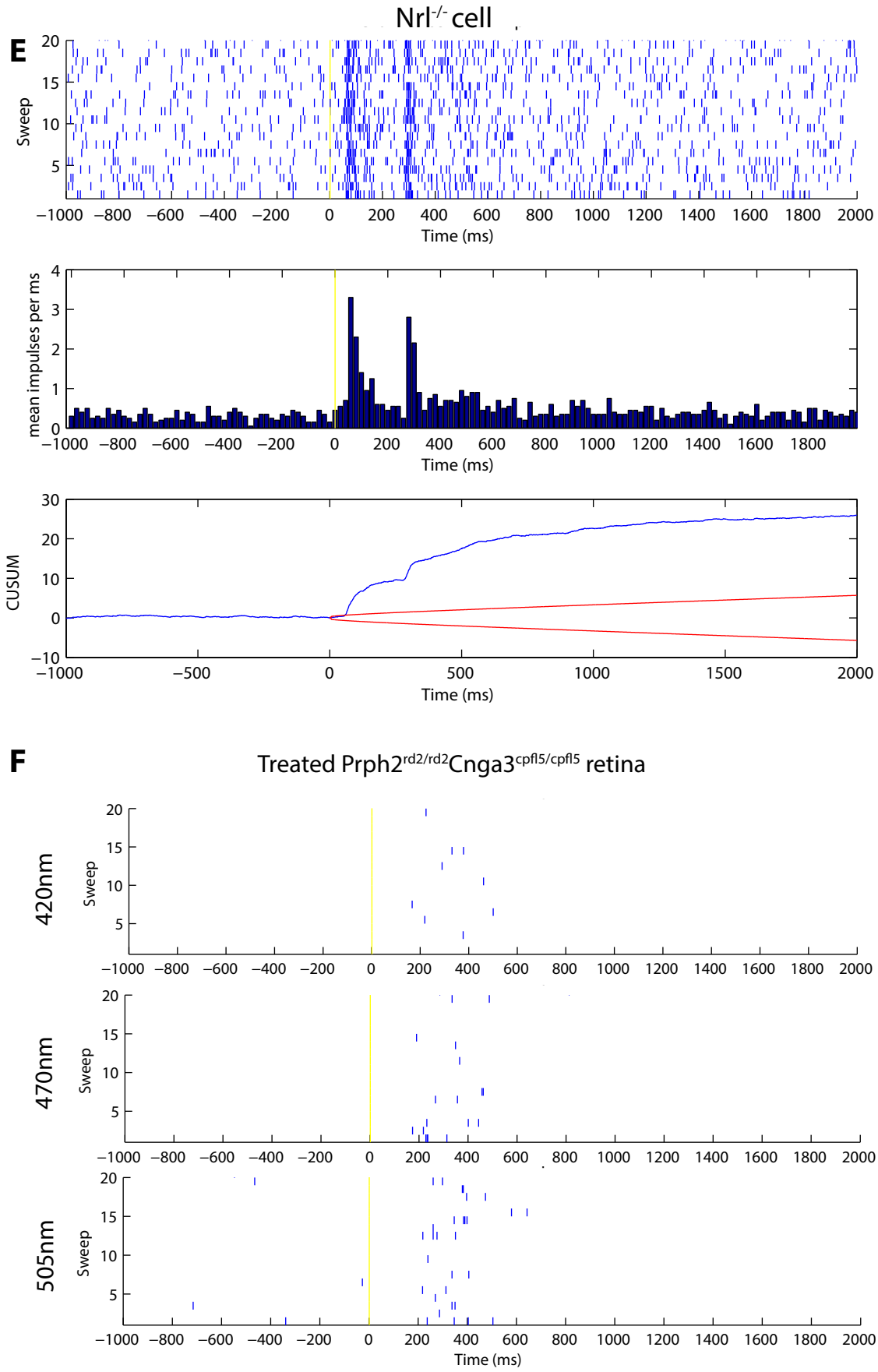
E
Nrl-/- cell
Sweep
Time (ms)
mean impulses per ms
CUSUM
F
Treated Prph2rd2/rd2Cnga3cpfl5/cpfl5 retina
420nm
470nm
505nm

6.2.2.2 Response to 420nm light

Figure 6.3 shows the number of responding cells compared to the total in all tested retinas using 420nm light at 2ND. The total number of responding cells varies between experiments; this is due to differences in the number of traces being excluded as noise, and the number of recordings judged to arise from more than one cell, during the spike sorting procedure. Table 6.3 shows the number of cells identified in each retina, and those found to be responding to light, as well as the number of clusters rejected due to a low baseline firing rate.

Table 6.3 Response to 420nm light

$Nrl^{-/-}$ control *(3 excluded)*		Untreated $Prph2^{rd2/rd2}Cnga3^{cpfl5/cpfl5}$ *(5 excluded)*		Treated $Prph2^{rd2/rd2}Cnga3^{cpfl5/cpfl5}$ *(21 excluded)*	
Responsive	Total	Responsive	Total	Responsive	Total
43	52	7	73	20	54
57	58	1	18	23	95
20	40	3	52	19	59
		17	72	5	57
		8	41	12	66
Totals					
120	150	36	256	79	331

Strong responses are seen in a high proportion of $Nrl^{-/-}$ cells (Figure 6.3C). Most cells also show a multiple phase response to light, with an increase in action potential frequency followed by a decrease, or vice versa. Many also appear to show a response to the end of the stimulus, at 200ms.

In $Prph2^{rd2/rd2}Cnga3^{cpfl5/cpfl5}$ retinas, the responses that could be seen did not show the rapid onset and offset of the cells in the $Nrl^{-/-}$ retina, instead showing a longer delay between stimulus onset and a change in spike frequency. These changes also appeared smaller in magnitude overall than in $Nrl^{-/-}$ cells. This is to be expected from a degenerating model, lacking outer segments and with functionless cones.

However, several cells in each retinal type were classified as light-responsive by the statistical analysis, but which do not show a change in spike frequency large enough to be easily seen by eye on the raster plots, as shown in Figure 6.3C-E.

This represents a limitation of the thresholding method used to determine cell response. While this approach allowed an automated and objective measurement of whether a cell responded to light, it meant that in a system with variable strengths of responses, any threshold set represents a compromise between retaining true outcomes and rejecting false positive outcomes. It is possible that these unclear responses represent the latter. However, the marked visible difference seen between the strong responses of the $Nrl^{-/-}$ cells and much weaker and less obvious responses from $Prph2^{rd2/rd2}Cnga3^{cpfl5/cpfl5}$ retinas (whether injected or not) indicate that some true responses may be too weak to be shown by visual inspection, but accurately identified by this statistical analysis.

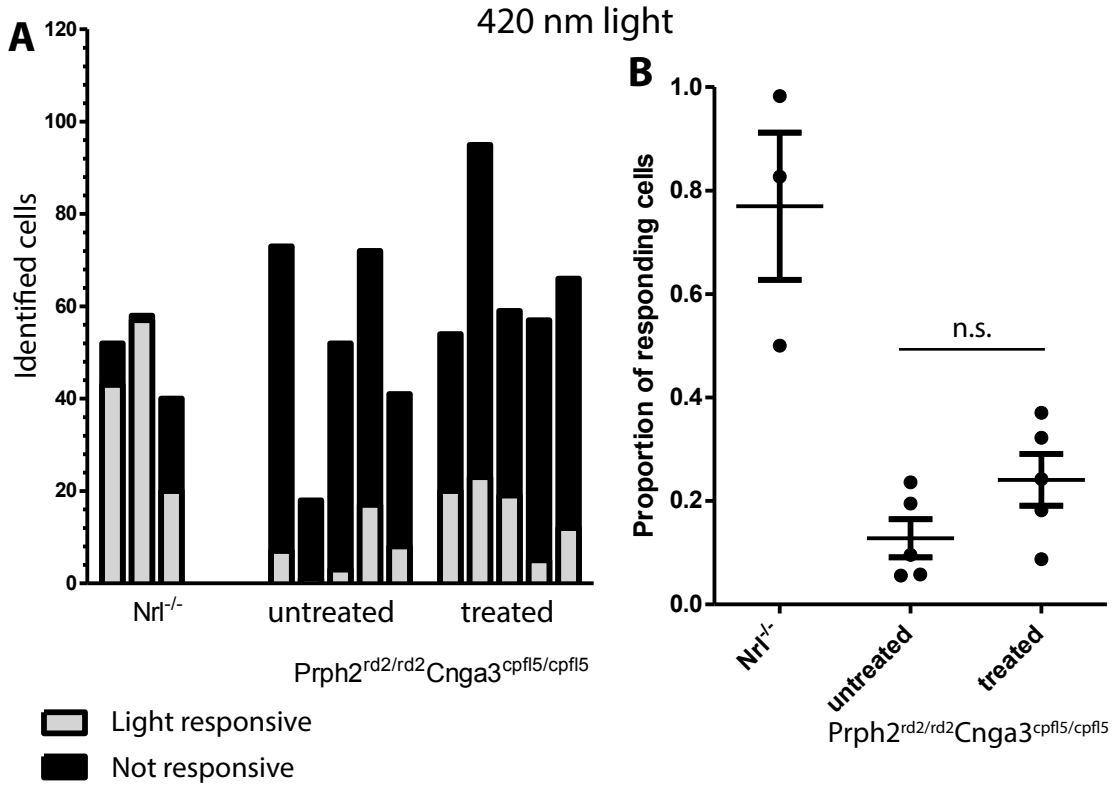
420 nm light
A
120
100
80
60
40
20
0
Identified cells
Nrl-/-
untreated
treated
Prph2rd2/rd2Cnga3cpfl5/cpfl5
Light responsive
Not responsive
B
1.0
0.8
0.6
0.4
0.2
0.0
Proportion of responding cells
n.s.
Nrl-/-
untreated
treated
Prph2rd2/rd2Cnga3cpfl5/cpfl5

Figure 6.3 Retinal ganglion cell responses to 420 nm light, measured by MEA.
Retinas used were Nrl$^{-/-}$, and Prph2$^{rd2/rd2}$Cnga3$^{cpfl5/cpfl5}$, with the latter either uninjected (untreated) or injected with 2x 200,000 P7/8 Nrl$^{-/-}$NrlGFP cells, 7-8 weeks before recording.
A The number of cells identified by spike sorting in each retina split into those determined to be light-responding (grey) and those which were not (black). The total number of identified cells is seen to vary between retinas.
B The proportion of total identified cells which were light-responsive in each processed retina. No significant difference was found between the proportions found in treated and untreated cells.

C-E Example responses of individual cells classed as responding from each retinal type, including the raster and cumulative sum plots.
In each retinal type, some cells classed as responding did not show a change in spike frequency large enough to be clearly seen in the raster plots (examples Cii, Di, Dv, Ev). Figure 6.4 investigates the likelihood of cells being falsely identified as responding. In all retinal types, however, clearly responding cells could also be seen, including putative ON responses (Cvi, Dii, Eii) and OFF responses (Civ, Dvi, Eiv, Evi), although these are more difficult to determine in the Prph2$^{rd2/rd2}$Cnga3$^{cpfl5/cpfl5}$ model, due to the unclear onset of response and the variable latency. Putative ON-OFF responses can be clearly seen only in Nrl$^{-/-}$ retinas (Ci, Ciii).

While responses in the Nrl$^{-/-}$ retinas (C) appeared in general to be larger in the change to prestimulus firing rate, and occur much more rapidly after stimulus presentation than in Prph2$^{rd2/rd2}$Cnga3$^{cpfl5/cpfl5}$ retinas, no such obvious differences in strength of response or speed of onset were seen between treated (E) and untreated (D) Prph2$^{rd2/rd2}$Cnga3$^{cpfl5/cpfl5}$ retinas.

C Individual cell recordings from Nrl$^{-/-}$ retinas

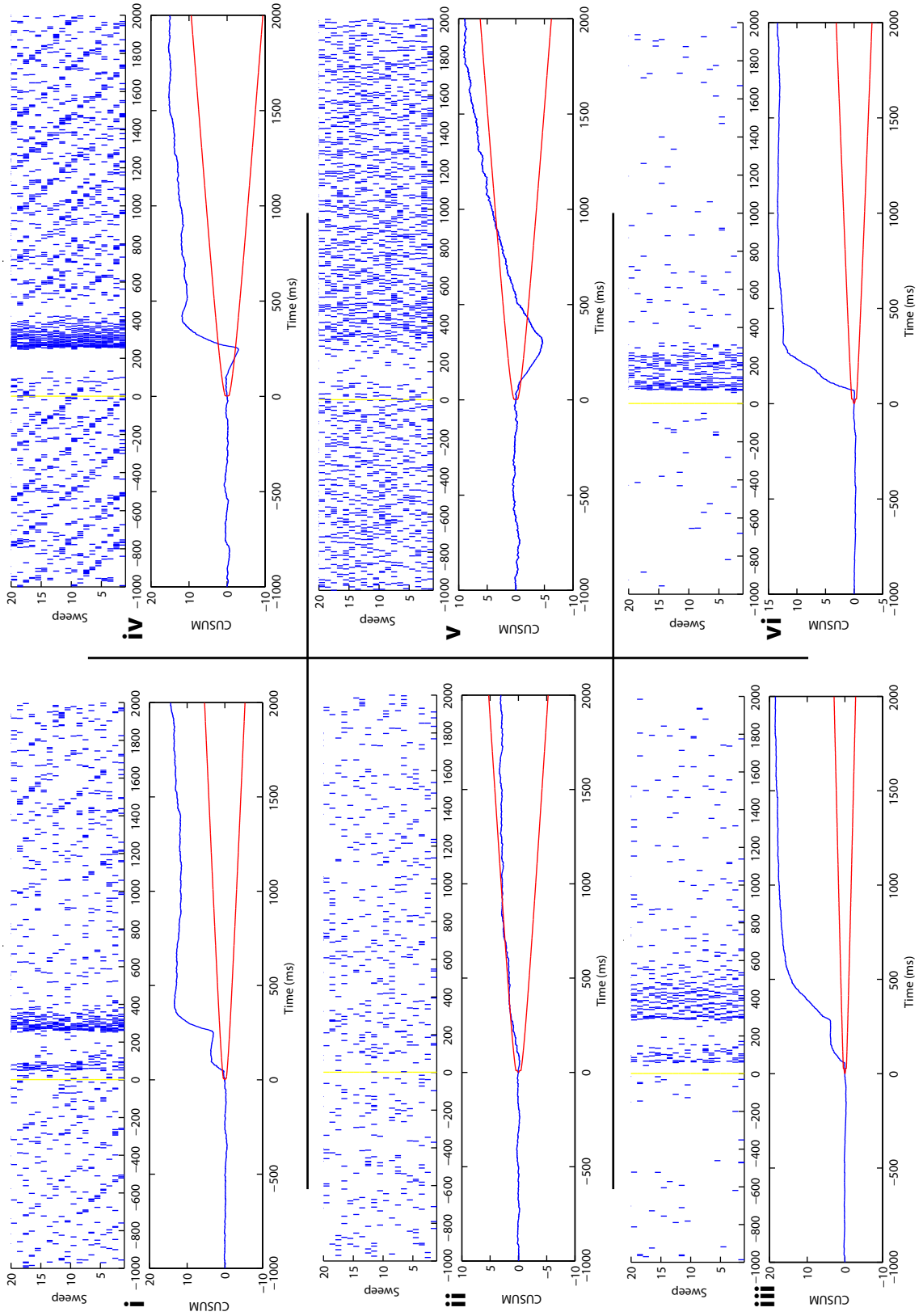

D Individual cell recordings from untreated Prph2$^{rd2/rd2}$Cnga3$^{cpfl5/cpfl5}$ retinas

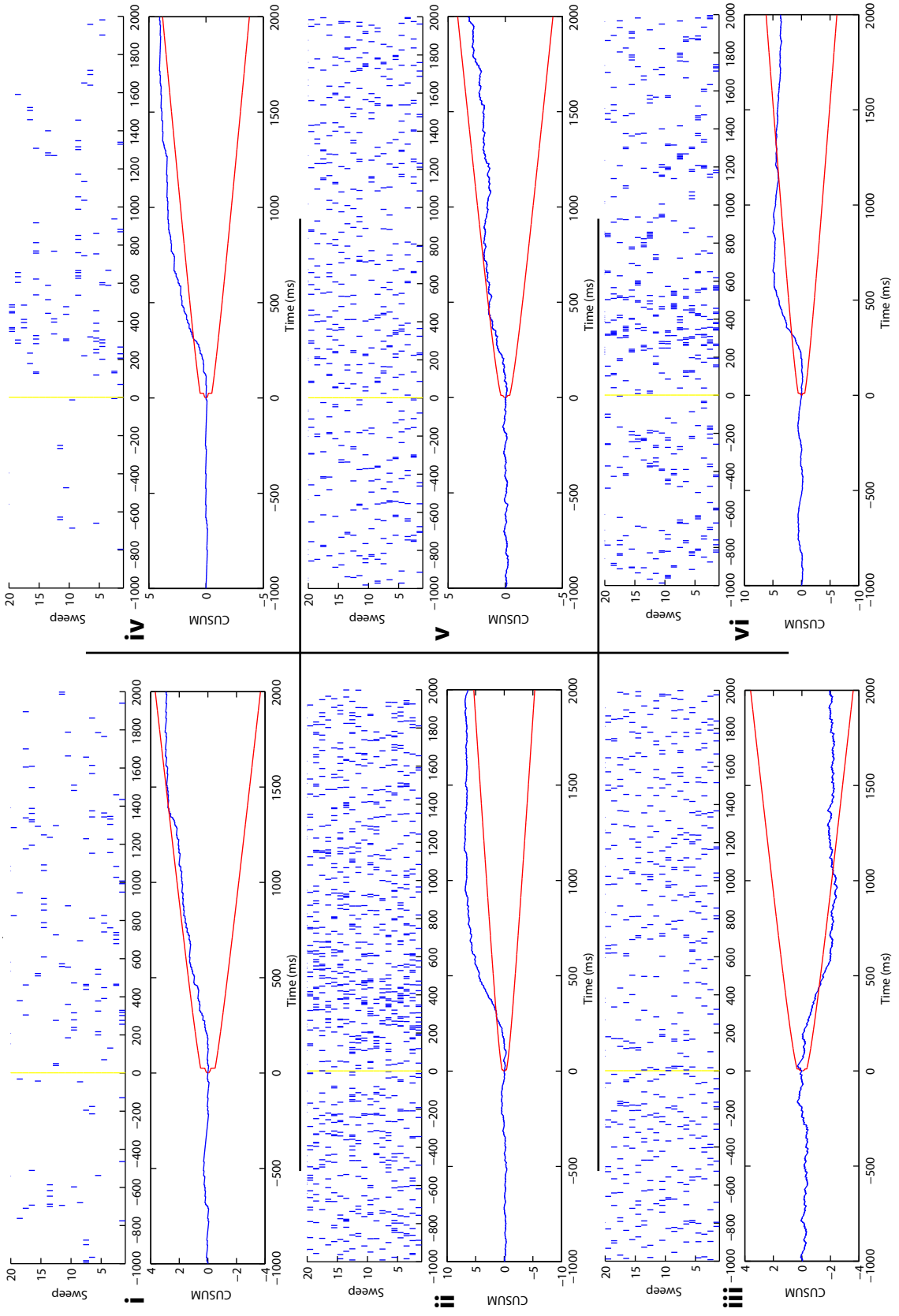

E Individual cell recordings from treated Prph2$^{rd2/rd2}$Cnga3$^{cpfl5/cpfl5}$ retinas

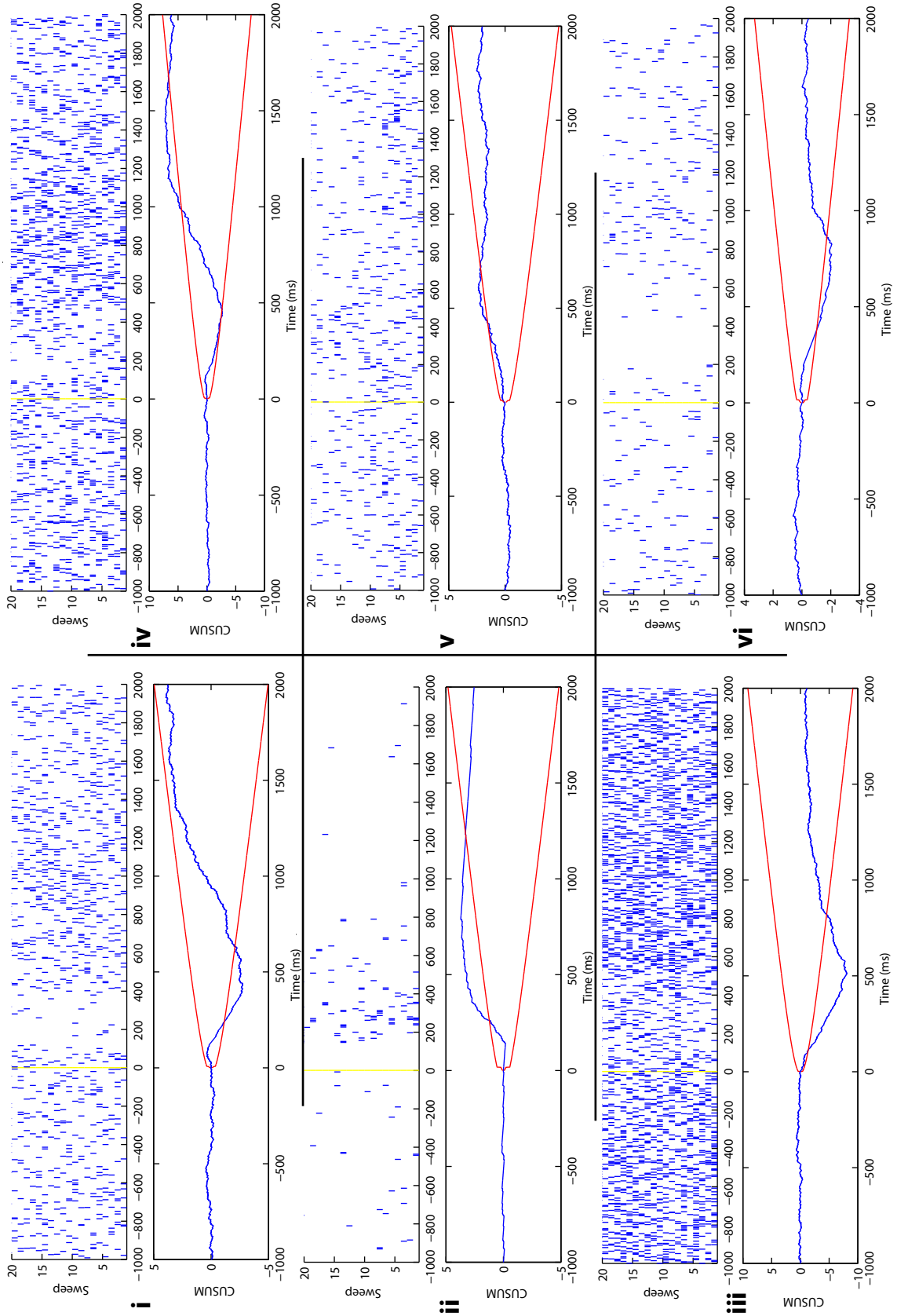

For these reasons, I analysed the recordings from the lowest light level condition used: the 420nm flash using 8ND filters (0.0002 μW, close to the maximum sensitivity of the power meter used), below the detection level of a normal WT retina. The number of cells shown to meet the threshold to be classified as responding in this condition are shown in Figure 6.4, together with examples of the spike data from these cells. While cells meeting these criteria could be found in all retinal conditions, the absolute number is very low, with only 20 out of 433 identified cells across all retinas being classed as responding; this can be used as a guide to estimate how many false positive outcomes can be expected in other stimulus levels. Only 3 out of 20 (15%) of the cells found to meet the threshold for responding at this lowest light level were also found to be responding in the 2ND 420nm light condition. This indicated that these observations were likely to be random events, and not likely to be consistent between retinal types or light conditions. For these analyses therefore, to avoid unnecessary exclusion of true responses, the thresholds were kept as described and the number of responding cells not adjusted.

Returning to the responses found with 420nm light, the total number of active channels in each recording indicated that responsive cells were more common in the treated retinas, with the three highest absolute numbers, and proportions of responding cells, found in this condition.

Transplantation itself is inherently variable and there is no way of accurately screening the recipient retinas for the number of GFP+ cells prior to MEA assessment. Moreover, there is additional uncertainty involved in finding areas of retina close to the injection site. Together, these underline the challenges in measuring any effect of transplantation in any given treated retina.

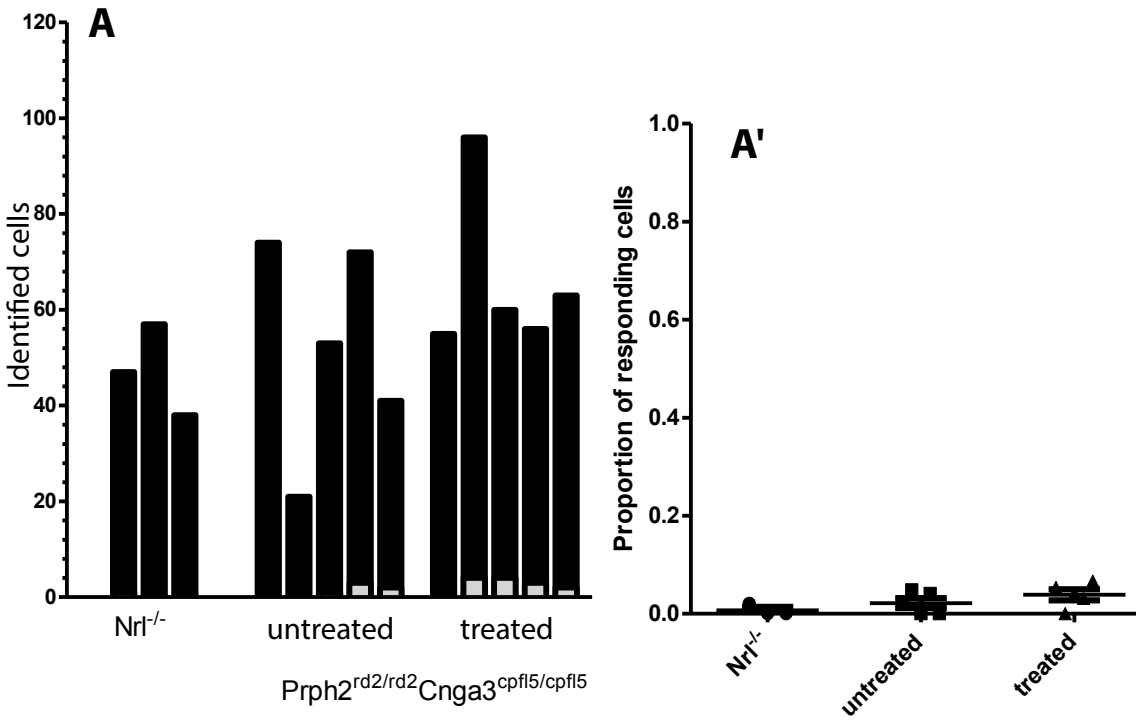

Figure 6.4 Responses at light intensities below detection level. A small number of cells in each condition reached the threshold to be judged as responding , showing that a small number of falsely identified responding cells will be given by this analysis. The total number of cells and those responding in each retina are shown (A), along with the proportion of responding cells (A').

B-D Examples of cells from this light level are shown from all three retinal types; these show that cells with particularly low spike rates (B) may fall into this category, as well as short violations of the threshold (D).

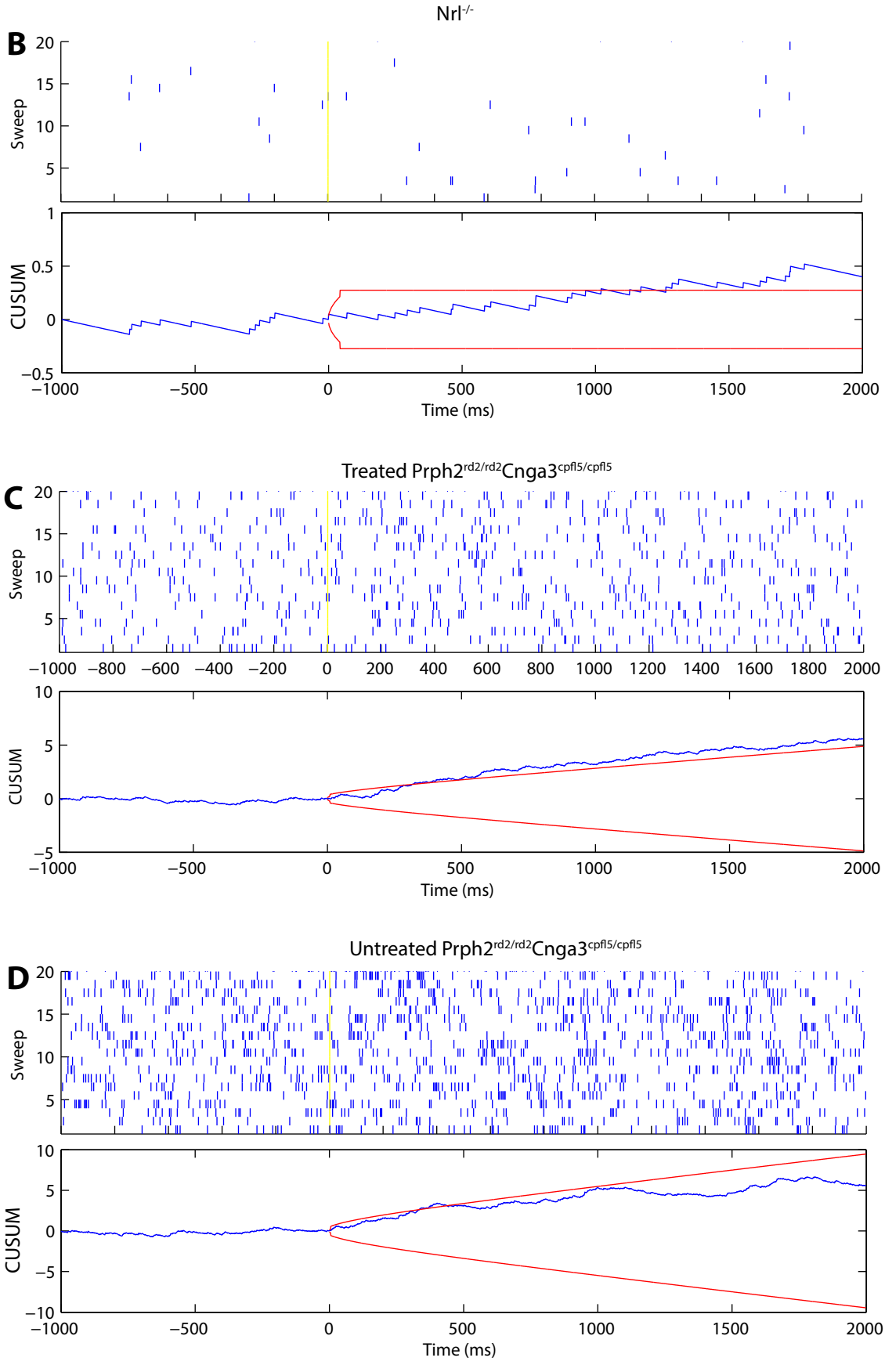
B
Nrl-/-
Sweep
CUSUM
Time (ms)
C
Treated Prph2rd2/rd2Cnga3cpfl5/cpfl5
Sweep
CUSUM
Time (ms)
D
Untreated Prph2rd2/rd2Cnga3cpfl5/cpfl5
Sweep
CUSUM
Time (ms)

However, although very low numbers of responding cells were found in the majority of untreated retinas, two showed higher levels of around 20% or more responding cells. Given this observation, and the number of recordings possible in this study, we cannot exclude the possibility that the observations from both treated and untreated retinas result from the variability in the response found in $Prph2^{rd2/rd2}Cnga3^{cpfl5/cpfl5}$ retinas rather than any effect of cell injections.

Combining all the cells within each condition of injected and uninjected retinas gives a total ratio of 79 responding, compared to 252 not responding (23.9%) in retinas which received cell injections, compared with 36 to 220 (14.1%) in control uninjected retinas. Comparing these proportions with Fisher's exact test shows significantly more responding cells in the injected conditions ($X^2(1)= 8.809$, $p = 0.003$).

However, the high level of variability between outcomes in each condition mean that combining these data in this way is likely to be inappropriate. The variation in the numbers of responding cells within conditions, and also of total cells identified can be seen in all retinal types, including the $Nrl^{-/-}$ retina. While variability might be expected from the treated retinas, as it is not guaranteed that an area of cell transplantation might be successfully located, for the other conditions this variation is likely to be due to experimental reasons.

Experimental variability could arise for a number of reasons, for example the strength of contact between the retina and the electrodes of the MEA, or the integrity of the MEA itself (these would be likely to explain differences in the total number of cells identified as such in each retinal preparation), but damage to the retina, and the health of the tissue could also affect the number of RGCs receiving input from light-responsive photoreceptors.

Furthermore, the intervention made – the injection of cells – was made on the scale of a whole retina, rather than at the level of independent cells. For this reason, comparisons treating each retina as a separate experiment are likely to give a closer estimate to the true outcome.

A comparison of the proportion of responding cells of each MEA preparation in each of the treated and untreated conditions was not significant: $t(8) = 1.808$, $p = 0.1081$. For comparisons of this kind however, the relatively small dataset provided by these experiments make it difficult to find statistically significant differences.

It is possible that the effect of cell transplantation would be an increase in the strength of response of individual RGCs, rather than the frequency of RGCs responding to light. The classification of cells as light-responsive by a threshold measurement does not easily allow for a comparison of the strength of response. Changes in the spike rate relative to a pre-stimulus level are by nature dependent on this baseline, which has been shown to vary substantially between cells, both in mean and variation. Small differences in response strength based on the spike rate would therefore also be largely driven by discrepancies in the baseline. While it is clearly seen that the $Nrl^{-/-}$ cells are in general stronger and quicker in onset, any differences between the treated and untreated $Prph2^{rd2/rd2}Cnga3^{cpfl5/cpfl5}$ retinas would be expected to be far less obvious, and responses of equivalent apparent strength were seen in both conditions. Given also that the significant responses of the $Prph2^{rd2/rd2}Cnga3^{cpfl5/cpfl5}$ retinas are in general only exceed the 3sd threshold by a small margin, changes to the spike rate would also be likely to be small relative to this threshold. As shown in Figure 6.3D and E, there are no clear differences in response latency or change in spike frequency between injected and uninjected $Prph2^{rd2/rd2}Cnga3^{cpfl5/cpfl5}$ retinas.

6.2.2.3 The effect of light wavelength

To determine whether the cells responding after injections of $Nrl^{-/-}$ cells fit a response profile of cone-like or rod-like cells, multiple wavelengths of LED light were used as a stimulus, with peaks at 420, 470 and 505nm. The cone-like photoreceptors produced by the $Nrl^{-/-}$ mutant mouse are most similar to S-cones, although they often also contain a variable amount of M-opsin. However, these cells have been shown to be dramatically reduced in response at wavelengths longer than 450nm (Daniele et al., 2005).

I therefore carried out a similar analysis on the recordings of tissue subjected to different wavelengths of light, subjected to the same neutral density filtration as described above. This gave optical power values of 147μW (420nm), 269 μW (470nm) and 156μW (505nm). It should be noted that the different stimuli were not presented in ascending order of wavelength, but rather in the sequence 420nm, 505nm, 470nm (with 20 sweeps for each wavelength) to prevent any difference seen from being the result of an unrelated change of retinal function over time. The number of cells responding in each condition, and those rejected due to low baseline spike rates, are shown in Tables 6.4 and 6.5, and Figure 6.5.

Table 6.4 Response to 470nm light

$Nrl^{-/-}$ *(2 excluded)*		Untreated $Prph2^{rd2/rd2}Cnga3^{cpfl5/cpfl5}$ *(7 excluded)*		Treated $Prph2^{rd2/rd2}Cnga3^{cpfl5/cpfl5}$ *(16 excluded)*	
Responsive	Total	Responsive	Total	Responsive	Total
40	52	3	71	18	55
53	58	1	15	26	96
10	41	7	53	21	58
		24	72	7	58
		9	41	5	73
Totals					
103	151	44	252	77	340

Table 6.5 Response to 505nm light

$Nrl^{-/-}$ *(2 excluded)*		Untreated $Prph2^{rd2/rd2}Cnga3^{cpfl5/cpfl5}$ *(11 excluded)*		Treated $Prph2^{rd2/rd2}Cnga3^{cpfl5/cpfl5}$ *(23 excluded)*	
Responsive	Total	Responsive	Total	Responsive	Total
8	52	10	70	23	54
55	58	1	16	28	93
6	41	4	52	19	60
		20	72	5	58
		7	41	14	67
Totals					
69	151	42	251	89	332

A reduction in the proportion of responding cells was evident in some $Nrl^{-/-}$ retinas with longer wavelength light but this effect was not constant across each retina tested, with one retina showing a 95% response rate even at 505nm – this retina also having the highest level of response at all wavelength values. Comparing traces from the same cell between wavelengths, as shown in Figure 6.5D, however, showed that even when response was maintained, in many cases at least, the apparent magnitude of this response was reduced, even when the cell was still responsive enough to be classed as such. For this reason, it is likely that these observations are the result of responses being weakened such that they fall below the threshold for detection.

In the $Prph2^{rd2/rd2}Cnga3^{cpfl5/cpfl5}$ retinas, however, no obvious reduction of the number of responding cells was found, as shown in Figure 6.5B,C. As noted above, in the $Nrl^{-/-}$ retina, even when S-opsin expressing cone-like cells are still responsive at higher wavelengths, the apparent strength of response is reduced. No such effect is clear in the responses from either group of $Prph2^{rd2/rd2}Cnga3^{cpfl5/cpfl5}$ retinas, as can be seen in Figure 6.5E,F (see also Figure 6.2F). Given that responses in these

retinas are much weaker in general than in the $Nrl^{-/-}$ mouse, it would be expected that such an effect would act to bring response levels down below the threshold level, which is not the case. For this reason, it can be concluded that the effect of wavelength expected from S-opsin containing cone-like cells does not occur in $Prph2^{rd2/rd2}Cnga3^{cpfl5/cpfl5}$ retinas. The lack of an obvious effect of wavelength in uninjected retinas shows that the model is an appropriate background for looking for the short-wavelength responses of $Nrl^{-/-}$ cells, although no such responses were evident in the injected retinas.

It also did not appear that treated $Prph2^{rd2/rd2}Cnga3^{cpfl5/cpfl5}$ retinas showed increased function relative to untreated retinas at any tested wavelength, with comparisons between the proportions of cells responding in each retina not significantly different with either 470nm light ($t(8)=0.9047$, $p = 0.3921$) or 505nm light ($t(8) = 1.768$, $p = 0.1151$).

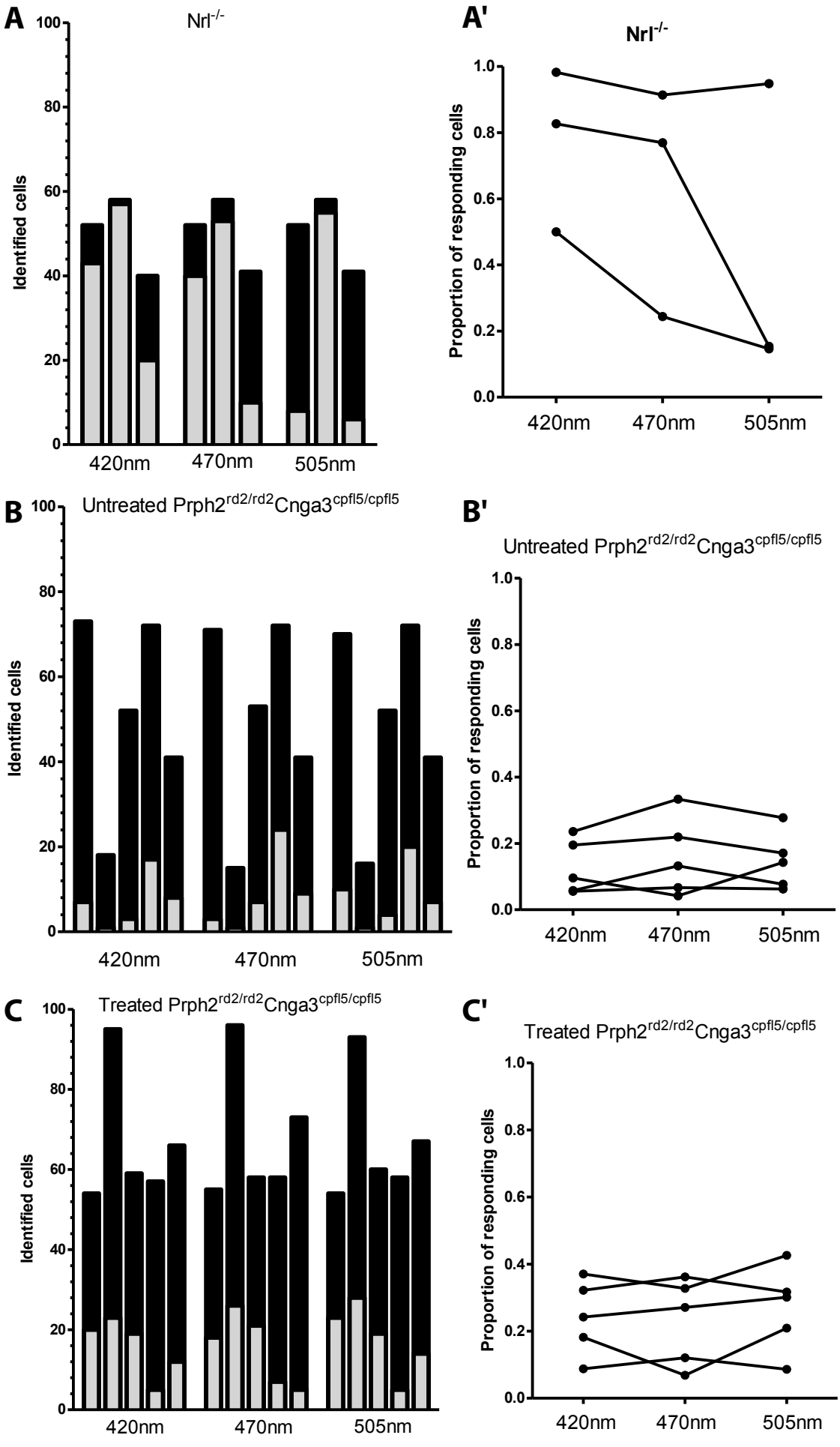
A
Nrl-/-
Identified cells
100
80
60
40
20
0
420nm
470nm
505nm
A'
Nrl-/-
Proportion of responding cells
1.0
0.8
0.6
0.4
0.2
0.0
420nm
470nm
505nm
B
Untreated Prph2rd2/rd2Cnga3cpfl5/cpfl5
Identified cells
B'
Untreated Prph2rd2/rd2Cnga3cpfl5/cpfl5
Proportion of responding cells
C
Treated Prph2rd2/rd2Cnga3cpfl5/cpfl5
Identified cells
C'
Treated Prph2rd2/rd2Cnga3cpfl5/cpfl5
Proportion of responding cells

Figure 6.5 The effect of wavelength on light response. LED light at 420, 470 and 505nm was used.

A-C Identified cells in each retina by wavelength of light stimulation, showing cells classified as responding (grey) and not responding to light (black).

A'-C' The proportion of total cells identified which respond to light (proportions from the same retinas are connected).

In $Nrl^{-/-}$ retinas, the number of responding cells drops substantially with longer wavelengths for two retinas, with the reduction smaller at 470nm than at 505nm. In the retina which does not show this pattern, looking at traces from the same cells at different wavelengths, the strength of these responses appear to be reduced at longer wavelengths. Examples of this are shown (D). These plots are from two cells (left and right) at the wavelengths specified, and are taken from the $Nrl^{-/-}$ retinal preparation which did not show a reduction in the number of responding cells. Although each cell reaches the threshold of response at each wavelength, the responses can be seen to decline in strength from 420nm to 505nm (note the deviation from the threshold lines in the cumulative sum plots) with the reduction in spike rate after removal of the stimulus at 200ms in particular being reduced with increasing wavelength in these examples.

This pattern of reduction is not seen in any of the $Prph2^{rd2/rd2}Cnga3^{cpfl5/cpfl5}$ retinas, and similar comparisons with the responses of individual cells do not show similar effects on the strength of response. E-F show the responses of cells in treated and untreated retinas at each wavelength, all meeting the threshold for responding.

D Individual cell recordings from Nrl$^{-/-}$ retinas

E Individual cell recordings from untreated Prph2$^{rd2/rd2}$Cnga3$^{cpfl5/cpfl5}$ retinas

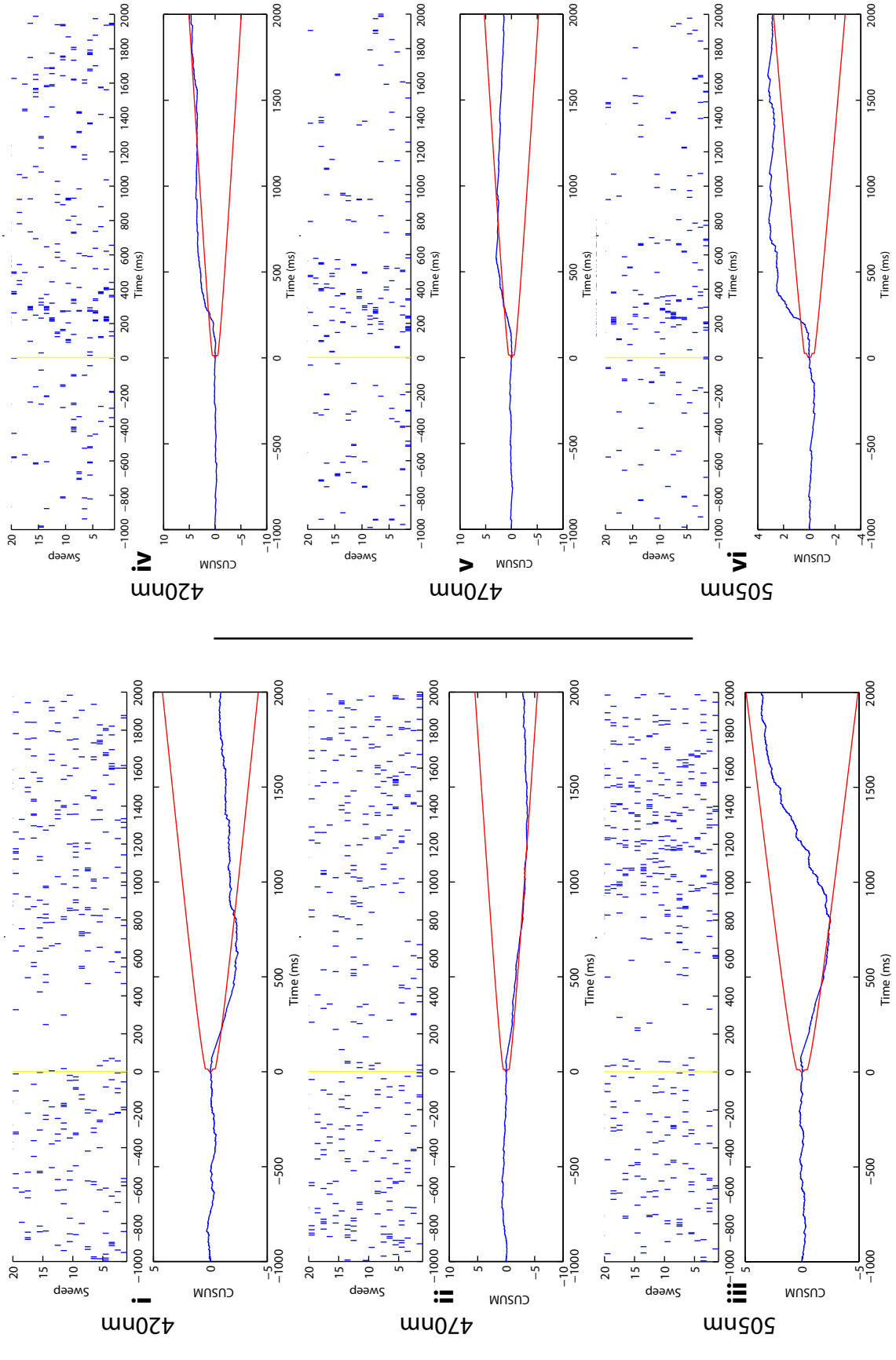

F Individual cell recordings from treated Prph2$^{rd2/rd2}$Cnga3$^{cpfl5/cpfl5}$ retinas

6.2.2.4 The effect of light intensity

Cone photoreceptors remain active at higher intensities of light than do rod photoreceptors, being used for human 'daylight' vision. Restoring cone-mediated retinal function would therefore allow vision at useful levels of light intensity.

The above experiments have shown that as a result of the rd2 mutation, rod cells in the $Prph2^{rd2/rd2}$ mouse begin to show responses at an abnormally high level of light intensity. Similarly, the $Cnga3^{cpfl5/cpfl5}$ mutation may reduce response at the highest intensity levels, as shown in section 6.2.1. It would be expected, therefore, that if the injection of photoreceptor precursor cells alleviated either of these problems, retinas treated in this way would show an increase in function relative to untreated controls at either higher or lower light intensities.

To investigate whether the responses in treated $Prph2^{rd2/rd2}Cnga3^{cpfl5/cpfl5}$ retinas behave differently at different light intensities, thus indicating a more cone-like response pattern, I analysed the recordings from retinas exposed to 420nm light at higher and lower light intensities (respectively 1ND and 3ND of neutral density filtration - 1340μW and 10.1μW optical power) than those assessed above. The results found are shown in Tables 6.6 and 6.7, and Figure 6.6.

Table 6.6 Response to 1ND 420nm light

Nrl$^{-/-}$ *(2 excluded)*		Untreated Prph2$^{rd2/rd2}$Cnga3$^{cpfl5/cpfl5}$ *(12 excluded)*		Treated Prph2$^{rd2/rd2}$Cnga3$^{cpfl5/cpfl5}$ *(18 excluded)*	
Responsive	Total	Responsive	Responsive	Total	Responsive
42	51	8	67	11	55
58	58	2	15	23	96
11	55	6	52	22	58
		21	71	3	58
		3	40	3	71
Totals					
111	164	40	245	62	338

Table 6.7 Response to 3ND 420nm light

Nrl$^{-/-}$ *(1 excluded)*		Untreated Prph2$^{rd2/rd2}$Cnga3$^{cpfl5/cpfl5}$ *(7 excluded)*		Treated Prph2$^{rd2/rd2}$Cnga3$^{cpfl5/cpfl5}$ *(20 excluded)*	
Responsive	Total	Responsive	Responsive	Total	Responsive
14	53	4	71	4	54
29	58	2	18	4	96
0	41	1	52	4	60
		3	72	1	54
		1	41	6	67
Totals					
43	152	11	254	19	331

Looking at the higher intensities, two Nrl$^{-/-}$ retinas showed little difference in response rate, with the number of cells changing by only one cell in each. A reduction in response could also be seen at these intensities in one retina, most likely representing eventual bleaching and fatigue of the remaining photoreceptors, although it could also be caused by reduction in tissue viability over time. This indicates that due to experimental variability, the effect of increasing light on retinas is not necessarily constant between all retinas of the same type.

In untreated Prph2$^{rd2/rd2}$Cnga3$^{cpfl5/cpfl5}$ retinas, a similar pattern was shown, with small increases (of four or fewer cells) shown in most retinas, indicating approximately constant response levels, and a reduction in one other. Likewise in treated retinas small increases were seen in two retinas and reductions in three others. There was no significant difference in the proportion of responding cells in in treated and untreated Prph2$^{rd2/rd2}$Cnga3$^{cpfl5/cpfl5}$ retinas at this light level $t(8) = 0.4728$, $p = 0.6490$. This indicated that treated and untreated retinas react similarly to high light intensities.

At lower intensities, reduction in response was evident in all retinal conditions, including treated and untreated Prph2$^{rd2/rd2}$Cnga3$^{cpfl5/cpfl5}$ retinas. An increase in responding cells was found between 3ND and 2ND in all Nrl$^{-/-}$ and treated retinas, and four out of five untreated Prph2$^{rd2/rd2}$Cnga3$^{cpfl5/cpfl5}$ retinas (with the exception being a single extra cell in the retina with the fewest total identified cells). In these retinas, although a very few cells could be found to be clearly responding (in both treated and untreated retina, see Figure 6.6D,E), the number of responding cells was close to that of cells stimulated at the very lowest light levels (see Figure 6.4) indicating that response at this intensity is close to negligible. Comparisons between the proportions of responding cells in treated and untreated Prph2$^{rd2/rd2}$Cnga3$^{cpfl5/cpfl5}$ retinas were not significant: $t(8) = 0.3640$, $p = 0.7253$.

In summary, there is no evidence that the injection of cone-like precursor cells allows improved function at lower light levels, or allows maintenance of response at higher levels.

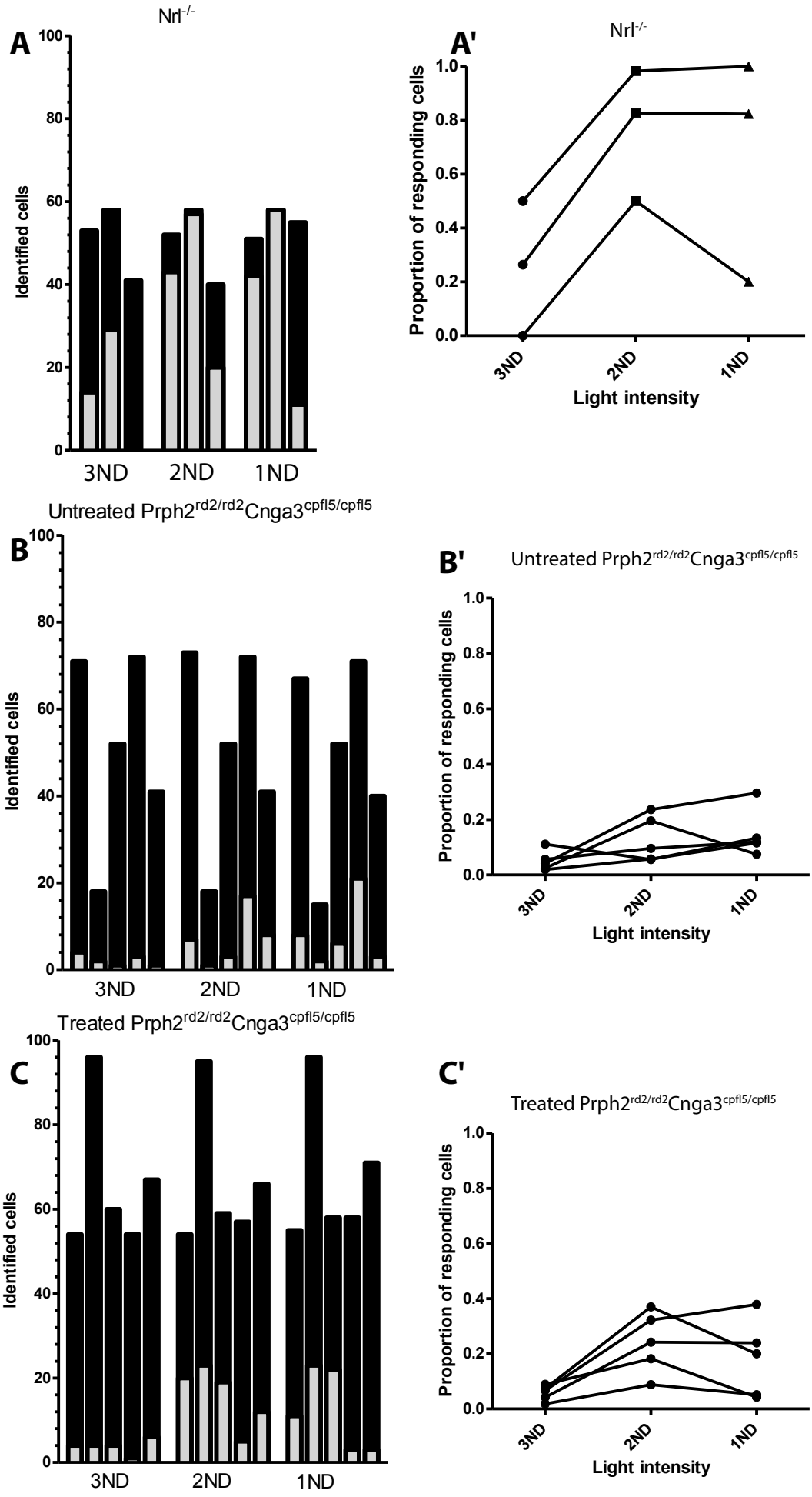
A
Nrl-/-
Identified cells
100
80
60
40
20
0
3ND
2ND
1ND
A'
Nrl-/-
Proportion of responding cells
1.0
0.8
0.6
0.4
0.2
0.0
3ND
2ND
1ND
Light intensity
B
Untreated Prph2rd2/rd2Cnga3cpfl5/cpfl5
Identified cells
100
80
60
40
20
0
3ND
2ND
1ND
B'
Untreated Prph2rd2/rd2Cnga3cpfl5/cpfl5
Proportion of responding cells
1.0
0.8
0.6
0.4
0.2
0.0
3ND
2ND
1ND
Light intensity
C
Treated Prph2rd2/rd2Cnga3cpfl5/cpfl5
Identified cells
100
80
60
40
20
0
3ND
2ND
1ND
C'
Treated Prph2rd2/rd2Cnga3cpfl5/cpfl5
Proportion of responding cells
1.0
0.8
0.6
0.4
0.2
0.0
3ND
2ND
1ND
Light intensity

Figure 6.6 The effect of light intensity on response. LED light at 420nm was used at 3 intensities, governed by neutral density filters such that light intensity at 3ND is one log below that at 2ND, and 1ND is one log above 2ND.

A-C Identified cells in each retina by wavelength of light stimulation, showing cells classified as responding (grey) and not responding to light (black).

A'-C' The proportion of total cells identified which respond to light (proportions from the same retinas are connected).

In $Nrl^{-/-}$ retinas, the number of responding cells increases substantially in all retinas between 3ND and 2ND, but is approximately maintained at this level at 1ND, except for one retina in which response falls,

Similarly, in both treated and untreated $Prph2^{rd2/rd2}Cnga3^{cpfl5/cpfl5}$ retinas, the number of responding cells is approximately constant between 2ND and 1ND, with a minority of retinas showing a reduction in responding cells.

At lower light intensities, the numbers of responding cells are lower in all treated and four out of five untreated retinas, and the numbers are similar to those seen at 8ND, the lowest intensity applied (Figure 6.4). While some cells were found showing clear responses, these cells were found in both treated (D) and untreated retinas (E).

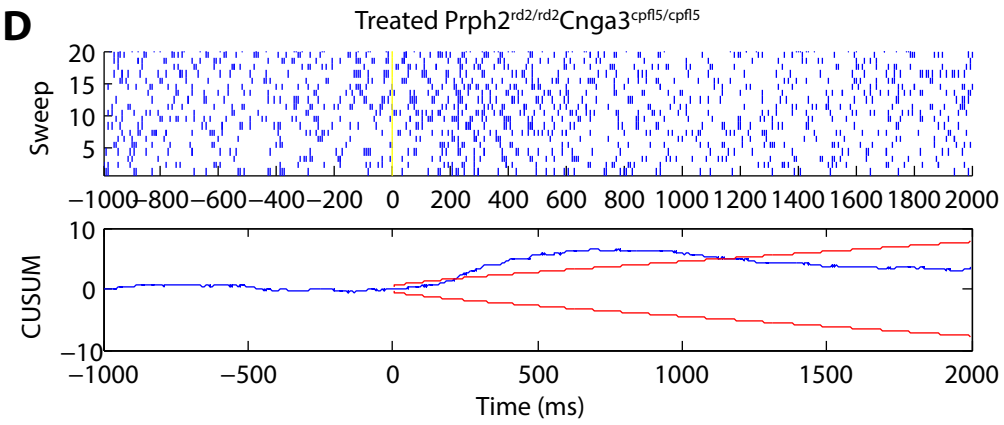
D
Treated Prph2rd2/rd2Cnga3cpfl5/cpfl5
Sweep
20
15
10
5
−1000 −800 −600 −400 −200 0 200 400 600 800 1000 1200 1400 1600 1800 2000
CUSUM
10
0
−10
−1000 −500 0 500 1000 1500 2000
Time (ms)

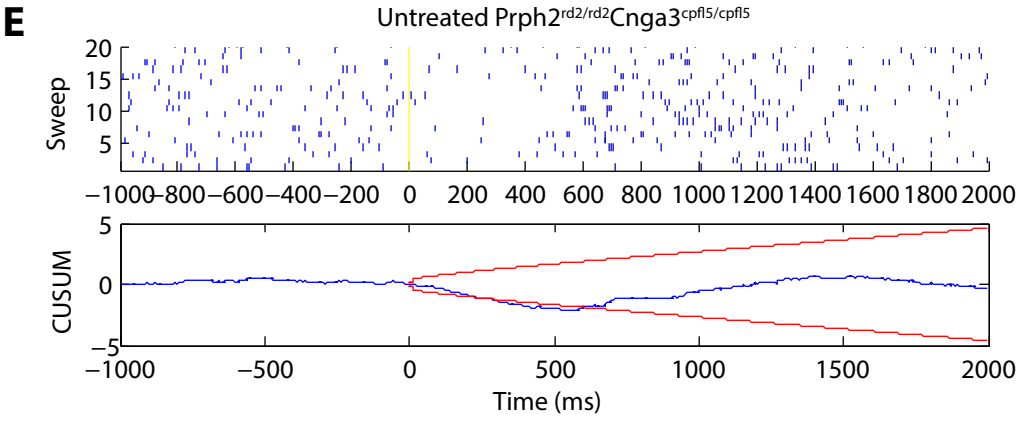
E
Untreated Prph2rd2/rd2Cnga3cpfl5/cpfl5
Sweep
20
15
10
5
−1000 −800 −600 −400 −200 0 200 400 600 800 1000 1200 1400 1600 1800 2000
CUSUM
5
0
−5
−1000 −500 0 500 1000 1500 2000
Time (ms)

6.3 Discussion

In this chapter, I looked at the effect of injecting $Nrl^{-/-}$ cone-like cells on the functional capacity of the degenerating retinas of $Prph2^{rd2/rd2}Cnga3^{cpfl5/cpfl5}$ double mutant mice. I used a multi-electrode array system to record from RGCs subjected to light exposure under a range of light levels and wavelengths. While robust responses could be found in control $Nrl^{-/-}$ retinas, responses from uninjected $Prph2^{rd2/rd2}Cnga3^{cpfl5/cpfl5}$ retinas were weak and delayed.

While there was a trend for an increase in the number of RGCs responding to light in treated $Prph2^{rd2/rd2}Cnga3^{cpfl5/cpfl5}$ retinas, it is not possible to conclude with certainty that this was due to the transplants per se. As untreated $Prph2^{rd2/rd2}Cnga3^{cpfl5/cpfl5}$ retinas exhibited a variable degree of residual response, with some showing proportions of responding cells at around 20% or more, it remains possible that the levels of response seen in treated retinas represents only variation in the ability of the MEA techniques to detect function in these retinas.

Changing the wavelength of the stimulus flash showed no clear effect on the cells either in treated or untreated $Prph2^{rd2/rd2}Cnga3^{cpfl5/cpfl5}$ retinas, either in terms of absolute numbers of responding cells, or in the apparent strength of those responses. Likewise, treated retinas do not show onset of response at lower intensities than untreated retinas, nor were they seen to improve response levels at higher light intensities. The lack of an effect of this kind indicates that if cells are affected by cell injections, they do not behave more similarly to the cone-like $Nrl^{-/-}$ cells that were injected.

These results contrast with those of a recent study (Santos-Ferreira et al., 2014) which also looked at the transplantation applications of $Nrl^{-/-}$ cells. In these

experiments, an MEA apparatus was also used to investigate the functional ability of cells transplanted in this way. The authors chose the cone-degenerating Pde6c$^{cpfl1/cpfl1}$ model as a recipient model without function at high light levels in order to detect the output of the transplanted cone-like cells. They found that response to high light levels was high, with 37% of recorded RGCs responding in these recipients, with no cells from uninjected retinas responding at these levels.

Given the low numbers of GFP+ cells found in the Pde6c$^{cpfl1/cpfl1}$ cone lacking or Cnga3$^{cpfl5/cpfl5}$ cone functionless models after transplantation in my experiments (means of 149 and 355 cells respectively, see section 5.2.3), it was decided for my experiments that it would be unlikely to expect many of the recording electrodes to be in close proximity to RGC cells receiving input from GFP+ cells.

In my results, however, it is not clear that the function of the transplanted cells, if present at all, is similar to that of cone or cone-like photoreceptors. A clear effect of stimulus wavelength similar to that of the Nrl$^{-/-}$ control retinas was not seen in experimental retinas that had received transplanted cells, nor in the uninjected Prph2$^{rd2/rd2}$Cnga3$^{cpfl5/cpfl5}$ double mutant mice.

This could be due to a number of factors. The residual function in untreated Prph2$^{rd2/rd2}$Cnga3$^{cpfl5/cpfl5}$ double mutants must occur from rod photoreceptors responding at abnormally high light levels, as shown in my ERG recordings. The spectral sensitivity of rhodopsin peaks at around 500nm, although it also displays sensitivity in the UV range (Wang et al., 2011). Although it is not clear to what extent the environment of the Prph2$^{rd2/rd2}$ retina might change this, it is likely that the responses seen in the untreated and, at least to some degree, the treated retinas are the result of residual rod-mediated activity.

If improvement in function were to be caused by cell transplantation, the mechanism by which this occurs would have to explain these observations. In Chapter 5, I concluded that the observations of GFP+ cells in recipient retinas after photoreceptor precursor transplantation are due in the majority not to the migration and integration of whole injected cells but to the transfer of material from injected cells to existing recipient cells.

While it is possible that any improvements in light sensitivity found after cell injection result only from the minority of cells that truly migrate into the retina, it is much more likely that material transferred from the injected cells to those of the recipient would account for any effect on function.

It might be expected that with gross transfer of some or all of the contents of injected cells to those in the recipient retina, as seen in rod-to-rod material transfer (Pearson et al. 2016, in press), that some of the defects preventing recipient cells from responding to light might be altered. For instance, the Cnga3 protein missing in the double mutant model might be replaced, completing the phototransduction cascade chain in recipient cone photoreceptors, which might express S-opsin, M-opsin or both. Alternatively (or additionally), a combination of rod and cone proteins in recipient rod photoreceptors as a result of material transfer might allow rhodopsin-based mechanisms of phototransduction, or the Prph2 present in injected cells could transfer to recipient cells, which could use it to allow the production of photopigment discs, thus improving the ability of these cells to respond to light.

6.3.1 Future possibilities

A likely explanation for the inconclusive results of my experiments is the extreme difficulty inherent in trying to determine an increase in function over a non-zero and variable baseline. An alternative to the methods used here would be to use a

different model with no residual function, but which also allows for a high number of GFP+ cells in the recipient ONL to be found after transplantation. While this was the initial aim of using the Prph2$^{rd2/rd2}$ model, unexpected abnormal residual rod response was found in this model, even after the introduction of the cpfl5 mutation.

The Nrl$^{-/-}$ model may represent an alternative model in which to assess function after transplantation of cones. As shown in Chapter 5, it supports robust transplantation outcomes, similar to the Prph2$^{rd2/rd2}$ model and much higher than the WT or any of the other types of degenerative retina studied. As it shows very high levels of cone function, but no rod function, the introduction of the cpfl5 mutation would be expected to remove all photoreceptor-mediated light responses from this model. Despite the early stage of cone loss which the Nrl$^{-/-}$ retina undergoes (Roger et al., 2012), this model would also have the advantage of increased stability over time, compared to the progressive degeneration of the Prph2$^{rd2/rd2}$ mouse. This would allow injection of mice at a later stage, and/or a longer post-transplantational window after which recordings could be taken, to allow for the maximum effect of transplantation.

It is not known, however, whether a cross between these models would in fact be suitable; just as in the case with the model used in these experiments, the results of combining mutant strains can be unpredictable. For example, the Cnga3$^{cpfl5/cpfl5}$ model exhibits delayed cone migration and subsequent mislocalisation of adult cones (Michalakis et al., 2005). The migration of the cone-like cells of the Nrl$^{-/-}$ model is not well understood, but interference with this process in all photoreceptors rather than the relatively very few cones affected in the Cnga3$^{cpfl5/cpfl5}$ model might have a particularly disruptive effect. Also, if a measure of redundancy exists in the phototransduction cascade which allows photoreceptors to bypass the use of

Cnga3, even at very low efficiency, the cumulative effect of an entire retina of cone-like cells might be enough to mask the response of any injected cells.

The MEA is a powerful tool to investigate the response of RGCs, and in an experimental paradigm allowing clear identification of responses occurring as a result of transplantation would be likely to enable investigation of how the retinal circuitry is affected by cell therapy. The experiments presented here, however, demonstrate that it too has limitations associated with variability and large data sets are thus required to make definitive conclusions.

Chapter 7 – Migration of cone precursor cells during development

7.1 Introduction

The development of neural tissue, such as the retina, involves the generation of several classes of cells with different specific functions, the forming of connections between these cells for the reception and processing of information, and the arrangement of these cells into an ordered tissue. Much research has been done into each of these aspects, with emphasis on the different behaviour of cells in different neural tissues. This chapter will address the migratory behaviour of the cone photoreceptors, which are the focus of this thesis.

In the area of cell therapy, an understanding of the developmental process in the tissue to be treated is crucial. Chapters 3 to 6 examined the outcomes seen after cone and cone-like cells were transplanted into recipient retina. This study, and previous work by this group and others, has shown that the developmental stage of the cells injected is critically important to the success of transplantation.

Initially, it was proposed that transplanted cells integrated by migration into recipient retina and matured to take up the position of adult photoreceptors in the ONL. This prompted a need for greater understanding of the motility of these cells in normal development. Indeed, work by others in the lab (Aghaizu N., PhD thesis, submitted) has demonstrated that rod photoreceptors undergo a period of migration immediately post terminal mitosis and can also be observed migrating into the host retina using real-time imaging of explants of transplanted retinas. It is not yet clear if they undergo a migratory process analogous to that shown in developmental tissue.

Moreover, as detailed in Chapters 4 and 5, recent evidence also indicates that this migration of donor cells accounts for only a small proportion of the reporter labelled cells we see in the host retina after transplantation. In the majority, material such as GFP (RNA and/or protein) is transferred from the injected cells to the photoreceptors that already exist in the recipient retina.

Regardless of the recent changes in our understanding of the mechanism underlying transplantation outcome, an understanding of the migratory process still informs other aspects of development. An example of this shown by the behaviour of neural progenitor cells during neurogenesis. In many neural tissue types, including the retina, a characteristic proliferative process of cell division and migration is undertaken. During this process, M-phase, where new cells are generated by at the apical edge of the developing tissue, the so-called ventricular zone (VZ), but progenitor cells can be found at positions basal to this during the other phases of the cell cycle (S-phase and G1-phase) (Sauer, 1935). They migrate through the tissue in a process called interkinetic nuclear migration (INM). During INM, cells are attached by processes to both limits of the developing tissue, and the motion shown appears to involve two distinct types of movement: a slow, stochastic movement in the basal direction, and a more rapid, directed apical movement triggered by progression through G2 phase (Leung et al., 2012; Norden et al., 2009). The function of INM is not agreed on, but there is growing evidence that it allows the exposure of progenitor cells to polarised signalling mechanisms and extrinsic cues which affect their subsequent behaviour and mediate differentiation (Baye and Link, 2008; Strzyz et al., 2015).

Migration after terminal mitosis is also evident in many cell types in the CNS, particularly in ordered, layered tissues, such as the cortex or the retina. Neurons, in particular, often need to take up a specific position in the tissue, depending on their

subtype. To produce the specialised light-sensitive tissue in the retina, for example, RGCs must migrate basally, away from the VZ, through the entire depth of the developing retina to the presumptive GCL, at the vitreal side of the retina, while bipolar, horizontal and amacrine cells must migrate to form the INL between the RGCs and the photoreceptors. The process of axon growth and synapse creation also involves the navigation of a cell through developing tissue. A number of mechanisms of neuronal migration happen in tandem with the production of an axon.

Photoreceptor migration

Cone photoreceptors are generated, as are the majority of retinal cells, in the VZ, at the apical margin of the immature retina, closest to the presumptive RPE. In adult retina, they are located in the equivalent area: the apical edge of the ONL, closest to the OLM and RPE. As a result, they do not obviously have to migrate to take up their adult position. A migratory phase of cone photoreceptor precursors has nevertheless been inferred from images of fixed tissue, in previous studies. During postnatal development, cone precursors are found dispersed through the depth of the developing ONL (Rich et al., 1997). These cells are also seen to adopt a spindle-shaped morphology characteristic of a moving cell body (Rakic, 1972; Zolessi et al., 2006). Cones have also been shown to undergo lateral migration a process most likely associated with their mosaic distribution: they can be seen located outside the column of clonally-related cells generated from a parent retinal progenitor cell (Reese et al., 1995).

Previous work carried out by the group using fixed retinal sections has shown a similar bidirectional radial pattern of postmitotic somal migration by rod photoreceptors (Warre-Cornish, PhD thesis, 2013). In addition, this work developed

time-lapse imaging techniques to examine the movement of rod precursors in explanted flat mounted NrlGFP murine retinas. The use of fixed tissue reveals little about the specifics of migration but did reveal a developmentally-related displacement of immature rods to positions basal to the VZ, which was later resolved as the retina matured. Real time imaging of live tissue approaches of the type developed are more powerful techniques for observing the migratory process in the nervous system, allowing for visualisation of the movement of cells *in vitro* as cell cultures, often in co-culture with glial cells or alternatively in slice preparations of neural tissue (Nadarajah and Parnavelas, 2002). In some organisms, such as zebrafish, live imaging can be carried out in sufficient detail *in vivo* due to the small size and relative transparency of these organisms (Zolessi et al., 2006). In murine retina, rod movements were displayed in real time (Warre-Cornish, PhD thesis, 2013).

Time lapse multiphoton imaging

The inevitable disruptions to tissue integrity and changes to the cellular environment that occur as a result of cultures and slices create uncertainty in the observations made using these methods. It is therefore desirable to maintain the tissue under observation in as similar a state to *in vivo* conditions as possible, which would also be likely to extend the duration of time over which the cells and their normal behaviour can be observed. With retinal tissue, an *ex vivo* whole flat mounted retina is likely to be the closest practical equivalent to the *in vivo* condition.

With the radial migration of cone photoreceptors occurring perpendicular to the surface presented by a flat mounted retina, this would require measuring the position of cell bodies by their depth in the tissue, which for the developing murine

ONL is approximately 50 μm. This is in contrast to using cell culture or a retinal slice where the position of cell bodies is in the imaging plane.

While confocal microscopy allows resolution of depth information by the exclusion of light from out-of-focus areas, it is limited by the depth to which the excitatory light wavelengths used can penetrate into tissue. Moreover, since with confocal microscopy the whole depth of the sample must be illuminated regardless of the plane to be imaged, the tissue is repeatedly exposed to very high levels of light for a long duration, which can cause rapid bleaching of labelling fluorophores and phototoxicity damage.

The technique of multiphoton imaging represents a partial solution to this problem. This approach excites the target fluorophore only at the plane to be imaged, by using photons of a multiple of the excitatory wavelength for that fluorophore. These photons are focussed at the plane to be imaged and only there do they reach a sufficient density to allow simultaneous absorption of multiple photons by a single fluorophore, thereby causing excitement. For example, to image a cell expressing eGFP (which has an excitatory peak of 420nm), a pulse laser of 840nm would be used. Two photons of 840nm would be sufficient to excite an eGFP molecule. This allows more frequent illumination without exposing the whole of the tissue to an excitatory wavelength, and additionally allows imaging at a greater depth into tissue, due to the reduced scattering of longer wavelength photons (Diaspro et al., 2005).

With the use of these techniques, the pattern of migration shown by rod precursors was assessed. At P0-1, the rod cells showed relatively slow movement with no obvious direction for most cells but with an average displacement in the basal direction away from the VZ, but with occasional periods of fast apical movement,

similar to the motion seen in INM, despite being shown by a postmitotic cell (Warre-Cornish, PhD thesis, 2013; Aghaizu N, PhD thesis, submitted).

In this chapter, initial results of looking at the migration of developing cone photoreceptors through live, time-lapse imaging will be shown and discussed.

7.2 Results

7.2.1 Evidence from fixed tissue

Images of fixed tissue (Figure 7.1, see also Chapter 3, Figure 3.2) taken from the transgenic cone reporter line Chrnb4.eGFP at developmental stages P0, 2, 3, 4, 6, 8, 10 and 12 confirm the immunohistochemical observations of (Rich et al., 1997), showing again that these cells originate in the VZ and are displaced from there between P2 and P12, before again taking up positions at the apical boundary of the ONL in adulthood. Additionally, by P3 and P4, processes could be seen from almost all cone photoreceptors spanning the entirety of the developing ONL, with basal processes terminating in a line suggesting the limits of the presumptive ONL. This was the case even before cone migration has begun, that is, while cell bodies are still located close to the VZ (P3). Similarly, at all later stages examined, processes were seen connecting the cell body of all cone precursors with the boundaries of the ONL. The presence of bipolar processes is similar to that described for neuronal cells undergoing somal translocation (see section 1.6.2.2), although with this method of migration the trailing process is generally retracted as the cell moves, rather than being maintained as is the case for cones. Additionally, this morphology is similar to that of neural or retinal progenitor cells undergoing INM (Del Bene et al., 2008).

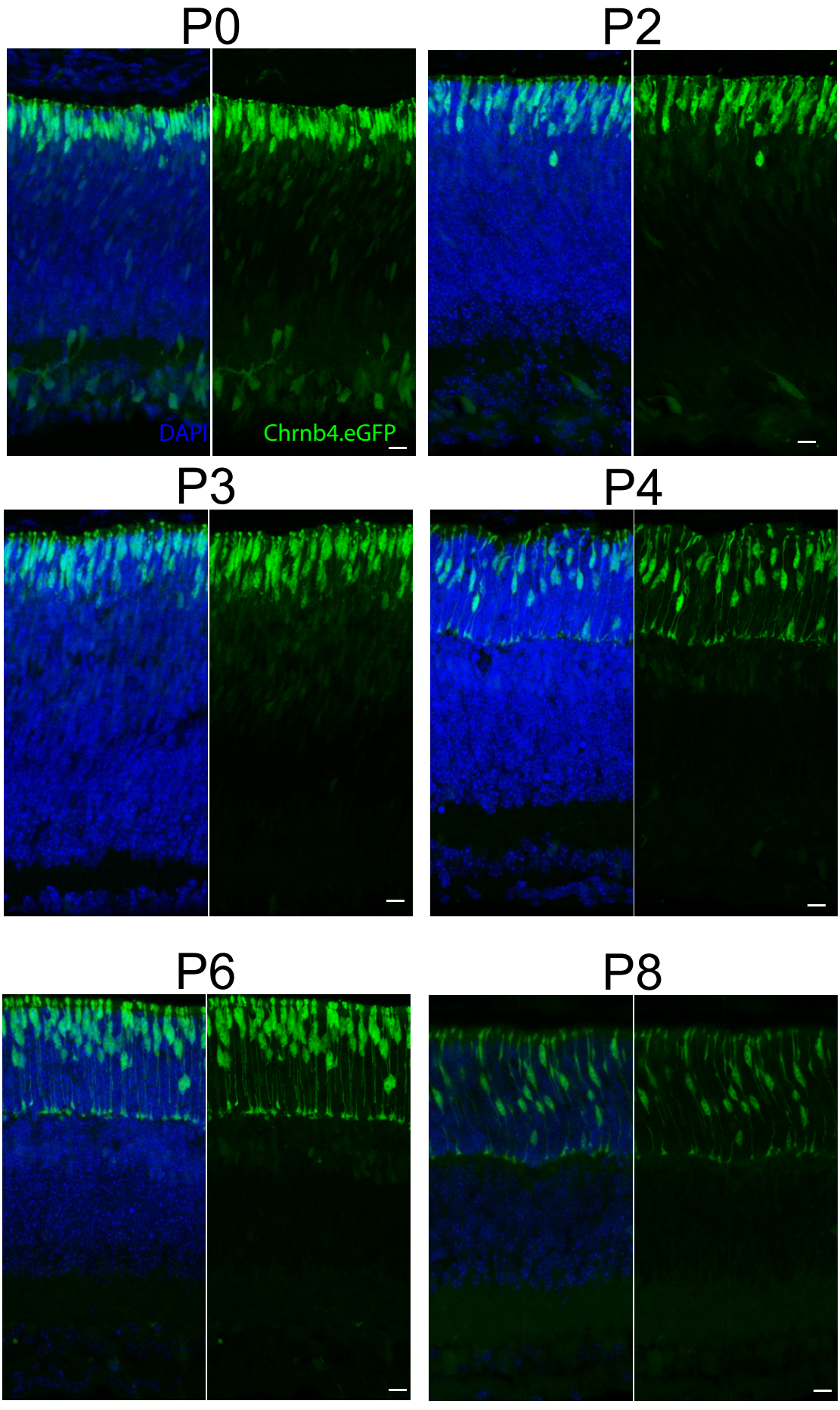
P0
P2
DAPI
Chrnb4.eGFP
P3
P4
P6
P8

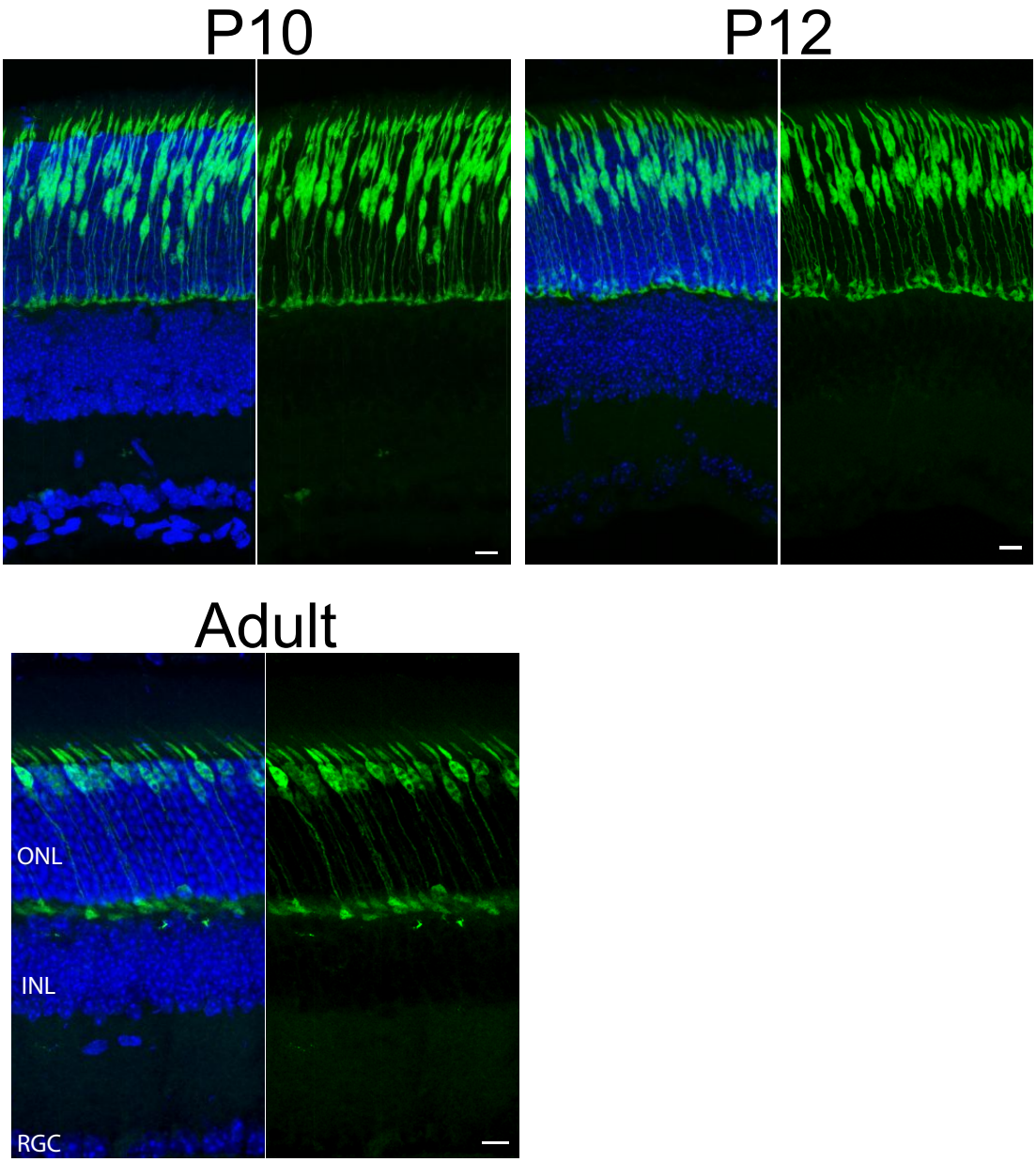

Figure 7.1 Evidence for cone migration in the Chrnb4.eGFP mouse.

z-stacks of confocal images taken from fixed retinal tissue of mice during the early postnatal period. Scale bars are 10µm. Before P3, the cone precursors (brightly GFP-expressing cells) are located at the apical surface of the neural retina. At and after P4, apical and basal processes spanning the entirety of the developing ONL can be seen, when the division between ONL and INL begins to become clear. Between P4 and P12, the cell bodies of the cone precursors can be seen to be displaced basally from the apical surface, but in adult tissue these cells are once again located here, against the OLM, indicating a period of bidirectional migration.

7.2.2 Live imaging of flat mounted *ex vivo* Chrnb4.eGFP retinas

To address the shortcomings of the study of fixed tissue, live imaging of *ex vivo* flat mounted retinas was used to give a clearer idea of the characteristics of the movement of individual cells. In Chapter 3, I showed that the Chrnb4 clearly labels cone precursors at early postnatal periods, and this model represented a suitable option for visualising live cones. For the survival of the tissue, and to provide conditions as close to those found *in vivo* as possible, imaging took place in a gas-controlled, heated environment.

NB For this section, additional material, primarily time-lapse films of migrating cells, can be found on the submitted CD-ROM. While not essential to the understanding of these results, this material is likely to give a better idea of the observations discussed below. Files are referred to as Supplementary Movie 1, 2, 3 etc.

7.2.2.1 Data collection and processing

P5/6 Chrnb4.eGFP retinas were used for imaging. This age, approximately halfway through the period of cone migration, was likely to provide an environment where the majority of the cells would be of the correct age to migrate, but where the process would be neither just beginning nor just ending. It also provided a compromise between the earlier ages where migration would not occur, and later ages where tissue survival in culture would be reduced.

P5/6 retinas were dissected and flat mounted with the photoreceptor layer upward on filter paper as described in section 2.5, with DMSO included in the imaging medium at a concentration of 1µl per 1ml imaging medium as a control for future pharmacological experiments (see below). Imaging was carried out overnight, at 37ºC and with 95% O_2, 5% CO_2, using a two-photon fluorescent microscope, and

using 840nm light to excite GFP. Every 10 minutes, a vertical stack of images was taken, separated by 1µm steps, from approximately 50µm below to 50µm above where GFP signal could be seen (for a total stack depth of between 150 and 200µm), to avoid losing the tissue through drift. Figures 2.3 and 2.4 show examples of the images generated in this way. The video files Supplementary Movie 1 and Supplementary Movie 2 show examples of the image stacks taken. Images were corrected for tissue drift.

Only successful imaging periods were taken forward for quantitative analysis. On some occasions, due to equipment failure or tissue drifting out of the imaging stack, most likely due to detachment from the filter paper, imaging was not successful for the whole period. On other occasions, tissue death occurred, with visible atrophy of cell bodies and a disruption of tissue. For example, imaging had to take place away from residual areas of RPE; the 840 nm infrared wavelength used for the laser is very strongly absorbed by the pigments in RPE cells, and when not removed, even small amounts can heat up the surrounding tissue, causing cell death and the disruption of tissue shape and integrity. An example of this happening can be seen on file Supplementary Movie 3.

Three sessions were successfully recorded from three separate retinas, with imaging times of 10h30, 11h and 11h40. As a control, P14 retina (N=1 retina) was used as a time point when cone migration would be expected to have ceased on the basis of the histological assessments shown in 7.2.1. In this tissue (see Supplementary Movie 4), GFP+ cells were observed to be located, and remain, at the apical surface of the retina, and did not move during the imaging period (approximately 4 hours 20 minutes).

To provide a quantitative assessment of the trajectory of these cells, cell tracking software (IMARIS) was used to measure the coordinates of the cells over time (see section 2.5). The z-coordinate (perpendicular to the imaging plane) was selected as representing the apico-basal axis. For each imaging session analysed, at least 100 cells identified and tracked by the software were assessed. Trajectories were individually verified to ensure that they represented only the cell body of a single precursor and corrected where necessary. Cells selected by the software were tracked for as much of the total imaging session as was possible. The trajectories of a total of 341 cells were generated in this way. The positions of the cells were recorded as μm relative to the most apical cell position recorded in each separate imaging session, which was held to indicate the apical limit. Comparing this position to the most basal position of a cell seen gave a total ONL thickness of between 61 and 71μm, depending on the imaging session.

7.2.2.2 Overview of migration

Figure 7.2 shows montage images of retinas imaged in this way, recalculated to show the xyz stack in xz view. Representative movies of cone migration are shown in Supplementary Movie 5. Note that the cells seen in these images are not necessarily represented in those measured with later *in silico* tracking, although they do form part of the complete data set.

Cells could be easily observed moving both apically and basally, with no obvious tendency for lateral motion. There was a notable visible difference in the nature of motion in these different directions, with examples of the types of motion found in these cells shown in Figure 7.3. Basal motion occurred relatively slowly, and rather than smooth gradual movement, displacement in this direction appeared to take place in a stochastic manner, with the overall basal displacement only seen when taken as an average over several time points. For several of the intermediate

images, cells did not appear to move at all, or even occasionally moved a small distance apically. By contrast, movements in the apical direction were rapid, with large changes in cell position detected between the 10 minute imaging intervals. Indeed, occasional cells were observed moving close to the full depth of the ONL in a single interval.

Intriguingly, several cells were observed displaying both types of movement at different points throughout the imaging session (Figure 7.3C, Figure 7.4B). Importantly, a small number of cells were found that returned to basally-directed movement after moving apically (Supplementary Movie 6). Together, these indicate that the majority of cone precursors did not migrate basally and then return apically just once, but instead cycled repeatedly between a basal and apical position.

Some basally moving cells were seen to progress beyond the boundary marked by the processes of other cones, into the putative OPL, where they appeared to remain stationary (Figure 7.3D, Supplementary Movie 7). Due to their clear GFP signal, these cells were held to be most likely cone precursors (see Chapter 3). Cone cells have been seen to be mislocalised in the OPL and even INL in mutant mouse models such as the Cnga3$^{cpfl5/cpfl5}$ model and those deficient in SUN- and KASH-domain containing proteins (Razafsky et al., 2012). Due to the relatively short period for which imaging could be carried out, it was not clear whether these cells eventually returned to the ONL. It is possible that in WT retina, cells which mislocalised in this way are removed by apoptosis, if they do not return to the ONL, or alternatively it is plausible that the disruption to the tissue caused by preparation for these experiments causes these events when they would otherwise not occur.

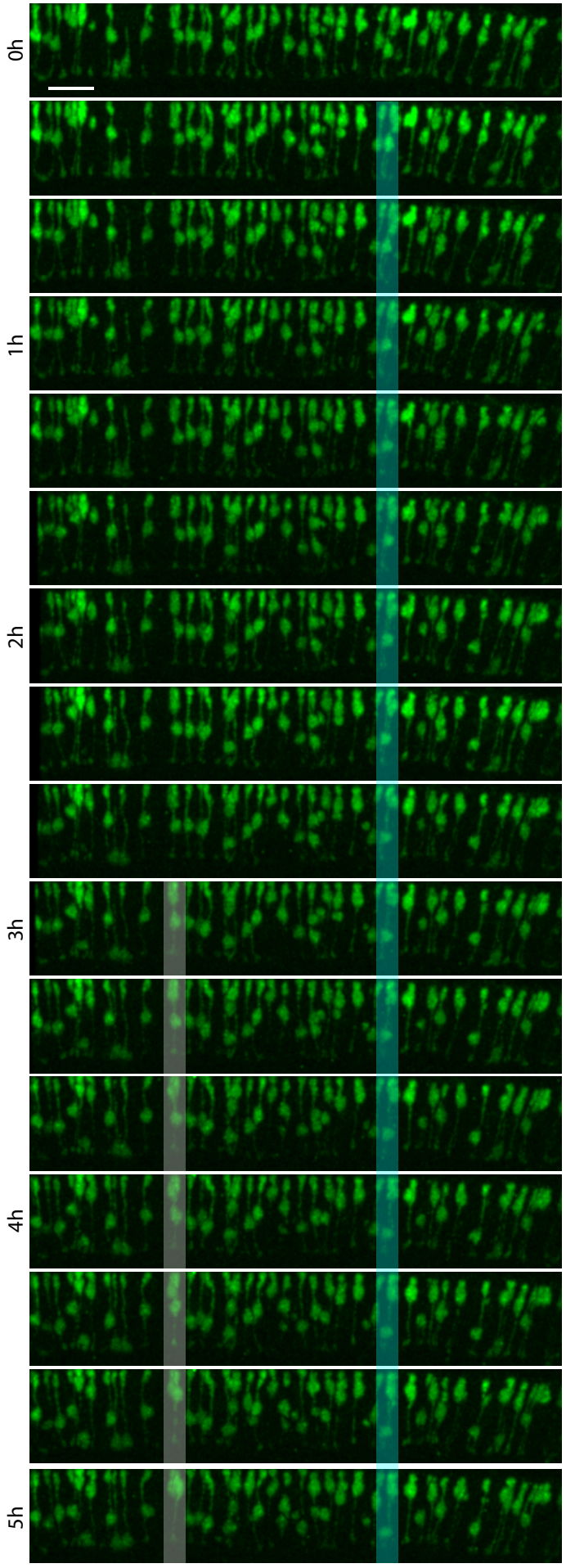

Figure 7.2 Montage images of a P5/6 Chrnb4.eGFP retina imaged every 10 minutes with a multiphoton microscope. This montage shows images taken 20 minutes apart. This image has been recalculated to simulate a side-on view, and shows a short section through the retina. Supplementary Video 5 shows the same view. Cells can be observed moving between consecutive time points, for example rapidly apically (grey boxes) and slowly basally (cyan boxes).

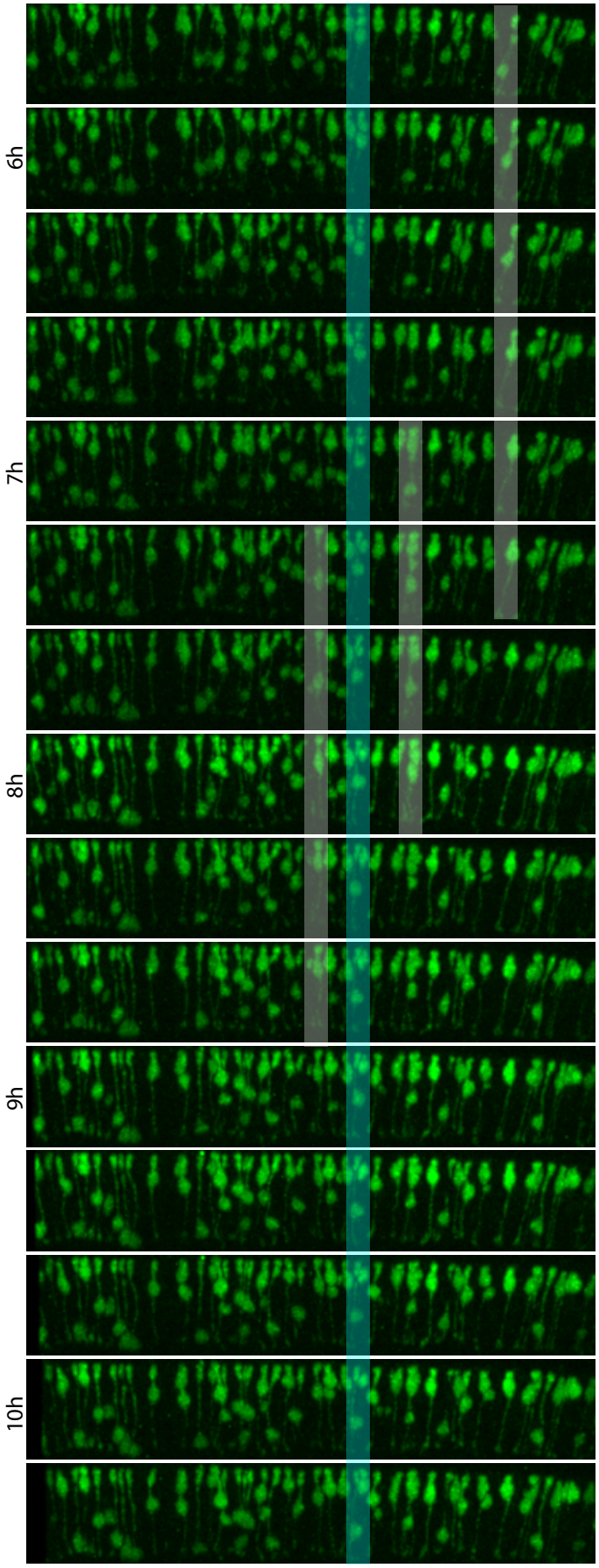
6h
7h
8h
9h
10h

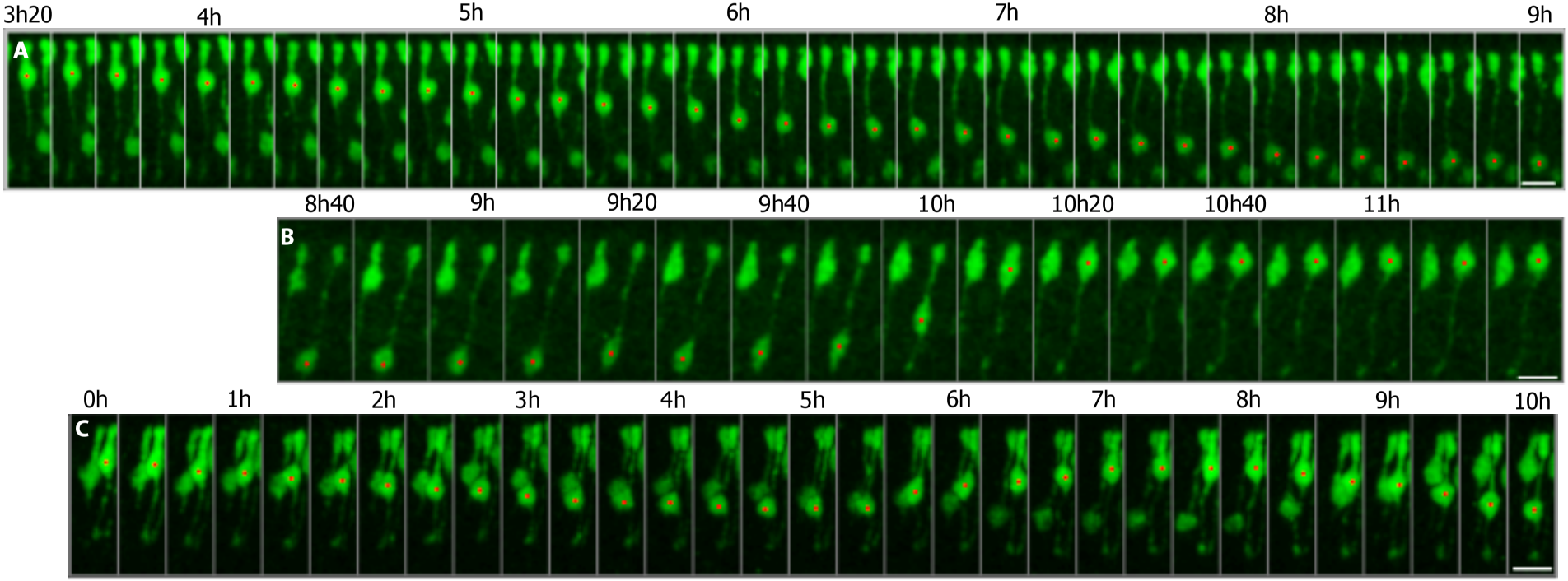

Figure 7.3 Live explanted flat-mounted retinae (postnatal day 6) were imaged using time-lapse multi-photon microscopy for periods of up to 12 hours. Many cells (marked with red dots) can be seen migrating slowly basally (A), and rapidly apically (B). Times are since the beginning of imaging, scale bars 10 µm. In contrast to previous assumptions, a significant proportion of cells are apparently undergoing multiple cycles of migration (C). The kinetics of this migration are similar to those described for interkinetic nuclear migration (IKNM) in cycling retinal and cortical progenitor cells.

A Slow basal movement of approximately 45µm over 300 minutes (frames 10 minutes apart).

B Fast apical movement of approximately 40µm over 20 minutes (frames 10 minutes apart).

C Basal movement followed by apical return and the subsequent resumption of basal movement (frames 20 minutes apart).

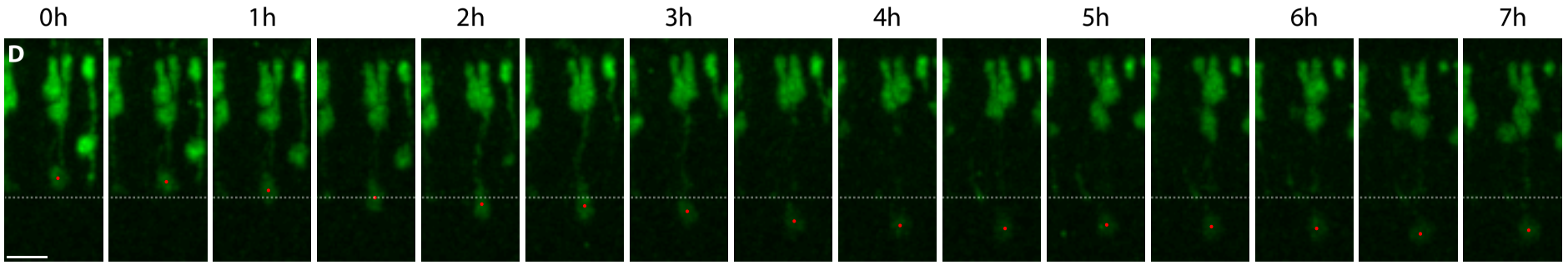

D Occasional cells were seen to move beyond the basal limit of the retina. Here, a cell (marked by red dots) moved beyond this limit (dashed line, approximated by the ends of the processes of neighbouring cells) and remained there throughout the imaging session (frames 30 minutes apart.)

Next, I sought to quantify the kinetics of cone cell migration. Figure 7.4A shows a kymograph of a cell tracked *in silico*, showing its position in the depth of the retina over time. A z coordinate value for each time point (black dots) could not always be found. For several of the following quantitative assessments, it was necessary to have a position value for each time and linear interpolation was used to generate a cell position for these gaps (red lines). In addition, to reduce the effect of fast fluctuations and variations in the location of the centre of the cell, a moving average filter was applied, with each position value replaced with the mean average of itself and the 2 values immediately before and after it (blue line), as illustrated in Figure 7.4A'. This did however mean the exclusion of positions at the very beginning and end of imaging sessions. (Thanks to Professor M Carandini for assistance with the computing necessary for these manipulations).

The trajectories of all cells were analysed for the presence of the different types of movement described qualitatively above, using filtered data to reduce the effects large fluctuations caused by tissue movement or inaccurate location of the centre of the cell. In addition, the criteria used were relatively strict, to avoid the inclusion of false positive traces. These movements are described in more detail below in sections 7.2.2.3 and 7.2.2.4 with a selection of trajectories shown in Figures 7.6A and 7.7A. Rapid apical movement was defined as a cell moving more than 10μm in the apical direction in 30 minutes, in keeping with similar work using rod photoreceptors, and approximating 1.5 cell lengths, which allowed unambiguous determination of movement. A total of 77 out of 341 analysed trajectories fit this definition (22.6%). A criterion for slow basal movement was set as 10μm movement in the basal direction over 12 time points, that is, 2 hours. 172 cells out of 341 (50.4%) were shown to meet this threshold.

A measurement of absolute displacement of all cells was carried out, as the difference between the first and last recorded position of each cell. On average, this was -11.7μm, indicating that on average, cells moved down in the time period. This measurement is imperfect, however, as rapid apical movements were relatively rare and would be more likely to be missed with the relatively short time of imaging, and would have a disproportionately small effect on this average. On the other hand, this does indicate that this migratory behaviour is likely to change over time, as without an increase in the proportion of apical movement, cells would all move to or beyond the basal limit of the tissue within a few days of a similar average displacement.

A total of 13 cells were judged by manual assessment to show evidence of more than one migratory cycle, either apical-basal-apical or basal-apical-basal movement, such as those shown in Figure 7.4B. Manual assessment was used for these cells due to the difficulty in classifying multiple similar, but discrete, periods of movement automatically, and the desire to avoid false-negative exclusions for either type of movement, as described in sections 7.2.2.3 and 7.2.2.4. Such exclusions are made more likely, as finding 3 separate motion periods within the achievable imaging period much reduced the number of effective time periods that could be analysed.

The proportion of cells, analysed in this way, which showed at least some form of the defined directed migration (slow basal or rapid apical) by the criteria defined above was 61.6% (210 cells out of 341 tracked). Since the imaging period comprised between 10 and 12 hours, a small fraction of the total period during development when cone migration occurs (P3 to P12 is approximately 216 hours) this indicates that it is very likely that most, if not all, cone precursor cells cells undergo cyclical migration, moving basally and returning apically multiple times during this period of development.

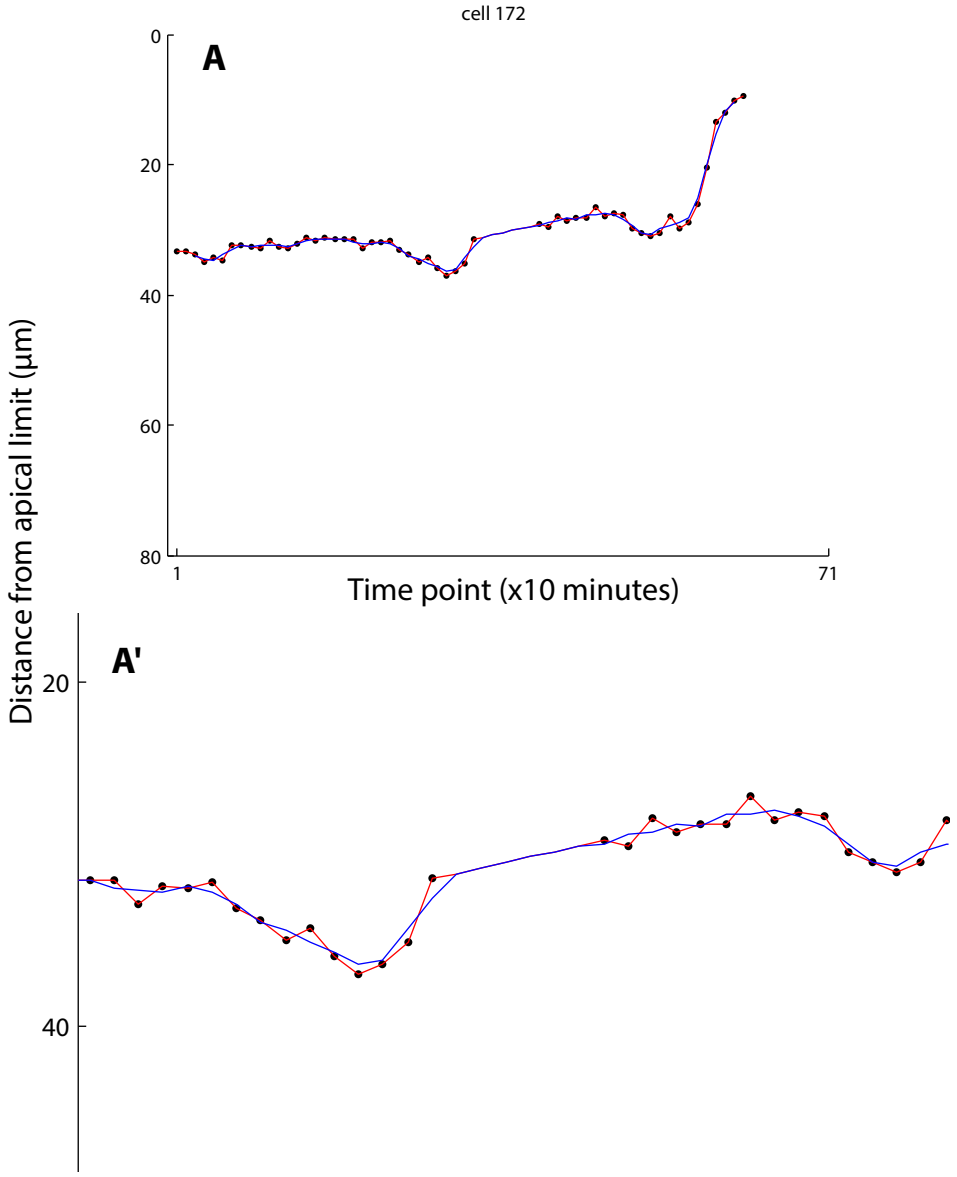

Figure 7.4 Cell trajectories. (NB for these and subsequent figures, cell numbers refer to the order in which they were assessed, with different imaging sessions providing cells 1-113, 114-240, and 241-341).

A An example of a kymograph of a cell, generated by tracking the position of cells *in silico.* The graph shows the distance of a cell from the apical limit over the 62 time points (10h20) that this cell was tracked. The z-position of a cell was taken to represent its position on the apico-basal axis (black dots). Missing values were generated by linear interpolation (red llines) and a moving linear average filter of 3 values (blue line) was used for some calculations to remove the effect of small fluctuations. A' shows an expanded view of one part of the trajectory.

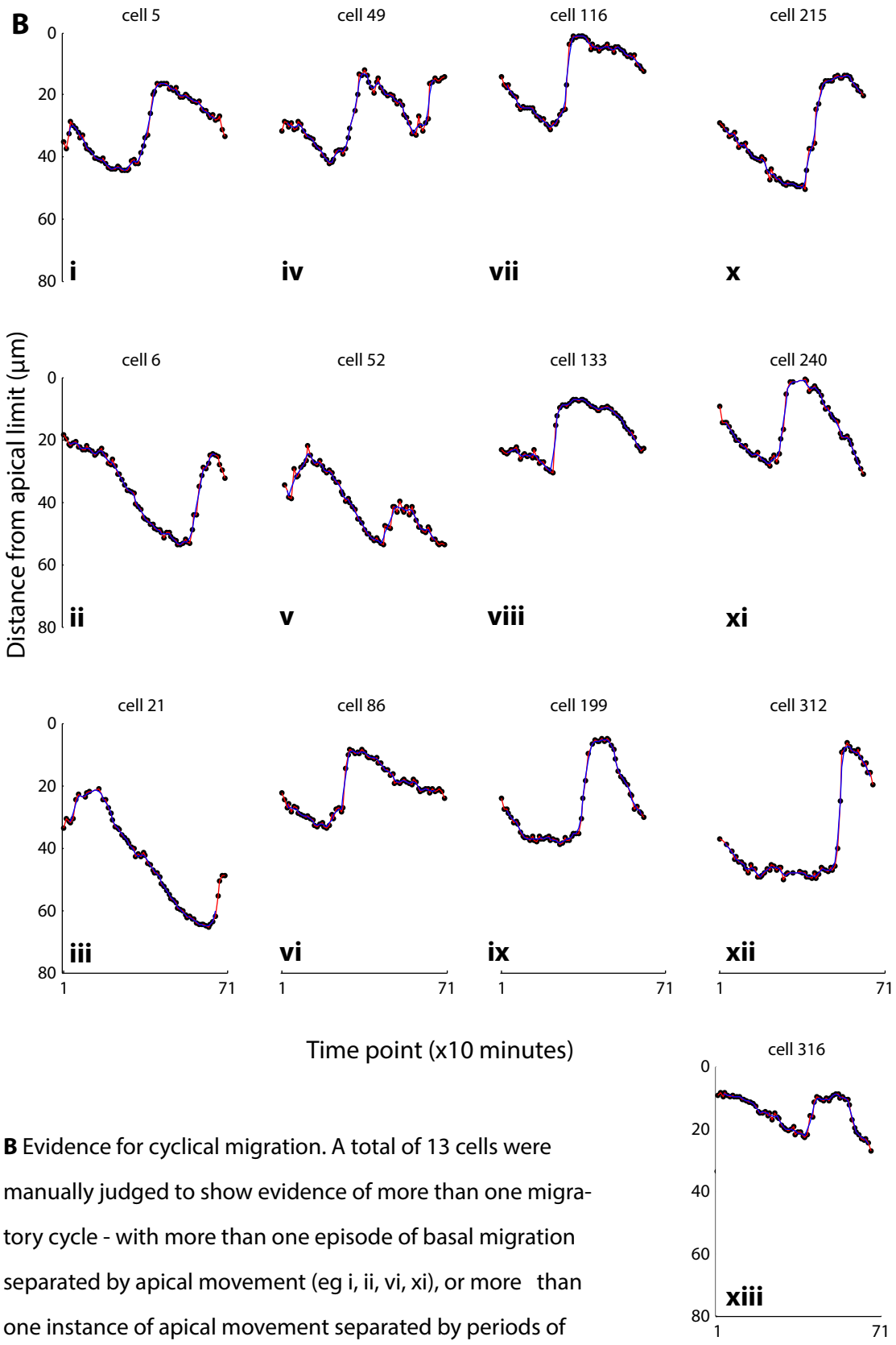

B Evidence for cyclical migration. A total of 13 cells were manually judged to show evidence of more than one migratory cycle - with more than one episode of basal migration separated by apical movement (eg i, ii, vi, xi), or more than one instance of apical movement separated by periods of basal movement (iii, iv, v). Some cells appear to lack a period of stationary behaviour (iii, iv, vi, xi) indicating that this may not be necessary for the progression of the migratory sequence.

Instantaneous velocity measurements were taken as the difference in a cell's z coordinate with that in the previous frame, to give μm moved in 10 minutes. Unfiltered data were used for these calculations, to allow the contribution of small random movements such as would be expected in a normal distribution, and to avoid artificial smoothing of central values. A histogram of these velocities (bins of 2μm) is shown in Figure 7.5A. The overwhelming majority of these 19292 recorded velocities are small, and approximately symmetrical around 0, with the average value -0.2μm. A small percentage of movements are larger (greater than 5 μm in 10 minutes), and particularly in the apical direction a very small number of very large velocities (between 10 and 45 μm in 10 minutes) are seen.

Plotting the values of the instantaneous velocities on an inverse normal graph showed the deviation from normality. This graph compares each velocity value found in my data with its equivalent value taken from a perfect normal distribution generated with the same mean and standard deviation. Section 2.5.2 describes the calculation of this measurement.

Figure 7.5B shows the inverse normal plots for the instantaneous velocities of these data. The straight line y=x shows conformity with the normal distribution, and deviation from it indicates a disparity. In the data shown, such deviations can be seen at the extremes, with positive displacement from the line on the right hand side indicating larger apical velocities than would be predicted by the normal distribution, and on the left hand side negative deflections indicating larger basal movements than predicted, although these latter changes were less marked.

The Mean squared displacement (MSD) gives a measure of cell body displacement over time, and can be used to ascertain whether motion is directed or random (see Section 2.5.2 and Huet et al. 2006) based on the gradient given when positions

further apart in time are compared. A linear relationship indicates that motion is random and unconstrained, while a negative curvature shows that movement is subject to constraints, and a positive curvature that movement is directed (Huet et al., 2006; Norden et al., 2009). Figure 7.5C shows the MSD for all cells analysed in these retinas, with the values for all cells averaged. Only the first 15 values are shown as this measurement quickly becomes less reliable as the lag between compared positions increases.

The extra sum-of squares F test was used to compare the goodness of fit of a straight-line against a second order quadratic equation with a positive curvature. The quadratic curve (described by $y= 0.00152x^2 + 0.375x – 2.2$) fit significantly better with the data: $F(1,5059) = 11.13$, $p=0.0009$, with the r^2 value = 0.1987 than did the linear fit. This shows that there is likely to be a directed aspect to the migration shown by these cells. However, since the vast majority of movements made within the imaging intervals are small, fit with a normal distribution and are symmetrical around 0, these directed movements have a comparatively small effect on this measurement, as evidenced by the small positive curvature.

To summarise, these measurements show that the distribution of velocities observed in the immature cone cells are not consistent with random, normally distributed motion, and that among the large amounts of small, stochastic motion, there are events that are directed movements which act to drive cone migration.

Next, I will examine the different types of motion seen separately, and in more detail.

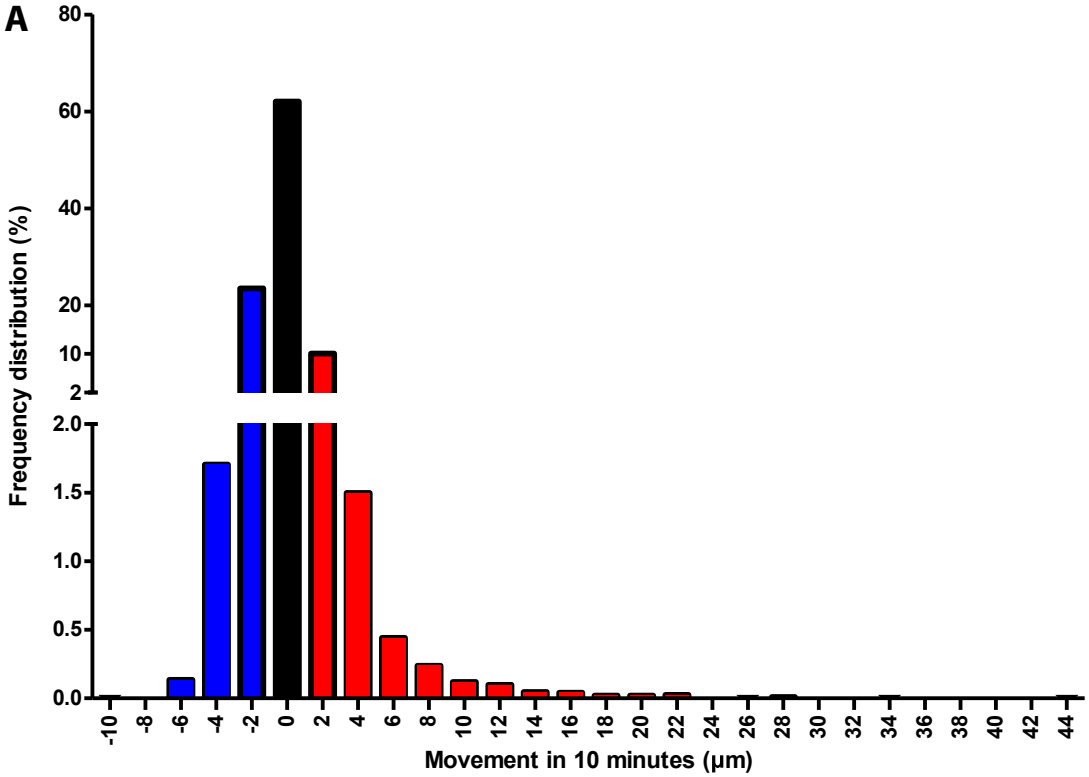
A
Frequency distribution (%)
80
60
40
20
10
2
2.0
1.5
1.0
0.5
0.0
-10 -8 -6 -4 -2 0 2 4 6 8 10 12 14 16 18 20 22 24 26 28 30 32 34 36 38 40 42 44
Movement in 10 minutes (µm)

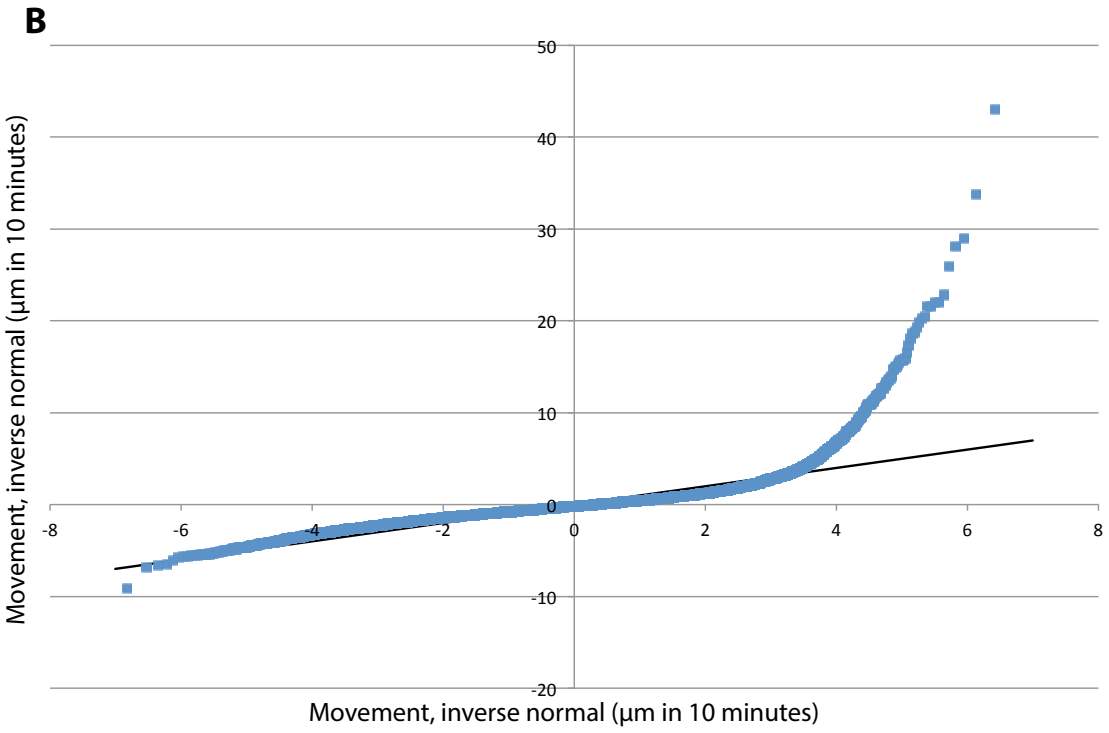
B
Movement, inverse normal (µm in 10 minutes)
50
40
30
20
10
0
-10
-20
-8 -6 -4 -2 0 2 4 6 8
Movement, inverse normal (µm in 10 minutes)

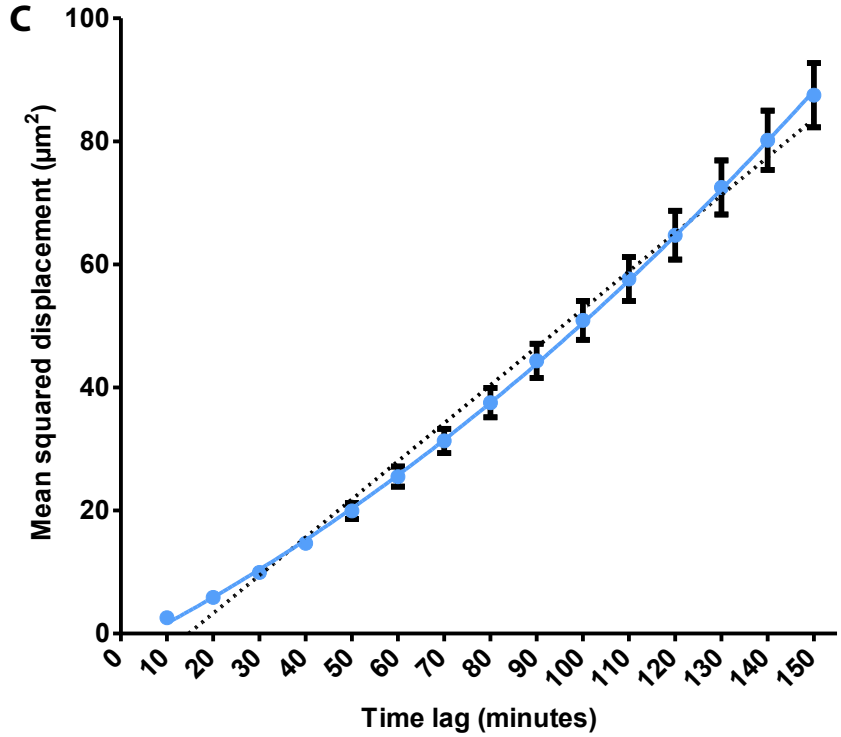

Figure 7.5 Overview of the motion of cone precursor cells.

A Histogram of the instantaneous velocities of all analysed trajectories - the distance travelled in 10 minutes between imaging events (19292 values, unfiltered data). Positive values (red) represent apical movements and negative values (blue) represent basal movements. The vast majority of the velocities were close to 0, with more than 95% less than 3µm and is approximately symmetrical around 0. More rapid motion can be seen in the apical direction.

B Inverse normal plot of the same instantaneous velocities. The black line y=x indicates conformity with a normal distribution with the same mean and standard deviation as the data. Deviation from this line indicates that the fast apical movements (right) are not the result of a normal distribution of movement.

C The mean squared displacement measurement was taken for all cells and averaged. These data are significantly better described by the second order quadratic curve with a positive curvature (blue line) as shown than by a linear fit (black dotted line), indicating that at least some of the migration behaviour shown by these cells is directed in nature. Error bars are SEM.

7.2.2.3 Rapid apical movement

Figure 7.6A shows the trajectory of selected cells that were classified as undergoing rapid apical movement. Figure 7.6B and C show all these recorded periods of apical movement arranged by the time of onset. Figure 7.6B, showing the trajectories by absolute distance from the apical limit of the retina, shows that cells can begin their apical movement from any position in the retina further than approximately 20μm from the apical limit (noting that of course apical movements initiated very close to the apical side would not be identified by the 10μm threshold). This indicates that apical movement is unlikely to be triggered by the approach of the migrating cell to the basal limit of the developing ONL.

The consequence of the apical movement, however, is the translocation of the cell closer to the apical limit of the tissue, although by no means *to* this limit. To illustrate, 60 minutes after the onset of apical movement, the position of the cells (excluding 5 cells where a position could not be found for this time) is a mean distance of 13.6μm from the apical boundary, with 50% of cells (32) within 10.5μm and 95% of cells (69) within 28μm, compared with a maximum apical-basal distance of between approximately 61 and 71μm, depending on the retina imaged (these observations are, of course, again subject to the restrictions imposed by the 10μm limit, which would exclude movements ending close to the basal boundary and other small jumps).

Supporting this, comparing the distance displaced in 60 minutes against the initial position in the retina using Pearson's correlation (Figure 7.6D) showed a highly significant correlation: $r = 0.6364$, $n = 72$, $p<0.0001$. This showed that the more basal a cell was on beginning its apical movement, the further it was likely to move. Since the majority of the movements were in excess of the threshold for apical

movement (46 out of 72 cells were displaced by more than 20μm in 60 minutes), it is very unlikely that this correlation was forced by the selection criteria.

Figure 7.6C shows the same apical movements relative to their position at the time of onset of movement, and extends to the positions from 40 minutes before this onset. This shows that the behaviour of the cells before the onset of apical movement is variable, with some cells moving slowly basally, others moving relatively slowly apically or even staying relatively stationary before beginning to move upwards. This suggests that the apical movement is also not simply triggered by a period of basal movement. Selected examples are included in Figure 7.6A. These grouped graphs also show that apical movements are of a similar gradient, indicating that the velocity of these movements is also similar.

Although the majority of apical movements exhibited very stereotyped kinetics, I also found evidence of slower movements in the apical direction. Applying the same criteria as for slower basal movements, that is, a minimum of 10μm movement over 2 hours, 36 cells (10.6%), which had not been classed as moving rapidly apically, were seen to move slowly apically. Examples of these can be seen in Figure 7.6E. Several of these cells (e.g. plots i-iv) might be classed as showing the same rapid apical movement as those identified above, but falling short of the arbitrary identification threshold for these cells. Others, however do appear to be moving relatively slowly apically for a prolonged period, in a manner similar to the basal movements described below.

In summary, therefore, periods of rapid apical cell movement are clearly distinct from the slow movement which characterises the majority of the imaging window.

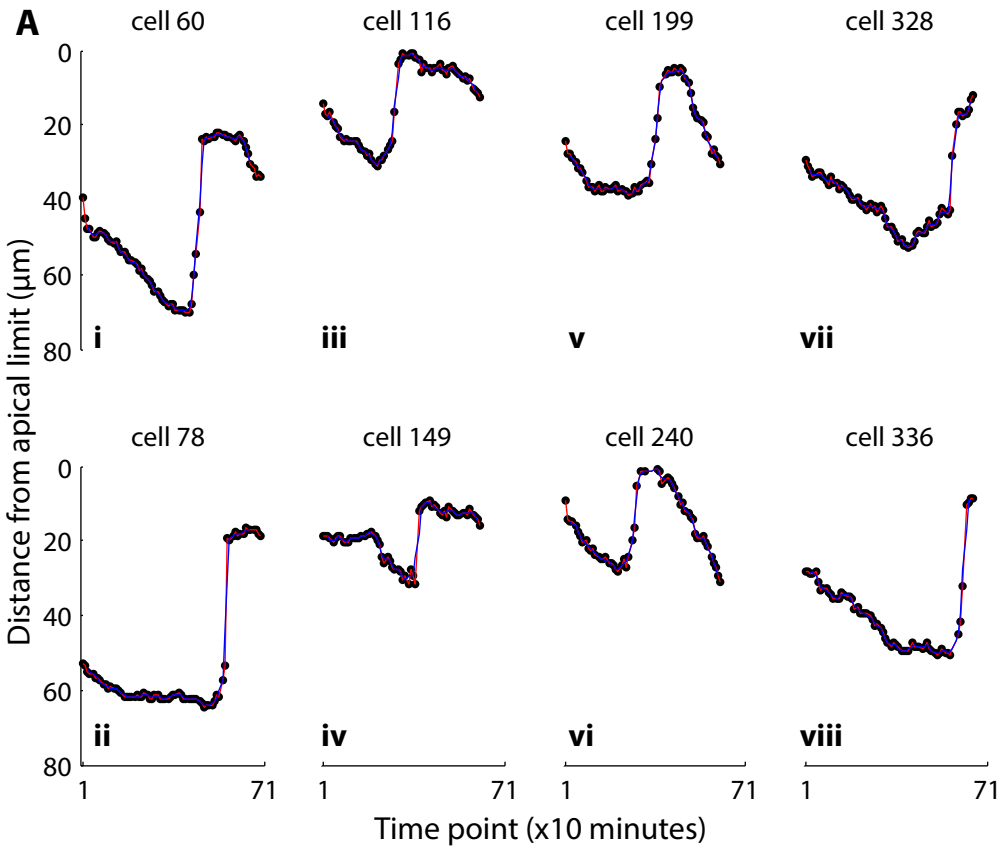
A
cell 60
cell 116
cell 199
cell 328
cell 78
cell 149
cell 240
cell 336
i
ii
iii
iv
v
vi
vii
viii
Distance from apical limit (µm)
Time point (x10 minutes)
0
20
40
60
80
1
71

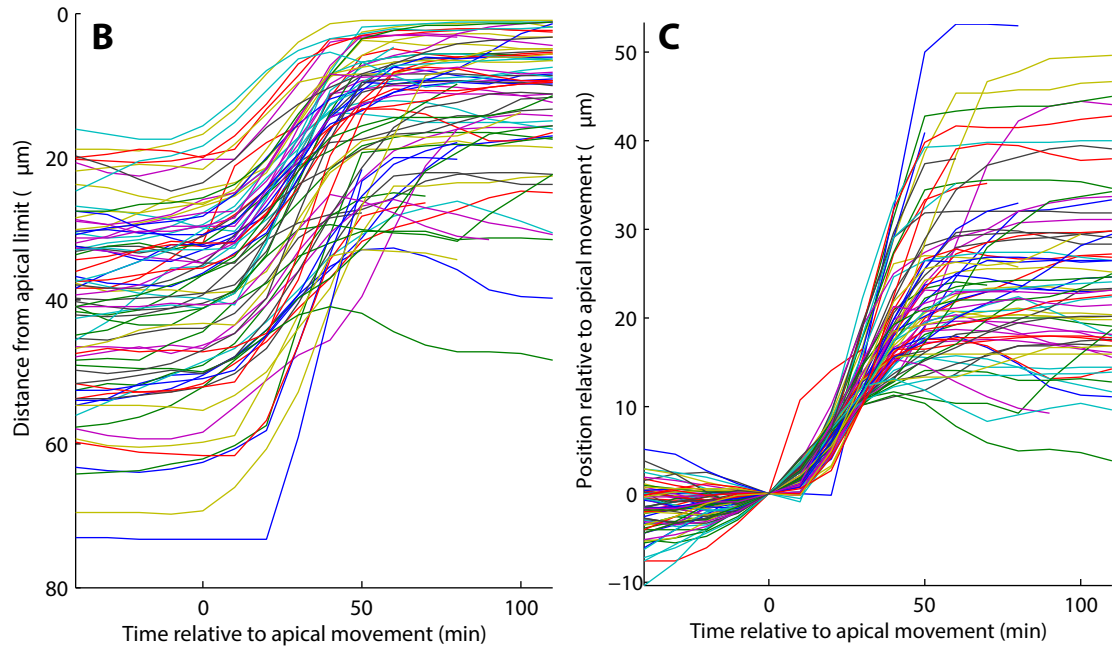
B
C
Distance from apical limit (µm)
Time relative to apical movement (min)
Position relative to apical movement (µm)
Time relative to apical movement (min)
0
20
40
60
80
50
100
−10
10
30

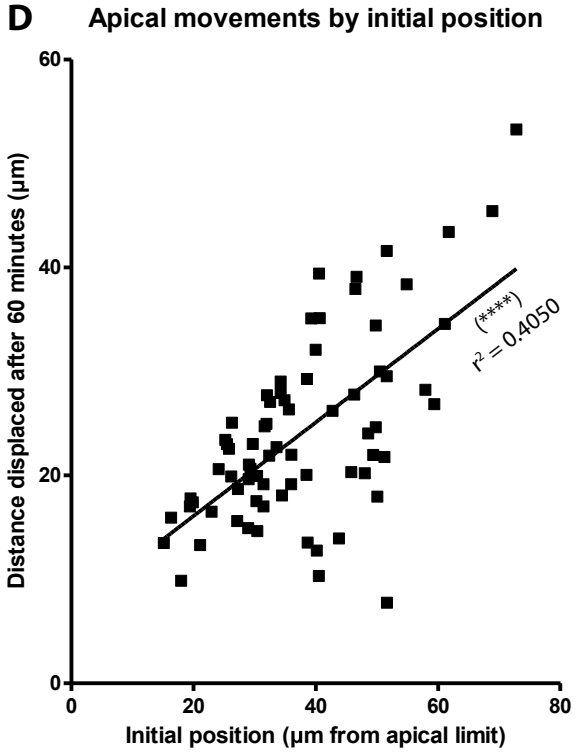

Figure 7.6 Analysis of rapid apical motion.

A Selected kymographs of cell position over time. These cells show rapid apical movement (defined as moving more than 10µm in 30 minutes). Recorded positions (black dots), linear interpolation of missing values (red line) and moving-average-filtered data (blue line) are shown. **B** All recorded apical movements (77 traces, filtered data) normalised by the time of onset (0). This shows that while apical movement can be initiated by cells throughout most of the depth of the developing ONL, the resulting cell position tends to be within the apical half of the ONL.

C All recorded apical movements (77 traces, filtered data) normalised by the time and position of the onset of movement, showing that the apical movement is stereotyped in nature, with a sigmoidal shape. The movement of the cells before the onset of apical movement is variable, with different cells seen to be stationary (A ii,v,viii), moving basally (A i,iv,vi) or relatively slowly apically (A iii,vii) immediately before this movement.

D The distance a cell moving rapidly apically is displaced 60 minutes after the onset of movement, compared with its initial position in the retina (72 cells). A strong correlation can be seen between these measurements.

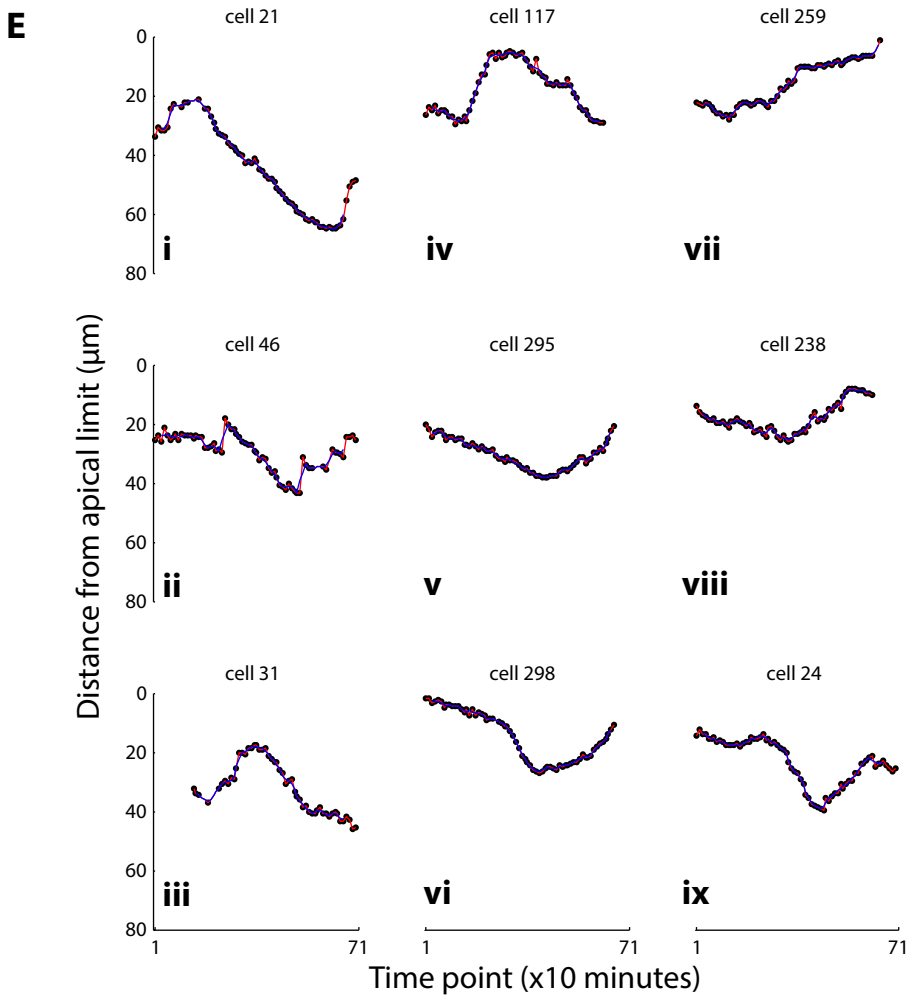

E To determine whether prolonged slow movement exists in the apical direction as it does basally, the same criterion of 10µm of movement in 120 minutes was applied. 36 cells were found to show this movement which did not also move rapidly apically. The kymographs of selected examples of these cells are shown. While some trajectories (i-iv) appeared to resemble the rapid movements seen in A, but not of the magnitude to meet the stricter speed and distance thresholds, others (v-ix) appeared to show a more gradual and prolonged apical movement period, similar to the basal movements shown in Figure 7.7.

7.2.2.4 Slow basal movement

A criterion for basal movement was set as 10μm movement in the basal direction over 12 time points (2 hours), as defined above, with 172 out of 341 (50.4%) cells analysed shown to meet this threshold.

In contrast to rapid apical movement, which was relatively stereotyped, the profile of these basal movements, including the velocity, duration and distance travelled varied considerably between cells, with examples shown in Figure 7.7A. Some cells moved basally at a relatively constant velocity for close to the entire duration of imaging, covering almost the entire depth of the ONL, while others moved for only a short time, or changed velocity during their trajectory. As a result, it should be noted that the threshold applied was likely to exclude basally moving cells which moved more slowly than average.

3 cells were shown to move 10μm basally in 30 minutes – that is, fulfilling the same speed criteria as were used to define rapid apical movements, these are shown in Figure 7.7B. As unusual as this finding was (compared to equivalent apical movements), it was not held to be indicative of a distinct mode of basal migration; as shown above in Figure 7.5, relatively modest instantaneous velocities of between 3 and 5μm in the basal direction were not excessively uncommon (around 1.7% of all velocities), and it might be expected 3 successive movements of this magnitude would occasionally arise in close proximity by chance.

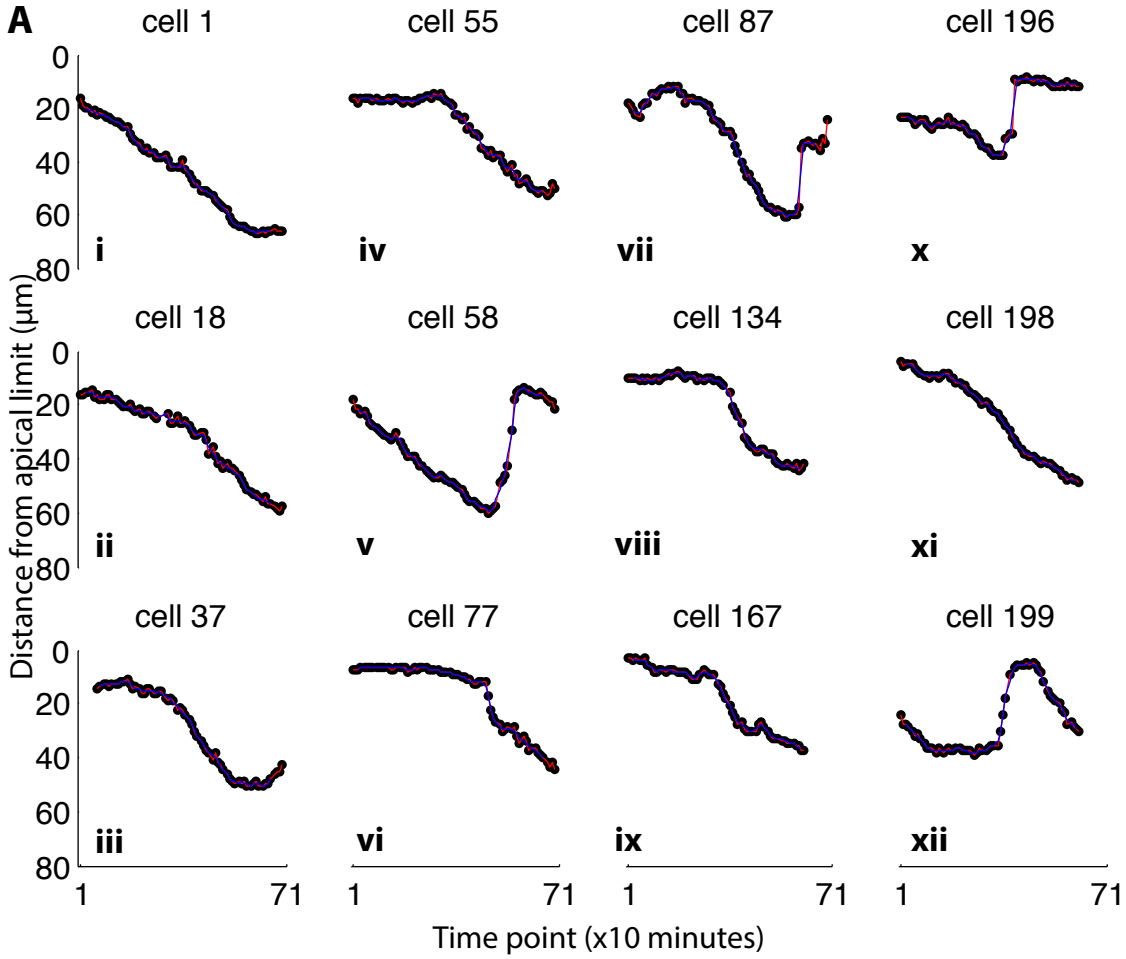

Figure 7.7 Overview of basal motion.

A Selected kymographs of the position of cells moving slowly basally over time (moving more than 10 µm basally over 120 minutes) Recorded positions (black dots), linear interpolation of missing values (red line) and moving-average-filtered data (blue line) are shown. The profile of basal movement can be seen to vary greatly between cells. Some cells moving basally at relatively constant velocity for almost the entirety of the imaging session and the entirety of the depth of the retina (i,xi). In other cells, the velocity of the basal movement appears to change over time (ii, ix). Basal movements can be seen to be prefaced most often by periods of relatively stationary behaviour (iv, vi, viii) and the end of a period of basal movement can lead to rapid apical movements (v, x), or another period of relatively stationary behaviour (i, iii).

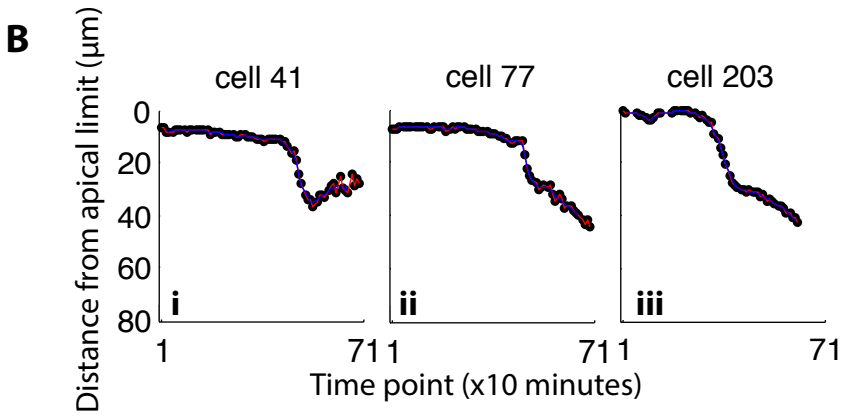

B To check for alternative modes of basal migration, cells moving 10µm basally in 30 minutes were identified, the same threshold applied to apically moving cells (Figure 7.X). 3 cells fit these criteria, with their trajectories shown here. Due to their rarity (<1%) and low velocity and displacement compared with the rapid apical movements seen, these were not held to indicate a separate mechanism of rapid basal migration, but rather the most rapid extremes of the same process shown by the cells in A.

7.2.2.5 Undirected stochastic movement and stationary cells

A total of 131 cells (38.4%) did not meet the criteria either for showing fast apical or slow basal movement, as shown above. It should be noted that a number of these cells would be included in the 'false negatives' – cells undergoing defined types of movement, but that did not pass the strict thresholds implemented. To reduce this effect, cells that did not move more than 10μm in either direction in any 120 minute period were identified, thereby excluding those cells showing slow apical movement as discussed in section 7.2.2.3, making a total of 114 cells (33.4%). On the other hand, periods of relatively stationary behaviour are exhibited by the majority of cells which do show directed movement (in either the basal or apical direction), and these cells are also excluded by these measurements.

A selection of the cells which did not show clear directed movement for the entirety of the imaging session are shown in Figure 7.8A, defined as not moving more than 10μm in either direction in 120 minutes, to exclude the cells which showed apical or basal movements of the types described above. Overlays of the trajectories of all cells are shown in Figure 7.8B, showing that the majority of these long-term stationary cells are located close to the apical edge of the retina. Taking the average position of each cell in this category over the entirety of its trajectory, 70% are within the most apical half of the retina (36μm) and 50% within 16 μm of the apical limit. This indicated that a large proportion of cells which remain stationary are located towards the apical surface of the retina, although it is not possible to determine whether these cells have not begun their migration cycles or have already taken up their adult position.

The directed nature of the cell movement seen in these experiments, in particular the rapid apical movements, strongly implicates an active mechanism of cell motility.

The difference between the rapid apical movements and the slower directed movements in the basal direction suggested that there might even be multiple mechanisms involved. In the next section, I investigate which cellular mechanisms might be involved.

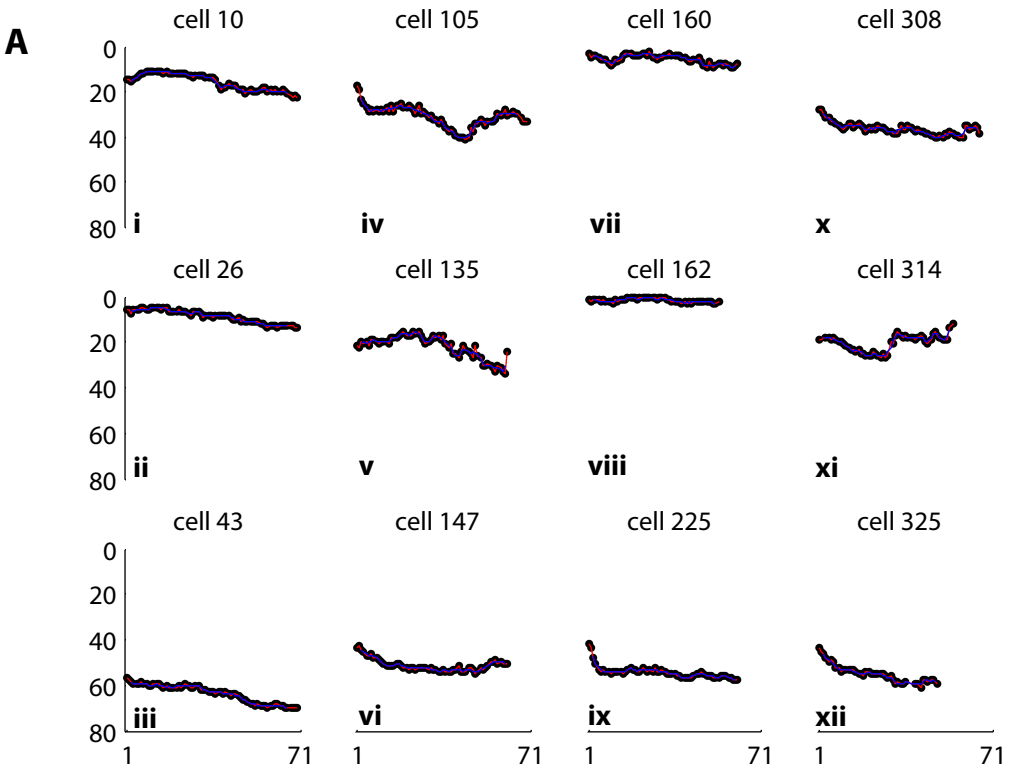
A
cell 10
cell 105
cell 160
cell 308
cell 26
cell 135
cell 162
cell 314
cell 43
cell 147
cell 225
cell 325
i
ii
iii
iv
v
vi
vii
viii
ix
x
xi
xii
0
20
40
60
80
1
71

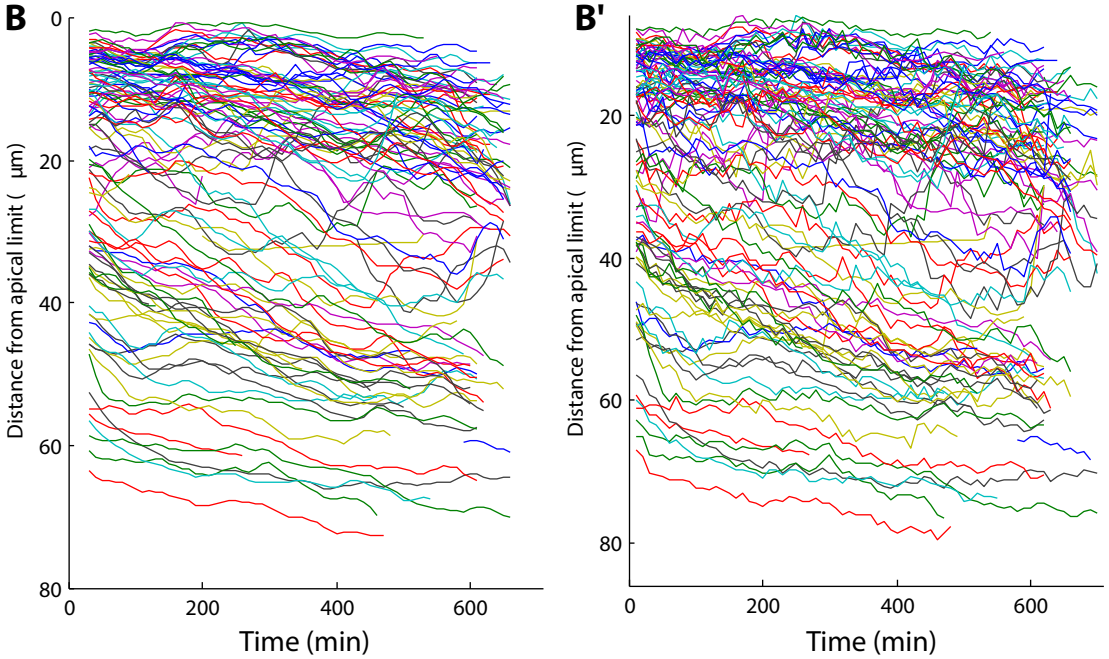
B
B'
Distance from apical limit (µm)
Time (min)
0
20
40
60
80
200
400
600

Figure 7.8 An overview of cells displaying relatively stationary behaviour.

A A selection of trajectories from cells which did not move more than 10µm in any given 120 minute period.

B Collecting all trajectories from cells which fit these criteria, showing their position in the ONL over time. These cells appear to be more often located in the apical portion of the retina, close to the apical limit, examples of which can also be seen in A (i, ii, vii, viii), although long-term stationary cells can also be seen in other parts of the ONL. Unfiltered data (B') shows that small fluctuations in position characterise the motion of these cells, leading to little change in position over time.

7.2.3 Pharmacological disruption of cell motility

The two major mechanisms for cell motility are the actomyosin system, which is the mechanism which drives muscle contraction, and the dynein/kinesin system named after the motor proteins which move cellular cargo along the cytoskeletal microtubules. Many previous studies looking at cell migration have used drugs that inhibit one or other of these systems to determine which has the greater contribution to the observed motion, with different forms of migration in different tissues shown to be driven by different mechanisms, as explained in section 1.6.

Ciliobrevin D is a small molecule antagonist of the dynein 1 motor protein and has been shown to prevent the movement of peroxisomes and melanosomes in cultured cells (Firestone et al., 2012). It was therefore used to examine the contribution of the dynein/kinesin system to the migratory behaviour seen in this tissue.

Imaging of P5/6 *ex vivo* flat mounted Chrnb4.eGFP retinas was carried out as before, with ciliobrevin D dissolved in DMSO, diluted in 1ml of imaging medium and then added to the imaging chamber, to make a final concentration of 25μM. Imaging of the tissue was carried out for at least 90 minutes before the addition of ciliobrevin D, to allow acclimatisation of the tissue and to ascertain both that the tissue was viable and that migration occurred before drug application. 3 separate successful imaging sessions were used, with durations of 4h30, 5h30 and 11h10 after drug application. Note that this is shorter on average than the sessions obtained with untreated retinas, partly due to the increased time needed for imaging before drug application, but also may be caused by a reduction in tissue survival time in the presence of ciliobrevin D. As a result, in some of the analyses below, I have attempted to correct for the effect of different imaging session lengths, and indicated in the text when and how this was done. Supplementary Movie 8 shows an xzt view

of a retina imaged in this way. The movement of the cells seen in this retina appears to be reduced, and, notably, the rapid apical movements common in untreated retinas were absent.

Processing of these images occurred as before, with 325 cells in total tracked across the 3 imaging sessions, and an ONL thickness of between 65 and 81μm. An overview of the data from these cells is shown in Figure 7.9, including a histogram of instantaneous velocities and an inverse normal plot of the same velocities, as in Figure 7.5. (Note that in plots of the trajectories of cells the maximum time is set to 71 time points, as with the data from untreated retinas, for ease of comparison). Although the instantaneous velocities are again shown to deviate from normality, in comparison to the equivalent measurements of untreated retinas, the incidence of rapid apical movements appears to be reduced for these cells (since instantaneous velocities require only the comparison of two consecutive positions, they were held to be relatively insensitive to the length of the imaging session, and so the entirety of all sessions were used). An analysis of the MSD measurements taken from cells from treated retinas shows that the overall displacement of these cells over time is significantly reduced, compared to cells in untreated retinas: $t(28) = 3.258$, $p = 0.0029$ (comparing the averages of the first 15 MSD values for each). However, the extra sum-of squares F test again showed that a quadratic curve (described by $y = 0.0007801x^2 + 0.1175x - 0.605$) fit significantly better with the data: $F(1,4778) = 12.23$, $p=0.0005$, with the r^2 value = 0.1447, than did a linear fit. This indicated some remaining influence of directed migration.

Rapid apical movement appeared to be almost completely abolished, with 0 out of 325 cells showing this kind of movement as defined by a movement of 10μm in 30 minutes. Similarly, only 2 cells were seen to move 10μm apically over 120 minutes, compared with 36 in untreated tissue. Two cells (numbers 94 and 100, as shown in

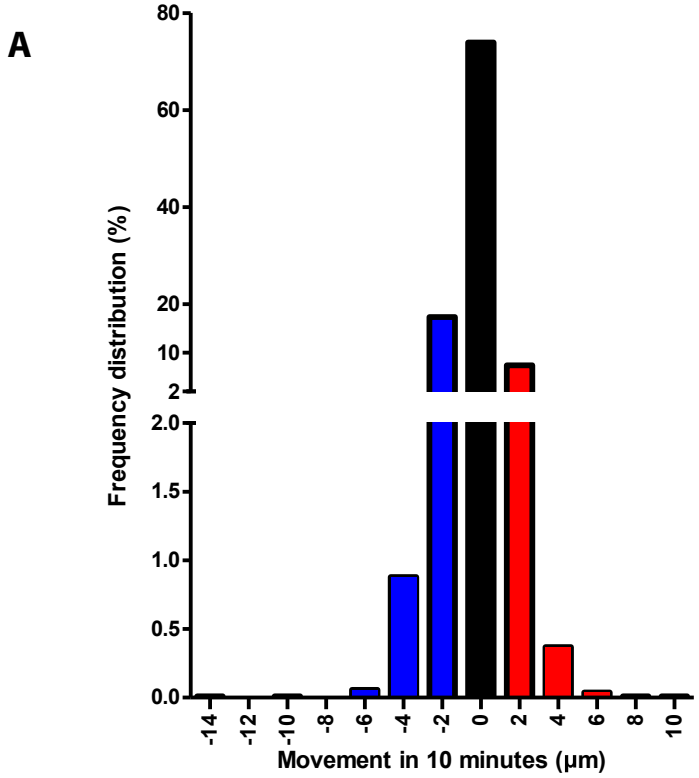
A
80
60
40
20
10
2
2.0
1.5
1.0
0.5
0.0
Frequency distribution (%)
-14
-12
-10
-8
-6
-4
-2
0
2
4
6
8
10
Movement in 10 minutes (µm)

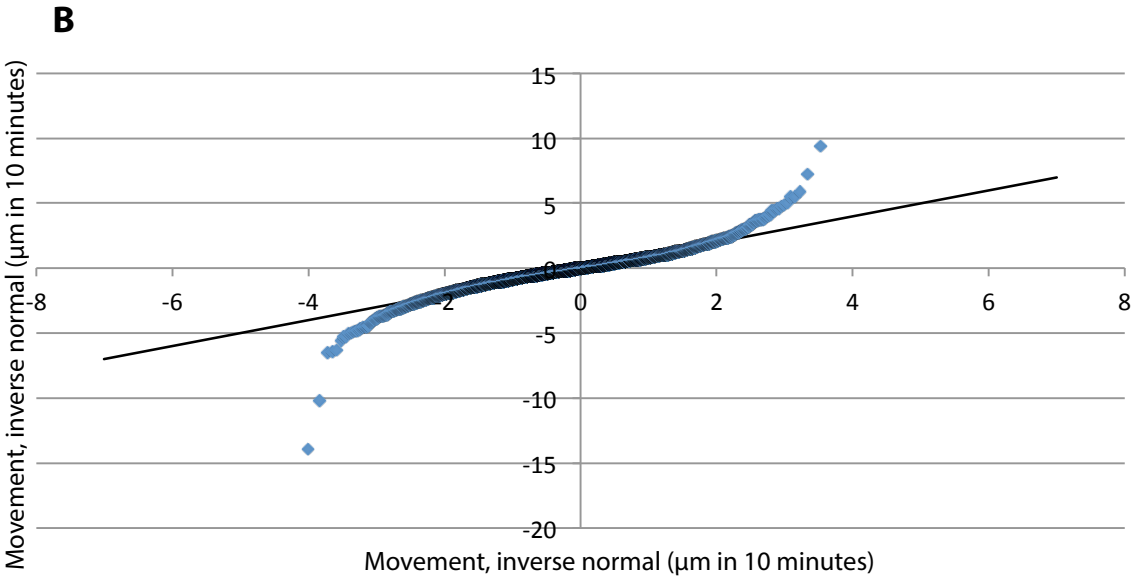
B
15
10
5
0
-5
-10
-15
-20
-8
-6
-4
-2
0
2
4
6
8
Movement, inverse normal (µm in 10 minutes)
Movement, inverse normal (µm in 10 minutes)

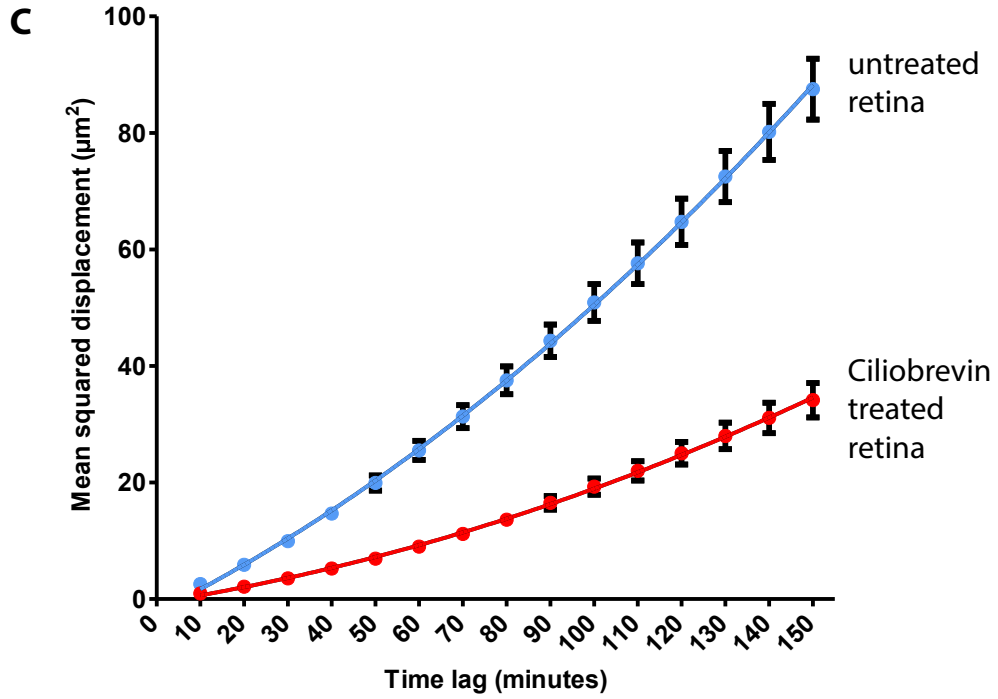

Figure 7.9 Overview of the motion of cone precursor cells in P5/6 Chrnb4.eGFP cells treated with 25µM Ciliobrevin D.

A Histogram of the instantaneous velocities of all analysed trajectories - the distance travelled in 10 minutes between imaging events (10586 values, unfiltered data). Positive values (red) represent apical movements and negative values (blue) represent basal movements. The vast majority of the velocities were close to 0, with more than 99% less than 3µm and is approximately symmetrical around 0. The rapid movements seen in the apical direction are much reduced from those seen with untreated retina (see Figure 7.6).

B Inverse normal plot of the same instantaneous velocities. The black line y=x indicates conformity with a normal distribution with the same mean and standard deviation as the data. Deviation from this line in the negative direction on the left and the positive direction on the right indicate that faster movements are undergone in these directions than would be predicted if these data came from a normal distribution, although the deviation in the apical direction is much reduced compared to untreated retinas.

C An MSD plot of displacements over time showed that overall movement was reduced in the treated retinas (red), compared to the untreated retinas (blue). error bars are SEM). The MSD plot of treated retinas was still better described by a positive curve than a linear fit.

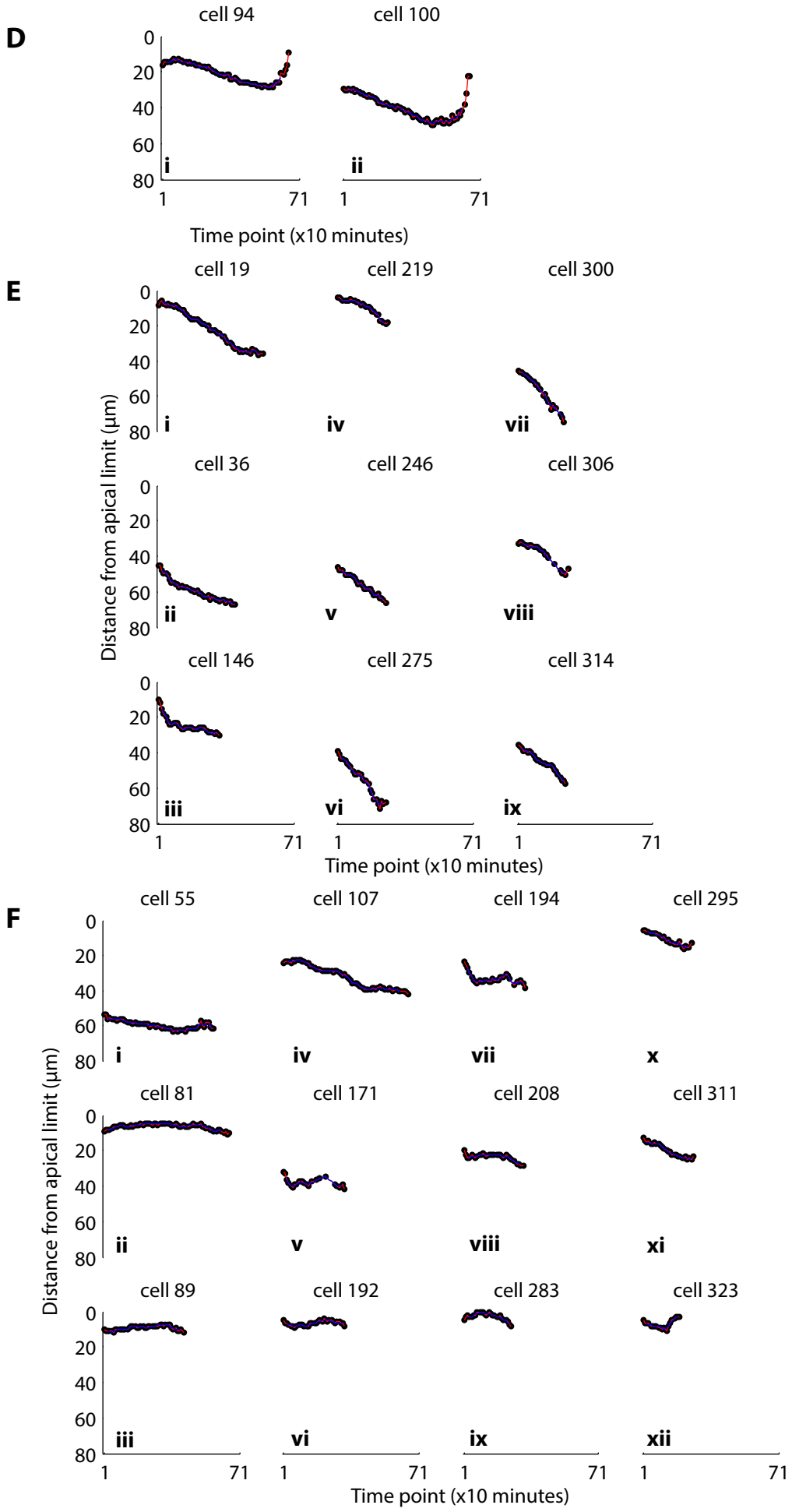
D
cell 94
cell 100
0
20
40
60
80
i
ii
1
71
Time point (x10 minutes)
E
cell 19
cell 219
cell 300
cell 36
cell 246
cell 306
cell 146
cell 275
cell 314
Distance from apical limit (µm)
iii
iv
v
vi
vii
viii
ix
Time point (x10 minutes)
F
cell 55
cell 107
cell 194
cell 295
cell 81
cell 171
cell 208
cell 311
cell 89
cell 192
cell 283
cell 323
x
xi
xii

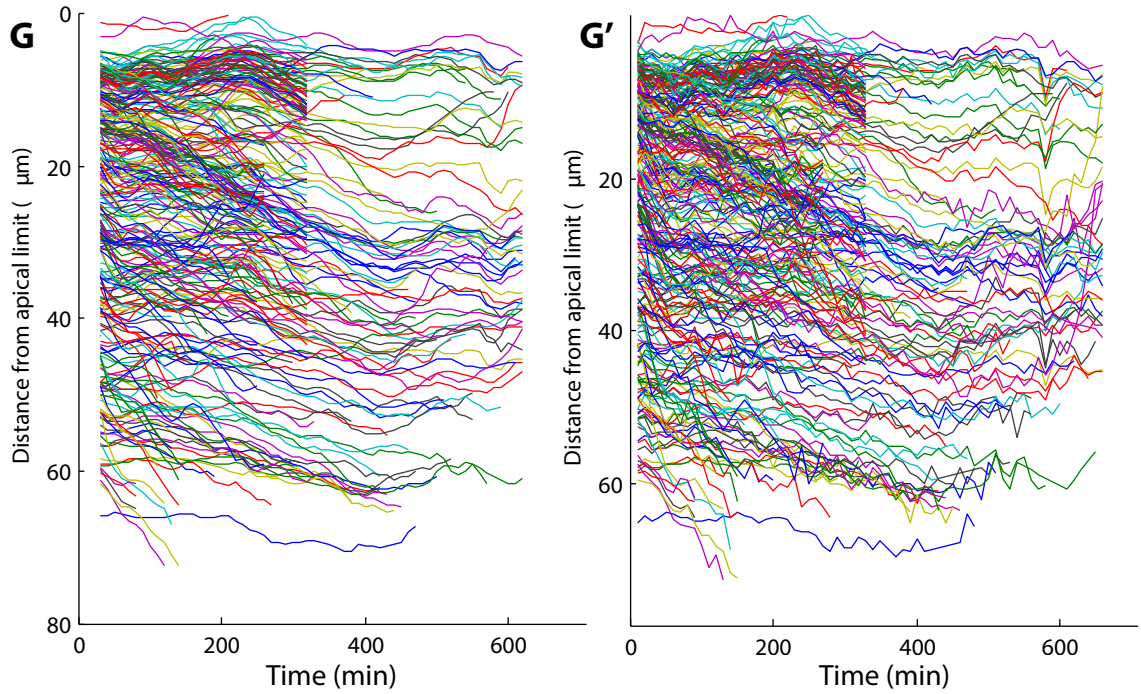

D-F Trajectories of cells from ciliobrevin D treated retinas. NB. For this figure, cell numbers refer to the order in which they were assessed, with different imaging sessions providing cells 1-111, 112-216, and 216-325.

D Rapid apical movements were almost entirely abolished. Two cells were found appearing to undergo rapid apical movement (over 10µm in 30 minutes), when only unfiltered data were used, from the same retina.

E The number of cells moving slowly basally (over 10µm in 120 minutes) were much reduced in some retinas, and apparently preserved in others, indicating a variable effect of the drug.

F As a result, the number of long-term stationary cells (never moving more than 10µm in 120 minutes) were increased. Many of these cells were located close to the apical limit (ii, iii, vi, ix, x, xi, xii) but others were not.

G All trajectories of cells classed as long-term stationary, including unfiltered data (G').

Figure 7.9D) did however appear to show rapid apical movements, and these were shown to move more than 10μm in 30 minutes, but only when unfiltered data were used. These both occurred at the end of the same imaging session (causing the exclusion by the filtered data), which was also the longest session including drug application – that is, the most comparable session to those using the untreated retinas. Comparable use of unfiltered data for the untreated retinas (without Ciliobrevin D) described above gave 89 instances of cells undergoing similar movement out of 341 total. Chi-square comparisons of these proportions showed an extremely significant difference, even when restricting the analysis only to the 111 cells from the session where these were seen ($X^2(1) = 30.75$, $p < 0.0001$).

These possible residual apical movements could be due to a number of factors: incomplete penetrance or effect of the drug, a reduction of its effect over time due to chemical or biological breakdown of the molecule, or the adaptation of the tissue to its effect. Alternatively, these cells could have been in the process of leaving the ONL entirely due to cell damage or death; as it was the end of the imaging session, this would not be apparent.

The proportion of cells that were judged to undergo directed basal movement was 46 out of 325 (14.2%) in the presence of Ciliobrevin D, compared with 172 out of 341 (50.4%) in control retina, showing a significant difference $X^2(1)= 99.51$, $p<0.0001$, indicating that this movement was much reduced, if preserved. Examples of cells meeting these criteria are shown in Figure 7.9B.

Due to the difference in imaging session length between untreated and treated retinas, I subsequently attempted to control for any effect this might have. Restricting the ciliobrevin D-treated data to the 111 cells in the longest imaging session (11h10), which was most comparable to the untreated sessions, this gave a

total of only 3 cells observed moving slowly basally at this rate, significantly different to the untreated values of 172 out of 341, $X^2(1)= 80.43$, $p<0.0001$.

Similarly, I also restricted the data from untreated retinas only to the equivalent portion of imaging time represented by the shortest imaging session (4h30), but took this portion from 1h30 to 6h of imaging time, to correct for the fact that the treated retinas were imaged for 90 minutes before drug application. I also restricted data from treated retinas to the first 4h30. This gave an imaging period of 4h30, or 27 time points for each retina. With these restrictions, a total of 42 out of 325 cells in untreated retina were found to be moving basally, compared with 53 out of 325 in the treated retinas. These proportions were not significantly different $X^2(1)= 1.193$, $p = 0.2748$.

This therefore indicated that while there is evidence that basal movement is much reduced by the application of ciliobrevin D, it remains much more common than apical movement. This also provides evidence that the effect of the drug might be variable between imaging preparations: the majority of the basal movements seen in ciliobrevin-treated retina came from a single imaging session.

The remainder of the cells (277 out of 325, or 85.2%) were therefore characterised as showing undirected stochastic movements, with examples shown in Figure 7.9F. Looking at the average positions of these long-term stationary cells, 60% were within the apical half of the ONL (41 μm), with 50% within 25μm of the apical limit. These average positions of these long-term stationary cells was however not significantly different from those in untreated tissue: $U(389) = 14039$, $p = 0.085$.

To summarise, the application of ciliobrevin D disrupts the processes of migration in cone photoreceptors. In particular, the rapid apical movement of cone precursors is

abolished, and the slower movement shown in the basal direction may also be affected, although the effect of the drug appears to vary. These data indicate a role for the dynein motor in cone precursor migration.

7.2.4 Description of CD-ROM files

Supplementary Movie 1 An image sequence of a single stack taken through the depth of a P5/6 Chrnb4.eGFP live explanted flat mounted retina. The scale bar is 50μm. Images are taken approximately 1μm apart in the z-direction and approximately 50μm below and above where GFP fluorescence is seen, giving a total depth of 179μm. This image is 277x277μm in the xy plane and sampled at 512x512, giving a voxel size of 0.54x0.54x1.00μm

Supplementary Movie 2 A stack of images of the same retina seen over time, with 10 minutes elapsing between the start of each stack being taken. 62 stacks were taken, meaning this represents 10h20 of imaging time, shown at 7 frames per second. Tissue drift can be seen in the xy plane over time.

Supplementary Movie 3 A similar view of a P8 Chrnb4.eGFP retina. A small patch of pigmented epithelial cells can be seen (marked on frame 1), and obvious cell death and tissue disruption quickly occurs around this area over time.

Supplementary Movie 4 A recalculated xzt view of a P14 Chrnb4.eGFP retina, showing no obvious movement of cone cells. Scale bar is 50μm.

Supplementary Movie 5 A recalculated xzt view of a P5/6 retina imaged in this way, showing 10h20 of imaging time, shown at 7 frames per second. This image is a stack of approximately 13.5μm (25 pixels) and has been treated with correction for 3D drift over time (ImageJ software, (Parslow et al., 2014)) Cells can be seen moving both basally and apically, with several examples of each clearly visible.

Supplementary Movie 6 A closer view of a similar xzt view, showing cells undergoing repeated motion (2 examples are marked) which move basally, then

rapidly apically, then return to basal movement. This movie is shown at 5 frames per second.

Supplementary Movie 7 Occasional cells can be seen moving basally beyond the limits of the developing ONL (as defined by the extent of the processes of surrounding cells), shown at 5 frames per second. Scale bar is 10μm.

Supplementary Movie 8 An xzt view of a retina treated with 25μM ciliobrevin D. Reduced cell movement is seen in these retinas, with apical movement in particular absent. Some loss of GFP signal is evident in this retina over time. Scale bar is 20μm.

7.3 Discussion

These experiments have allowed visualisation of the movement of individual developing cone photoreceptors for the first time, and allowed identification of the major features of the migration of these cells.

The presence of processes connecting the cell bodies to both edges of the ONL was initially suggestive of the nuclear translocation method of migration discussed above and in the introduction. However, the method of migration shown by the cones showed a striking similarity to INM, a mode of migration previously ascribed to proliferating progenitor cells, indicating that similar molecular mechanisms might underlie this postmitotic motion. In particular, and further to previous work, the evidence that individual cells undergo bidirectional migration multiple times is most similar to the migration profile of proliferating RPCs undergoing INM.

While the selection of the developmental age of P5/6 allowed visualisation of cells during a period of high migration, this leaves questions unanswered regarding the beginning and end of the developmental period of migration. Retinas from P2/3 or

P12/13 would be likely to allow for the tracking of cells beginning migration and taking up their final adult positions, respectively. In particular, determining whether the latter, final movement differed in any way from the apical movement seen in younger tissue would be an important step. However, the relatively limited length of time for which imaging can be carried out, even with multiphoton techniques, would mean it would be difficult to determine whether a given cell was indeed migrating for the first or final time – an imaging session would have to track the same cell from either before any cells were seen to move or until all cells were stationary to find this with certainty. A change in the balance of migration types during development would be more easily found: in my experiments I found that, on average, a tracked cell exhibited a net 12μm displacement in the basal direction during an imaging period of 10 to 12 hours, which, while a crude metric, illustrates that the migratory pattern seen at the developmental times I used must be reversed at some stage, whether by cessation of basal movements or an increase in the frequency of apical migration.

Use of the dynein inhibitor ciliobrevin D implicated the dynein-kinesin mechanism in driving the apical motion at least. The dynein motor works to transport cellular cargo towards the minus-ends of microtubules, which are typically located at the cell centrosome (Doxsey, 2001). The centrosome is located towards the apical limit of the retina (Aghaizu N., PhD thesis, submitted) throughout the period of migration, which would be in keeping with dynein being the driving force behind rapid apical movement, but would not explain the effect seen on basally directed movement seen in some treated retinas.

It should be noted, however, that these methods of pharmacological intervention are prone to having off-target effects, that is, the activity of ciliobrevin D could have affected cell motion in indirect ways, such as by causing cell death or a general

reduction in cytoskeletal integrity. Indeed, in these experiments tissue survival time appeared to be reduced with the addition of the drug, and furthermore the effect of drug on the presence of basal movement in particular was very variable between imaging sessions, with some preparations showing an almost total loss of basal movements, and others where it is apparently completely preserved.

Further, the cone precursors studied in these experiments represent a small proportion of the total cell population of the retina. Other cells are dividing and migrating at this developmental age, and the effect of the application of the drug on these cells is unknown. For example, the observed variable effect of Ciliobrevin D on basal movement could be due to effects on the movement and division of RPCs, which could be failing to rise to the VZ and divide. More investigation, and more specific interventions would therefore be necessary to draw firm conclusions regarding the cellular processes behind these observations.

Several other pharmacological agents exist which would allow the targeting of separate components of the actin/myosin or dynein/kinesin mechanisms, but a more targeted method of intervention would be likely to give more reliable results. For example, specific knockdown of certain motor protein components using cell-specific interference RNA or antisense oligonucleotide techniques would allow the function of these components to be locally and reversibly reduced.

Even with approaches such as these, however, uncovering the mechanisms in use may be less than straightforward. The striking difference between apical and basal motion seen with cone precursors suggests that different mechanisms may well be responsible for the overall migration. However, with the interaction between the two unknown, it may not be possible to separate the effects of intervention by observing the loss or retention of particular modes of migration.

For example, if the proteins that drive apical movement were successfully abolished, and those causing basal movement preserved, but basal movement is only triggered by an apical position of a cell, then basal movements would be rapidly lost once all cells were positioned close to the basal edge of the retina. This could explain the loss of basal movement shown in some ciliobrevin D treated retinas in my experiments.

The differing views in the literature over the mechanisms governing similar cell migratory activity suggest that caution should be used in concluding which applies in any one case. To illustrate, in INM, dynein-mediated motion has been implicated as explaining the apical motion seen in this process (Del Bene et al., 2008; Kulikova et al., 2011; J. Tsai et al., 2010; Xie et al., 2007), a finding similar that described here for post-mitotic cones, but others studies have indicated that the process continues after disruption of this mechanism (Norden et al., 2009) and that disrupting the actomyosin complex has a greater effect on INM (Schenk et al., 2009) (a more detailed discussion of this literature can be found in section 1.6.1).

As processes connecting the cell body of migrating cones to each boundary of the ONL were seen even at very early ages, another major type of neuronal migration that this resembles is that of somal translocation. This is a mechanism independent of glial cells. Somal translocation has been shown to be unaffected by the inhibition of myosin II or kinesin (Hawthorne et al., 2010) and appears to depend on the action of dynamin. On the other hand, somal translocation is usually characterised as involving the withdrawal of the trailing process as the cell approaches its final location, which does not occur with these cells.

Other forms of neuronal migration are dependent on glial cells, with the leading processs making contact with those of existing glia which have grown along the migration path. While Müller glia do span the depth of the retina, they are the final retinal cell type to differentiate, with a peak at P4 (Marquardt and Gruss, 2002), after the beginning of cone migration, although before this time they are progenitors with a bipolar morphology, spanning the depth of the tissue. It is also not clear why cones would require the guidance of the glial cells at the time of migration, since as shown above they appear to develop distinct processes along the trajectory of their migration before beginning the process. In previous work from this group, however, close spatial associations between migrating rod photoreceptors and Müller glia were found (Warre-Cornish, PhD thesis, 2013). It is possible that the development of the processes seen from all cone precursors at P4 are grown with the guidance of existing tracts in the retina, possibly those of RPCs or nascent Müller glia.

These differences from the major forms of postmitotic neural migration suggest that INM may indeed be a better model for understanding the movement exhibited by postmitotic photoreceptors. These results compare with similar experiments carried out using neonatal NrlGFP retina both previously (Warre-Cornish, PhD thesis, 2013) and currently (Aghaizu, PhD thesis, submitted), with fluorescent labelled rod precursor cells; in these studies, the movement undergone by rods was found to be very similar to that of cones, with a slow, stochastic basal and a dynein-dependent rapid directed apical motion.

7.3.1 The function of migration

The reason for this migratory step is still unclear. Given that rod precursors move in a very similar way, but do not have the specified adult location at the apical edge of

the ONL which the cones do, it is not evident that it is a specific and necessary process to allow cones to find their final position.

Also, the existence of processes throughout the whole of the developing ONL from all cone photoreceptors seen at P3, at the very beginning of migration makes it unlikely that the migration is necessary for the cell to develop its axon and determine the place where it must make a synaptic connection, as is the case with some migratory behaviour in other parts of the CNS.

Furthermore, the discovery of a cyclical mode of migration, with cells moving basally and then apically multiple times during development, again suggests that the migration itself is not directly for the purpose of moving the photoreceptor precursors to their final position. The similarity of the movement observed in these experiments to that of INM suggests that similar purposes may underlie the two processes. While there is no clear consensus for the ultimate purpose of INM, it is generally supposed that the basal movement seen is necessary to allow access to the apical surface for cells to divide.

A possible explanation on these lines could be that the basal cell movement seen both in INM and in my observations is driven passively by the genesis of new cells by mitosis at the apical surfaces. As cells divide and grow, they take up an increased amount of space and might exert force on surrounding cells, pushing them basally, away from the area of division. The rapid apical movement of cone precursors under this explanation would therefore be an active process to maintain the cell within the ONL. This is also proposed as an explanation for the very similar migration seen in INM (Norden et al., 2009), and evidence has been seen that when mitosis is inhibited by arresting cells in S-phase during neurogenesis in the brain,

that the basal movement of progenitor cells is concomitantly reduced (Kosodo et al., 2011).

Also supporting this idea within the context of postmitotic migration are the effects seen in models where migration is disrupted. In mice with mutations in SUN- and KASH- domain containing proteins, components of LINC complexes, cones are mislocalised basally from their usual position and some are found in the OPL and INL (Razafsky et al., 2012), which could indicate that when migration mechanisms are disrupted the cells are pushed down by dividing progenitor cell above them but cannot move back up again, causing some of them to leave the ONL. Of course, the converse might not be apparent with these kinds of observation; if cells were unable to move basally but could still move apically they could leave the ONL entirely and be lost or removed by the immune system.

On the other hand, cone cell genesis peaks at late embryonic stages (approximately E15.5) and is almost complete by birth, yet postmitotic cone cells remain at the apical surface for several days until the initiation of migration after P2, as shown by my results and other studies. During this period, mitosis is continuing as rod precursor genesis approaches its peak, and ganglion, amacrine and bipolar cells are also produced (Marquardt and Gruss, 2002), and in fact total neurogenesis peaks around birth (Young, 1985), but this apparently does not cause the cone cells to be pushed away from the apical surface between E15.5 and P2. On the other hand, the end of photoreceptor migration at around P10-12 coincides with the decline in neurogenesis in the retina. Given that only the cone photoreceptors – a very small population – are visualised in these experiments, it is possible that the movement of other cells allows for sufficient access to the ventricular zone for mitosis to continue, during the time that the cone precursors are stationary. The far more numerous rod photoreceptors, for example, are seen to undergo migration

around birth, much sooner relative to their mitosis than the cones (Warre-Cornish, PhD Thesis, 2013; Aghaizu. PhD Thesis, submitted).

The evidence that disruption of the dynein/kinesin mechanism of cell movement prevents the slow directed movement shown by cone precursors is inconclusive, but such a disruption would indicate that this process is unlikely to be wholly passive. On the other hand, as discussed above, the off-target effects of ciliobrevin D application could affect the process of neurogenesis to such an extent that the downward force on the cone precursors is removed. Again, the use of cell-specific RNAi techniques may allow targeted interventions sufficient to determine whether other cells affect these process.

To conclude, while many questions remain, the migration characterised by these experiments shows, for the first time, that the postmitotic cone photoreceptors in the mouse undergo cyclical migration within the developing ONL during the early postnatal period. Future work will need to characterise the beginning and end of the migration period, while any attempts to determine the mechanism and purpose of this process will have to be carried out with an appreciation of the behaviour of other retinal cell types at this time, as well as the effects of intervention on the whole retina.

Chapter 8 – Synthesis and final conclusions

8.1 Summary of research findings

This thesis aimed to extend previous work in the field of photoreceptor replacement therapy for the treatment of retinal degenerative diseases to use cone photoreceptors. Although the majority of previous work had focussed on rod photoreceptor transplantation, proof-of-principle for cone transplantation had already been demonstrated, where mixtures of cone and rod cells had been injected into recipient mice (Lakowski et al., 2010), and subsequent apparently integrated GFP+ cells in the recipient retina had occasionally been shown to be cone-like in appearance, and display cone-specific protein markers. My experiments attempted to develop this work further, to develop resources that would allow transplantation of only cone cells, and to improve the outcomes of transplantation, such that appropriate treatments of cone-related disease treatment could be produced.

I discussed a number of mouse models suitable for investigating these aims in Chapter 3. I concluded that the Chrnb4.eGFP model represented the best source of true cone precursors, as well as a way of tracking developing cones. I also determined that the $Nrl^{-/-}$/NrlGFP and $Nr2e3^{rd7/rd7}$CrxGFP mice could be used as sources of enriched populations of cone-like precursors. Through qPCR analysis, I showed that the transcriptomes of the cells isolated from these models were consistent with cone photoreceptors.

In Chapter 4, I used the Chrnb4.eGFP as a source of true cone cells. I transplanted these cells at E15.5, P1 and P8 into WT and $Nrl^{-/-}$ recipients. In the WT recipient,

although GFP+ cells were found in the recipient ONL after transplantation, they overwhelmingly resembled rod photoreceptors, as was the case after the transplantation of CrxGFP cells in previous studies (Lakowski et al., 2010).

In Chapter 5, I found similar results using fate restricted $Nrl^{-/-}$ cells, which lack the ability to become rod cells. After transplantation, these too appeared to resemble rods after integration into the recipient, and only rarely were GFP+ cells found which stained for the nuclear cone marker Rxrγ. Somewhat more common were cells that expressed cone-arrestin, but these were still a small minority.

While the results using true cones from the Chrnb4.eGFP model suggested that it might be the case that cone cells are not fully committed to their eventual fate, and are able to differentiate into cells resembling rod photoreceptors, the similar results found with the $Nrl^{-/-}$ cells made this explanation less likely. I discussed recent work from the group and others which proposed an alternative explanation for the results seen after the transplantation of photoreceptor cells. These found that while integration of transplanted cells occurred, the majority of the GFP+ cells in recipient retina after cell injection are the result of material transfer: the exchange of a variety of RNA and/or proteins, including GFP, between recipient and donor cells. Preliminary results from the extension of this work to the transplantation of $Nrl^{-/-}$ NrlGFP cone-like cells into DsRed-expressing recipients indicated that with these cells, too, the majority of GFP+ cells found after transplantation are also DsRed+, that is, they contain donor- and recipient-specific proteins.

In the light of these data, I concluded that the greater part of my results were also due to the process of material transfer, with GFP and other cell contents moving from injected cells in the subretinal space into existing recipient cells in the ONL, rather than the donor cells themselves migrating into the recipient ONL.

I also attempted to determine the effect of transplantations of cone-like cells on the light response of recipient retinas (Chapter 6). Recordings were made from the RGCs of Prph2$^{rd2/rd2}$Cnga3$^{cpfl5/cpfl5}$ double mutant mice, which had received injections of Nrl$^{-/-}$ donor cells. While I was not able to conclude that these retinas were improved in their ability to respond to light, or converted to a response pattern more similar to cone photoreceptors, other studies using these techniques have indeed shown functional improvement. Therefore, it is likely that the injection of cone-like cells has the potential to increase the light response of recipient retina.

Finally, in Chapter 7 I investigated the migratory behaviour which cone precursors display during development. Through time-lapse imaging techniques, I was able to describe the trajectory of these cells for the first time, and determined that they display a mode of movement very similar to that of proliferating progenitor cells, known as interkinetic nuclear migration, which has not been reported before in postmitotic cells. I showed that it is likely the microtubular motor protein dynein that drives the rapid apical movement seen in these cells, but that the slower basal movement seen may be an active or passive process.

Despite the interesting implications for retinal development, the re-evaluation of photoreceptor transplantation prompted by recent evidence implicating material transfer means that the relevance of this migration to transplantation may be minimal. Recent work from the group (Pearson et al. 2016, in press) suggests, however that a proportion of transplanted donor cells do migrate into the ONL across the OLM, but it is as yet unclear what, if any, migratory behaviour they display once inside the recipient retina.

8.2 Future directions

8.2.1 Material transfer

The key outstanding question regards the mechanisms underlying the material transfer which underlies the rescue resulting from photoreceptor transplantation. While existing theories are detailed in Section 5.3.2, this debate is still very much in its infancy, and due to the large number of disparate observations that any mechanism would have to explain, a full understanding of how this process occurs may be some way distant.

By whatever means, material transfer appears to be a robust process, able to transport a wide array of proteins, including those necessary for cell function. There is evidence that degeneration occurring as a result of genetic mutation can be halted by the provision of healthy replacement proteins. The reintroduction of Nrl-expression in the $Nrl^{-/-}$ mouse has been shown to prevent the degeneration (secondary cone loss) seen in this model (Montana et al., 2013), even in adult cells. Functional improvements after transplantation seen in previous studies (Pearson et al., 2012) are evidence that despite the unexpected explanation, cell therapy has the potential of treating degenerative disease.

In this event, my results have shown that cone precursors behave similarly to rods after transplantation, and while the efficiency of material transfer appears to be reduced using these cells, it is also apparent that those interventions that have been shown to increase outcome using rod cells equally apply to cones. If better evidence for functional improvement by the introduction of these cells can be found (see the discussion for Chapter 6), it will be possible to determine in which contexts cone transplantation may be of clinical benefit.

However, if, as some recent evidence suggests (Pearson et al. 2016, in press), material transfer is a frequent but transient occurrence, the influx of functional material to degenerating cells may not be sufficient to provide effective long-term treatment to recipient retinas, either in terms of restoring function or preventing cell death. Additionally, the lack of efficiency, likelihood of a recipient immune response and difficulty in obtaining large numbers of cells for transplantation means that this approach may not be the most effective way of repairing recipient cells.

From a clinical point of view, the existence of material transfer represents a reduction in how useful cell transplantation could be as a treatment for retinal degenerative diseases. The major advantage proposed for cell transplantation is the provision of new photoreceptors and the restoration of lost function, rather than the slowing of cell loss or even the repair of remaining photoreceptors. With the majority of the resulting outcome of cell transplantation being dependent on the remaining recipient photoreceptors taking up material from injected cells, this restoration of lost function may not be possible with current approaches.

8.2.2 Alternative approaches and applications

Gene therapy, using viruses or other vectors to provide intact copies of mutant genes, represents a targeted and practical method to repair specific genetic defects in patients. While the advantage of cell therapy is that it aims to treat heterogeneous conditions with a range of causes, and replace lost photosensitive cells, developments in genetic and other techniques may also be able to address these problems.

New approaches in this area are attempting to find solutions to the problem of restoring light-sensitive cells in diseases where photoreceptors die. A promising

possibility is the conversion of existing retinal cells other than the photoreceptors to be photosensitive. Small molecule 'photoswitch' drugs have been discovered which enable control of neuronal excitability with light, such as acrylamide-azobenzene-quaternary ammonium (AAQ) which blocks K^+ channels until photoisomerised by short wavelength light, thus controlling the membrane potential of cells. Application of AAQ has been shown to confer light responses to RGCs, and in mice lacking rods or cones, behavioural measurements of light response (light avoidance) and the pupillary reflex have been restored (Polosukhina et al., 2012). Similarly, optogenetic methods, introducing genes for the production of light-sensitive ion channels, could imbue surviving cells with the capacity to respond to light, without the need to replace photoreceptors.

In advanced cases of retinal degeneration the entirety of the ONL can be lost and this may represent a more promising target for injection of new photoreceptor cells (whether or not material transfer occurs would be incidental in this case), as there would not be recipient photoreceptors to take up material. Injection of Nrl GFP+ rod precursor cells into the Pde6b$^{rd1/rd1}$ mouse, which loses its ONL by 3 weeks of age, has been seen to lead to the organisation of injected cells into a polarised arrangement resembling the ONL (Barber et al., 2013; Singh et al., 2013), with injected cells showing signs of segment development, as well as improvement of the pupillary reflex and an increase in light avoidance behavioural measurement. Human iPS cells injected into the Pde6b$^{rd1/rd1}$ mouse have recently been shown to partially restore visual function, as shown by light aversion, pupillometry and ERG measurements (Barnea-Cramer et al., 2016). Consistent with this, initial results from this group have suggested that injections of photoreceptor precursors into the Pde6b$^{rd1/rd1}$ mouse lead to restoration of function as measured by MEA recordings (K. Powell, pers. comm.).

Transplantation of partial retinal sheets represents one method of replacing a lost ONL. However, creating renewable sources of dissociated cells is likely to be easier than similar sources of ordered retinal sheets; however, as despite advances in the production of tissue similar to developing retina using stem cell techniques, ethical sources of whole human neural tissue are still not available.

In cone cells in particular, the use of sheets and/or dissociated cells should still be applicable in the context of human treatment. In the macula, cone photoreceptors predominate, and in the fovea cell bodies and processes are displaced from the light path, leading to a much thinned retina. Loss of photoreceptors in these areas would therefore be expected to lead to areas that could favour a more integrative outcome of transplantation. This could be investigated by the use of cone transplantation techniques in models such as the $Pde6b^{rd1/rd1}$ mouse.

Alternatively, cell therapy using different source cells may well represent effective treatments. For example, RPE injection is beginning to be tested as a method of treating diseases such as dry AMD which affect this cell layer (Schwartz et al., 2016, 2014) with some evidence of improving visual acuity in these conditions.

To conclude, the future of photoreceptor-based cell therapy as a method of treating retinal degenerative diseases will depend on a re-evaluation of the underlying mechanisms, in the light of this study and other lines of evidence. While cone cell replacement in theory represents the best method of restoring vision in degenerative diseases where these cells are lost, more evidence, particularly regarding transplantation into late stage degeneration, will be required to determine whether this approach is feasible.

Appendix A – Genetic codes, PCR conditions and primers

Table A1 PCR primers and protocol details for genotyping

Genotype	F Primer (5' to 3')	R Primer (3' to 5')	Amplicon (bp)	Kit used	Method of Analysis
cpfl5	TAGGCCATCCCATCCTGTCA	CTGGACCAGTCAAGTCCGTG	182	Promega	Sequencing
EGFP (Chrnb4.EGFP)	CCTACGGCGTGCAGTGCTTCAGC	CGGCGAGCTGCACGCTGCGTCCTC	Approx. 300	HotStar Taq (Qiagen)	Band detection
Rd1	CACACCCCCGGCTGATCACTG	CTGAAAGTTGAACATTTCATC	Approx 300	Promega	Sequencing
Rd8	GCACAATAGAGATTGGAGGC	TGTCTACATCCACCTCACAG	Approx 250	Promega	Sequencing
$Nrl^{-/-}$	GGGCTCCACACCATACAG	AGAGGCCCTTCCATAGAGAC	216	Promega	Band detection
Prph2 - rd2 mutant	GACCCAGATTGCCTGTGGCA	TGAGCCACAGCAGACGTTGG	393	Promega	Band detection
Prph2 – wild-type variant	CCAGAAATAGGTTCGCTGTCC	GATGGTCATAGCTGTAGTGCG	330	Promega	Band detection

Table A2 PCR conditions for genotyping

Genotype	Initial denaturation	Denaturation	Annealing	Extension	Final Extension	Cycles
cpfl5	2m 95^{o}C	30s 95^{o}C	50s 60^{o}C	30s 72^{o}C	5m 72^{o}C	35
EGFP (Chrnb4. EGFP)	15m 95^{o}C	45s 94^{o}C	45s 60^{o}C	60s 72^{o}C	10m 72^{o}C	30
Rd1	5m 95^{o}C	30s 95^{o}C	30s 55^{o}C	45s 72^{o}C	10m 72^{o}C	30
Rd8	2m 95^{o}C	30s 95^{o}C	30s 59^{o}C	30s 72^{o}C	5m 72^{o}C	35
Nrl$^{-/-}$	7m 95^{o}C	10s 96^{o}C	30s 62^{o}C	90s 72^{o}C	7m 68^{o}C	30
Prph2	5m 95^{o}C	30s 95^{o}C	30s 56^{o}C	45s 72^{o}C	10m 72^{o}C	35

Table A3 qPCR primers and details

Gene	F primer (5' to 3')	R primer (5' to 3')	Amplicon (bp)	Probe number
Arr3	GCTAACCTGCCC TGTTCAGTA	TTCAAAGTCAA CCCCACAGG	75	64
Chrnb4	GCTCCTCGTCTC TCTGTTCG	CATCCATCAGC TTCTCCTCTG	77	64
En2	GACCGGCCTTCT TCAGGT	CCTGTTGGTCT GAAACTCAGC	132	110
Fgfr4	AATCGTATTGGA GGCATTCG	TCCGAGGGTAC CACACTTTC	71	47
Gnat2	CATGTCCACACT AGGCATTGAC	GCCAGGTTGTT GAGCTGTCT	72	21
Opn1mw (M-opsin)	ATCGTGCTCTGC TACCTCCA	TTTCTGTTGCTT TGCCACTG	60	5
Pde6c	CGAAGGTGAAGG TGACTGAAG	GCTGCCTCCTA AATCTGTGG	86	4
Rxrγ	CAGAAGTGCCTG GTCATGG	CCTCACTCTCT GCTCGCTCT	82	82
Opn1sw (S-opsin)	CAACCCCATCAT CTACTGCTT	GACACGTCAGA TTCGTCTGC	96	4
Thrβ2	ATGCATCTATGTT GGCATGG	GCTTGGCTAGC CTCTTGCT	62	42
Nrl	TTCTGGTTCTGACA GTGACTACG	TGGGACTGAGCA GAGAGAGG	77	53
Nr2e3	CAGCCAGCCTGT GAGGTT	AGAAGCTCAAT GCGCTCAG	81	32
Rhodopsin	ACCTGGATCATG GCGTTG	TGCCCTCAGGG ATGTACC	70	32
B-actin	AAGGCCAACCGT GAAAAGAT	ACCAGAGGCAT AC	110	56

Appendix B – Material Transfer

This section contains selected figures and data from ‘Donor and host photoreceptors engage in material transfer following transplantation of post-mitotic photoreceptor precursors’, (Pearson et al. 2016, in press). Figure legends are also adapted from this study. The entirety of this paper is submitted as supplementary information, on the accompanying CD-ROM. Figure B8 is not however from this paper, but is preliminary data regarding the extension of this work to use $Nrl^{-/-}$ cone-like cells.

These figures accompany the results to Chapter 5, specifically section 5.2.7, in which I discuss material transfer between donor and recipient cells as an explanation for the outcome of cell transplantation.

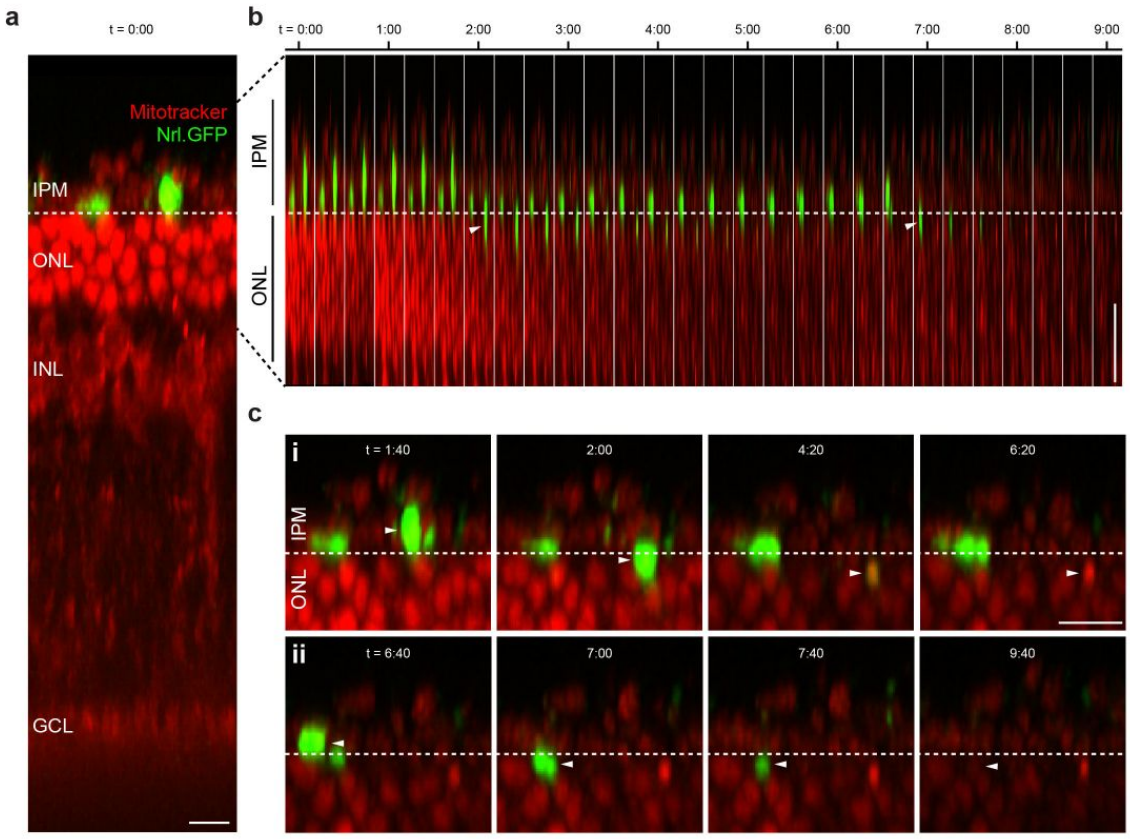

Figure B1 Real-time imaging shows that transplanted donor cells can move into the ONL of recipient retina. NrlGFP precursor cells were injected into 12 week old Prph2rd2/rd2 recipient mice. 3 days after transplantation live explanted retinas were imaged with 2-photon fluorescence live-imaging. Both donor and recipient cells were labelled using Mitotracker Orange before recording. Scale bars 10 µm.

a At the beginning of recordings, GFP+ donor cells were readily observed subretinally, adjacent to the ONL. A dashed white line indicates the presumptive position of the OLM.

b Time course of cell movement. Two GFP+ donor cells (white arrowheads) can be seen penetrating the OLM and subsequently locating in the recipient ONL. GFP signal subsequently declines in both cells after movement, but Mitotracker signal is still apparent.

c Expanded views of the first (i) and second (ii) cells seen moving into the recipient ONL in (b).

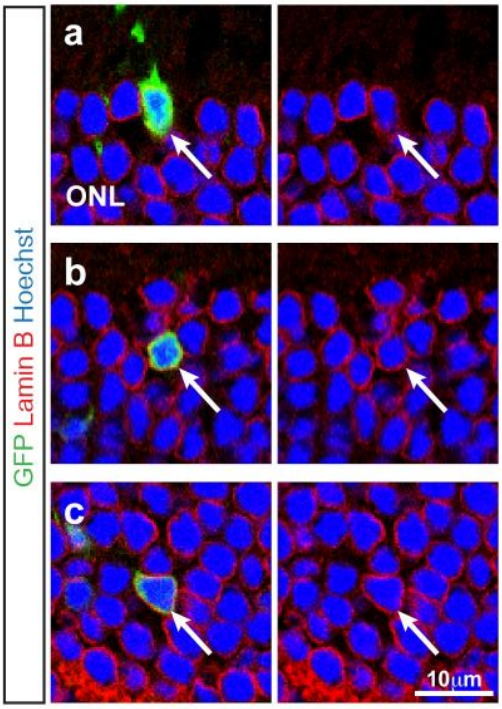

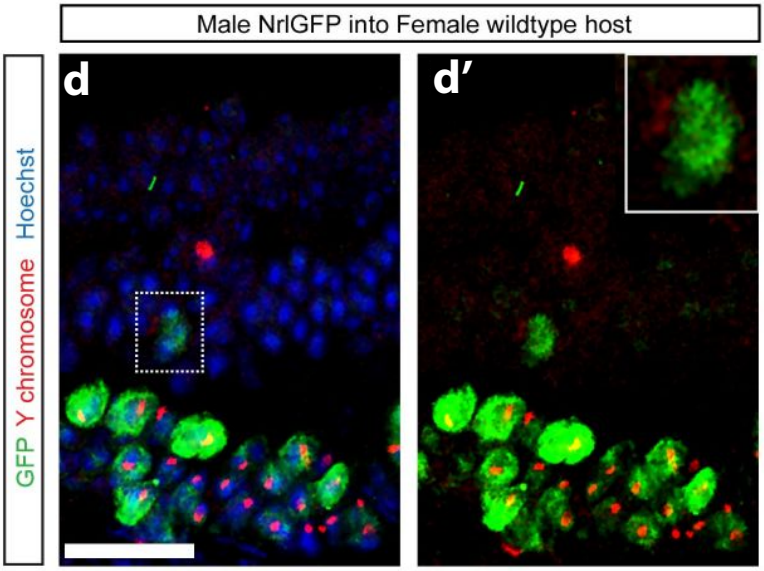

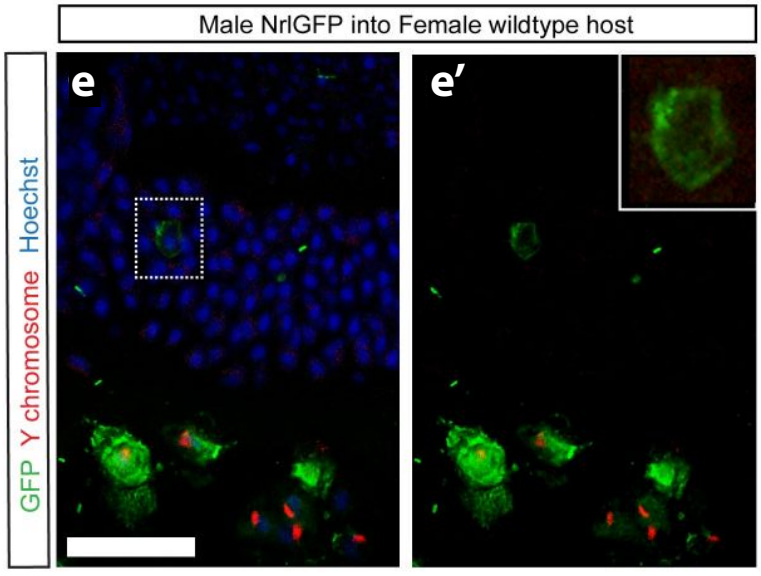

Figure B2 Material transfer is not the result of nuclear fusion

a-c Gnat1$^{-/-}$ and WT retinas received transplantation of NrlGFP post-mitotic photoreceptor precursor cells. Lamin B staining shows that GFP+ cells only ever presented a single nuclear envelope (red) and nucleus (blue)

d,e FISH-labelling of the male Y-chromosome after transplantation of male donor NrlGFP photoreceptor precursor cells into female recipients. Y-chromosome labelling is readily seen in GFP+ donor cells remaining in the subretinal space, but not in female recipient tissue. Occasional GFP+ cells in recipient retina label for the Y-chromosome (d, see insert) but the large majority do not (e).

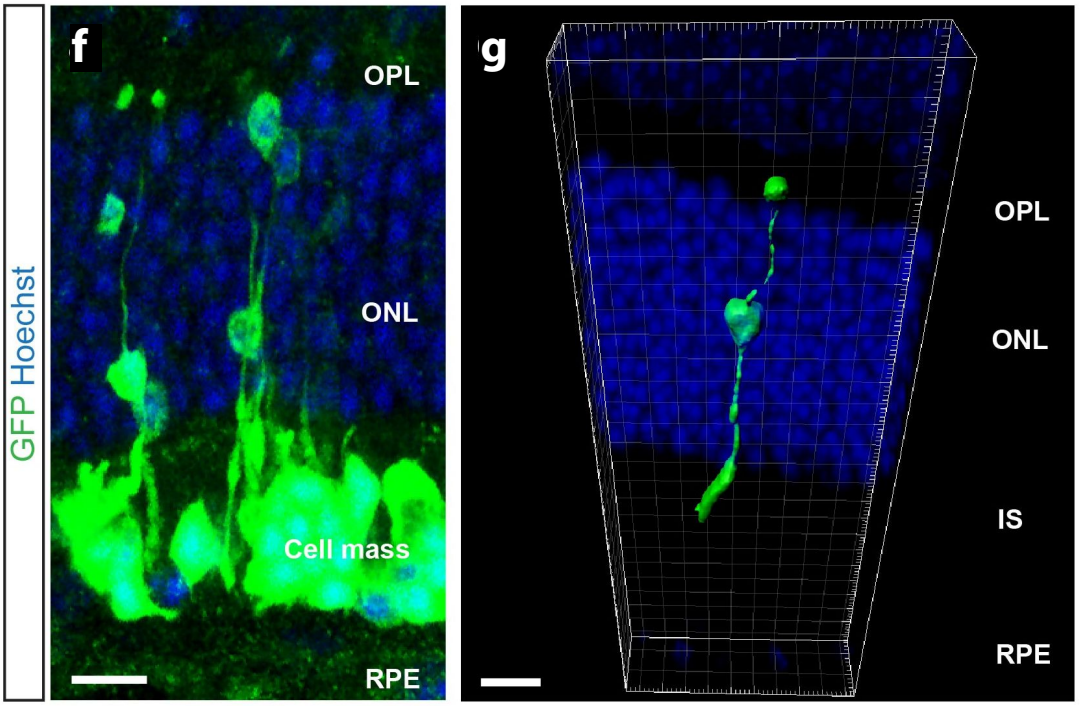

f,g After transplantation of NrlGFP post-mitotic photoreceptor precursor cells many GFP+ cells are found close to a cell mass of donor cells in the subretinal space (f), but several are not (g). 3d reconstruction of this cell indicates that no connections exist between it and any other GFP+ cell.

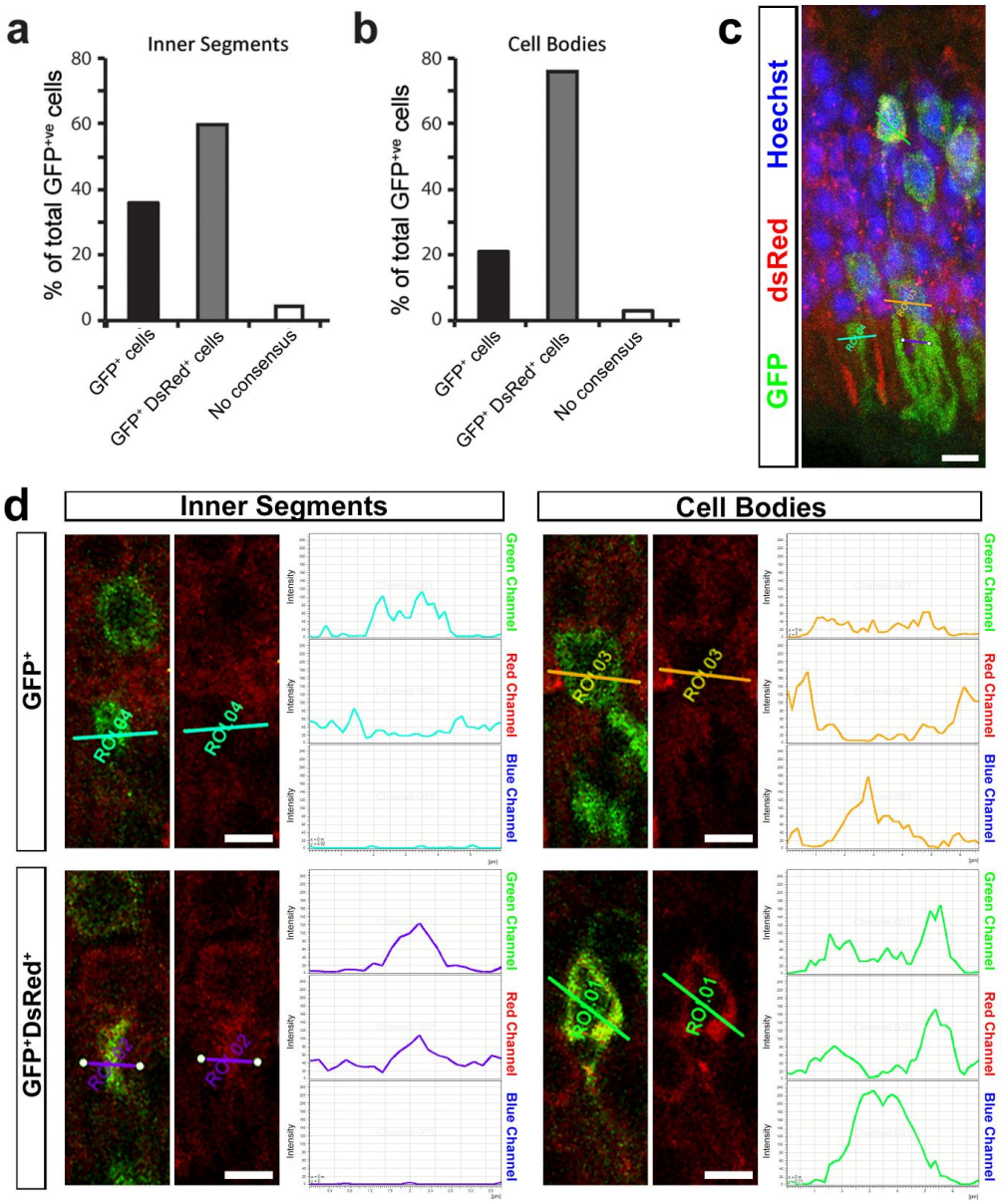

Figure B3 Donor and recipient reporters are found within some recipient cells after transplantation. NrlGFP donor cells were injected into DsRed+ recipients. 5-6 weeks post transplantation, fluorescence levels were measured in a line across the nucleus or inner segment of a GFP+ cell in recipient ONL by two assessors.

a,b The proportion of analysed cells which expressed GFP only (GFP+), or both DsRed and GFP (GFP+/DsRed+), looking at the expression levels in inner segments (a) and cell bodies (b). 36% of GFP+ inner segments were identified as showing an increase in GFP signal and a concomitant decrease in DsRed fluorescence, while 60% showed unchanged or increased DsRed signal, indicating a cell containing both reporters.

c GFP+ cells in the recipient ONL, showing the region of interest (ROI) lines used to assess fluorescence levels.

d The ROIs in (c) showing both nuclei and inner segments displaying GFP+ only (upper) and GFP+/DsRed+ (lower) patterns of fluorescence.

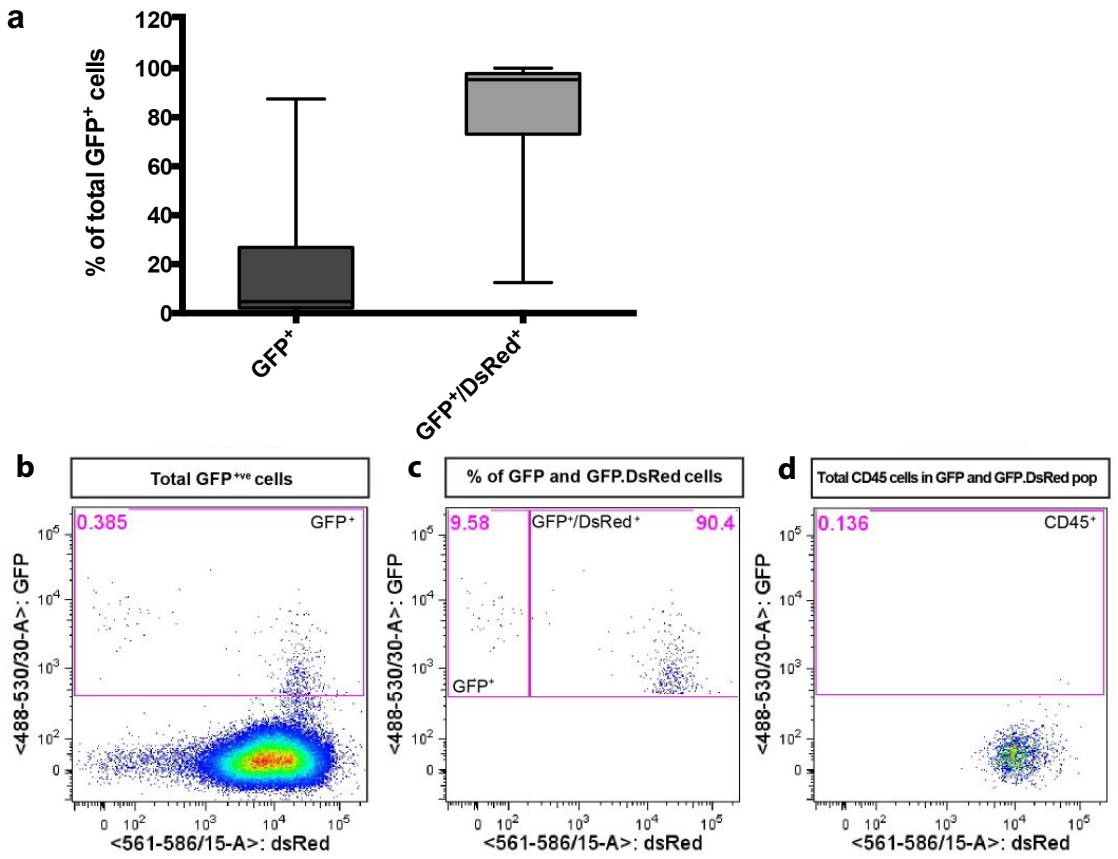

Figure B4 Host and donor-derived reporter proteins can be found in host cells after transplantation, as shown by flow cytometry DsRed retinas received transplantation of NrlGFP post-mitotic photoreceptor precursor cells. 5-6 weeks post transplantation retinas were dissociated and examined by flow cytometry for the presence of each reporter.

a Box plots showing median and range for % of GFP+ only and GFP/DsRed photoreceptors in each recipient retina analysed.

b-d Fluorescence plots showing DsRed (x-axis) and GFP (y-axis) fluorescence strength.

b In dissociated recipient retina the majority of cells expressed only DsRed, with some cells expressing GFP (here 0.385%).

c Of the GFP+ cells isolated, the majority (here 90.4%) also expressed DsRed (right hand side), indicating that they are recipient cells having taken up GFP from donor cells. A minority expressed only GFP.

d Only 0.016% of GFP+DsRed+ cells were also CD45+ (0.136% of the total CD45+ population), indicating that these cells were not macrophages or other leukocytes.

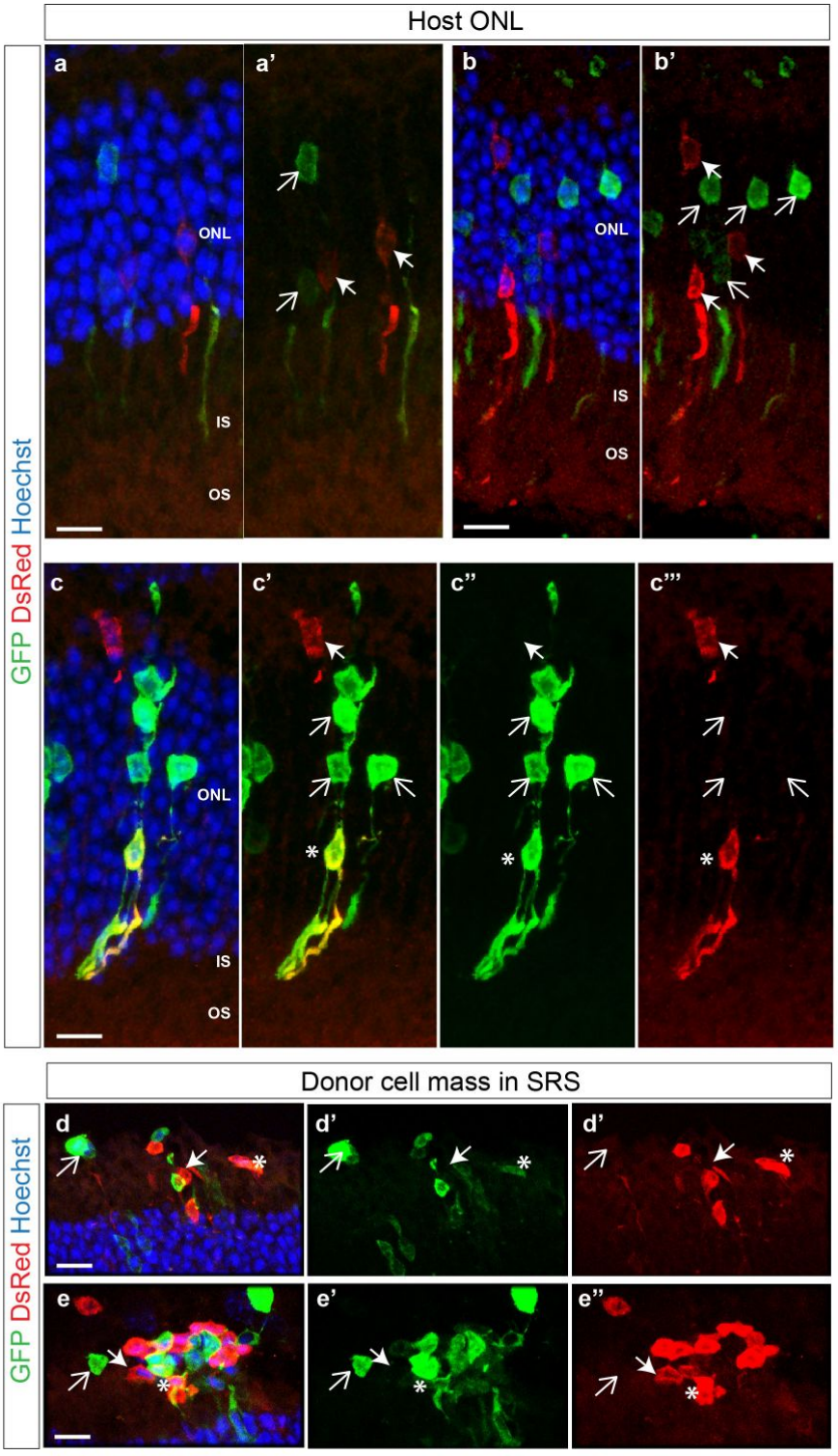

Figure B5 Material transfer involves interaction between donor and host photoreceptors A mixed population of NrlGFP and DsRed donor cells (sorted to enrich photoreceptor precursor cells by labelling for CD73) were injected into WT and Gnat1-/- recipients. GFP+ (open arrow) and DsRed+ (closed arrow) cells were found in mixed combinations in recipient ONL, and not in colour-concordant columns (a-c). Occasional cells in the host retina were seen to express both reporters (c, *). Similarly, in the subretinal space (d), cell masses with cells expressing GFP or DsRed were found, with very occasional cells expressing both. Scale bar 10µm.

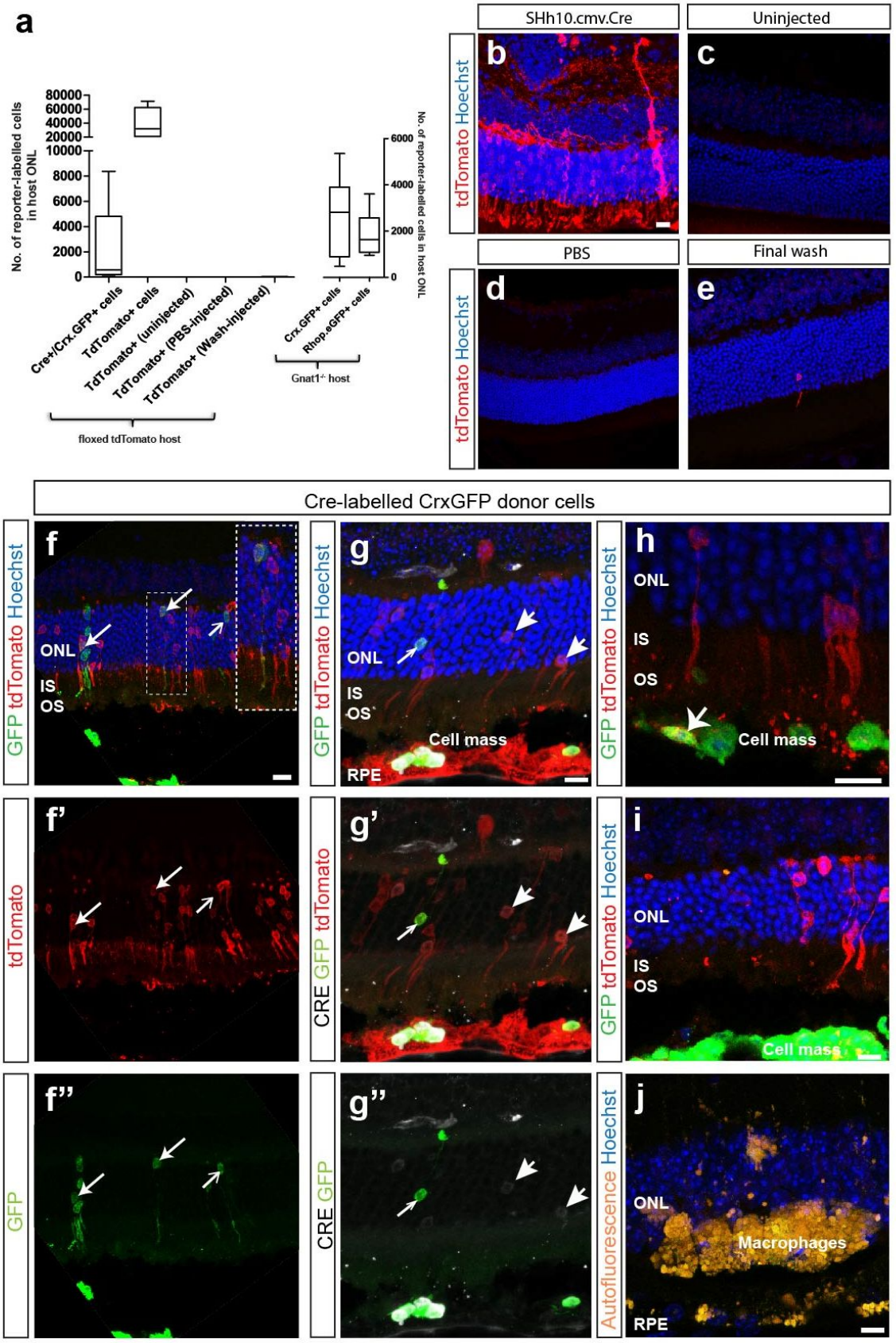
a
No. of reporter-labelled cells in host ONL
80000
60000
40000
20000
10000
8000
6000
4000
2000
0
No. of reporter-labelled cells in host ONL
6000
4000
2000
0
Cre+/Crx.GFP+ cells
TdTomato+ cells
TdTomato+ (uninjected)
TdTomato+ (PBS-injected)
TdTomato+ (Wash-injected)
Crx.GFP+ cells
Rhop.eGFP+ cells
Gnat1-/- host
floxed tdTomato host
SHh10.cmv.Cre
Uninjected
b
c
tdTomato Hoechst
PBS
Final wash
d
e
tdTomato Hoechst
Cre-labelled CrxGFP donor cells
GFP tdTomato Hoechst
f
ONL
IS
OS
g
ONL
IS
OS
Cell mass
RPE
h
ONL
IS
OS
Cell mass
tdTomato
f'
CRE GFP tdTomato
g'
GFP tdTomato Hoechst
i
ONL
IS
OS
Cell mass
GFP
f''
CRE GFP
g''
Autofluorescence Hoechst
j
ONL
Macrophages
RPE

Figure B6 Wide-spread recombination and expression of floxed reporters after transplantation of Cre-expressing donor cells

Adult floxed tdTomato reporter mouse retina received transplantation of CrxGFP+ donor cells virally transduced to produce Cre recombinase. Scale bars 10µm.

a Box plot showing reporter-labelled photoreceptors in recipient retina 5-6 weeks after transplantation.

b-e Injection of ShH10.CMV.iCre virus induced tdTomato expression (b). Injection of the final supernatant (e) from cell preparation led to very few tdTomato+ cells (22 +/- 20 cells per eye), indicating virus carryover did not occur in large amounts. No tdTomato expression was seen in uninjected (c) or PBS-injected (d) eyes.

f Cells expressing both GFP and tdTomato were seen in recipient ONL after transplantation, indicating transfer of both Cre and GFP from donor cells and recombination in recipient cells. Significantly higher numbers of tdTomato+ cells not also expressing GFP are seen than GFP+ cells (approximately 18-fold, see (a)), in particular close to the subretinal cell mass, indicating that more cells have received donor-derived material than contain GFP at any one time, whereas Cre recombination is permanent. GFP+TdTomato+ cells can be seen surrounded by GFP-TdTomato+ cells (Insert).

g Immunostaining for Cre shows robust expression in donor cells in the subretinal space and weaker presence in some reporter labelled cells within recipient retina.

h Some cells in the subretinal cell mass expressed GFP and tdTomato, indicating bidirectional material transfer.

i Cells expressing tdTomato were found in areas without GFP+ cells but with donor-derived cells in the subretinal space.

j Few if any cells expressing either reporter were seen in retinas where rejection of the cell mass occurred.

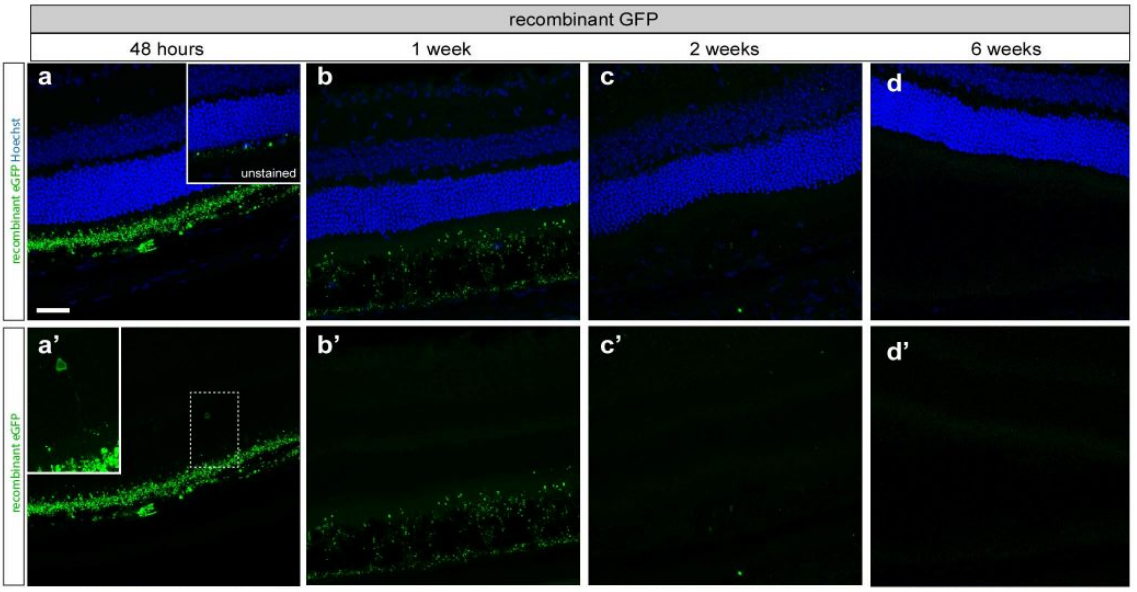
recombinant GFP
48 hours
1 week
2 weeks
6 weeks
a
b
c
d
unstained
recombinant eGFP Hoechst
a'
b'
c'
d'
recombinant eGFP

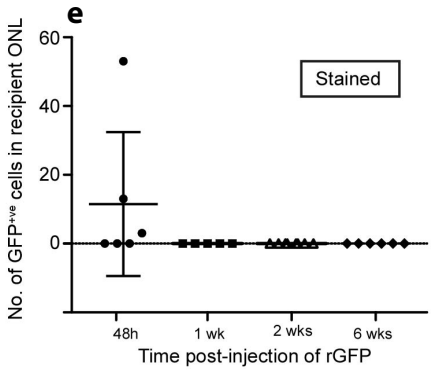
e
No. of GFP+ve cells in recipient ONL
60
40
20
0
Stained
48h
1 wk
2 wks
6 wks
Time post-injection of rGFP

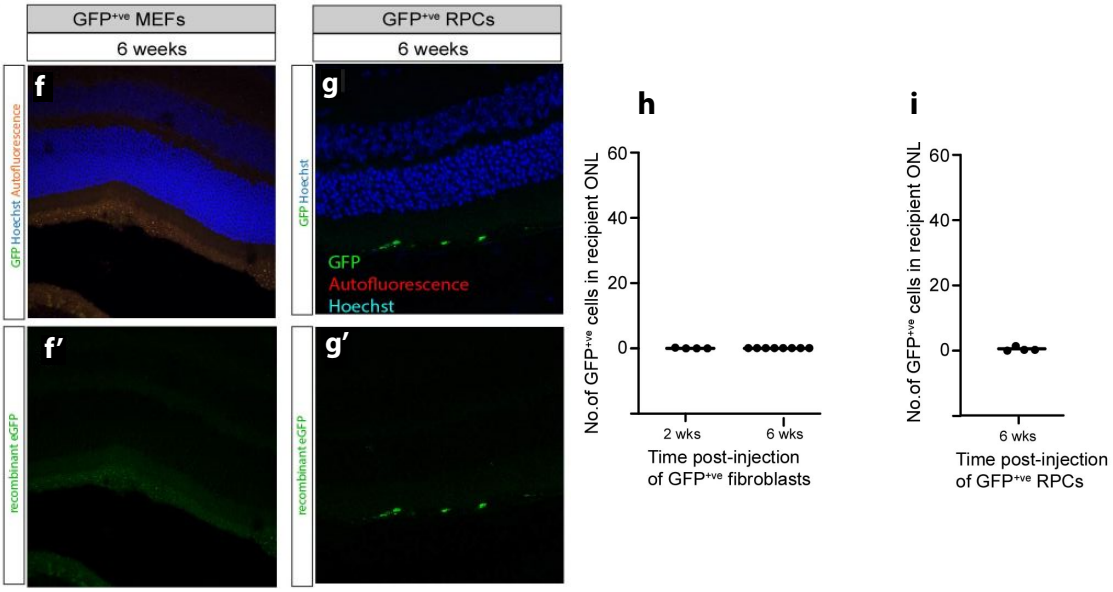
GFP+ve MEFs
6 weeks
GFP+ve RPCs
6 weeks
f
g
GFP Hoechst Autofluorescence
GFP Hoechst
GFP
Autofluorescence
Hoechst
f'
g'
recombinant eGFP
h
No.of GFP+ve cells in recipient ONL
60
40
20
0
2 wks
6 wks
Time post-injection
of GFP+ve fibroblasts
i
No.of GFP+ve cells in recipient ONL
60
40
20
0
6 wks
Time post-injection
of GFP+ve RPCs

Figure B7 Material transfer is specific to photoreceptor precursor donor cells, and not the result of free protein uptake from the environment

a-e Adult retinas injected with recombinant eGFP show very few GFP+ cells in recipient retina. Residual eGFP is seen at short periods after injection (48h, 1 week). The numbers of GFP+ cells seen are shown in (e), they are seen only at 48h after injection, and only after immunostaining to enhance eGFP signal.

f-i Injection of other GFP+ cell types does not result in material transfer. GFP+ mouse embryonic fibroblasts did not survive in the retinal space after transplantation (f, h) in any recipient retinas after 2 or 6 weeks, although autofluorescent macrophages were seen.

GFP+ retinal precursor cells from cba.GFP+ mice were transplanted into adult Gnat1$^{-/-}$ recipients (g,i). While donor cells were found in the subretinal space, in only one of four eyes were any GFP+ cells (3) found in the recipient ONL.

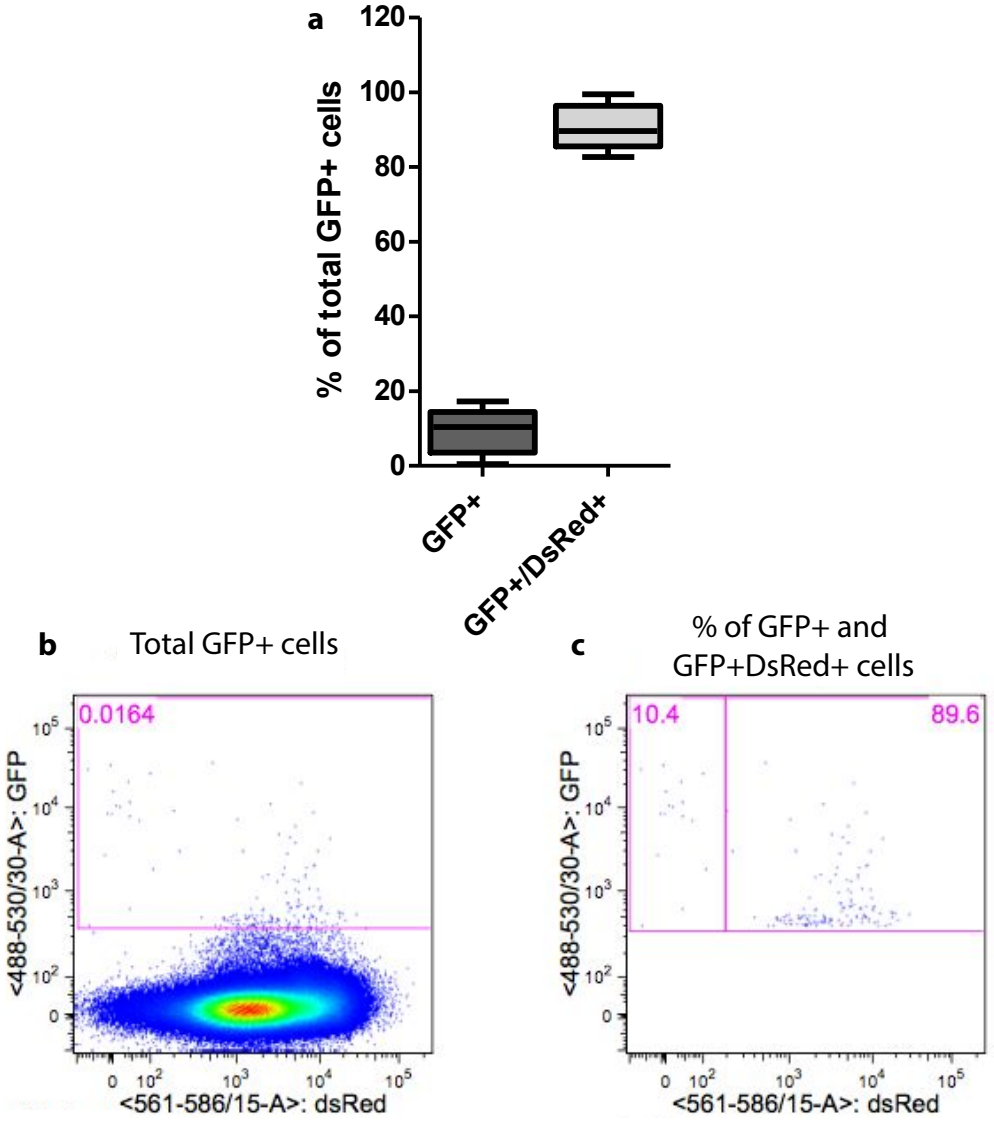

Figure B8 Preliminary data shows evidence for material transfer using Nrl$^{-/-}$ donor cells

DsRed retinas received transplantation of 200,000 Nrl$^{-/-}$NrlGFP post-mitotic photoreceptor precursor cells (5 retinas, two occasions). 2 weeks post transplantation, retinas were dissociated and examined by flow cytometry for the presence of each fluorescence reporter.

a Box plots showing median and range for % of GFP+ only and GFP+/DsRed+ photoreceptors in each recipient retina analysed.

b-c Fluorescence plots showing DsRed (x-axis) and GFP (y-axis) fluorescence strength for an example retina.

b In dissociated recipient retina the majority of cells expressed only DsRed, with some cells expressing GFP (here 0.0164%, 154 cells).

c Of the GFP+ cells isolated, the majority (here 89.6%) also expressed DsRed, indicating that they are recipient cells having taken up GFP from donor cells. A minority expressed only GFP.

Bibliography

Aghaizu, N.D., PhD Thesis 2016. Mechanisms of rod photoreceptor motility in development and following transplantation.

Akimoto, M., Cheng, H., Zhu, D., Brzezinski, J. a, Khanna, R., Filippova, E., Oh, E.C.T., Jing, Y., Linares, J.-L., Brooks, M., Zareparsi, S., Mears, A.J., Hero, A., Glaser, T., Swaroop, A., 2006. Targeting of GFP to newborn rods by Nrl promoter and temporal expression profiling of flow-sorted photoreceptors. Proc. Natl. Acad. Sci. U. S. A. 103, 3890–5. doi:10.1073/pnas.0508214103

Alexiades, M.R., Cepko, C., 1996. Quantitative analysis of proliferation and cell cycle length during development of the rat retina. Dev. Dyn. 205, 293–307. doi:10.1002/(SICI)1097-0177(199603)205:3<293::AID-AJA9>3.0.CO;2-D

Ali, R.R., Sarra, G.M., Stephens, C., Alwis, M.D., Bainbridge, J.W., Munro, P.M., Fauser, S., Reichel, M.B., Kinnon, C., Hunt, D.M., Bhattacharya, S.S., Thrasher, a J., 2000. Restoration of photoreceptor ultrastructure and function in retinal degeneration slow mice by gene therapy. Nat. Genet. 25, 306–10. doi:10.1038/77068

Altshuler, D., Lo Turco, J.J., Rush, J., Cepko, C., 1993. Taurine promotes the differentiation of a vertebrate retinal cell type in vitro. Development 119, 1317–1328.

Alvarez-Dolado, M., Pardal, R., Garcia-Verdugo, J.M., Fike, J.R., Lee, H.O., Pfeffer, K., Lois, C., Morrison, S.J., Alvarez-Buylla, A., 2003. Fusion of bone-marrow-derived cells with Purkinje neurons, cardiomyocytes and hepatocytes. Nature 425, 968–973. doi:10.1038/nature02069

Applebury, M.L., Antoch, M.P., Baxter, L.C., Chun, L.L., Falk, J.D., Farhangfar, F., Kage, K., Krzystolik, M.G., Lyass, L. A, Robbins, J.T., 2000. The murine cone photoreceptor: a single cone type expresses both S and M opsins with retinal spatial patterning. Neuron 27, 513–523.

Araki, M., 2007. Regeneration of the amphibian retina: Role of tissue interaction and related signaling molecules on RPE transdifferentiation. Dev. Growth Differ. 49, 109–120. doi:10.1111/j.1440-169X.2007.00911.xs

Arshavsky, V.Y., 2002. Like night and day: Rods and cones have different pigment regeneration pathways. Neuron 36, 1–3. doi:10.1016/S0896-6273(02)00937-6

Azadi, S., Ca, A.R., 2002. Thyroid-b2 and the retinoid RAR-a , RXR-c and ROR-b2 receptor mRNAs ; expression pro ¢ les in mouse retina , retinal explants and neocortex 13, 6–11.

Bainbridge, J.W., Smith, A.J., Barker, S.S., Robbie, S., Henderson, R., Balaggan, K., Viswanathan, A., Holder, G.E., Stockman, A., Tyler, N., Petersen-Jones, S., Bhattacharya, S.S., Thrasher, A.J., Fitzke, F.W., Carter, B.J., Rubin, G.S., Moore, A.T., Ali, R.R., 2008. Effect of gene therapy on visual function in Leber's congenital amaurosis. N Engl J Med 358, 2231–2239. doi:10.1056/NEJMoa0802268

Bainbridge, J.W.B., Mehat, M.S., Sundaram, V., Robbie, S.J., Barker, S.E., Ripamonti, C., 2015. Long-Term Effect of Gene Therapy on Leber ' s Congenital Amaurosis. N. Engl. J. Med. 372, 1887–1897. doi:10.1056/NEJMoa1414221.Long-Term

Barber, A.C., Hippert, C., Duran, Y., West, E.L., Bainbridge, J.W.B., Warre-cornish, K., Luhmann, U.F.O., Lakowski, J., Sowden, J.C., 2013. Repair of the degenerate retina by photoreceptor transplantation. doi:10.1073/pnas.1212677110/-/DCSupplemental.www.pnas.org/cgi/doi/10.1073/pnas.1212677110

Barnea-Cramer, A.O., Wang, W., Lu, S.-J., Singh, M.S., Luo, C., Huo, H., McClements, M.E., Barnard, A.R., MacLaren, R.E., Lanza, R., Hartong, D.T., Berson, E.L., Dryja, T.P., Barber, A.C., Luo, J., Singh, M.S., Pearson, R.A., Lamba, D.A., Gust, J., Reh, T.A., Schmitt, S., Schwartz, S.D., Schwartz, S.D., Song, W.K., Lamba, D.A., Karl, M.O., Ware, C.B., Reh, T.A., Osakada, F., Ikeda, H., Sasai, Y., Takahashi, M., Hirami, Y., Lamba, D.A., Zhou, L., Torre, A. La, Lamba, D.A., Jayabalu, A., Reh, T.A., Eiraku, M., Sasai, Y., Jin, Z.B., Okamoto, S., Xiang, P., Takahashi, M., Osakada, F., Takahashi, K., Meyer, J.S., Mellough, C.B., Sernagor, E., Moreno-Gimeno, I., Steel, D.H., Lako, M., Nakano, T., Decembrini, S., Koch, U., Radtke, F., Moulin, A., Arsenijevic, Y., Reichman, S., Zhong, X., Kaewkhaw, R., Zhou, S., Gouras, P., Du, J., Kjeldbye, H., Yamamoto, S., Zack, D.J., Kwan, A.S., Wang, S., Lund, R.D., Tucker, B.A., Gonzalez-Cordero, A., Eberle, D., Schubert, S., Postel, K., Corbeil, D., Ader, M., Koso, H., Lakowski, J., Eberle, D., Santos-Ferreira, T., Grahl, S., Ader, M., Lakowski, J., Warren, L., Ni, Y., Wang, J., Guo, X., Bowes, C., Farber, D.B., Lolley, R.N., Rong, H., Craft, C.M., Chang, B., Assawachananont, J., Cehajic-Kapetanovic, J., West, E.L., Lakowski, J., MacLaren, R.E., Yao, J., Eng, L.F., Ghirnikar, R.S., Dahl, D., Zhang, Y., Arner, K., Ehinger, B., Perez, M.T., Harvey, R.J., De'Sperati, C., Strata, P., Misslin, R., Belzung, C., Vogel, E., Busskamp, V., Swaroop, A., Kim, D., Forrest, D., Haider, N.B., Stingl, K., Zrenner, E., Cramer, A.O., MacLaren, R.E., Thompson, S., Sun, J., Punzo, C., Cepko, C., 2016. Function of human pluripotent stem cell-derived photoreceptor progenitors in blind mice. Sci. Rep. 6, 29784. doi:10.1038/srep29784

Bartsch, U., Oriyakhel, W., Kenna, P.F., Linke, S., Richard, G., Petrowitz, B., Humphries, P., Farrar, G.J., Ader, M., 2008. Retinal cells integrate into the outer nuclear layer and differentiate into mature photoreceptors after subretinal transplantation into adult mice. Exp. Eye Res. 86, 691–700. doi:10.1016/j.exer.2008.01.018

Baye, L.M., Link, B. a, 2008. Nuclear migration during retinal development. Brain Res. 1192, 29–36. doi:10.1016/j.brainres.2007.05.021

Berson, E., 2007. Long-term visual prognoses in patients with retinitis pigmentosa: the Ludwig von Sallmann lecture. Exp. Eye Res. 85, 7–14. doi:10.1016/j.exer.2007.03.001.Long-Term

Birch, D.G., Anderson, J.L., Fish, G.E., 1999. Yearly rates of rod and cone functional loss in retinitis pigmentosa and cone-rod dystrophy. Ophthalmology 106, 258–268. doi:10.1016/S0161-6420(99)90064-7

Blatt, M., Wiseman, S., Domany, E., 1996. Superparamagnetic Clustering of Data. Phys. Rev. Lett. 76, 3251–3254. doi:10.1103/PhysRevLett.76.3251

Boesze-Battaglia, K., 2000. Fusion between retinal rod outer segment membranes and model membranes: functional assays and role for peripherin/rds. Methods Enzymol. 316, 65–86. doi:S0076-6879(00)16717-5 [pii]

Boesze-Battaglia, K., Goldberg, A.F.X., Dispoto, J., Katragadda, M., Cesarone, G., Albert, A.D., 2003. A soluble peripherin/Rds C-terminal polypeptide promotes membrane fusion and changes conformation upon membrane association. Exp. Eye Res. 77, 505–514. doi:10.1016/S0014-4835(03)00151-9

Boesze-Battaglia, K., Kong, F., Lamba, O.P., Stefano, F.P., Williams, D.S., 1997. Purification and light-dependent phosphorylation of a candidate fusion protein, the photoreceptor cell peripherin/rds. Biochemistry 36, 6835–6846. doi:10.1021/bi9627370

Bowmaker, J.K., Dartnall, H.J., 1980. Visual pigments of rods and cones in a human retina. J. Physiol. 298, 501–11. doi:10.1017/CBO9781107415324.004

Bringmann, A., Pannicke, T., Grosche, J., Francke, M., Wiedemann, P., Skatchkov, S.N., Osborne, N.N., Reichenbach, A., 2006. Müller cells in the healthy and diseased retina. Prog. Retin. Eye Res. 25, 397–424. doi:10.1016/j.preteyeres.2006.05.003

Brooks, M.J., Rajasimha, H.K., Roger, J.E., Swaroop, A., 2011. Next-generation sequencing facilitates quantitative analysis of wild-type and Nrl(-/-) retinal transcriptomes. Mol. Vis. 17, 3034–54.

Brzezinski, J.A., Reh, T.A., 2015. Photoreceptor cell fate specification in vertebrates. Development 142, 3263–3273. doi:10.1242/dev.127043

Brzezinski, J.A. th, Kim, E.J., Johnson, J.E., Reh, T.A., 2011. Ascl1 expression defines a subpopulation of lineage-restricted progenitors in the mammalian retina. Development 138, 3519–3531. doi:10.1242/dev.064006

Burke, B., 2012. It takes KASH to hitch to the SUN. Cell 149, 961–3. doi:10.1016/j.cell.2012.05.004

Burke, B., Roux, K.J., 2009. Nuclei take a position: managing nuclear location. Dev. Cell 17, 587–97. doi:10.1016/j.devcel.2009.10.018

Buzsáki, G., 2004. Large-scale recording of neuronal ensembles. Nat. Neurosci. 7, 446–451. doi:10.1038/nn1233

Cepko, C.L., Austin, C.P., Yang, X., Alexiades, M., Ezzeddine, D., 1996. Cell fate determination in the vertebrate retina. Proc. Natl. Acad. Sci. U. S. A. 93, 589–95. doi:10.1017/CBO9781107415324.004

Chang, B., Grau, T., Dangel, S., Hurd, R., Jurklies, B., Sener, E.C., Andreasson, S., Dollfus, H., Baumann, B., Bolz, S., Artemyev, N., Kohl, S., Heckenlively, J., Wissinger, B., 2009. A homologous genetic basis of the murine cpfl1 mutant and human achromatopsia linked to mutations in the PDE6C gene. Proc. Natl. Acad. Sci. U. S. A. 106, 19581–6. doi:10.1073/pnas.0907720106

Chen, J., 2005. The Rod Photoreceptor-Specific Nuclear Receptor Nr2e3 Represses

Transcription of Multiple Cone-Specific Genes. J. Neurosci. 25, 118–129. doi:10.1523/JNEUROSCI.3571-04.2005

Chen, J., Makino, C.L., Peachey, N.S., Baylor, D.A., Simon, M.I., 1995. Mechanisms of rhodopsin inactivation in vivo as revealed by a COOH-terminal truncation mutant. Science (80-.). 267, 374–377. doi:10.1126/science.7824934

Chen, S., Wang, Q.-L., Nie, Z., Sun, H., Lennon, G., Copeland, N.G., Gilbert, D.J., Jenkins, N.A., Zack, D.J., 1997. Crx, a Novel Otx-like Paired-Homeodomain Protein, Binds to and Transactivates Photoreceptor Cell-Specific Genes. Neuron 19, 1017–1030. doi:10.1016/S0896-6273(00)80394-3

Cheng, H., Aleman, T.S., Cideciyan, A. V., Khanna, R., Jacobson, S.G., Swaroop, A., 2006. In vivo function of the orphan nuclear receptor NR2E3 in establishing photoreceptor identity during mammalian retinal development. Hum. Mol. Genet. 15, 2588–2602. doi:10.1093/hmg/ddl185

Cheng, H., Khan, N.W., Roger, J.E., Swaroop, A., 2011. Excess cones in the retinal degeneration rd7 mouse, caused by the loss of function of orphan nuclear receptor Nr2e3, originate from early-born photoreceptor precursors. Hum. Mol. Genet. 20, 4102–15. doi:10.1093/hmg/ddr334

Cheng, H., Khanna, H., Oh, E.C.T., Hicks, D., Mitton, K.P., Swaroop, A., 2004. Photoreceptor-specific nuclear receptor NR2E3 functions as a transcriptional activator in rod photoreceptors. Hum. Mol. Genet. 13, 1563–1575. doi:10.1093/hmg/ddh173

Chiu, M., Zack, D., Wang, Y., Nathans, J., 1994. Murine and bovine blue cone pigment genes: cloning and characterization of two new members of the S family of visual pigments. Genomics.

Chiu, M.I., Nathans, J., 1994. A sequence upstream of the mouse blue visual pigment gene directs blue cone-specific transgene expression in mouse retinas. Vis. Neurosci. 11, 773–780.

Chung, S.H., Shen, W., Gillies, M.C., 2013. Laser Capture Microdissection-Directed Profiling of Glycolytic and mTOR Pathways in Areas of Selectively Ablated Müller Cells in the Murine Retina. Investig. Opthalmology Vis. Sci. 54, 6578. doi:10.1167/iovs.13-12311

Corbo, J.C., Cepko, C.L., 2005. A hybrid photoreceptor expressing both rod and cone genes in a mouse model of enhanced S-cone syndrome. PLoS Genet. 1, e11. doi:10.1371/journal.pgen.0010011

Cornish, E.E., Natoli, R.C., Hendrickson, A., Provis, J.M., 2004. Differential distribution of fibroblast growth factor receptors (FGFRs) on foveal cones: FGFR-4 is an early marker of cone photoreceptors. Mol. Vis. 10, 1–14.

Craig, S.E.L., Calinescu, A.-A., Hitchcock, P.F., 2008. Identification of the molecular signatures integral to regenerating photoreceptors in the retina of the zebra fish. J. Ocul. Biol. Dis. Infor. 1, 73–84. doi:10.1007/s12177-008-9011-5

Curcio, C.A., Sloan, K.R., Kalina, R.E., Hendrickson, A.E., 1990. Human Photoreceptor Topography . J. Comp. Neurol. 523, 497–523.

Daniele, L.L., Lillo, C., Lyubarsky, A.L., Nikonov, S.S., Philp, N., Mears, A.J., Swaroop, A., Williams, D.S., Pugh, E.N., 2005. Cone-like morphological, molecular, and electrophysiological features of the photoreceptors of the Nrl knockout mouse. Invest. Ophthalmol. Vis. Sci. 46, 2156–67. doi:10.1167/iovs.04-1427

Davey, N.J., Ellaway, P.H., Stein, R.B., 1986. Statistical limits for detecting change in the cumulative sum derivative of the peristimulus time histogram. J. Neurosci. Methods 17, 153–66. doi:10.1016/0165-0270(86)90068-3

de Jong, P.T.V.M., 2006. Age-Related Macular Degeneration. N. Engl. J. Med. 355, 1474–1485. doi:10.1056/NEJMra062326

Decembrini, S., Cananzi, M., Gualdoni, S., Battersby, A., Allen, N., Pearson, R.A., Ali, R.R., De Coppi, P., Sowden, J.C., 2011. Comparative analysis of the retinal potential of embryonic stem cells and amniotic fluid-derived stem cells. Stem Cells Dev. 20, 851–63. doi:10.1089/scd.2010.0291

Del Bene, F., Wehman, A.M., Link, B. a, Baier, H., 2008. Regulation of neurogenesis by interkinetic nuclear migration through an apical-basal notch gradient. Cell 134, 1055–65. doi:10.1016/j.cell.2008.07.017

Den Hollander, A.I., Ghiani, M., De Kok, Y.J.M., Wijnholds, J., Ballabio, A., Cremers, F.P.M., Broccoli, V., 2001. Isolation of Crb1, a mouse homologue of Drosophila crumbs, and analysis of its expression pattern in eye and brain. Mech. Dev. 110, 203–207. doi:10.1016/S0925-4773(01)00568-8

Di Foggia, V., Makwana, P., Ali, R.R., Sowden, J.C., 2016. Induced Pluripotent Stem Cell Therapies for Degenerative Disease of the Outer Retina: Disease Modeling and Cell Replacement. J. Ocul. Pharmacol. Ther. 0, jop.2015.0143. doi:10.1089/jop.2015.0143

Diaspro, A., Chirico, G., Collini, M., 2005. Two-photon fluorescence excitation and related techniques in biological microscopy. Q. Rev. Biophys. 38, 97–166. doi:10.1017/S0033583505004129

Doxsey, S., 2001. Re-evaluating centrosome function. Nat. Rev. Mol. Cell Biol. 2, 688–698. doi:10.1038/35089575

Eberle, D., Kurth, T., Santos-Ferreira, T., Wilson, J., Corbeil, D., Ader, M., 2012. Outer segment formation of transplanted photoreceptor precursor cells. PLoS One 7, e46305. doi:10.1371/journal.pone.0046305

Ebrey, T., Koutalos, Y., 2001. Vertebrate Photoreceptors. Prog. Retin. Eye Res. 20, 49–94. doi:10.1016/S1350-9462(00)00014-8

Eiraku, M., Takata, N., Ishibashi, H., Kawada, M., Sakakura, E., Okuda, S., Sekiguchi, K., Adachi, T., Sasai, Y., 2011. Self-organizing optic-cup morphogenesis in three-dimensional culture. Nature 472, 51–56. doi:10.1038/nature09941

Ezzeddine, Z.D., Yang, X., DeChiara, T., Yancopoulos, G., Cepko, C.L., 1997. Postmitotic cells fated to become rod photoreceptors can be respecified by CNTF treatment of the retina. Development 124, 1055–67.

Farjo, R., Skaggs, J.S., Nagel, B.A., Quiambao, A.B., Nash, Z.A., Fliesler, S.J., Naash, M.I.,

2006. Retention of function without normal disc morphogenesis occurs in cone but not rod photoreceptors. J. Cell Biol. 173, 59–68. doi:10.1083/jcb.200509036

Fei, Y., 2003. Development of the cone photoreceptor mosaic in the mouse retina revealed by fluorescent cones in transgenic mice. Mol. Vis. 9, 31–42.

Fei, Y., Hughes, T.E., 2001. Transgenic expression of the jellyfish green fluorescent protein in the cone photoreceptors of the mouse. Vis. Neurosci. 18, 615–623.

Firestone, A.J., Weinger, J.S., Maldonado, M., Barlan, K., Langston, L.D., O'Donnell, M., Gelfand, V.I., Kapoor, T.M., Chen, J.K., 2012. Small-molecule inhibitors of the AAA+ ATPase motor cytoplasmic dynein. Nature 484, 125–129. doi:10.1038/nature10936

Franze, K., Grosche, J., Skatchkov, S.N., Schinkinger, S., Foja, C., Schild, D., Uckermann, O., Travis, K., Reichenbach, A., Guck, J., 2007. Muller cells are living optical fibers in the vertebrate retina. Proc. Natl. Acad. Sci. 104, 8287–8292. doi:10.1073/pnas.0611180104

Fujieda, H., Bremner, R., Mears, A.J., Sasaki, H., 2009. Retinoic acid receptor-related orphan receptor alpha regulates a subset of cone genes during mouse retinal development. J. Neurochem. 108, 91–101. doi:10.1111/j.1471-4159.2008.05739.x

Furukawa, T., Morrow, E.M., Cepko, C.L., 1997. Crx, a novel otx-like homeobox gene, shows photoreceptor-specific expression and regulates photoreceptor differentiation. Cell 91, 531–541. doi:10.1016/S0092-8674(00)80439-0

Furukawa, T., Morrow, E.M., Li, T., Davis, F.C., Cepko, C.L., 1999. Retinopathy and attenuated circadian entrainment in Crx-deficient mice. Nat. Genet. 23, 466–470. doi:10.1038/70591

Gallina, D., Todd, L., Fischer, A.J., 2014. A comparative analysis of Müller glia-mediated regeneration in the vertebrate retina. Exp. Eye Res. 123, 121–130. doi:10.1016/j.exer.2013.06.019

Ghosh, F., Juliusson, B., Arnér, K., Ehinger, B., 1999. Partial and full-thickness neuroretinal transplants. Exp. Eye Res. 68, 67–74. doi:10.1006/exer.1998.0582

Ghosh, F., Wong, F., Johansson, K., Bruun, A., Petters, R.M., 2004. Transplantation of Full-Thickness Retina in the Rhodopsin Transgenic Pig. Retina 24, 98–109. doi:10.1097/00006982-200402000-00014

Ghosh, K.K., Bujan, S., Haverkamp, S., Feigenspan, A., Wässle, H., 2004. Types of Bipolar Cells in the Mouse Retina. J. Comp. Neurol. 469, 70–82. doi:10.1002/cne.10985

Gong, S., Zheng, C., Doughty, M.L., Losos, K., Didkovsky, N., Schambra, U.B., Nowak, N.J., Joyner, A., Leblanc, G., Hatten, M.E., Heintz, N., 2003. A gene expression atlas of the central nervous system based on bacterial artificial chromosomes. Nature 425, 917–925.

Gonzalez-Cordero, A., West, E.L., Pearson, R. a, Duran, Y., Carvalho, L.S., Chu, C.J., Naeem, A., Blackford, S.J.I., Georgiadis, A., Lakowski, J., Hubank, M., Smith, A.J., Bainbridge, J.W.B., Sowden, J.C., Ali, R.R., 2013. Photoreceptor precursors derived from three-dimensional embryonic stem cell cultures integrate and mature within adult

degenerate retina. Nat. Biotechnol. 31, 741–747. doi:10.1038/nbt.2643

Gosens, I., den Hollander, A.I., Cremers, F.P.M., Roepman, R., 2008. Composition and function of the Crumbs protein complex in the mammalian retina. Exp. Eye Res. 86, 713–726. doi:10.1016/j.exer.2008.02.005

Graca, A.B., 2016. Anna's Thesis.

Grinvald, A., Lieke, E., Frostig, R.D., Gilbert, C.D., Wiesel, T.N., 1986. Functional architecture of cortex revealed by optical imaging of intrinsic signals. Nature 324, 361–364. doi:10.1038/324361a0

Guadagni, V., Novelli, E., Piano, I., Gargini, C., Strettoi, E., 2015. Pharmacological approaches to retinitis pigmentosa: A laboratory perspective. Prog. Retin. Eye Res. 48, 62–81. doi:10.1016/j.preteyeres.2015.06.005

Gualdoni, S., Baron, M., Lakowski, J., Decembrini, S., Smith, A.J., Pearson, R.A., Ali, R.R., Sowden, J.C., 2010. Adult ciliary epithelial cells, previously identified as retinal stem cells with potential for retinal repair, fail to differentiate into new rod photoreceptors. Stem Cells 28, 1048–1059. doi:10.1002/stem.423

Haider, N.B., Demarco, P., Nystuen, A.M., Huang, X., Smith, R.S., McCall, M. a, Naggert, J.K., Nishina, P.M., 2006. The transcription factor Nr2e3 functions in retinal progenitors to suppress cone cell generation. Vis. Neurosci. 23, 917–29. doi:10.1017/S095252380623027X

Haider, N.B., Jacobson, S.G., Cideciyan, a V, Swiderski, R., Streb, L.M., Searby, C., Beck, G., Hockey, R., Hanna, D.B., Gorman, S., Duhl, D., Carmi, R., Bennett, J., Weleber, R.G., Fishman, G. a, Wright, a F., Stone, E.M., Sheffield, V.C., 2000. Mutation of a nuclear receptor gene, NR2E3, causes enhanced S cone syndrome, a disorder of retinal cell fate. Nat. Genet. 24, 127–31. doi:10.1038/72777

Haider, N.B., Naggert, J.K., Nishina, P.M., 2001. Excess cone cell proliferation due to lack of a functional NR2E3 causes retinal dysplasia and degeneration in rd7/rd7 mice. Hum. Mol. Genet. 10, 1619–26.

Hajrasouliha, A.R., Jiang, G., Lu, Q., Lu, H., Kaplan, H.J., Zhang, H.-G., Shao, H., 2013. Exosomes from retinal astrocytes contain antiangiogenic components that inhibit laser-induced choroidal neovascularization. J. Biol. Chem. 288, 28058–67. doi:10.1074/jbc.M113.470765

Hartline, H.K., 1969. Visual receptors and retinal interaction. Science 164, 270–8. doi:10.1017/CBO9781107415324.004

Hartong, D.T., Berson, E.L., Dryja, T.P., 2006. Retinitis pigmentosa 1795–1809. doi:10.1136/bmj.2.1512.1419-a

Hatten, M.E., 1987. Glial-Guided Granule Neuron Migration Video Microscopic Study in vitro : A High-Resolution 7.

Hatten, M.E., York, N., 1995. Motility and Cytoskeletal Granule Neurons Organization of Migrating Cerebellar 5.

Hauswirth, W.W., Aleman, T.S., Kaushal, S., Cideciyan, A. V, Schwartz, S.B., Wang, L.,

Conlon, T.J., Boye, S.L., Flotte, T.R., Byrne, B.J., Jacobson, S.G., 2008. Treatment of leber congenital amaurosis due to RPE65 mutations by ocular subretinal injection of adeno-associated virus gene vector: short-term results of a phase I trial. Hum. Gene Ther. 19, 979–90. doi:10.1089/hum.2008.107

Hawthorne, A.L., Wylie, C.J., Landmesser, L.T., Deneris, E.S., Silver, J., 2010. Serotonergic neurons migrate radially through the neuroepithelium by dynamin-mediated somal translocation. J. Neurosci. 30, 420–30. doi:10.1523/JNEUROSCI.2333-09.2010

Hippert, C., Graca, A.B., Barber, A.C., West, E.L., Smith, A.J., Ali, R.R., Pearson, R. a., 2015. Müller Glia Activation in Response to Inherited Retinal Degeneration Is Highly Varied and Disease-Specific. PLoS One 10, e0120415. doi:10.1371/journal.pone.0120415

Huet, S., Karatekin, E., Tran, V.S., Fanget, I., Cribier, S., Henry, J.-P., 2006. Analysis of transient behavior in complex trajectories: application to secretory vesicle dynamics. Biophys. J. 91, 3542–59. doi:10.1529/biophysj.105.080622

Iandiev, I., Biedermann, B., Bringmann, A., Reichel, M.B., Reichenbach, A., Pannicke, T., 2006. Atypical gliosis in Müller cells of the slowly degenerating rds mutant mouse retina. Exp. Eye Res. 82, 449–457. doi:10.1016/j.exer.2005.07.018

Ishikawa, Y., Mine, S., 1983. Aminoadipic acid toxic effects on retinal glial cells. Jpn. J. Ophthalmol. 27, 107–18.

Jadhav, A.P., Cho, S.-H., Cepko, C.L., 2006a. Notch activity permits retinal cells to progress through multiple progenitor states and acquire a stem cell property. Proc. Natl. Acad. Sci. U. S. A. 103, 18998–9003. doi:10.1073/pnas.0608155103

Jadhav, A.P., Mason, H. a, Cepko, C.L., 2006b. Notch 1 inhibits photoreceptor production in the developing mammalian retina. Development 133, 913–923. doi:10.1242/dev.02245

Jeon, C., Strettoi, E., Masland, R.H., 1998. The Major Cell Populations of the Mouse Retina 18, 8936–8946.

Jia, L., Oh, E.C.T., Ng, L., Srinivas, M., Brooks, M., Swaroop, A., Forrest, D., 2009. Retinoid-related orphan nuclear receptor RORbeta is an early-acting factor in rod photoreceptor development. Proc. Natl. Acad. Sci. U. S. A. 106, 17534–9. doi:10.1073/pnas.0902425106

Jiang, C., Klassen, H., Zhang, X., Young, M., 2010. Laser injury promotes migration and integration of retinal progenitor cells into host retina. Mol. Vis. 16, 983–90.

Johnson, P.T., Williams, R.R., Cusato, K., Reese, B.E., 1999. Rods and cones project to the inner plexiform layer during development. J. Comp. Neurol. 414, 1–12.

Keays, K.M., Owens, G.P., Ritchie, A.M., Gilden, D.H., Burgoon, M.P., 2005. Laser capture microdissection and single-cell RT-PCR without RNA purification. J. Immunol. Methods 302, 90–98. doi:10.1016/j.jim.2005.04.018

Kelley, M.W., Turner, J.K., Reh, T. a, 1994. Retinoic acid promotes differentiation of photoreceptors in vitro. Development 120, 2091–2102.

Kevany, B., Palczewski, K., 2010. Phagocytosis of retinal rod and cone photoreceptors.

Physiology 25, 8–15. doi:10.1152/physiol.00038.2009.Phagocytosis

Kinkl, N., Hageman, G.S., Sahel, J. a, Hicks, D., 2002. Fibroblast growth factor receptor (FGFR) and candidate signaling molecule distribution within rat and human retina. Mol. Vis. 8, 149–160.

Kinouchi, R., Takeda, M., Yang, L., Wilhelmsson, U., Lundkvist, A., Pekny, M., Chen, D.F., 2003. Robust neural integration from retinal transplants in mice deficient in GFAP and vimentin. Nat. Neurosci. 6, 863–868. doi:10.1038/nn1088

Klassen, H.J., Ng, T.F., Kurimoto, Y., Kirov, I., Shatos, M., Coffey, P., Young, M.J., 2004. Multipotent retinal progenitors express developmental markers, differentiate into retinal neurons, and preserve light-mediated behavior. Investig. Ophthalmol. Vis. Sci. 45, 4167–4173. doi:10.1167/iovs.04-0511

Koike, C., Nishida, A., Ueno, S., Saito, H., Sanuki, R., Sato, S., Furukawa, A., Aizawa, S., Matsuo, I., Suzuki, N., Kondo, M., Furukawa, T., 2007. Functional roles of Otx2 transcription factor in postnatal mouse retinal development. Mol. Cell. Biol. 27, 8318–29. doi:10.1128/MCB.01209-07

Kosodo, Y., Suetsugu, T., Suda, M., Mimori-Kiyosue, Y., Toida, K., Baba, S. a, Kimura, A., Matsuzaki, F., 2011. Regulation of interkinetic nuclear migration by cell cycle-coupled active and passive mechanisms in the developing brain. EMBO J. 30, 1690–1704. doi:10.1038/emboj.2011.81

Kruger, A., Matulla, B., Wolzt, M., Pieh, S., Strenn, K., Findl, O., Eichler, H.G., Schmetterer, L., 1998. Short-term oral pentoxifylline use increases choroidal blood flow in patients with age-related macular degeneration. Arch. Ophthalmol. (Chicago, Ill. 1960) 116, 27–30. doi:10.1128/AAC.03728-14

Kulikova, S., Abatis, M., Heng, C., Lelievre, V., 2011. Interkinetic nuclear migration: Reciprocal activities of dynein and kinesin. Cell Adh. Migr. 5, 277–279. doi:10.4161/cam.5.4.17432

Kunchithapautham, K., Coughlin, B., Crouch, R.K., Rohrer, B., 2009. Cone Outer Segment Morphology and Cone Function in the *Rpe65* $^{-/-}$ *Nrl* $^{-/-}$ Mouse Retina Are Amenable to Retinoid Replacement. Investig. Opthalmology Vis. Sci. 50, 4858. doi:10.1167/iovs.08-3008

Lakowski, J., Baron, M., Bainbridge, J., Barber, a C., Pearson, R. a, Ali, R.R., Sowden, J.C., 2010. Cone and rod photoreceptor transplantation in models of the childhood retinopathy Leber congenital amaurosis using flow-sorted Crx-positive donor cells. Hum. Mol. Genet. 19, 4545–59. doi:10.1093/hmg/ddq378

Lamba, D.A., Gust, J., Reh, T.A., 2009. Transplantation of Human Embryonic Stem Cell-Derived Photoreceptors Restores Some Visual Function in Crx-Deficient Mice. Cell Stem Cell 4, 73–79. doi:10.1016/j.stem.2008.10.015

Lee, S.-R., Kim, H.-Y., Rogowska, J., Zhao, B.-Q., Bhide, P., Parent, J.M., Lo, E.H., 2006. Involvement of matrix metalloproteinase in neuroblast cell migration from the subventricular zone after stroke. J. Neurosci. 26, 3491–5.

doi:10.1523/JNEUROSCI.4085-05.2006

Leung, L., Klopper, a. V., Grill, S.W., Harris, W. a., Norden, C., 2012. Apical migration of nuclei during G2 is a prerequisite for all nuclear motion in zebrafish neuroepithelia. Development 139, 2635–2635. doi:10.1242/dev.085456

Lim, L.S., Mitchell, P., Seddon, J.M., Holz, F.G., Wong, T.Y., 2012. Age-related macular degeneration. Lancet 379, 1728–1738. doi:10.1016/S0140-6736(12)60282-7

Lipinski, D.M., Yusuf, M., Barnard, A.R., Damant, C., Charbel Issa, P., Singh, M.S., Lee, E., Davies, W.L., Volpi, E. V, MacLaren, R.E., 2011. Characterization of a dominant cone degeneration in a green fluorescent protein-reporter mouse with disruption of Loci associated with human dominant retinal dystrophy. Invest. Ophthalmol. Vis. Sci. 52, 6617–23. doi:10.1167/iovs.11-7932

Liu, H., Etter, P., Hayes, S., Jones, I., Nelson, B., Hartman, B., Forrest, D., Reh, T. a, 2008. NeuroD1 regulates expression of thyroid hormone receptor 2 and cone opsins in the developing mouse retina. J. Neurosci. 28, 749–756. doi:10.1523/JNEUROSCI.4832-07.2008

Ma, J., Kabiel, M., Tucker, B. a, Ge, J., Young, M.J., 2011. Combining chondroitinase ABC and growth factors promotes the integration of murine retinal progenitor cells transplanted into Rho(-/-) mice. Mol. Vis. 17, 1759–1770. doi:193 [pii]

Ma, J., Norton, J., Allen, A., Burns, J., 1995. Retinal degeneration slow (rds) in mouse results from simple insertion of at haplotype-specific element into protein-coding exon II. Genomics 28, 212–9. doi:10.1006/geno.1995.1133

Mack, A.F., Papanikolaou, D., Lillo, C., 2003. Investigation of the migration path for new rod photoreceptors in the adult cichlid fish retina. Exp. Neurol. 184, 90–96. doi:10.1016/S0014-4886(03)00131-6

Maclaren, R.E., Groppe, M., Barnard, A.R., Cottriall, C.L., Tolmachova, T., Seymour, L., Clark, K.R., During, M.J., Cremers, F.P.M., Black, G.C.M., Lotery, A.J., Downes, S.M., Webster, A.R., Seabra, M.C., 2014. Retinal gene therapy in patients with choroideremia: initial findings from a phase 1/2 clinical trial. Lancet 6736, 1–9. doi:10.1016/S0140-6736(13)62117-0

MacLaren, R.E., Groppe, M., Barnard, A.R., Cottriall, C.L., Tolmachova, T., Seymour, L., Clark, K.R., During, M.J., Cremers, F.P.M., Black, G.C.M., Lotery, A.J., Downes, S.M., Webster, A.R., Seabra, M.C., 2014. Retinal gene therapy in patients with choroideremia: initial findings from a phase 1/2 clinical trial. Lancet 6736, 1–9. doi:10.1016/S0140-6736(13)62117-0

MacLaren, R.E., Pearson, R.A., MacNeil, A., Douglas, R.H., Salt, T.E., Akimoto, M., Swaroop, A., Sowden, J.C., Ali, R.R., 2006. Retinal repair by transplantation of photoreceptor precursors. Nature 444, 203–7. doi:10.1038/nature05161

Maguire, A.M., Simonelli, F., Pierce, E.A., Pugh, E.N., Mingozzi, F., Bennicelli, J., Banfi, S., Marshall, K.A., Testa, F., Surace, E.M., Rossi, S., Lyubarsky, A., Arruda, V.R., Konkle, B., Stone, E., Sun, J., Jacobs, J., Dell'Osso, L., Hertle, R., Ma, J., Redmond, T.M.,

Zhu, X., Hauck, B., Zelenaia, O., Shindler, K.S., Maguire, M.G., Wright, J.F., Volpe, N.J., McDonnell, J.W., Auricchio, A., High, K.A., Bennett, J., 2008. Safety and efficacy of gene transfer for Leber's congenital amaurosis. N. Engl. J. Med. 358, 2240–8. doi:10.1056/NEJMoa0802315

Marquardt, T., Gruss, P., 2002. Generating neuronal diversity in the retina: one for nearly all. Trends Neurosci. 25, 32–38.

Matsuda, T., Cepko, C.L., 2004. Electroporation and RNA interference in the rodent retina in vivo and in vitro. Proc. Natl. Acad. Sci. U. S. A. 101, 16–22. doi:10.1073/pnas.2235688100

McIlvain, V. a, Knox, B.E., 2007. Nr2e3 and Nrl can reprogram retinal precursors to the rod fate in Xenopus retina. Dev. Dyn. 236, 1970–9. doi:10.1002/dvdy.21128

Mears, a J., Kondo, M., Swain, P.K., Takada, Y., Bush, R. a, Saunders, T.L., Sieving, P. a, Swaroop, a, 2001. Nrl is required for rod photoreceptor development. Nat. Genet. 29, 447–52. doi:10.1038/ng774

Michalakis, S., Geiger, H., Haverkamp, S., Hofmann, F., Gerstner, A., Biel, M., 2005. Impaired opsin targeting and cone photoreceptor migration in the retina of mice lacking the cyclic nucleotide-gated channel CNGA3. Invest. Ophthalmol. Vis. Sci. 46, 1516–24. doi:10.1167/iovs.04-1503

Milam, A., Rose, L., 2002. The nuclear receptor NR2E3 plays a role in human retinal photoreceptor differentiation and degeneration. Proc. ….

Misson, J.P., Austin, C.P., Takahashi, T., Cepko, C.L., Caviness, V.S., 1991. The alignment of migrating neural cells in relation to the murine neopallial radial glial fiber system. Cereb. Cortex 1, 221–9.

Montana, C.L., Kolesnikov, A. V, Shen, S.Q., Myers, C. a, Kefalov, V.J., Corbo, J.C., 2013. Reprogramming of adult rod photoreceptors prevents retinal degeneration. Proc. Natl. Acad. Sci. U. S. A. 1–6. doi:10.1073/pnas.1214387110

Mori, M., Ghyselinck, N.B., Chambon, P., Mark, M., 2001. Systematic immunolocalization of retinoid receptors in developing and adult mouse eyes. Invest. Ophthalmol. Vis. Sci. 42, 1312–1318.

Morrow, E.M., Belliveau, M.J., Cepko, C.L., 1998. Two phases of rod photoreceptor differentiation during rat retinal development. J. Neurosci. 18, 3738–3748.

Nadarajah, B., Alifragis, P., Wong, R.O.L., Parnavelas, J.G., 2003. Neuronal migration in the developing cerebral cortex: observations based on real-time imaging. Cereb. Cortex 13, 607–11.

Nadarajah, B., Brunstrom, J.E., Grutzendler, J., Wong, R.O., Pearlman, a L., 2001. Two modes of radial migration in early development of the cerebral cortex. Nat. Neurosci. 4, 143–50. doi:10.1038/83967

Nadarajah, B., Parnavelas, J.G., 2002. Modes of neuronal migration in the developing cerebral cortex. Nat. Rev. Neurosci. 3, 423–32. doi:10.1038/nrn845

Naik, R., Mukhopadhyay, A., Ganguli, M., 2009. Gene delivery to the retina: focus on non-

viral approaches. Drug Discov. Today 14, 306–315. doi:10.1016/j.drudis.2008.09.012

Nelson, R., 2001. Visual Responses of Ganglion Cells, in: The Organization of the Retina and Visual System. pp. 1–61.

Ng, L., Hurley, J.B., Dierks, B., Srinivas, M., Salto, C., Vennstrom, B., Reh, T.A., Forrest, D., 2001. A thyroid hormone receptor that is required for the development of green cone photoreceptors. Nat Genet 27, 94–8. doi:10.1038/83829

Ng, L., Ma, M., Curran, T., Forrest, D., 2009. Developmental expression of thyroid hormone receptor β2 protein in cone photoreceptors in the mouse. Neuroreport 20, 627–631. doi:10.1097/WNR.0b013e32832a2c63.Developmental

Nikonov, S.S., Kholodenko, R., Lem, J., Pugh, E.N., 2006. Physiological Features of the S- and M-cone Photoreceptors of Wild-type Mice from Single-cell Recordings. J. Gen. Physiol. 127, 359–374. doi:10.1085/jgp.200609490

Norden, C., Young, S., Link, B. a, Harris, W. a, 2009. Actomyosin is the main driver of interkinetic nuclear migration in the retina. Cell 138, 1195–208. doi:10.1016/j.cell.2009.06.032

Ogden, T.E., 1975. The receptor mosaic of Aotes trivirgatus: distribution of rods and cones. J Comp Neurol 163, 193–202. doi:10.1002/cne.901630205

Oh, E., Cheng, H., Hao, H., Jia, L., Khan, N., Swaroop, A., 2008. Rod differentiation factor NRL activates the expression of nuclear receptor NR2E3 to suppress the development of cone photoreceptors. Brain Res. 16–29. doi:10.1016/j.brainres.2008.01.028.Rod

Oh, E.C.T., Khan, N., Novelli, E., Khanna, H., Strettoi, E., Swaroop, A., 2007. Transformation of cone precursors to functional rod photoreceptors by bZIP transcription factor NRL. Proc. Natl. Acad. Sci. U. S. A. 104, 1679–1684. doi:10.1073/pnas.0605934104

Osakada, F., Ikeda, H., Mandai, M., Wataya, T., Watanabe, K., Yoshimura, N., Akaike, A., Akaike, A., Sasai, Y., Takahashi, M., 2008. Toward the generation of rod and cone photoreceptors from mouse, monkey and human embryonic stem cells. Nat. Biotechnol. 26, 215–24. doi:10.1038/nbt1384

Pang, J.J., Alexander, J., Lei, B., Deng, W., Zhang, K., Li, Q., Chang, B., Hauswirth, W.W., 2010. Achromatopsia as a potential candidate for gene therapy, in: Advances in Experimental Medicine and Biology. pp. 639–646. doi:10.1007/978-1-4419-1399-9_73

Parslow, A., Cardona, A., Bryson-Richardson, R.J., 2014. Sample Drift Correction Following 4D Confocal Time-lapse Imaging e51086. doi:doi:10.3791/51086

Pearring, J.N., Salinas, R.Y., Baker, S.A., Arshavsky, V.Y., 2013. Protein sorting, targeting and trafficking in photoreceptor cells. Prog. Retin. Eye Res. 36, 24–51. doi:10.1016/j.preteyeres.2013.03.002

Pearson, R., 2014. Advances in repairing the degenerate retina by rod photoreceptor transplantation. Biotechnol. Adv. 1–7. doi:10.1016/j.biotechadv.2014.01.001

Pearson, R.A., Barber, A.C., Rizzi, M., Hippert, C., Xue, T., West, E.L., Duran, Y., Smith, A.J., Chuang, J.Z., Azam, S.A., Luhmann, U.F.O., Benucci, A., Sung, C.H., Bainbridge,

J.W., Carandini, M., Yau, K.-W., Sowden, J.C., Ali, R.R., 2012. Restoration of vision after transplantation of photoreceptors. Nature 485, 99–103. doi:10.1038/nature10997

Pearson, R.A., Barber, A.C., West, E.L., MacLaren, R.E., Duran, Y., Bainbridge, J.W., Sowden, J.C., Ali, R.R., 2010. Targeted disruption of outer limiting membrane junctional proteins (Crb1 and ZO-1) increases integration of transplanted photoreceptor precursors into the adult wild-type and degenerating retina. Cell Transplant. 19, 487–503. doi:10.3727/096368909X486057

Pearson, R. a, Lüneborg, N.L., Becker, D.L., Mobbs, P., 2005. Gap junctions modulate interkinetic nuclear movement in retinal progenitor cells. J. Neurosci. 25, 10803–14. doi:10.1523/JNEUROSCI.2312-05.2005

Pearson, R., Gonzalez-Cordero, A., West, E.., Ribeiro, J.R., Aghaizu, N.D., Goh, D., Sampson, R.D., Georgiadis, A., Waldron, P.., Duran, Y., Naeem, A., Kloc, M., Cristante, E., Kruczek, K., Sowden, J.C., Smith, A.J., Ali, R.R., 2016. Donor and host photoreceptors engage in material transfer following transplantation of post-mitotic photoreceptor precursors. Nat. Commun.

Penfold, P.L., Madigan, M.C., Gillies, M.C., Provis, J.M., 2001. Immunological and aetiological aspects of macular degeneration. Prog. Retin. Eye Res. 20, 385–414. doi:10.1016/S1350-9462(00)00025-2

Peng, G.H., Ahmad, O., Ahmad, F., Liu, J., Chen, S., 2005. The photoreceptor-specific nuclear receptor Nr2e3 interacts with Crx and exerts opposing effects on the transcription of rod versus cone genes. Hum. Mol. Genet. 14, 747–764. doi:10.1093/hmg/ddi070

Pollak, J., Wilken, M.S., Ueki, Y., Cox, K.E., Sullivan, J.M., Taylor, R.J., Levine, E.M., Reh, T. a, 2013. ASCL1 reprograms mouse Muller glia into neurogenic retinal progenitors. Development 140, 2619–31. doi:10.1242/dev.091355

Polosukhina, A., Litt, J., Tochitsky, I., Nemargut, J., Sychev, Y., De Kouchkovsky, I., Huang, T., Borges, K., Trauner, D., Van Gelder, R.N., Kramer, R.H., 2012. Photochemical restoration of visual responses in blind mice. Neuron 75, 271–82. doi:10.1016/j.neuron.2012.05.022

Qiu, G., Seiler, M.J., Mui, C., Arai, S., Aramant, R.B., de Juan, E., Sadda, S., 2005. Photoreceptor differentiation and integration of retinal progenitor cells transplanted into transgenic rats. Exp. Eye Res. 80, 515–25. doi:10.1016/j.exer.2004.11.001

Quiroga, R.Q., Nadasdy, Z., Ben-Shaul, Y., 2004. Unsupervised spike detection and sorting with wavelets and superparamagnetic clustering. Neural Comput. 16, 1661–1687. doi:10.1162/089976604774201631

Radtke, N.D., Aramant, R.B., Petry, H.M., Green, P.T., Pidwell, D.J., Seiler, M.J., 2008. Vision Improvement in Retinal Degeneration Patients by Implantation of Retina Together with Retinal Pigment Epithelium. Am. J. Ophthalmol. 146. doi:10.1016/j.ajo.2008.04.009

Rakic, P., 1972. Mode of cell migration to the superficial layers of fetal monkey neocortex. J.

Comp. Neurol. 145, 61–83. doi:10.1002/cne.901450105

Rakic, P., Knyihar-Csillik, E., Csillik, B., 1996. Polarity of microtubule assemblies during neuronal cell migration. Proc. Natl. Acad. Sci. U. S. A. 93, 9218–22.

Razafsky, D., Blecher, N., Markov, A., Stewart-Hutchinson, P.J., Hodzic, D., 2012. LINC complexes mediate the positioning of cone photoreceptor nuclei in mouse retina. PLoS One 7, e47180. doi:10.1371/journal.pone.0047180

Reese, B.E., Harvey, a R., Tan, S.S., 1995. Radial and tangential dispersion patterns in the mouse retina are cell-class specific. Proc. Natl. Acad. Sci. U. S. A. 92, 2494–8.

Rich, K.A., Zhan, Y., Blanks, J.C., 1997. Migration and synaptogenesis of cone photoreceptors in the developing mouse retina. J. Comp. Neurol. 388, 47–63.

Roberts, M.R., Hendrickson, A., McGuire, C.R., Reh, T. a, 2005. Retinoid X receptor (gamma) is necessary to establish the S-opsin gradient in cone photoreceptors of the developing mouse retina. Invest. Ophthalmol. Vis. Sci. 46, 2897–2904. doi:10.1167/iovs.05-0093

Robinson, S.R., Rapaport, D.H., Stone, J., 1985. Cell Division in the Developing Cat Retina Occurs in Two Zones A utoradiography The protocol of Fraser 7 for staining mitotic figures Thymidine autoradiography Three observations obtained with thymidine auto- 19, 101–109.

Roger, J.E., Ranganath, K., Zhao, L., Cojocaru, R.I., Brooks, M., Gotoh, N., Veleri, S., Hiriyanna, A., Rachel, R. a, Campos, M.M., Fariss, R.N., Wong, W.T., Swaroop, A., 2012. Preservation of cone photoreceptors after a rapid yet transient degeneration and remodeling in cone-only Nrl-/- mouse retina. J. Neurosci. 32, 528–41. doi:10.1523/JNEUROSCI.3591-11.2012

Rouaux, C., Arlotta, P., 2013. Direct lineage reprogramming of post-mitotic callosal neurons into corticofugal neurons in vivo. Nat. Cell Biol. 15, 214–21. doi:10.1038/ncb2660

Sakaguchi, D.S., Van Hoffelen, S.J., Young, M.J., 2003. Differentiation and morphological integration of neural progenitor cells transplanted into the developing mammalian eye. Ann. N. Y. Acad. Sci. 995, 127–39.

Samardzija, M., Caprara, C., Heynen, S.R., Willcox DeParis, S., Meneau, I., Traber, G., Agca, C., von Lintig, J., Grimm, C., 2014. A mouse model for studying cone photoreceptor pathologies. Invest. Ophthalmol. Vis. Sci. 55, 5304–13. doi:10.1167/iovs.14-14789

Samardzija, M., Von lintig, J., Tanimoto, N., Oberhauser, V., Thiersch, M., Seeliger, M., Remé, C.E., Grimm, C., Wenzel, A., 2008. R91W mutation in Rpe65 leads to milder early-onset retinal dystrophy due to the generation of low levels of 11-cis-retinal. Hum. Mol. Genet. 17, 281–292. doi:10.1093/hmg/ddm304

Samson, M., Emerson, M.M., Cepko, C.L., 2009. Robust marking of photoreceptor cells and pinealocytes with several reporters under control of the Crx gene. Dev. Dyn. 238, 3218–25. doi:10.1002/dvdy.22138

Santos-Ferreira, T., Postel, K., Stutzki, H., Kurth, T., Zeck, G., Ader, M., 2014. Daylight

vision repair by cell transplantation. Stem Cells 1–15. doi:10.1002/stem.1824

Sauer, F.C., 1935. Mitosis in the neural tube. J. Comp. Neurol. 62, 377–405. doi:10.1002/cne.900620207

Schaar, B.T., McConnell, S.K., 2005. Cytoskeletal coordination during neuronal migration. Proc. Natl. Acad. Sci. U. S. A. 102, 13652–7. doi:10.1073/pnas.0506008102

Schaeren-Wiemers, N., André, E., Kapfhammer, J.P., Becker-André, M., 1997. The expression pattern of the orphan nuclear receptor RORbeta in the developing and adult rat nervous system suggests a role in the processing of sensory information and in circadian rhythm. Eur. J. Neurosci. 9, 2687–701.

Schenk, J., Wilsch-Bräuninger, M., Calegari, F., Huttner, W.B., 2009. Myosin II is required for interkinetic nuclear migration of neural progenitors. Proc. Natl. Acad. Sci. U. S. A. 106, 16487–92. doi:10.1073/pnas.0908928106

Schwartz, S.D., Regillo, C.D., Lam, B.L., Eliott, D., Rosenfeld, P.J., Gregori, N.Z., Hubschman, J.-P., Davis, J.L., Heilwell, G., Spirn, M., Maguire, J., Gay, R., Bateman, J., Ostrick, R.M., Morris, D., Vincent, M., Anglade, E., Del Priore, L. V, Lanza, R., 2014. Human embryonic stem cell-derived retinal pigment epithelium in patients with age-related macular degeneration and Stargardt's macular dystrophy: follow-up of two open-label phase 1/2 studies. Lancet 6736, 1–8. doi:10.1016/S0140-6736(14)61376-3

Schwartz, S.D., Tan, G., Hosseini, H., Nagiel, A., 2016. Subretinal Transplantation of Embryonic Stem Cell-Derived Retinal Pigment Epithelium for the Treatment of Macular Degeneration: An Assessment at 4 Years. Invest. Ophthalmol. Vis. Sci. 57, ORSFc1-9. doi:10.1167/iovs.15-18681

Seiler, M.J., Thomas, B.B., Chen, Z., Wu, R., Sadda, S.R., Aramant, R.B., 2008. Retinal transplants restore visual responses: Trans-synaptic tracing from visually responsive sites labels transplant neurons. Eur. J. Neurosci. 28, 208–220. doi:10.1111/j.1460-9568.2008.06279.x

Shen, S.-W., Duan, C.-L., Chen, X.-H., Wang, Y.-Q., Sun, X., Zhang, Q.-W., Cui, H.-R., Sun, F.-Y., 2015. Neurogenic effect of VEGF is related to increase of astrocytes transdifferentiation into new mature neurons in rat brains after stroke. Neuropharmacology. doi:10.1016/j.neuropharm.2015.11.012

Shoukimas, G.M., Hinds, J.W., 1978. The development of the cerebral cortex in the embryonic mouse: an electron microscopic serial section analysis. J. Comp. Neurol. 179, 795–830. doi:10.1002/cne.901790407

Siegert, S., Cabuy, E., Scherf, B.G., Kohler, H., Panda, S., Le, Y.-Z., Fehling, H.J., Gaidatzis, D., Stadler, M.B., Roska, B., 2012. Transcriptional code and disease map for adult retinal cell types. Nat. Neurosci. 15, 487–495. doi:10.1038/nn.3032

Siegert, S., Scherf, B.G., Del Punta, K., Didkovsky, N., Heintz, N., Roska, B., 2009. Genetic address book for retinal cell types. Nat. Neurosci. 12, 1197–1204. doi:10.1038/nn.2370

Silva, A.O., Ercole, C.E., McLoon, S.C., 2003. Regulation of ganglion cell production by Notch signaling during retinal development. J. Neurobiol. 54, 511–524.

doi:10.1002/neu.10156

Singh, M.S., Charbel Issa, P., Butler, R., Martin, C., Lipinski, D.M., Sekaran, S., Barnard, A.R., MacLaren, R.E., 2013. Reversal of end-stage retinal degeneration and restoration of visual function by photoreceptor transplantation. Proc. Natl. Acad. Sci. U. S. A. 110, 1101–6. doi:10.1073/pnas.1119416110

Smiley, S., Nickerson, P.E., Comanita, L., Daftarian, N., El-Sehemy, A., Tsai, E.L.S., Matan-Lithwick, S., Yan, K., Thurig, S., Touahri, Y., Dixit, R., Aavani, T., De Repentingy, Y., Baker, A., Tsilfidis, C., Biernaskie, J., Sauvé, Y., Schuurmans, C., Kothary, R., Mears, A.J., Wallace, V.A., 2016. Establishment of a cone photoreceptor transplantation platform based on a novel cone-GFP reporter mouse line. Sci. Rep. 6, 22867. doi:10.1038/srep22867

Smith, A.J., Bainbridge, J.W., Ali, R.R., 2009. Prospects for retinal gene replacement therapy. Trends Genet. 25, 156–165. doi:10.1016/j.tig.2009.02.003

Smith, D.K., He, M., Zhang, C.-L., Zheng, J.C., 2016. The therapeutic potential of cell identity reprogramming for the treatment of aging-related neurodegenerative disorders. Prog. Neurobiol. doi:10.1016/j.pneurobio.2016.01.006

Smith, W., Assink, J., Klein, R., Mitchell, P., Klaver, C.C., Klein, B.E., Hofman, A., Jensen, S., Wang, J.J., de Jong, P.T., 2001. Risk factors for age-related macular degeneration: Pooled findings from three continents. Ophthalmology 108, 697–704.

Sodhi, P., Hartwick, A.T., 2014. Adenosine modulates light responses of rat retinal ganglion cell photoreceptors througha cAMP-mediated pathway. J Physiol 592, 4201–4220. doi:10.1113/jphysiol.2014.276220

Sodhi, P., Hartwick, A.T.E., 2016. Muscarinic acetylcholine receptor-mediated stimulation of retinal ganglion cell photoreceptors. Neuropharmacology 108, 305–315. doi:10.1016/j.neuropharm.2016.04.001

Solecki, D.J., 2012. Sticky situations: recent advances in control of cell adhesion during neuronal migration. Curr. Opin. Neurobiol. 22, 791–8. doi:10.1016/j.conb.2012.04.010

Solecki, D.J., Model, L., Gaetz, J., Kapoor, T.M., Hatten, M.E., 2004. Par6alpha signaling controls glial-guided neuronal migration. Nat. Neurosci. 7, 1195–203. doi:10.1038/nn1332

Solecki, D.J., Trivedi, N., Govek, E.-E., Kerekes, R. a, Gleason, S.S., Hatten, M.E., 2009. Myosin II motors and F-actin dynamics drive the coordinated movement of the centrosome and soma during CNS glial-guided neuronal migration. Neuron 63, 63–80. doi:10.1016/j.neuron.2009.05.028

Solovei, I., Kreysing, M., Lanctôt, C., Kösem, S., Peichl, L., Cremer, T., Guck, J., Joffe, B., 2009. Nuclear Architecture of Rod Photoreceptor Cells Adapts to Vision in Mammalian Evolution. Cell 137, 356–368. doi:10.1016/j.cell.2009.01.052

Starr, D. a., 2003. ANChors away: an actin based mechanism of nuclear positioning. J. Cell Sci. 116, 211–216. doi:10.1242/jcs.00248

Stoorvogel, W., Kleijmeer, M.J., Geuze, H.J., Raposo, G., 2002. The biogenesis and

functions of exosomes. Traffic 3, 321–330. doi:tra030502 [pii]

Strzyz, P.J., Lee, H.O., Sidhaye, J., Weber, I.P., Leung, L.C., Norden, C., 2015. Interkinetic Nuclear Migration Is Centrosome Independent and Ensures Apical Cell Division to Maintain Tissue Integrity. Dev. Cell 32, 203–219. doi:10.1016/j.devcel.2014.12.001

Stuck, M.W., Conley, S.M., Naash, M.I., 2012. Defects in the outer limiting membrane are associated with rosette development in the Nrl-/- retina. PLoS One 7, e32484. doi:10.1371/journal.pone.0032484

Suzuki, T., Akimoto, M., Imai, H., Ueda, Y., Mandai, M., Yoshimura, N., Swaroop, A., Takahashi, M., 2007. Chondroitinase ABC treatment enhances synaptogenesis between transplant and host neurons in model of retinal degeneration. Cell Transplant. 16, 493–503. doi:10.1017/CBO9781107415324.004

Suzuki, T., Mandai, M., Akimoto, M., Yoshimura, N., Takahashi, M., 2006. The simultaneous treatment of MMP-2 stimulants in retinal transplantation enhances grafted cell migration into the host retina. Stem Cells 24, 2406–2411. doi:10.1634/stemcells.2005-0587

Swaroop, A., Kim, D., Forrest, D., 2010. Transcriptional regulation of photoreceptor development and homeostasis in the mammalian retina. Nat. Rev. Neurosci. 11, 563–76. doi:10.1038/nrn2880

Takahashi, K., Yamanaka, S., 2006. Induction of Pluripotent Stem Cells from Mouse Embryonic and Adult Fibroblast Cultures by Defined Factors. Cell 126, 663–676. doi:10.1016/j.cell.2006.07.024

Tan, M.H., Smith, A.J., Pawlyk, B., Xu, X., Liu, X., Bainbridge, J.B., Basche, M., McIntosh, J., Tran, H.V., Nathwani, A., Li, T., Ali, R.R., 2009. Gene therapy for retinitis pigmentosa and Leber congenital amaurosis caused by defects in AIPL1: effective rescue of mouse models of partial and complete Aipl1 deficiency using AAV2/2 and AAV2/8 vectors. Hum. Mol. Genet. 18, 2099–114. doi:10.1093/hmg/ddp133

Tapley, E.C., Starr, D. a, 2013. Connecting the nucleus to the cytoskeleton by SUN-KASH bridges across the nuclear envelope. Curr. Opin. Cell Biol. 25, 57–62. doi:10.1016/j.ceb.2012.10.014

Taylor, T.B., Vishnu, P., Michie, S. a, Raja, R., Horner, N., Kunitake, S.T., 2002. Molecular Diagnostic Techniques High-Quality RNA from Cells Isolated by Laser Capture Microdissection 33, 5–8.

Terada, N., Hamazaki, T., Oka, M., Hoki, M., Mastalerz, D.M., Nakano, Y., Meyer, E.M., Morel, L., Petersen, B.E., Scott, E.W., 2002. Bone marrow cells adopt the phenotype of other cells by spontaneous cell fusion. Nature 416, 542–545. doi:10.1038/nature730

Tobergte, D.R., Curtis, S., 2011. Ranibizumab and Bevacizumab for Neovascular Age-Related Macular Degeneration. N. Engl. J. Med. 364, 1897–1908. doi:10.1056/NEJMoa1102673

Tropepe, V., Coles, B., Chiasson, B., Horsford, D., Elia, A., McInnes, R., Van der Kooy, D., 2000. Retinal Stem Cells in the Adult Mammalian Eye. Science (80-.). 287, 2032–

2036. doi:10.1126/science.287.5460.2032

Tsai, J.-W., Lian, W.-N., Kemal, S., Kriegstein, A.R., Vallee, R.B., 2010. Kinesin 3 and cytoplasmic dynein mediate interkinetic nuclear migration in neural stem cells. Nat. Neurosci. 13, 1463–1471. doi:10.1038/nn.2665

Tsai, J., Lian, W., Kemal, S., 2010. Kinesin 3 and cytoplasmic dynein mediate interkinetic nuclear migration in neural stem cells. Nat. … 13, 1463–1471. doi:10.1038/nn.2665.An

Tucker, B. a, Park, I.-H., Qi, S.D., Klassen, H.J., Jiang, C., Yao, J., Redenti, S., Daley, G.Q., Young, M.J., 2011. Transplantation of adult mouse iPS cell-derived photoreceptor precursors restores retinal structure and function in degenerative mice. PLoS One 6, e18992. doi:10.1371/journal.pone.0018992

Ueki, Y., Wilken, M.S., Cox, K.E., Chipman, L., Jorstad, N., Sternhagen, K., Simic, M., Ullom, K., Nakafuku, M., Reh, T.A., 2015. Transgenic expression of the proneural transcription factor Ascl1 in Müller glia stimulates retinal regeneration in young mice. Proc. Natl. Acad. Sci. U. S. A. 112, 13717–22. doi:10.1073/pnas.1510595112

Vallee, R.B., Seale, G.E., Tsai, J.-W., 2009. Emerging roles for myosin II and cytoplasmic dynein in migrating neurons and growth cones. Trends Cell Biol. 19, 347–55. doi:10.1016/j.tcb.2009.03.009

Vaughan, P.S., Leszyk, J.D., Vaughan, K.T., 2001. Cytoplasmic dynein intermediate chain phosphorylation regulates binding to dynactin. J. Biol. Chem. 276, 26171–9. doi:10.1074/jbc.M102649200

Walch, O.J., Zhang, L.S., Reifler, A.N., Dolikian, M.E., Forger, D.B., Wong, K.Y., 2015. Characterizing and modeling the intrinsic light response of rat ganglion-cell photoreceptors. J. Neurophysiol. 114, 2955–2966. doi:10.1152/jn.00544.2015

Wall, D.S., Mears, A.J., McNeill, B., Mazerolle, C., Thurig, S., Wang, Y., Kageyama, R., Wallace, V.A., 2009. Progenitor cell proliferation in the retina is dependent on Notch-independent Sonic hedgehog/Hes1 activity. J. Cell Biol. 184, 101–112. doi:10.1083/jcb.200805155

Wang, D.Y., Chan, W.M., Tam, P.O.S., Baum, L., Lam, D.S.C., Chong, K.K.L., Fan, B.J., Pang, C.P., 2005. Gene mutations in retinitis pigmentosa and their clinical implications. Clin. Chim. Acta. 351, 5–16. doi:10.1016/j.cccn.2004.08.004

Wang, M., Wong, W.T., 2014. Microglia-Müller cell interactions in the retina. Adv. Exp. Med. Biol. 801, 333–8. doi:10.1007/978-1-4614-3209-8_42

Wang, Y. V, Weick, M., Demb, J.B., 2011. Spectral and temporal sensitivity of cone-mediated responses in mouse retinal ganglion cells. J. Neurosci. 31, 7670–7681. doi:10.1523/JNEUROSCI.0629-11.2011

Warre-Cornish, K., 2013. Migration and maturation of rod photoreceptor precursors in transplant and development. University College London.

Warre-Cornish, K., Barber, A.C., Sowden, J.C., Ali, R.R., Pearson, R. a, 2014. Migration, Integration and Maturation of Photoreceptor Precursors Following Transplantation in the Mouse Retina. Stem Cells Dev. 1–14. doi:10.1089/scd.2013.0471

Wässle, H., 2004. Parallel processing in the mammalian retina. Nat. Rev. Neurosci. 5, 747–757. doi:10.1038/nrn1497

Wässle, H., Puller, C., Muller, F., Haverkamp, S., 2009. Cone contacts, mosaics, and territories of bipolar cells in the mouse retina. J Neurosci 29, 106–117. doi:10.1523/JNEUROSCI.4442-08.2009

Wenzel, A., von Lintig, J., Oberhauser, V., Tanimoto, N., Grimm, C., Seeliger, M.W., 2007. RPE65 is essential for the function of cone photoreceptors in NRL-deficient mice. Invest. Ophthalmol. Vis. Sci. 48, 534–42. doi:10.1167/iovs.06-0652

West, E.L., Gonzalez-Cordero, A., Hippert, C., Osakada, F., Martinez-Barbera, J.P., Pearson, R. a, Sowden, J.C., Takahashi, M., Ali, R.R., 2012. Defining the integration capacity of embryonic stem cell-derived photoreceptor precursors. Stem Cells 30, 1424–35. doi:10.1002/stem.1123

West, E.L., Pearson, R.A., Barker, S.E., Luhmann, U.F.O., Maclaren, R.E., Barber, A.C., Duran, Y., Smith, A.J., Sowden, J.C., Ali, R.R., 2010. Long-term survival of photoreceptors transplanted into the adult murine neural retina requires immune modulation. Stem Cells 28, 1997–2007. doi:10.1002/stem.520

West, E.L., Pearson, R.A., Duran, Y., Maclaren, R.E., 2012. Europe PMC Funders Group Manipulation of the Recipient Retinal Environment by Ectopic Expression of Neurotrophic Growth Factors Can Improve Transplanted Photoreceptor Integration and Survival 21, 871–887. doi:10.3727/096368911X623871.Manipulation

West, E.L., Pearson, R.A., Tschernutter, M., Sowden, J.C., MacLaren, R.E., Ali, R.R., 2008. Pharmacological disruption of the outer limiting membrane leads to increased retinal integration of transplanted photoreceptor precursors. Exp. Eye Res. 86, 601–611. doi:10.1016/j.exer.2008.01.004

Willems, E., Leyns, L., Vandesompele, J., 2008. Standardization of real-time PCR gene expression data from independent biological replicates. Anal. Biochem. 379, 127–129. doi:10.1016/j.ab.2008.04.036

Wong, A.A., Brown, R.E., 2007. Age-related changes in visual acuity, learning and memory in C57BL/6J and DBA/2J mice. Neurobiol. Aging 28, 1577–1593. doi:10.1016/j.neurobiolaging.2006.07.023

Xie, Z., Moy, L.Y., Sanada, K., Zhou, Y., Buchman, J.J., Tsai, L.-H., 2007. Cep120 and TACCs control interkinetic nuclear migration and the neural progenitor pool. Neuron 56, 79–93. doi:10.1016/j.neuron.2007.08.026

Yamashita, T., Sonoda, S., Suzuki, R., Arimura, N., Tachibana, K., Maruyama, K., Sakamoto, T., 2007. A novel bubble liposome and ultrasound-mediated gene transfer to ocular surface: RC-1 cells in vitro and conjunctiva in vivo. Exp. Eye Res. 85, 741–748. doi:10.1016/j.exer.2007.08.006

Yang, R.B., Robinson, S.W., Xiong, W.H., Yau, K.W., Birch, D.G., Garbers, D.L., 1999. Disruption of a retinal guanylyl cyclase gene leads to cone-specific dystrophy and paradoxical rod behavior. J. Neurosci. 19, 5889–97.

Yao, J., Tucker, B.A., Zhang, X., Checa-Casalengua, P., Herrero-Vanrell, R., Young, M.J., 2011. Robust cell integration from co-transplantation of biodegradable MMP2-PLGA microspheres with retinal progenitor cells. Biomaterials 32, 1041–1050. doi:10.1016/j.biomaterials.2010.09.063

Yaron, O., Farhy, C., Marquardt, T., Applebury, M., Ashery-Padan, R., 2006. Notch1 functions to suppress cone-photoreceptor fate specification in the developing mouse retina. Development 133, 1367–1378. doi:10.1242/dev.02311

Ying, Q.-L., Nichols, J., Evans, E.P., Smith, A.G., 2002. Changing potency by spontaneous fusion. Nature 416, 545–548. doi:10.1038/nature729

Yoshida, N., Ikeda, Y., Notomi, S., Ishikawa, K., Murakami, Y., Hisatomi, T., Enaida, H., Ishibashi, T., 2013. Clinical evidence of sustained chronic inflammatory reaction in retinitis pigmentosa. Ophthalmology 120, 100–105. doi:10.1016/j.ophtha.2012.07.006

Yoshida, S., Mears, A.J., Friedman, J.S., Carter, T., He, S., Oh, E., Jing, Y., Farjo, R., Fleury, G., Barlow, C., Hero, A.O., Swaroop, A., 2004. Expression profiling of the developing and mature Nrl-/- mouse retina: identification of retinal disease candidates and transcriptional regulatory targets of Nrl. Hum. Mol. Genet. 13, 1487–503. doi:10.1093/hmg/ddh160

Young, M.J., Ray, J., Whiteley, S.J., Klassen, H., Gage, F.H., 2000. Neuronal differentiation and morphological integration of hippocampal progenitor cells transplanted to the retina of immature and mature dystrophic rats. Mol. Cell. Neurosci. 16, 197–205. doi:10.1006/mcne.2000.0869

Young, R.W., 1985. Cell differentiation in the retina of the mouse. Anat. Rec. 212, 199–205. doi:10.1002/ar.1092120215

Yu, J., Lei, K., Zhou, M., Craft, C.M., Xu, G., Xu, T., Zhuang, Y., Xu, R., Han, M., 2011. KASH protein Syne-2/Nesprin-2 and SUN proteins SUN1/2 mediate nuclear migration during mammalian retinal development. Hum. Mol. Genet. 20, 1061–73. doi:10.1093/hmg/ddq549

Zhang, X., Lei, K., Yuan, X., Wu, X., Zhuang, Y., Xu, T., Xu, R., Han, M., 2009. SUN1/2 and Syne/Nesprin-1/2 complexes connect centrosome to the nucleus during neurogenesis and neuronal migration in mice. Neuron 64, 173–87. doi:10.1016/j.neuron.2009.08.018

Zhong, X., Gutierrez, C., Xue, T., Hampton, C., Vergara, M.N., Cao, L.-H., Peters, A., Park, T.S., Zambidis, E.T., Meyer, J.S., Gamm, D.M., Yau, K.-W., Canto-Soler, M.V., 2014. Generation of three-dimensional retinal tissue with functional photoreceptors from human iPSCs. Nat. Commun. 5, 389–400. doi:10.1038/ncomms5047

Zolessi, F.R., Poggi, L., Wilkinson, C.J., Chien, C.-B., Harris, W. a, 2006. Polarization and orientation of retinal ganglion cells in vivo. Neural Dev. 1, 2. doi:10.1186/1749-8104-1-2